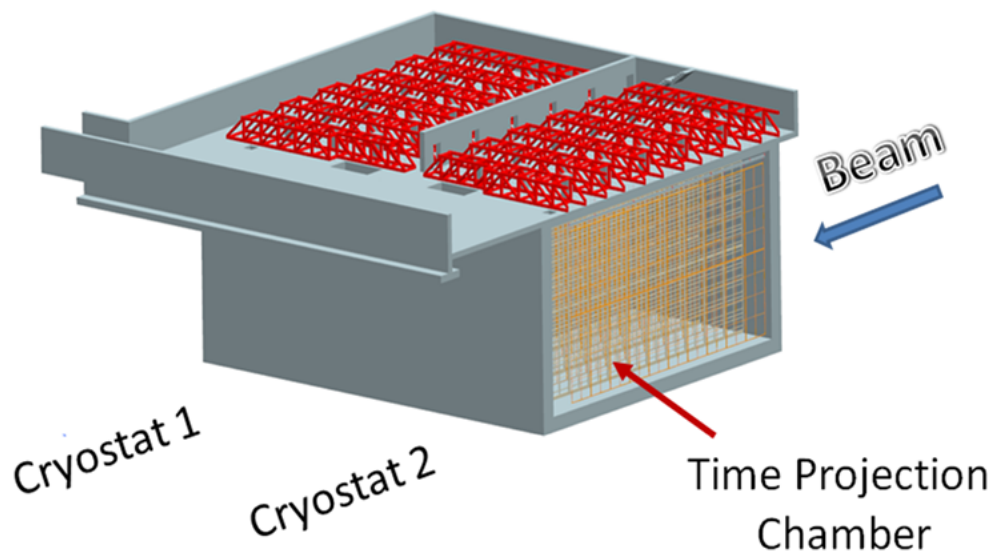# Long-Baseline Neutrino Experiment (LBNE) Project

Conceptual Design Report

Volume 4: The Liquid Argon Detector at the Far Site

September 10, 2012

Contents

Acronyms, Abbreviations and Units

A	ampere (also mA, kA)
ADC	analog-to-digital converter
APA	anode plane assembly
APD	avalanche photodiodes
ArgoNeuT	Mini LArTPC Exposure to Fermilab's NuMI Beam
ASIC	application-specific integrated circuit
atm	atmosphere
B	byte (also MB, GB, etc.)
b	barn, a measure of cross section; bit (also Mb, Gb, etc.)
bar	bar (also mbar, etc.)
barg	bar gauge
BGR	band-gap reference
Bis-MSB	1,4-bis[2-(2-methylphenyl)ethenyl]-benzene, a wavelength-shifting chemical
Bq	becquerel
C	coulomb
CAD	computer-aided design
CDF	one of two decommissioned collider detectors at Fermilab's Tevatron, along with D-Zero
CDR	Conceptual Design Report

CF	conventional facilities
cf	cubic foot (also ft^3)
CFD	computerized fluid dynamics
cfm	cubic feet per meter (also ft^3/m)
Ci	curie
CP	charge parity
CPA	cathode plane assembly
D-Zero	one of two decommissioned collider detectors at Fermilab's Tevatron, along with CDF
DAQ	data acquisition
DC	direct current
DCM	Data concentrator modules
DCM	data concentrator module
DOE	Department of Energy
DUSEL	Deep Underground Science and Engineering Laboratory
EM	electromagnetic
ENC	equivalent noise charge
ESH	Environment, Safety and Health
eV	electron-volt (also keV, MeV, GeV)
F	farad (also pF, nF)
FEM	front-end module
FESHM	Fermilab's ES&H Manual
FFT	Fast Fourier Transform
FIRUS	Fire and Utilities; Fermilab site-wide, high-reliability, remote monitoring system used to monitor building fire panels and various utilities throughout the lab
FLARE	Fermilab Liquid Argon Experiments
FPGA	field-programmable gate array

FR-4	flame resistant 4
FSE	field-shaping electrode
ft	foot or feet
G	gauss (also mG) or gradient (in magnets)
g	gram (also mg, kg)
G10/FR4	a fire rated electrical-grade dielectric made with and epoxy material reinforced with a woven fiberglass mat
gal	gallon
GAr	gaseous argon
GLACIER	NASA's General Laboratory Active Cryogenic International Space Station Experiment Refrigerator
gpm	gallons per minute (also gal/min)
GTT	Gaztransport & Technigaz
h	hour
HSSD	High Sensitivity Smoke Detection
HV	high voltage
HVAC	heating, ventilation and air conditioning
Hz	hertz (s-1)
ICARUS	Imaging Cosmic and Rare Underground Signals, experiment at the LNGS
IHI	Ishikawajima-Harima Heavy Industries
in	inch
INFN	Istituto Nazionale della Fiscia Nucleare
IT	integration prototype
IU	Indiana University
K	kelvin
l	liter
LANNDD	Liquid Argon Neutrino and Nucleon Decay Detector

LAPD	Liquid Argon Purity Demonstrator
LAr	liquid argon
LAr-FD	LBNE's Liquid Argon Far Detector
LAr1	one-kiloton LAr prototype for LBNE's LAr-FD
LArSoft	a reconstruction software package for LAr detectors
LArTPC	liquid argon time projection chamber
LBNE	Long-Baseline Neutrino Experiment
LED	light-emitting diode
LEM	large electron multiplier
LEMO	a push-pull connector made by the LEMO company in Switzerland
LHe	liquid helium
LN	liquid nitrogen, also written LN_2 and LN2
LNG	liquefied natural gas
LNGS	Gran Sasso National Laboratory
LOTO	lockout/tagout; an OSHA safety practice
LPG	liquefied petroleum gas
LVDS	low-voltage differential signaling
m	meter (also nm, micron, mm, cm, km)
MCT	membrane cryostat test
MICA	type of dielectric material used in capacitors
MicroBooNE	A 100-ton LArTPC located along Fermilab's Booster neutrino beamline
min	minute
MINERvA	A neutrino-scattering experiment that uses the NuMI beamline at Fermilab
MINOS	Main Injector Neutrino Oscillation Search, a Fermilab experiment
MIP	minimum ionizing particle
MIT	Massachusetts Institute of Technology

MOS	metal-oxide semiconductor
MOSFET	metal-oxide-semiconductor field-effect transistor
MS	mega samples
MTS	Materials Test Stand
MTU	master timing unit
MUX	multiplex
N	newton
N or N2	nitrogen
NASA	National Aeronautics and Space Administration
NBTI	negative bias temperature instability
NC	neutral current
NICADD	Northern Illinois Center for Accelerator and Detector Development NOvA
NIM	Nuclear Instruments and Methods (journal)
NIST	National Institute of Standards and Technology
NOvA	NuMI Off-Axis Neutrino Appearance experiment at Fermilab
NPO	type of dielectric material used in capacitors
NSF	National Science Foundation
OD	outer diameter
ODH	oxygen deficiency hazard
OPERA	Oscillation Project with Emulsion-Racking Apparatus, at CERN and LNGS
OSHA	Occupational Safety and Health Administration
P5	Particle Physics Project Prioritization Panel
Pa	pascal
PC	personal computer
PC-4	Fermilab building, Proton Center building number 4
PCI	peripheral component interconnect

PDA	photon detection assembly
PDE	photon-detection efficiency
PE	photo-electron
PLC	programmable logic controller
PMT	photomultiplier tube
PPE	personnel protective equipment
PRV	pressure-relief valve
psi	pounds per square inch
QC	quality control
QFP	quad flat pack
R	roentgen
rad	radian (also mrad)
RC	resistive capacitive
ROOT	An object oriented framework for large-scale data analysis developed at CERN
s	second (also ns, μs, ms)
S/N	signal-to-noise
scfm	standard cubic foot per minute
SCR	silicon controlled rectifier
SDSTA	South Dakota Science and Technology Authority
SHV	safe high voltage, a type of HV cable connector
SIMOPS	simultaneous operations study
SiPM	Silicon photomultiplier
SM	stress-migration
SS	stainless steel
SURF	Sanford Underground Research Facility (in Lead, S.D., the LBNE Far Site)

T	Tesla
t	ton
TC	thermal cycling
TDDB	time-dependent dielectric breakdown
TDU	timing distribution unit
TPB	tetraphenyl butadiene, a wavelength shifting chemical
TPM	TPC module
USB	universal serial bus
UV	ultraviolet
V	volt (also mV, kV, MV)
VA	volt-ampere (also mVA, kVA, MVA)
VAC	Volts alternating current (also mVAC, kVAC)
VME	a computer bus standard
VUV	vacuum ultraviolet light
VUV	vacuum ultraviolet
W	watt (also mW, kW, MW)
WARP	Wimp Argon Program
WBS	Work Breakdown Structure
WLS	wavelength shifter
yd	yard

List of Figures

List of Tables

1   Introduction

1.1   Introduction to the LBNE Project

The Long-Baseline Neutrino Experiment (LBNE) Project team has prepared this Conceptual Design Report (CDR) which describes a world-class facility to enable a compelling research program in neutrino physics. The ultimate goal in the operation of the facility and experimental program is to measure fundamental physical parameters, explore physics beyond the Standard Model and better elucidate the nature of matter and antimatter.

Although the Standard Model of particle physics presents a remarkably accurate description of the elementary particles and their interactions, it is known that the current model is incomplete and that a more fundamental underlying theory must exist. Results from the last decade, revealing that the three known types of neutrinos have nonzero mass, mix with one another and oscillate between generations, point to physics beyond the Standard Model. Measuring the mass and other properties of neutrinos is fundamental to understanding the deeper, underlying theory and will profoundly shape our understanding of the evolution of the universe.

1.1.1   About this Conceptual Design Report

The LBNE Conceptual Design Report is intended to describe, at a conceptual level, the scope and design of the experimental and conventional facilities that the LBNE Project plans to build to address a well-defined set of neutrino-physics measurement objectives. At this Conceptual Design stage the LBNE Project presents a *Reference Design* for LBNE and alternative designs that are still under consideration for particular elements.

The scope includes

- an intense neutrino beam aimed at a far site

- detectors located downstream of the neutrino source

- a massive neutrino detector located at the far site

- construction of conventional facilities at both the near and far sites

The selected near and far sites are Fermi National Accelerator Laboratory (Fermilab), in Batavia, IL and Sanford Underground Research Facility (SURF), respectively. The latter is the site of the formerly proposed Deep Underground Science and Engineering Laboratory (DUSEL) in Lead, South Dakota.

This CDR is organized into six stand-alone volumes, one to describe the overall LBNE Project and one for each of its component L2 projects:

- Volume 1: The LBNE Project

- Volume 2: The Beamline at the Near Site

- Volume 3: Detectors at the Near Site

- Volume 4: The Liquid Argon Detector at the Far Site

- Volume 5: Conventional Facilities at the Near Site

- Volume 6: Conventional Facilities at the Far Site

Volume 1 is intended to provide readers of varying backgrounds an introduction to LBNE and to the following volumes of this CDR. It contains high-level information and refers the reader to topic-specific volumes and supporting documents, also listed in Section 1.1.5. Each of the other volumes contains a common, brief introduction to the overall LBNE Project, an introduction to the individual L2 project and a detailed description of its conceptual design.

1.1.2   LBNE and the U.S. Neutrino-Physics Program

In its 2008 report, the Particle Physics Project Prioritization Panel (P5) recommended a world-class neutrino-physics program as a core component of the U.S. particle physics program [3]. Included in the report is the long-term vision of a large detector at the formerly proposed Deep Underground Science and Engineering Laboratory (DUSEL) in Lead, S.D. (now SURF), and a high-intensity neutrino source at Fermilab.

On January 8, 2010, the Department of Energy (DOE) approved the Mission Need for a new long-baseline neutrino experiment that would enable this world-class program and firmly establish the U.S. as the leader in neutrino science. The LBNE Project is designed to meet this Mission Need.

With the facilities provided by the LBNE Project, the LBNE Science Collaboration proposes to mount a broad attack on the science of neutrinos with sensitivity to all known parameters in a single experiment. The focus of the program will be the explicit demonstration of leptonic CP violation, if it exists, by precisely measuring the asymmetric oscillations of muon-type neutrinos and antineutrinos into electron-type neutrinos and antineutrinos.

The experiment will result in precise measurements of key three-flavor neutrino-oscillation parameters over a very long baseline and a wide range of neutrino energies, in particular, the CP-violating phase in the three-flavor framework and the mass ordering of neutrinos. The unique features of the experiment – the long baseline, the broad-band beam, and the high resolution of the detector – will enable the search for new physics that manifests itself as deviations from the expected three-flavor neutrino-oscillation model. The scientific goals and capabilities of LBNE are outlined in Volume 1 of this CDR and the 2010 Interim Report of the Long-Baseline Neutrino Experiment Collaboration Physics Working Groups [4].

Siting the Far Detector deep underground, a scope opportunity that LBNE may seek to pursue in the future with non-DOE funding, would provide opportunities for research in additional areas of physics, such as nucleon decay and neutrino astrophysics, in particular, studies of neutrino bursts from supernovae occurring in our galaxy.

1.1.3   LBNE Project Organization

The LBNE Project Office at Fermilab is headed by the Project Director and assisted by the Project Manager, Project Scientist and Systems Engineer. Project Office support staff include a Project Controls Manager and supporting staff, a Financial Manager, an Environment, Safety and Health (ES&H) Manager, a Computing Coordinator, Quality Assurance, Procurement and Risk Managers, a documentation team and administrative support. The Project organization is shown in Figure 1–1.

The Beamline, Liquid Argon Far Detector and Conventional Facilities L2 Projects are managed by the Project Office at Fermilab, while the Near Detector Complex L2 Project is managed by a Project Office at Los Alamos National Laboratory (LANL).

More information on Project Organization can be found in Volume 1 of this CDR. A full description of LBNE Project management is contained in the LBNE Project Management Plan [5].

1.1.4   Principal Parameters of the LBNE Project

The principal parameters of the major Project elements are given in Table 1–1.
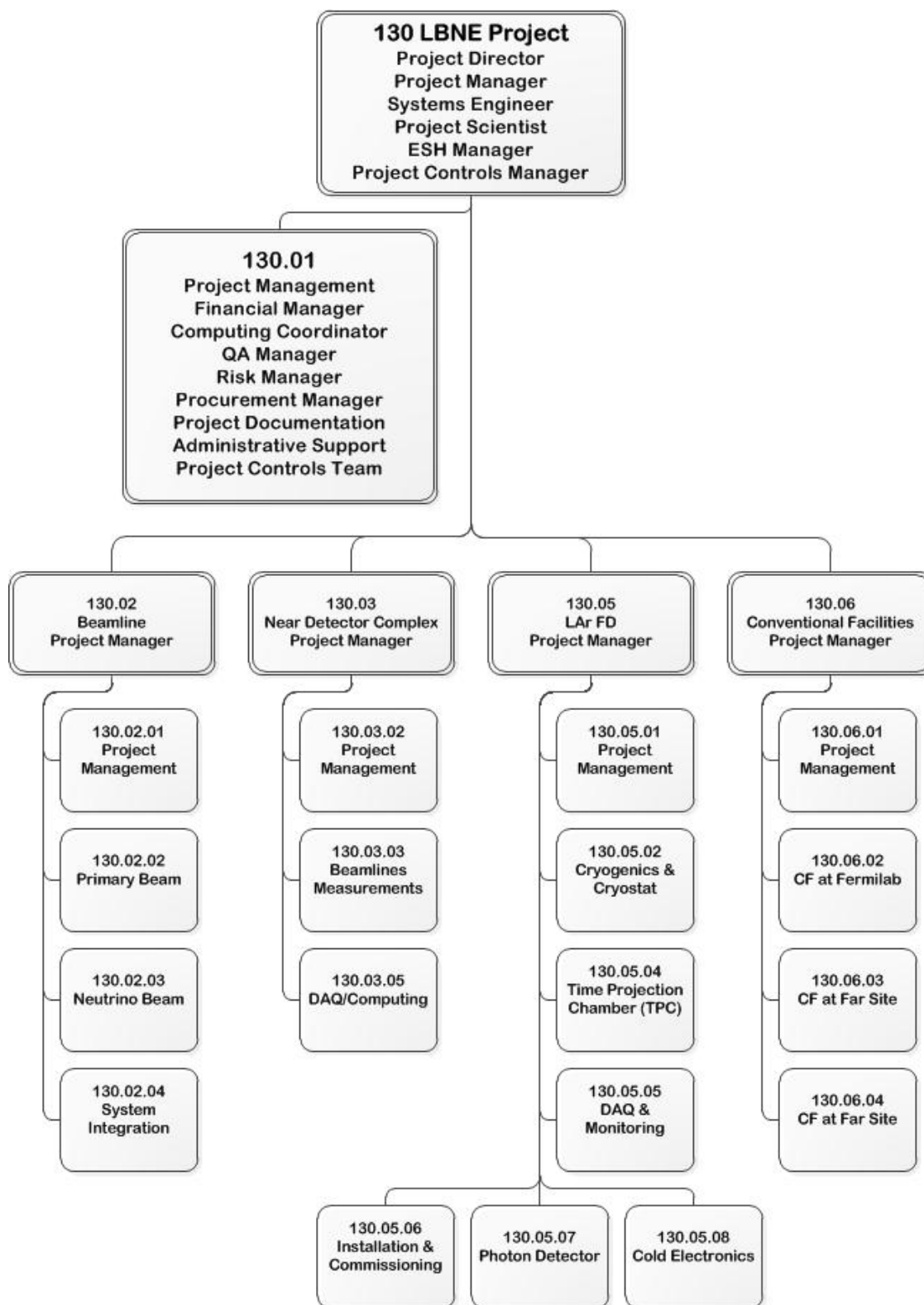
Figure 1–1: Organization chart for the LBNE Project (to WBS Level 3)

Table 1–1: LBNE Principal Parameters

Project Element Parameter	Value
Near- to Far-Site Baseline	1,300 km
Primary Proton Beam Power	708 kW, upgradable to 2.3 MW
Protons on Target per Year	6.5×10^{20}
Primary Beam Energy	60 – 120 GeV (tunable)
Neutrino Beam Type	Horn-focused with decay volume
Neutrino Beam Energy Range	0.5 – 5 GeV
Neutrino Beam Decay Pipe Diameter × Length	4 m × 203.7 m
Far Detector Type	LArTPC
Far Detector Active (Fiducial) Mass	13.5 (10) kton
Far Detector Depth	3 m overburden

1.1.5 Supporting Documents

A host of information related to the CDR is available in a set of supporting documents. Detailed information on risk analysis and mitigation, value engineering, ES&H, costing, project management and other topics not directly in the design scope can be found in these documents, listed in Table 1–2. Each document is numbered and stored in LBNE's document database, accessible via a username/password combination provided by the Project. Project documents stored in this database are made available to internal and external review committees through Web sites developed to support individual reviews.

Table 1–2: LBNE CD-1 Documents

Title	LBNE Doc Number(s)
Alternatives Analysis	4382
Case Study Report; Liquid Argon TPC Detector	3600
Configuration Management Plan	5452
DOE Acquisition Strategy for LBNE	5442
DOE Preliminary Project Execution Plan	5443
Integrated Environment, Safety and Health Management Plan	4514
LAr-FD Preliminary ODH Analysis	2478
LBNE Reconfiguration Final Report	Linked from LBNE web site (lbne.fnal.gov) under "Reports and Documents"
Global Science Objectives, Science Requirements and Traceback Reports	4772

Parameter Tables, Far Detector	3383
Preliminary Hazard Analysis Report	4513
Preliminary Security Vulnerability Assessment Report	4826
Procurement Plan	5329
Project Management Plan	2453
Project Organization Chart	5449
Quality Assurance Plan	2449
Report on the Depth Requirements for a Massive Detector at Homestake	0034
Requirements, Beamline	4835
Requirements, Far Detector	3747
Requirements, Far Site Conventional Facilities	4958
Requirements, Near Detectors	5579
Requirements, Near Site Conventional Facilities	5437
Risk Management Plan	5749
Value Engineering Report	3082
Work Breakdown Structure (WBS)	4219

1.2 Introduction to the Liquid Argon Far Detector

1.2.1 Overview

The Far Detector conceptual design for LBNE is a liquid argon time projection chamber (LArTPC). The basic components of this type of detector include a cryostat to contain the liquid argon (LAr), a TPC detection mechanism immersed in the LAr, readout electronics and a cryogenic system to keep the LAr temperature at 87 K and maintain the required purity.

The LBNE Far Detector LArTPC, referred to as the LAr-FD, consists of two large cryostats as shown in Figure 1–2, each of which holds a total of 9.4 kton of LAr. The active (instrumented) LAr mass of each is 6.7 kton and its fiducial mass, as defined for neutrino-oscillation studies, is 5 kton.

A uniform electric field is created within the LArTPC volume between cathode planes and anode wire planes. Charged particles passing through the TPC ionize electrons that drift to the anode wire planes. The bias voltage is set on the anode plane wires so that ionization
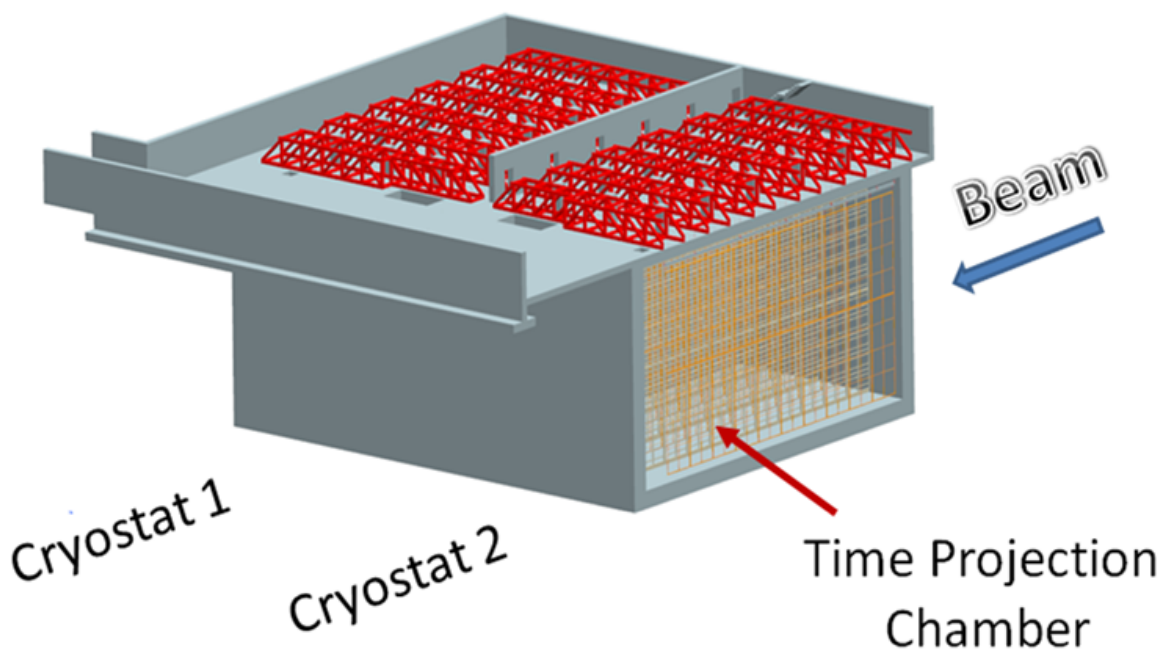
Figure 1–2: LAr-FD configuration. The beam enters from the east, placing Detector (cyrostat) 1 north of Detector 2.

electrons drift between the first several (induction) planes and are collected on the last (collection) plane. Readout electronics amplify and continuously digitize the induced waveforms on the sensing wires at 2 MHz, and transmit these data to the data acquisition (DAQ) system for processing. The wire planes are oriented at different angles allowing a 3D reconstruction of the particle trajectories. In addition to these basic components, a photon-detection system provides a trigger for galactic supernova neutrino interactions.

The design of the LAr-FD has been developed and refined over the past three years. The starting point was the ICARUS T600 system [6], and the process was informed and guided by the experience with small LArTPCs in the U.S., particularly ArgoNeuT [7] and the development of designs for MicroBooNE [8]. The LAr-FD concept is designed for assembly from small, independent elements that can be repeated almost indefinitely in any dimension to form the entire assembly within a large cryostat. Each of the standalone unit cells includes an independent mechanical structure to support the elements it contains. To a large extent, scaling from detector volumes containing anywhere from a few to several hundred such elements is straightforward with small and predictable risk.

The LAr-FD will require 3 m of 2.7 g/cm^3 shielding material on top of, and on the sides of, the detector to provide as much as 300 m of 20-degree low-angle cosmic-ray muon shielding. To accomplish this, the detector will be located in an excavated pit, nestled into a hillside. The facilities for housing the detector are described in Volume 6 of this CDR.

1.2.2 Location and Layout

The proposed location of the LAr-FD on the SURF site is shown in Figure 1–3.

Figure 1–4 zooms in to show the proposed orientation of the installation with respect to its surroundings, and Figure 1–5 zooms in further to show the proposed configuration of the detector and ancillary buildings. The building and related conventional facilities are described in Volume 6 of this CDR.

The LAr-FD Detector Hall will be erected above two side-by-side pits that will be excavated in the surface rock near the Oro Hondo fan site. The long axis of the detector modules will point towards Fermilab, parallel to and in line with the neutrino beamline. The below-grade rectangular pits inside of which the cryostats fit, will have dimensions of 18 m wide by 18 m high by 30 m long. The pits will be separated by a 3 m wide concrete septum. A roof support wall, constructed above the concrete septum, will be perforated with passageways to provide easy access and ventilation throughout the building. The configuration is illustrated in Figures 1–6 and 1–7. Primary egress will be through the truck entrances and stairways. Secondary egress will be provided by a personnel passageway at the near (east) end of the building.

Minimal head-height is required above the cryostats except at a high bay at the far (west) end where TPC components will be rigged into place through the 2-m $\times$ 4-m hatches in each cryostat. A 15-ton crane will be provided in the high bay. Two truck entrances will be provided at each end of the high bay to facilitate parallel construction and installation in the cryostats.

The nitrogen refrigerator and cryogenic storage tanks will be located outside. Cryogenic supply and return lines will be routed through one of the truck entrances or through a dedicated pipe chase.

1.2.3 Cryostat Construction

The cryostat construction uses commercial stainless-steel membrane technology engineered and produced by industry. These vessels are widely deployed in liquefied natural gas (LNG) tanker ships and tanks, and are typically manufactured in sizes much larger than that of the LAr-FD. This is an inherently clean technology, in that the primary membrane panels are constructed of polished SS, with passive insulation.

The LAr-FD cryostat reference design was selected on the recommendation of the experienced engineering consultants from ARUP USA, Inc. [9] after consideration of an alternative design that uses segmented, internally self-supporting, evacuable, modular cryostats. Evacuation, in particular, appears not to be necessary; in September 2011, the Fermilab Liquid Argon Purity
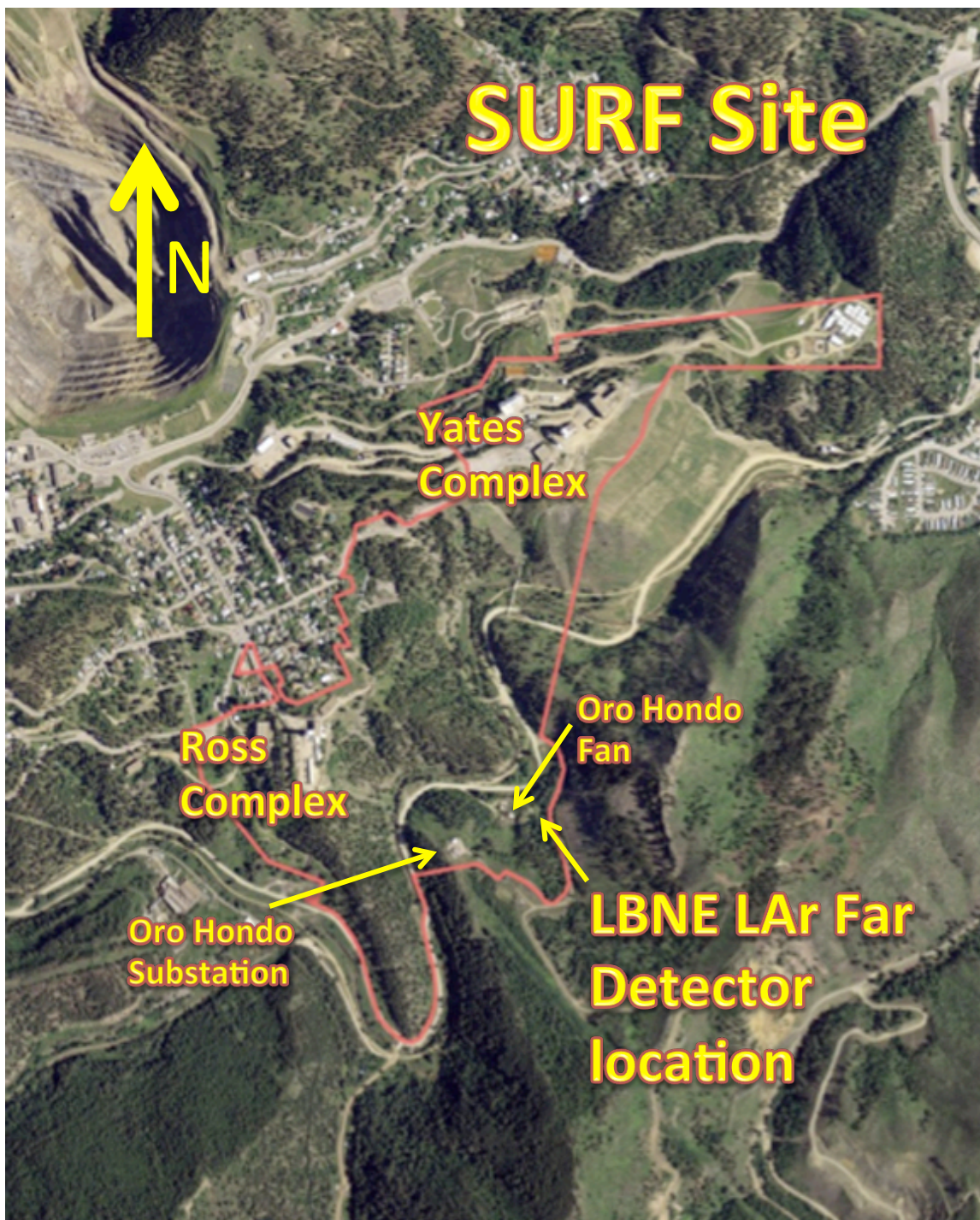
Figure 1–3: Location of LAr-FD on the SURF site in Lead, SD.
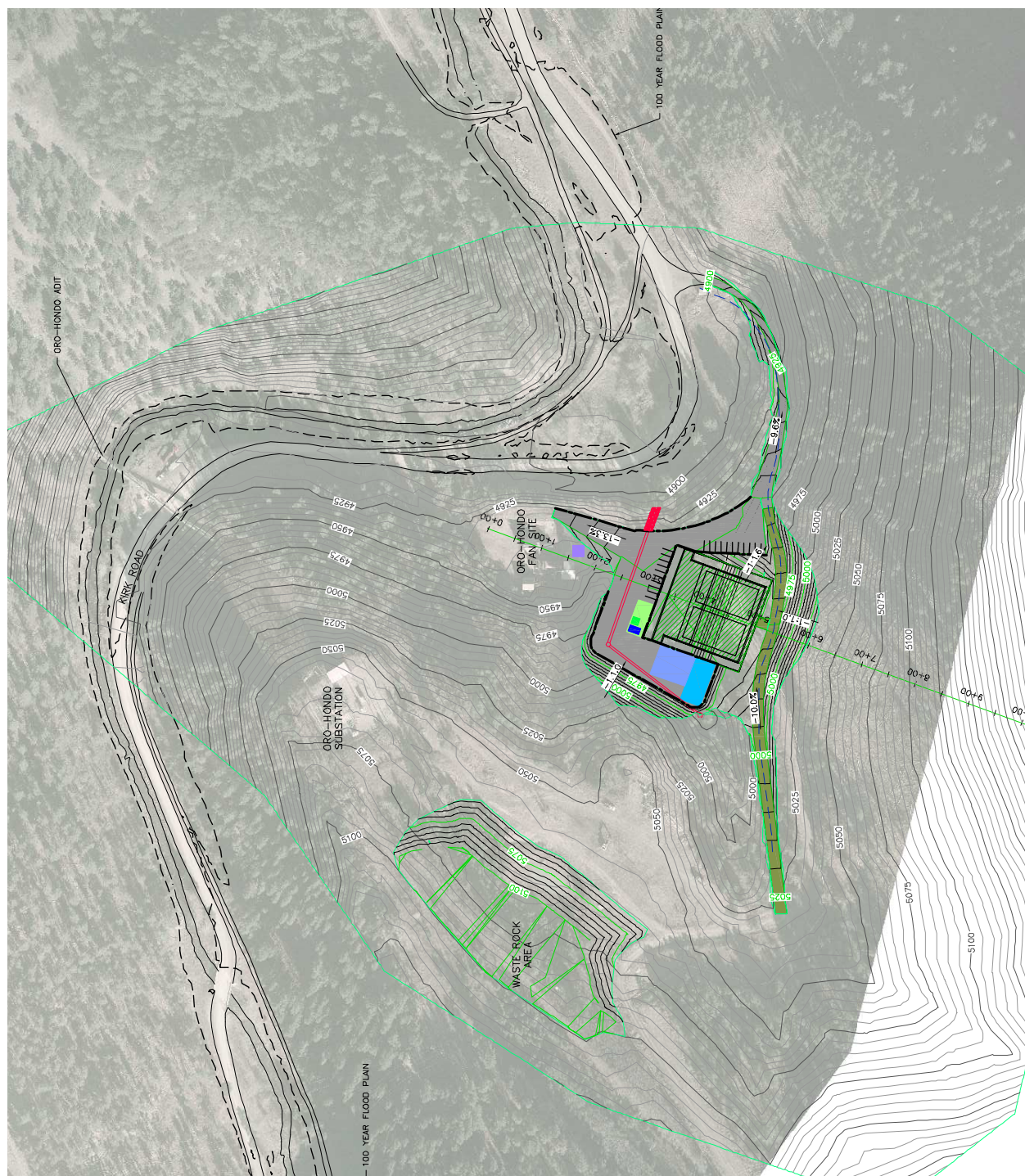
Figure 1–4: LAr-FD configuration with respect to the site (North points up)
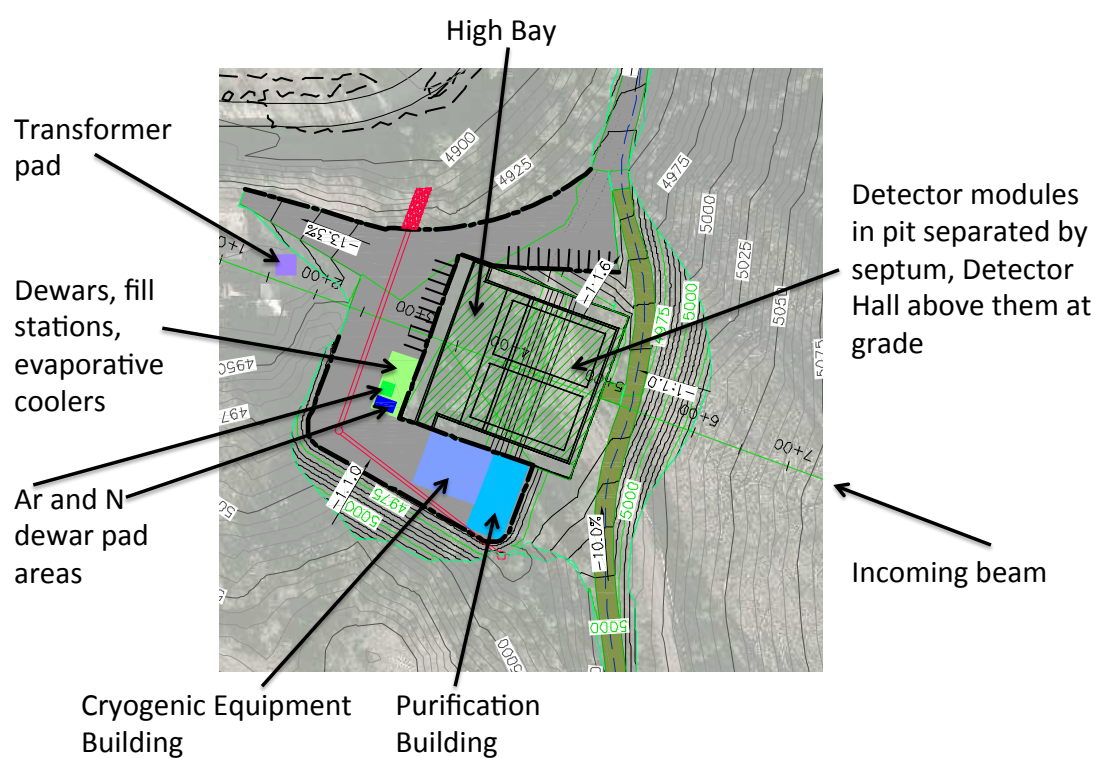
Figure 1–5: LAr-FD configuration and ancillary buildings (North points up)
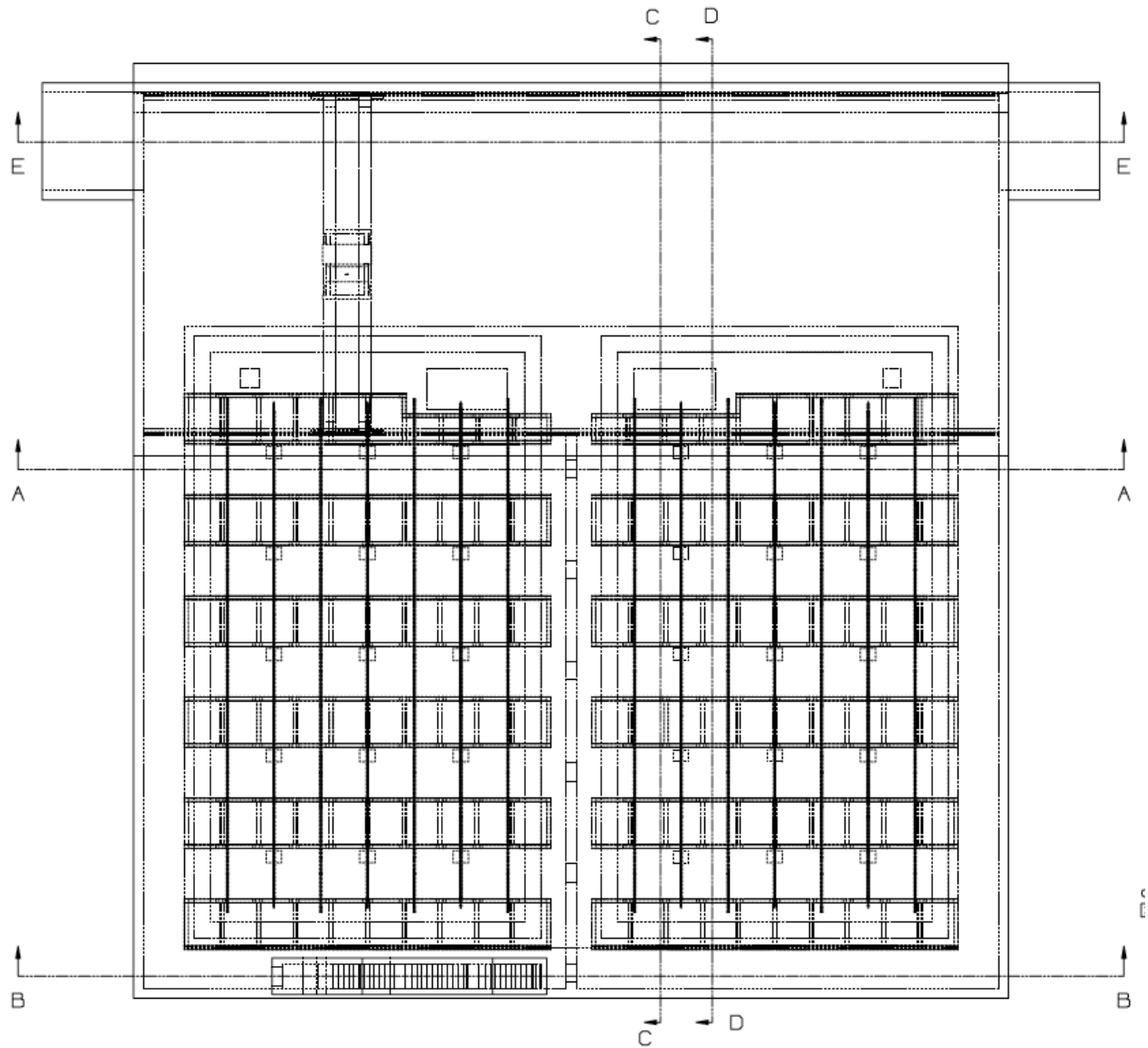
Figure 1–6: Plan view of two-cryostat detector showing trusswork on top of detector; beam enters at bottom of illustration; high bay is from the A-A line upwards.
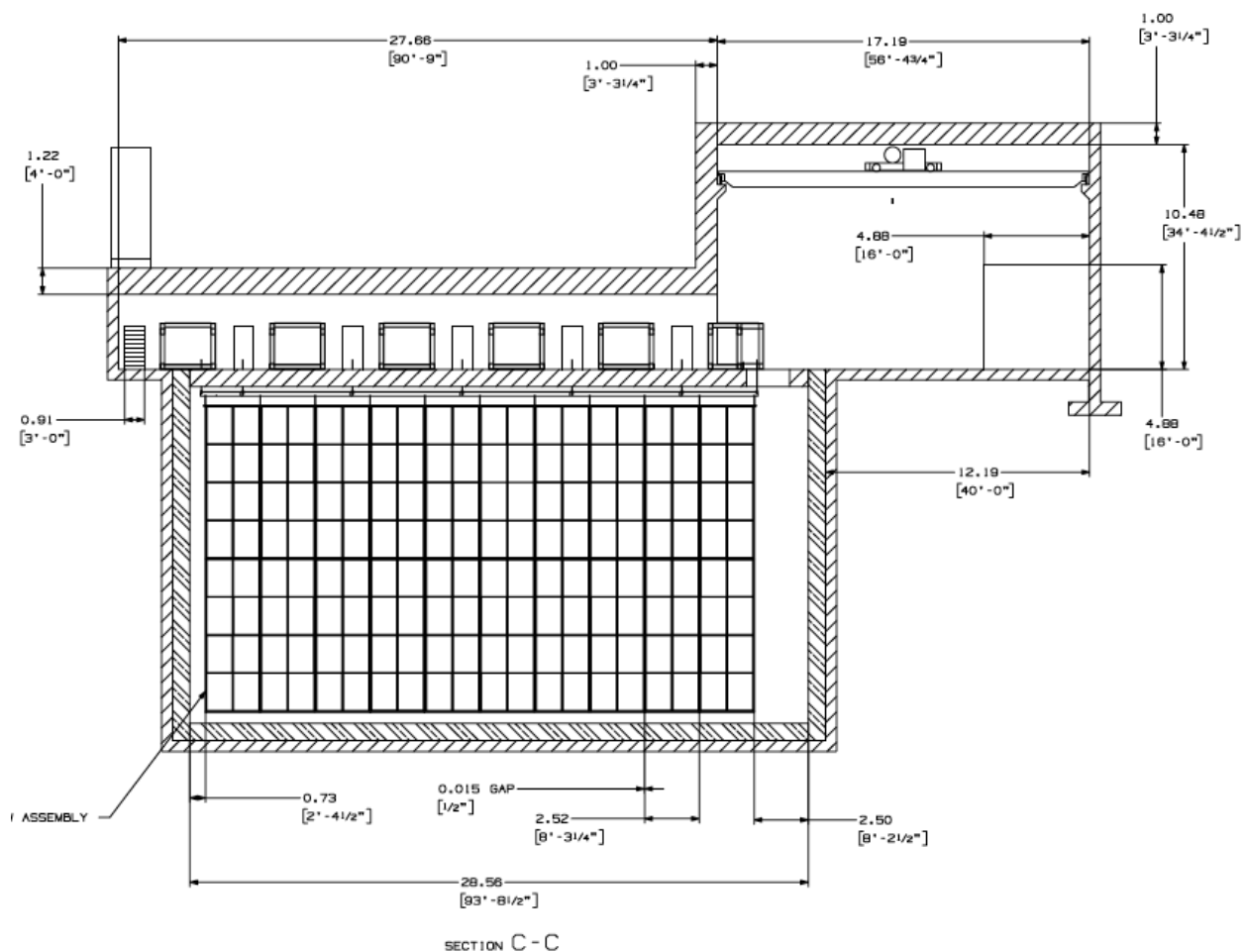
Figure 1–7: Vertical slice of detector (e.g., the cross section C-C in Figure 1–6), viewed from the right-hand side of that figure. Detector elements are shown in the cryostat, trusswork is above in the Detector Hall, and the high bay is to the right.

Demonstrator (LAPD) achieved purity levels of less than 100 ppt oxygen-equivalent, using the method that is planned for use in the LAr-FD (the method is described in Section 8.3.3). This confirms that the method works, obviating the risk to LBNE that an evacuable vessel will be required. Operation of a 35-ton prototype using membrane-cryostat technology will provide a further demonstration.

The LAr-FD membrane cryostats are hermetically sealed containers supported by the surrounding rock. This "in-ground" configuration offers access only from the top and protects against possible cryogen leaks out of the tank. The side walls consist of a series of membranes, foam insulation and reinforced concrete poured against the shotcrete covered rock. The inner (primary) membrane liner, made of stainless steel, is corrugated to provide strain relief from temperature-related expansion and contraction. The basic components of the membrane tank are illustrated in Figure 1–8.
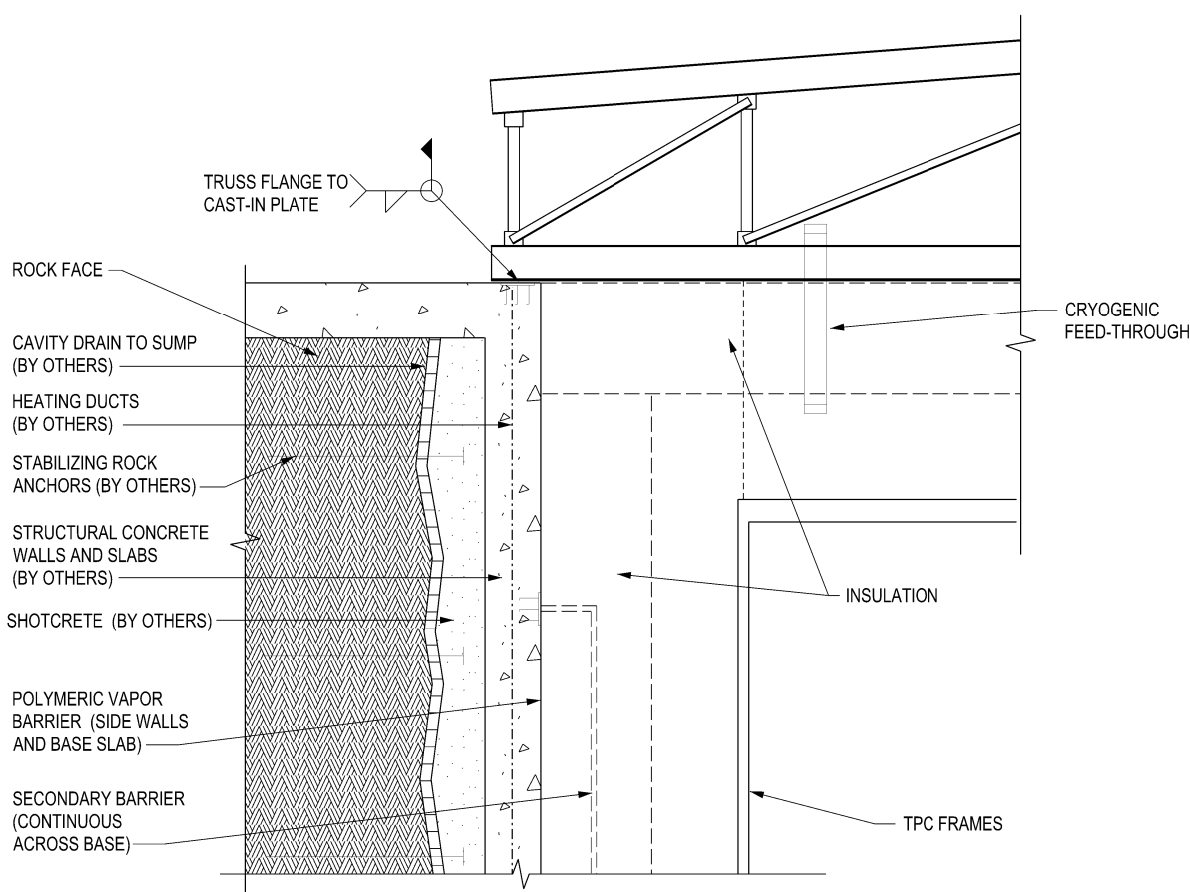
Figure 1–8: Composite system as installed for the LAr-FD reference design

1.2.4   Cryogenic Systems

The LAr must be initially transferred to the cryostats and must be kept cold, pure and circulating smoothly during operations in order to maintain a sufficiently long drift lifetime for the ionization electrons. The major cryogenic systems used to perform these functions include the cryogen supply for cool-down and fill, gas filtration, argon condensing, liquid filtration and circulation and argon purity analysis.

The overall cryogenic system layout and location is intended to optimize safety and efficiency. It is designed to minimize:

- the risk of personnel injury to any Oxygen Deficiency Hazard (ODH)

- heat ingress to the cryogenic system

- the volume of the argon system external to the cryostat and hence the potential for argon escape or contamination

- and to provide safe access to refrigeration equipment that requires periodic maintenance

The re-condensers and purifiers will be located in the Cryogenic Equipment Building. A 50-m^3 LAr receiving dewar and a 50-m^3 LN dewar will be located on an adjacent pad. Three liquid nitrogen (LN) refrigerators (two operating and one spare) will provide a cooling capacity of 165 kW.

The required flow rate of liquid argon to be sent for purification is expected to decrease over time as impurities are slowly removed from the system . The initial maximum flow rate will be 51 m^3/hr (224 gpm) from each cryostat, resulting in a complete volume turnover every five days. Longer term, the rate will decrease to 25 m^3/hr with a turnover time of 10 days. As point of comparison, ICARUS T600 has a maximum turnover rate of eight to ten days.

1.2.5   LAr Purification

The purification of LAr is accomplished with standard industrial equipment, using molecular sieves and chemically reducing materials, which is scalable within the contemplated range to accommodate the estimated irreducible material-outgassing from warm materials in the ullage (the vapor space above the liquid argon).

1.2.6   Time Projection Chamber

The Time Projection Chamber (TPC) is the active detection element of the LAr-FD. The construction concept is shown schematically in Figure 1–9. The TPC is located inside the cryostat vessel and is completely submerged in LAr at 87 K. Its active volume is 14 m high, 14 m wide and 25 m long in the beam direction. It has four rows of Cathode Plane Assemblies (CPA) planes interleaved with three rows of Anode Plane Assemblies (APA) planes that are oriented vertically, parallel to the beamline, with the electric field applied perpendicular to the planes. The maximum electron-drift distance between a cathode and an adjacent anode is 2.3 m. Both the cathode and anode plane assemblies are 2.5 m wide and 7 m high. Two 7-m modules (either APA or CPA) stack vertically to instrument the 14-m active depth. In each row, 10 such stacks are placed edge-to-edge along the beam direction, forming the 25-m active length of the detector. Each cryostat houses a total of 60 APAs and 80 CPAs. A "field cage" surrounds the top and ends of the detector to ensure uniformity of the electric field. The field cage is assembled from panels of FR-4 sheets with parallel copper strips connected to resistive divider networks.

Each APA has three wire planes that are connected to readout electronics; two induction planes (labeled U and V in Figure 1–9) and one collection plane (X). A fourth wire plane, grid plane (G), is held at a bias voltage but is not instrumented with readout electronics. The grid plane improves the signal-to-noise ratio on the U plane and provides electrostatic discharge protection for the readout electronics.

1.2.7   Electronics, Readout and Data Acquisition

Requirements for low noise and for extreme purity of the LAr motivate locating the front-end electronics in the LAr (hence "cold electronics"). By placing the electronics close to the anode wires the capacitance is minimized thereby minimizing the electronic noise. In-cryostat electronics also has the advantage of reducing the number of cables and feedthroughs needed, thereby reducing the resulting Ar contamination. The use of CMOS electronics in this application is particularly attractive since the series noise of this process has a noise minimum at 87 K. The large number of readout channels required to instrument the LAr-FD TPCs motivates the use of CMOS ASICs. Signal zero-suppression and multiplexing will be implemented in the ASIC, minimizing the number of cables and feedthroughs in the ullage gas, and therefore reducing contamination from cable outgassing. Figure 1–10 shows the conceptual architecture of a front-end electronics design that meets the requirements for LAr-FD. The entire electronics chain is immersed in the LAr.

All signal feedthroughs will be placed at the top of the cryostat, where they are easily installed, are always accessible, are at low hydrostatic pressure and pose no risk of LAr leakage. The cold electronic system will include digitization, buffering, and some level of digital output multiplexing. Output data links will include redundancy to eliminate the

two sets of
G,U,V,X wire planes

cold electronics boards

detail cross section of the
electronics enclosures

concept of the APAs, and
wire wrapping arrangement

installation of APAs inside the crypstat

Cryostat access
hatch,
plugged when
cryostat is filled

Wire and Cathode
frames are transported
in halves which are
joined in cryostat

Cathode Plane Assemblies   Anode Plane Assemblies

Field Cage

Foam Insulation

Concrete Liner

cross section view of the TPC componets inside the cryostat

Figure 1–9: TPC modular construction concept

effect of any single-point failure.
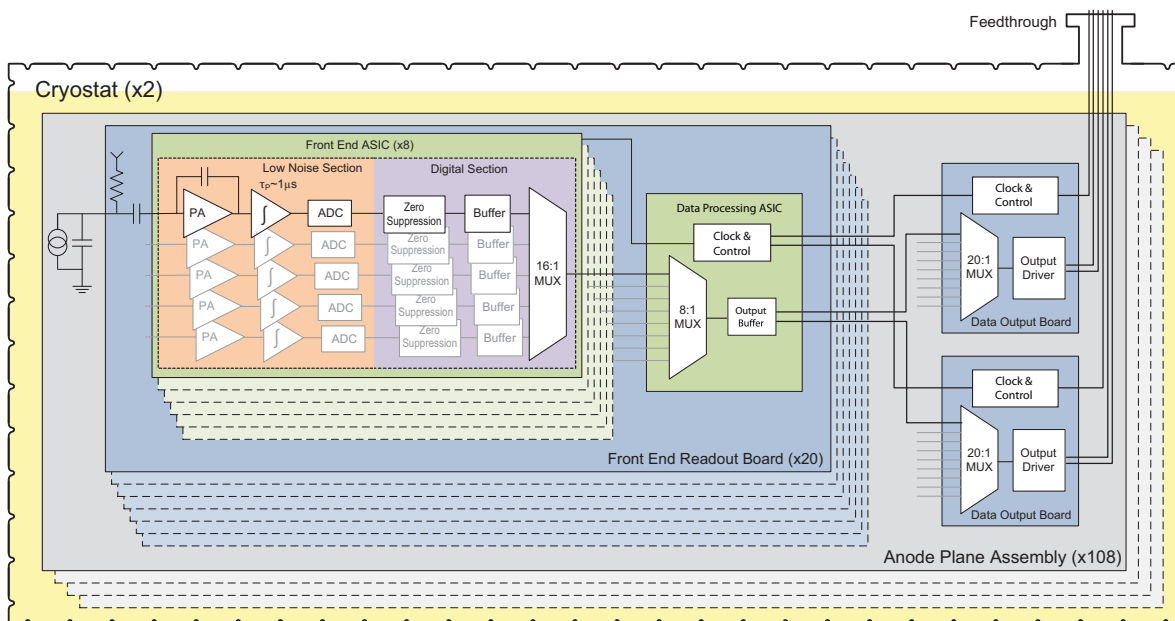
Figure 1–10: Conceptual front-end electronics architecture

1.2.8   Photon-Detection System

Identification of the different possible charged-particle types depends on accurate measurements of ionization along tracks. This requires accurate determination of the time of interaction, or event time, t_e, which leads to the absolute location of the event along the drift axis, and allows the determination of Q_0, the true ionization charge.

For non-accelerator physics events, t_e is not known a priori. However, LAr is an excellent scintillator, generating of order 10^4 128-nm photons per MeV of deposited energy. Detection of scintillation photons provides a prompt signal that allows unambiguous location of particle positions along the drift axis.

Photon detection is also important for mitigating the effects of the significant cosmic ray backgrounds expected for a surface detector.

The photon-detection system consists of acrylic light-guides that lead to small photomultiplier tubes (PMTs), as shown in Figure 1–11. Approximately 5% of the converted photons incident on a light guide are captured within it and travel to the PMT. A wavelength-shifting coating on the light guides efficiently converts the scintillation photon wavelength from 128 nm to 428 nm where the PMT is most sensitive. The fast PMT signals will be

routed out of the cryostat to standard readout electronics.
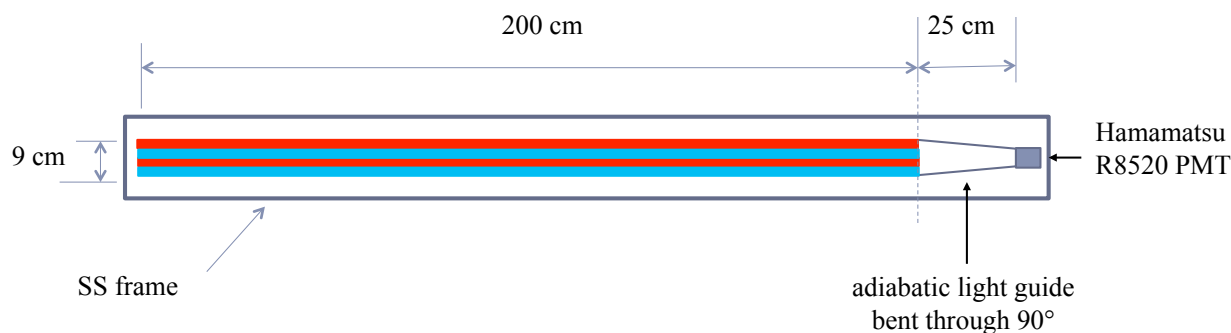
Figure 1–11: Light Guide Paddle: four adiabatic light guides bent onto a single R8520-MOD PMT.

Ten light-guide and PMT assemblies, or "paddles", will be installed within each APA frame prior to wire winding. The PMT signals will be used as a software "trigger" in the DAQ to define the event time, t_e, for non-accelerator events. This system provides a t_e signal throughout the entire detector in contrast to a system similar to that used in MicroBooNE and ICARUS, where light detection elements are restricted to locations outside the detector volume.

1.2.9   Detector Installation and Operation

Detector components will be shipped in sealed containers to the Far Site by truck and delivered to the building. The containers will be moved to a clean area over the hatches where components will be lowered through the access hatch into each cryostat.

The construction of the two cryostats and the installation and commissioning activities will be staged such that both TPCs can be tested cold while one cryostat still remains available as a potential LAr storage vessel. The LAr in one cryostat can be transferred to the other, and back again, if necessary, until all the tests complete successfully. Once both TPCs are known to work properly at LAr temperature, the second fill will take place.

To protect the membrane on the floor of the cryostat during TPC installation, a temporary floor will be installed. After each pair of APAs is installed, they will be connected to the DAQ system and the wire integrity tested. All wires on previously installed APA pairs will also be tested. The wire integrity test will be performed during cryostat cool-down as well. A relatively slow cool-down rate will ensure that the temperature-induced stresses in the APA frames and wires are kept well below the level experienced during testing.

An installation and integration detector mock-up will be constructed at Fermilab to confirm that interfaces between detector systems are well defined and to refine the installation

procedures.

1.3   Principal Parameters

The principal parameters of the LAr-FD are given in Table 1–3.

Table 1–3: LAr-FD Principal Parameters

Parameter	Value
Total Active (Fiducial) Mass	13.5 (10) kton
Number of Detector Modules (Cryostats)	2
Drift Cell Configuration within Module	3 wide × 2 high × 10 long drift cells
Drift Cell Dimensions	2 × 2.3 m wide (drift) × 7 m high × 2.5 m long
Detector Module Dimensions	13.9 m wide × 14 m high × 25.3 m long
Anode Wire Spacing	∼5 mm
Wire Planes (Orientation from vertical)	Grid (0°), Induction 1 (45°), Induction 2 (-45°), Collection (0°)
Drift Electric Field	500 V/cm
Maximum Drift Time	1.4 ms

1.3.1   Design Considerations

TPCs operated to date have been constructed with an anode wire spacing in the range of 3 mm (ICARUS) to 4.8 mm (Fermilab cosmic-ray stand). The amount of ionization charge collected on the wires increases with larger wire spacing, resulting in a better signal-to-noise ratio without serious consequences (the radiation length of LAr is ~ 30 times larger than the typical wire spacing). The electron-π^0 separation efficiency of a TPC with 5-mm wire spacing is only a few percent lower than one with 3-mm wire spacing. It is also clear that a TPC with larger wire spacing requires fewer wires and readout channels, resulting in lower cost.

Only two wire planes are required to reconstruct events in three dimensions, however three wire planes will be used to provide N+1 redundancy. The third will improve the pattern-recognition efficiency for a subset of multi-track events in which trajectories can overlap in two views. The collection-plane wires are most commonly used for calorimetric reconstruction and are oriented vertically (0°) to minimize both the wire length and the electronics noise.

A study of wire orientation has shown that for a TPC with three instrumented wire planes, the optimum orientation of the induction plane wires should be between $\pm 40°$ and $\pm 60°$ when the collection plane wires are at $0°$ [10]. The ideal orientation for the more isotropic low-energy events, e.g., supernova-neutrino interactions, is $\pm 60°$. The selected induction-plane wire orientation of $\pm 45°$ has better position resolution in the vertical direction than $\pm 30°$ and has shorter wires compared to a wire orientation of $\pm 60°$. The induction plane wires are wrapped around the APA frames so that the readout electronics can be located on the top or bottom of the TPC. As a result, it is natural to arrange the APAs vertically in a two-high confugration.

Access to the top of the cryostat is required to install and connect cabling. Therefore, risk of personnel injury and detector damage, both of which increase with height, along with optimal cryostat shape form the primary considerations for the detector height, 14 m. The height of the APA has been chosen, accordingly, to be 7 m, resulting in 7-m-long collection-plane wires and 10-m-long induction plane wires.

The 2.5 m width of the APA was chosen to facilitate construction and to allow standard, over-the-road transport.

The choice of cryostat width is based on the desired cryostat shape and building roof span. From a cryogenics standpoint, the ideal cryostat for a modular TPC would be a cube since membrane-cryostat capital and operating costs scale linearly with the surface area. Due to the resulting detector height, a cube shape is not ideal for building construction however for cryostats of this size.

A drift field of 500 V/cm was chosen based on experience from similar detectors such as ICARUS, ArgoNeuT and the Fermilab cosmic-ray test stand. At this electric field, $\sim 30\%$ of the ionization electrons produced by the passage of a minimum ionizing particle (MIP) recombine and create scintillation light that provides a fast trigger. The remaining ionization electrons drift to the APA and produce wire-plane signals. The TPC could function at higher or lower drift fields but the relative yields of scintillation light and ionization electrons would change. The use of a higher drift field would require more care in the design of the high-voltage systems. The electron drift velocity is 1.6 mm/μs at 500 V/cm. For a maximum drift distance of 2.3 m and a drift field of 500 V/cm, the required voltage on the cathode plane is 114 kV. This is within the range of commercially available high-voltage cables and within the range of current designs for cryogenic feedthroughs.

The maximum drift cell length of 2.3 m was chosen based on experience from other detectors and on the need to mitigate the effects of space charge due to the high flux of cosmic rays. The required minimum signal-to-noise ratio of 10:1 ensures that the tracking efficiency will be 100% throughout the entire drift cell. The TPC must be capable of detecting the smallest signal (1 MeV) produced in interactions that LBNE will study. This situation occurs when a MIP travels parallel to a wire plane and perpendicular to the orientation of the wires in the plane. A MIP loses 2.1 MeV of energy in each cm of travel, producing $\sim$ 40,000

ionization electrons along every 5 mm section of the track. About 28,000 electrons escape recombination and, ignoring the effects of LAr purity and diffusion, would all drift to one collection plane wire. The capacitance due to the maximum-length 10-m wire is 226 pF resulting in an equivalent noise charge (ENC) of 530 electrons in the CMOS amplifiers. The signal-to-noise ratio would therefore be 53:1 if all of the ionization electrons arrived at the wire.

Ionization electrons will be lost due to impurities in the LAr. The fraction that survive passage to the anode planes is $e^{-t/\tau}$, where t is the drift time and τ is the drift-electron lifetime. The maximum drift time is the maximum drift length divided by 1.6 mm/μs which equals 1.4 ms for LBNE. The ICARUS detector has achieved a drift electron lifetime of 6 – 7 ms. The Materials Test Stand (described in Section 8.3.1) regularly achieves a drift-electron lifetime of 8 – 10 ms. The Fermilab Liquid Argon Purity Demonstrator achieved a liftime of > 3 ms during initial tests. Based on this experience, and by careful selection of materials in the ullage, a drift-electron lifetime at least as good as ICARUS is expected. The signal-to-noise ratio would be 36:1 for a drift electron lifetime of 6 ms. A minimum lifetime of 0.9 ms is required to meet the 10:1 signal-to-noise ratio requirement.

The cloud of drifting ionization electrons will spread out in space due to the effects of diffusion. The maximum transverse RMS width of the electron cloud is 2 mm for the chosen drift distance and drift field, well matched to both the chosen wire spacing and electronics sampling rate.

1.4   Detector Development Program

The feasibility of the LAr-FD as a detector has been demonstrated by a series of tests, prototypes and smaller experiments, and most impressively by the current state of the ICARUS experiment currently taking data at Gran Sasso. Many of the development activities related to drift lifetime, cold electronics, mechanical design, analysis tools and cryostat construction in the U.S. are described in the *Integrated Plan for LArTPC Neutrino Detectors in the US* [11]. This program includes non-LBNE activities such as the Fermilab Materials Test Stand, Fermilab electronics test stand, LAPD, photon detection, ArgoNeuT and Mi-croBooNE as well as LBNE activities such as the 35-ton prototype. The development plan is described in detail in Chapter 8.

1.5   Participants and Organization

The design for the LBNE Far Detector is being carried out by an LBNE L2 project team, headed at Fermilab but with participants also from Brookhaven National Laboratory, participating LBNE institutions and has included an engineering design firm, Arup USA, Inc.,
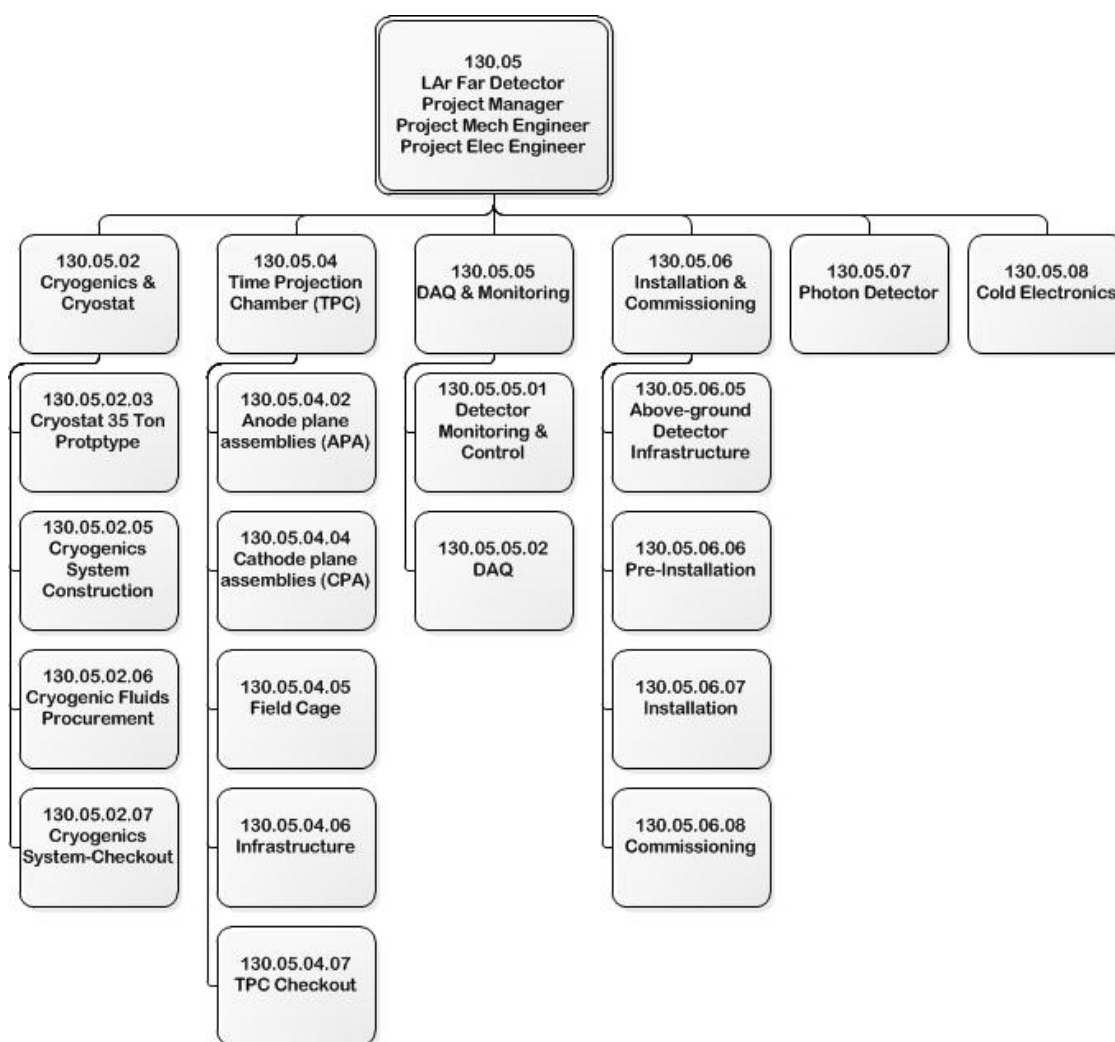
Figure 1–12: Organization chart for the Far Detector L2 Project (to WBS Level 4)

to assist with cryostat and cryogenic-plant design. This firm also provided valuable cost-estimating expertise.The South Dakota Science and Technology Authority (SDSTA) owns and manages the SURF site, which is the location planned for detector construction.

The LBNE Far Detector development effort is managed by the Work Breakdown Structure (WBS) Level 2 Manager for the Far Detector L2 Project. The supporting team includes a WBS Level 3 Manager for each of its component systems: Cryogenics & Cryostat, Time Projection Chamber (TPC) and Electronics, Data Acquisition (DAQ), Installation & Commissioning and Photon Detector. Figure 1–12 shows an organization chart down to Level 4 (L4).

The Conventional Facilities Level 3 Far Site Manager is the LBNE Project liaison with the LAr-FD L2 Project to ensure the detector requirements are met; this person is responsible

for all LBNE scope at the Far Site. Management of SURF and the organizational relationship between it and the LBNE Project and Fermilab are described in the SDSTA-Fermilab-LBNL Memorandum of Understanding (MOU) [12] and the LBNE Project Management Plan [5].

2 Cryogenics System and Cryostat (WBS 130.05.02)

The scope of the Cryostat and Cryogenics subsystem includes the design, procurement, fabrication, testing, delivery and installation oversight of (a) a cryostat to contain the liquid argon (LAr) and the TPC, and (b) a comprehensive cryogenics system that meet the required performance for acquiring, maintaining and purifying the LAr in the detector. This chapter describes a reference design for these interdependent detector elements.

The scope of the reference-design membrane cryostat encompasses the following components:

- Two 5-kton (fiducial mass) cryostats for a LAr-FD

- LAr tanker truck receiving facilities

- Transfer system to deliver LAr to the detector cryostats

- Boil-off gas reliquefaction equipment

- LAr-purification facilities

- Cryostat-purge facilities

- LAr transfer equipment

2.1 Introduction

The conceptual reference design for the LAr-FD specifies two rectangular vessels each measuring 15.6 m in width, 16.0 m in height and 28.6 m in length, and containing a total mass of 9.4 kton of LAr, as illustrated in Figure 1–2.

2.1.1 Cryostat Design

A membrane cryostat design commonly used for liquid natural gas (LNG) storage and transport tanker ships (Figure 2–1) will be used. A membrane vessel uses a stainless-steel liner to contain the liquid cryogen. The pressure loading of the liquid cryogen is transmitted through rigid foam insulation to the surrounding rock, which provides external support for the liner. The membrane liner is corrugated to provide strain relief resulting from temperature-related expansion and contraction (Figure 2–2).
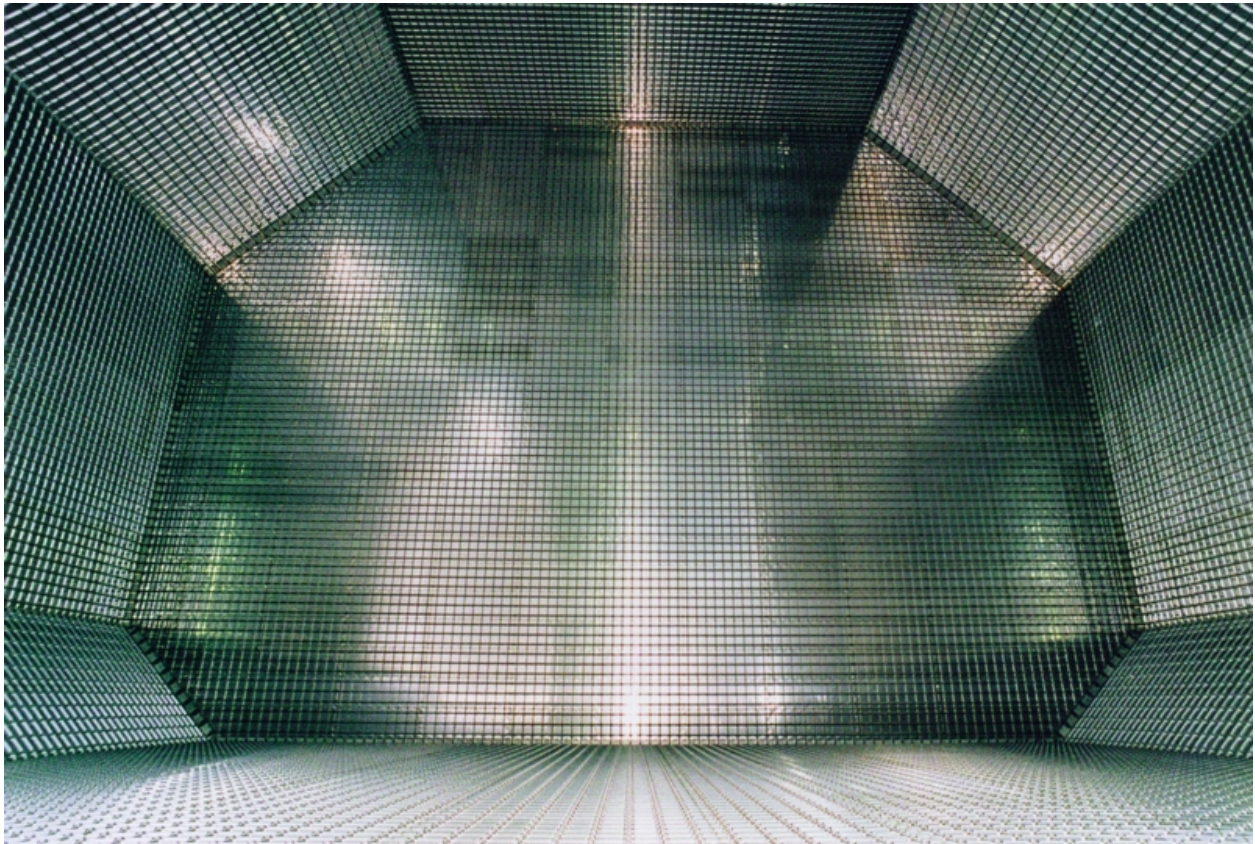
Figure 2–1: Interior of a LNG ship tanker. The tank shown is 24 m high by 35 m wide with interior grid-like corrugations on a 0.34-m pitch. By comparison, a single LAr-FD cryostat is 16 m high by 15.6 m wide.

The advantages offered by the membrane design relative to a self-supporting cryostat are:

- Efficient use of the excavated volume due to the cryostat's direct attachment to the rock on floor and sides, which reduces the civil construction costs for the project

- Higher ratio of usable (fiducial) mass to total mass

During the conceptual design studies two membrane cryostat vendors have been identified.

Figure 2–2: Primary membrane section (courtesy GTT)

Those vendors are GTT (Gaztransport & Technigaz) and IHI (Ishikawajima-Harima Heavy Industries). Each is technically capable of delivering a membrane cryostat that meets the design requirements for the LAr-FD. To provide clarity, only one vendor is represented in this CDR (GST system from GTT); this is for informational purposes only and should not be construed as preferring GTT over IHI. Nothing inherent in the IHI design changes the design approach.

2.1.2 Cryogenic Systems Design

The cryogenic systems and their layout is shown in Figure 2–3, and described in Sections 2.3 through 2.7. Conceptual design studies and studies done by ARUP, USA [9] indicate that the implementation strategy for the cryogenics system is independent of the cryostat design.

2.1.3 Design Parameters

The requirements and parameters for the cryostat and cryogenic system design are within the LAr-FD requirements documentation [13] [14] and the parameter tables [15], respectively. The overarching system requirements are to provide a high-purity, stable liquid argon environment for the TPC and to provide mechanical support for the TPC. For components that pass through the ullage (the vapor space above the LAr), no sources of reliquefaction may be present. Tables 2–1 and 2–2 offer a brief overview of parameters for a single cryostat of LAr-FD.
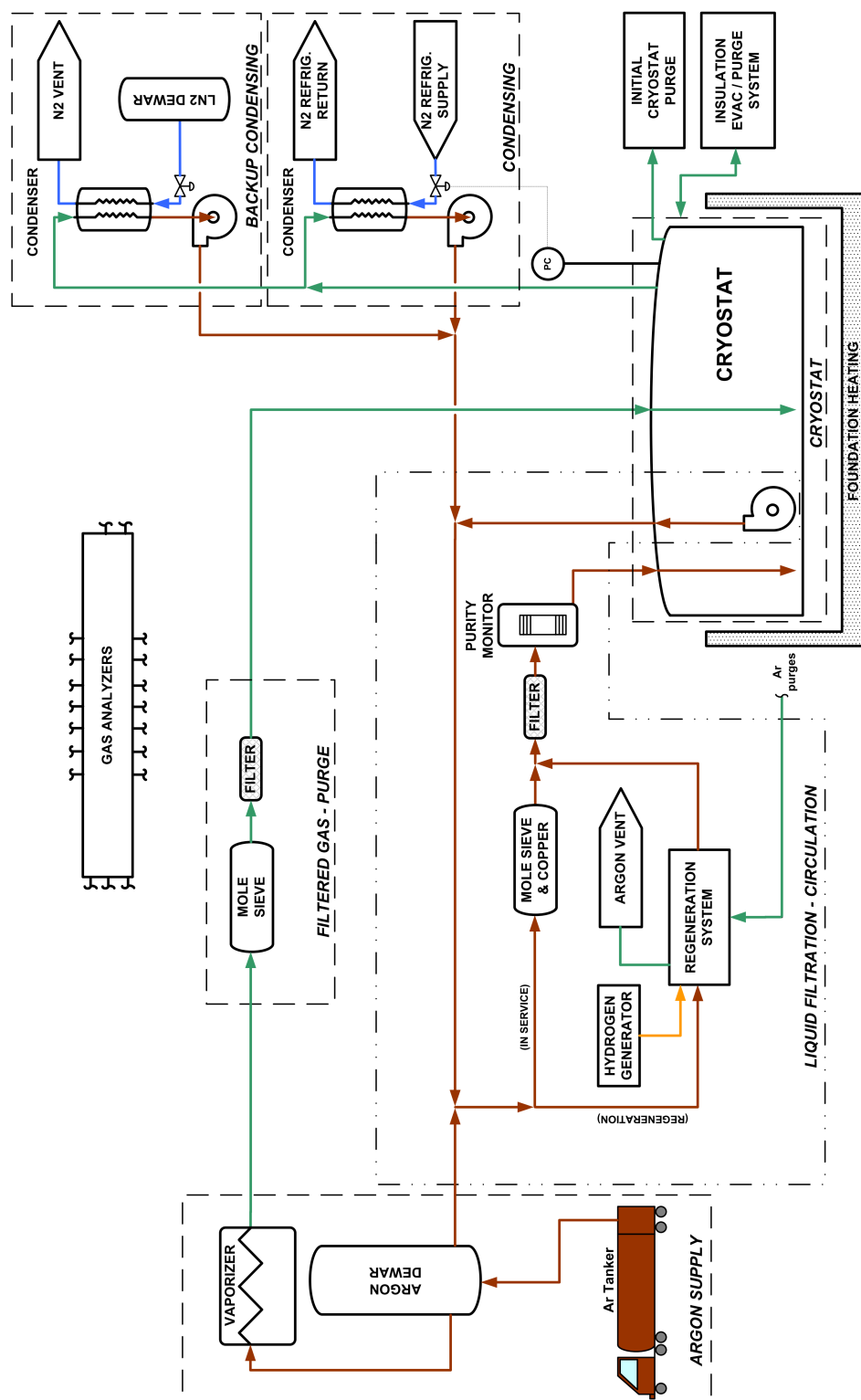
Figure 2–3: Process flow diagram of cryogenic system; only critical controls are shown

Table 2–1: Design parameters for one LAr-FD Cryostat

Parameter	Value
Total Cryostat Volume:	7,100 m^3
Total LAr Volume:	6,700 m^3
LAr Total Mass:	9.4 kton
Inner Height of the Tank:	16.0 m
Inner Width of the Tank:	15.6 m
Inner Length of the Tank:	28.6 m
Insulation:	Reinforced Polyurethane; inner layer is 40 cm thick, outer layer is 40 cm thick
Primary Membrane(GTT):	1.2-mm thick type 304L stainless steel with corrugations on 340 mm × 503 mm rectangular pitch
Secondary Containment(GTT):	≈ 0.07-mm thick aluminum between fiberglass cloth; overall thickness is 0.8 mm located between insulation layers
Outer Concrete Layer:	0.5 m thick, inner surface treated with a vapor barrier
LAr Temperature:	87 ± 1 K at 130 mbarg
Depth of the Liquid (Liquid Head):	15.0 m
Design Operating Pressure (Above Liquid):	130 mbarg
Design Operating Pressure (Bottom of Liquid):	2186 mbarg
Rated Pressure Capacity of Tank:	0.52 MPa abs

Table 2–2: Summary of parameters for the membrane cryostat

Property	Reference-Design Cryostat
Type of crane	15 ton bridge crane
Base slab	Reinforced concrete
Side walls	Reinforced concrete
Concrete heating system	Redundant / Replaceable Electric system
Roof	Pre-fabricated steel truss modules with lower steel plate
Vapor barrier	Polymeric on concrete surfaces / steel plate on roof
Insulation / Secondary barrier / Membrane	GST system by GTT
TPC	Individual 2.5 x 7m frames lowered through 2m x 4m roof hatch. Assembled within cryostat and suspended by hangers passing through the roof.
LAr containment system	Full containment: Membrane / Secondary Barrier / Concrete Liner

2.2   Cryostat Configuration

This section describes the configuration of the cryostat tanks only. The rails for TPC support and transfer, the installation of which is the responsibility of this WBS element, are described as part of the detector pre-installation activities in Section 7.3.1.

2.2.1   Sides and Bottom of Tank

The membrane tank walls consist of several layers. The layers are, in order from inside to outside, stainless-steel primary membrane, insulation, thin aluminum secondary membrane, more insulation, polymeric vapor barrier, concrete, shotcrete and rock. The secondary membrane contains the LAr in case of any primary membrane leaks and the vapor barrier prevents water ingress into the insulation. This "in-ground" tank arrangement (i.e., offering access only from the top) protects against possible cryogen leaks out of the tank — there is no place for the liquid cryogen to go because it is surrounded on all sides by rock. The basic components of the membrane tank are illustrated in Figure 1–8. Bolted connections (not shown in the figure) will be made between the truss and structural elements in the concrete.

2.2.2   Concrete Liner and Vapor Barrier

The formed concrete liner will be poured against shotcrete on the sides and bottom of the excavated volume. Conduits and heating elements will be embedded in the concrete liner to maintain rock temperatures above freezing to preclude any problems associated with freezing water and heaving. The embedded conduits are encased approximately midway in the concrete side walls, end walls and bottom floor slab as depicted in Figure 2–4. The concrete liner and conduits are provided under the conventional facilities scope. The heating elements are provided by LAr-FD scope.
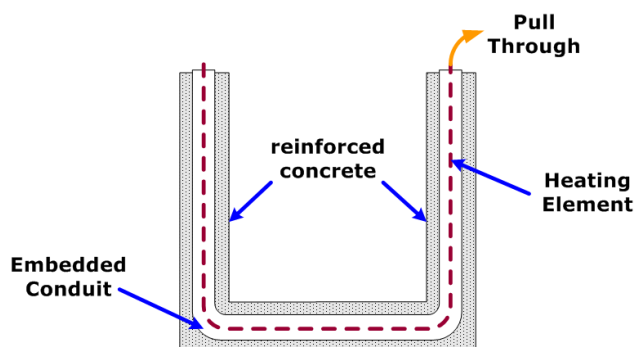
Figure 2–4: End view of concrete liner showing embedded conduits for heating elements (Courtesy Arup)

Table 2–3: Heat load calculation (Thickness = 0.8 m for all)

Element	Area (m^2)	κ (W/m-K)	$\triangle$T (K)	Heat input (kW)
Base	482	0.0283	191	3.3
End walls	551	0.0283	191	3.7
Side walls	988	0.0283	191	6.7
Roof	482	0.0283	207	3.7
Total				17.3

A vapor barrier is required on all internal surfaces of the concrete liner (base slab, side walls, end walls) and the roof to prevent the ingress of any water vapor into the insulation space. If water vapor were permitted to migrate into the insulation space it could freeze and degrade the thermal performance of the insulation. The barrier must also reliably absorb the stresses and strains from all normal loading conditions. The selected vapor barrier material is a polymeric liner for the side and bottom surfaces. This has been used extensively in onshore LNG tank applications. The vapor barrier for the top will be solid steel plate welded together and to the underside of the roof truss. The vapor barrier (floor, walls and top) is provided under the CF scope.

2.2.3   Insulation System and Secondary Membrane

The membrane cryostat requires insulation applied to all internal surfaces of the concrete liner (base slab, side walls, end walls) and roof in order to control the heat ingress and hence the required refrigeration load. Choosing a reasonable, maximum insulation thickness of 0.8 m, and given an average thermal conductivity coefficient for the insulation material of $\kappa \approx 0.0283$ W/m-K, the heat input from the surrounding rock is expected to be 17.3 kW total. This is shown in table 2–3.

The insulation material is a solid reinforced polyurethane foam, manufactured as composite panels (1 m × 3 m from GTT, 3-m × 8-m from IHI). The panels get laid out in a grid, with 3-cm gaps between them (that will be filled with loose fiberglass) and fixed onto anchor bolts embedded into the concrete at ∼3-meter intervals. The composite panels contain the 40-cm thick outermost insulation layer, the secondary membrane and the 40-cm innermost insulation layer. After positioning adjacent composite panels and filling the 3-cm gap, the secondary membrane is spliced together by epoxying an additional overlapping layer of secondary membrane over the joint. All seams are covered so that the secondary membrane is a continuous liner. Figure 2–5 illustrates how the layers come together at a corner.

The secondary membrane is comprised of a thin aluminum sheet and fiberglass cloth. The fiberglass-aluminum-fiberglass composite is very durable and flexible with an overall thickness of ∼1 mm. The secondary membrane is placed 40 cm in from the concrete (40 cm from
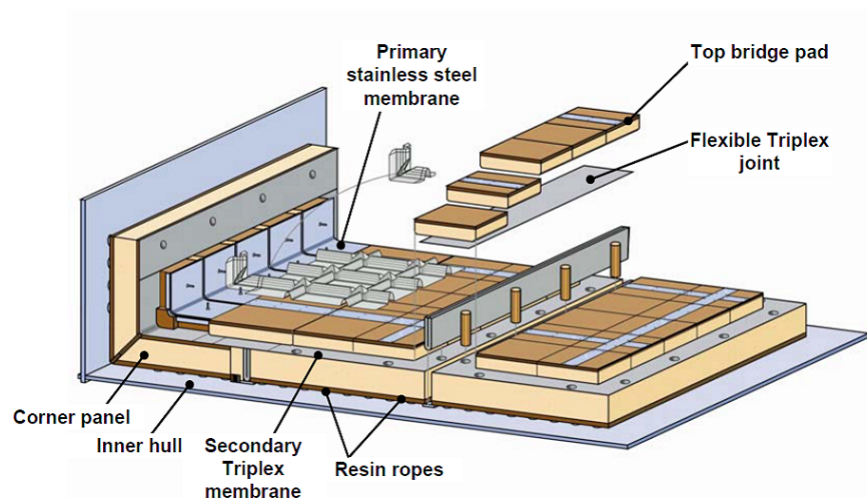
Figure 2–5: Membrane corner detail

the primary membrane), within the insulation space. It surrounds the internal tank on the bottom and sides, and it separates the insulation space into two distinct, leak-tight, inner and outer volumes. The outer, 40-cm thick volume of insulation separates this membrane from the concrete. This sheet is connected to embedded metal plates in the vertical concrete wall at the upper edge of the tank. In the unlikely event of an internal leak from the cryostat's primary membrane into the inner insulation space, it will prevent the liquid cryogen from migrating all the way through to the concrete liner where it would degrade the insulation thermal performance and could possibly cause thermal stress cracks in the surrounding concrete. The liquid cryogen, in the case of leakage through the inner (primary) membrane will escape to the secondary membrane volume, which gets purged with GAr at the rate of one volume exchange per day.

2.2.4 Tank Layers as Packaged Units

Membrane tank vendors have a "cryostat in a kit" design that incorporates insulation and secondary barriers into packaged units. See Figure 2–6. Figure 1–8 illustrates how these layers would be used in the LAr-FD reference design.

2.2.5 Top of Tank

The stainless-steel primary membrane, intermediate insulation layers and vapor barrier continue across the top of the detector, providing a vapor-tight seal. Note that no secondary membrane is used or required for the cryostat top. The cryostat roof is a steel truss structure that bridges the detector. Stiffened steel plates are welded to the underside of the truss to form a flat vapor barrier surface onto which the roof insulation attaches directly;
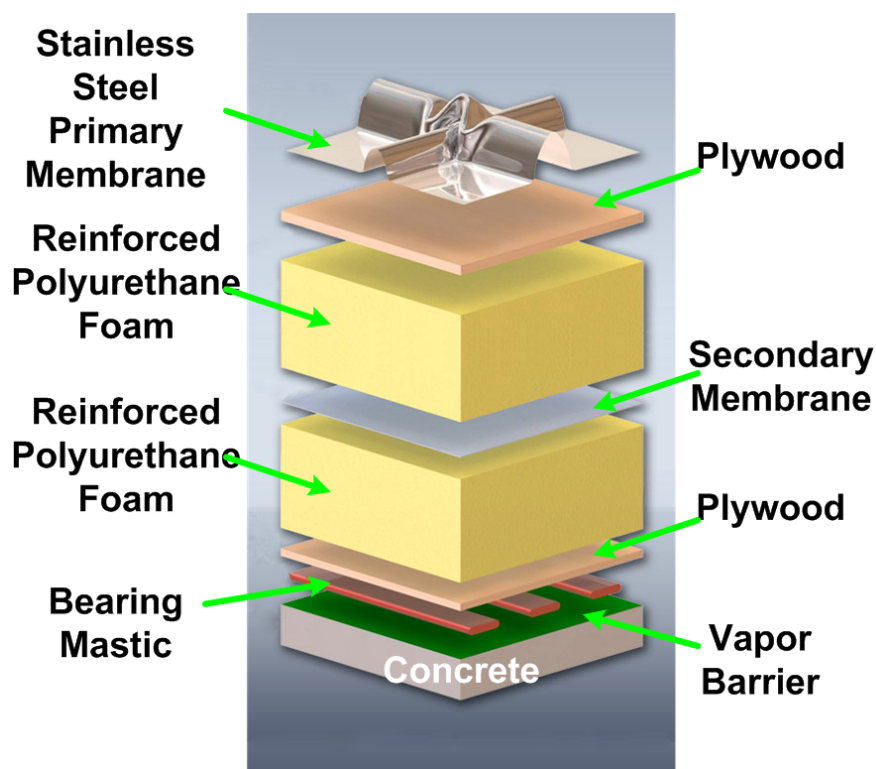
Figure 2–6: GST composite system from GTT

this is described more fully below. Fully fabricated roof trusses are placed across the roof with a 2.5-m spacing. Field-fabricated truss members and steel plates are welded between the prefabricated trusses to connect the two prefabricated sections. The roof is built up of alternating prefabricated and field-fabricated "in-fill" roof sections. This configuration was selected during the screening process because it provides an efficient, gas-tight solution that can be readily constructed within the excavated volume.

The truss structure rests on the top of the concrete wall as shown in Figure 1–8 where a positive structural connection between the concrete and the truss is made to resist the internal upward force caused by the slightly pressurized argon in the ullage space (roof truss design pressure during cryostat relieving is 350 mbarg, roof truss maximum deflection is 76 mm). The hydrostatic load of the LAr in the cryostat is carried by the floor and the side walls. Everything else within the cryostat (TPC planes, electronics, sensors, cryogenic- and gas-plumbing connections) is supported by the steel plates under the truss structure. All piping and electrical penetrations into the interior of the cryostat are made through this top plate to minimize the potential for leaks.

Studs are welded to the underside of the steel roof plates to bolt the insulation panels. Insulation plugs are inserted into the bolt-access holes after panels are mounted. The primary membrane panels (also manufactured in smaller sheets) are first tack-welded then fully welded to complete the inner cryostat volume. Feed-through ports as shown in Figure 2–7

are located at regular intervals within the corrugation pattern of the primary membrane to accommodate TPC hangers, electrical and fiber-optic cables, and piping. The roof truss will be anchored to the top of the poured-concrete liner walls to resist the uplift caused by internal tank overpressure. The roof truss will be pre-fabricated off-site in ∼2 m wide, fully-welded modules and transported to the Detector Hall as required by the installation schedule.

Figure 2–7: Nozzle in roof membrane cryostat (Figure courtesy GTT)

The prefabricated steel roof-truss modules are relatively lightweight (∼ 8,000 kg each) and require only moderate crane capacity. If the steel trusses need to be separated into smaller pre-fabricated units for transport to the site, assembly within the detector pit prior to installation is relatively straightforward.

Some equipment, such as monitoring instrumentation and pumps, will be installed within wells extending through the roof structure. All connections into the cryostat will be made above the maximum liquid level and mostly located on the roof of the cryostat.

2.3   LAr Circulation and Temperature-Profile Modeling

The liquid circulation in the LAr-FD cryostats has been modeled using computational fluid dynamics modeler software (ANSYS CFX).

A field cage, described in Section 3.6, was modeled with half-inch slots cut every five inches, yielding a 10% porosity. Standard insulation thermal conductivity of 0.0283 W/m-K was used to model the heat flux into the LAr, and used an exterior temperature of 278 K and an internal temperature of 87.15 K. From the results the temperature stability requirement

on LAr-FD was chosen to be ±1 K. The model in Figures 2–8 and 2–9 clearly identifies convective currents flowing through the entire liquid bath with the highest velocities < 0.034 m/s, and a temperature gradient much less than 0.1 K across the entire fluid body. This indicates conformity with LAr-FD requirements and parameters.
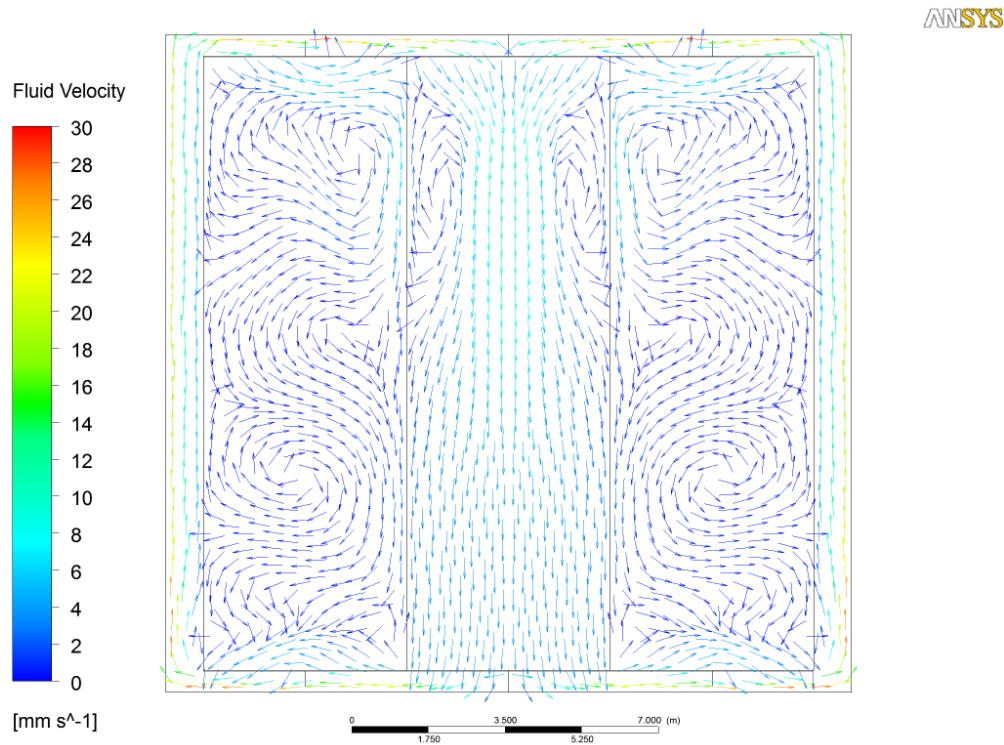
Figure 2–8: LAr velocity profile

2.4   Leak Prevention

The primary membrane will be subjected to several leak tests and weld remediation, as necessary. All (100%) of the welds will be tested by an Ammonia Colorimetric Leak Test (ASTM E1066-95) in which welds are painted with a reactive yellow paint before injecting gas with 25% ammonia into the bottom insulation space of the tank. Wherever the paint turns purple or blue, a leak is present. Both membrane cryostat manafucturers use this technique for certifying that a cryostat is leak-tight. Any and all leaks will be repaired. The test lasts a minimum of 20 hours and is sensitive enough to detect defects down to 0.003 mm in size and to a 10^{-7} std-cm^3/s leak rate (equivalent leak at standard pressure and temperature, 1 atm and 273 K). Both membrane cryostat manafucturers use this technique for certifying that a cryostat is leak-tight.

To prevent infiltration of water-vapor or oxygen through microscopic membrane leaks (below detection level) the insulation spaces will be continuously purged to provide one volume
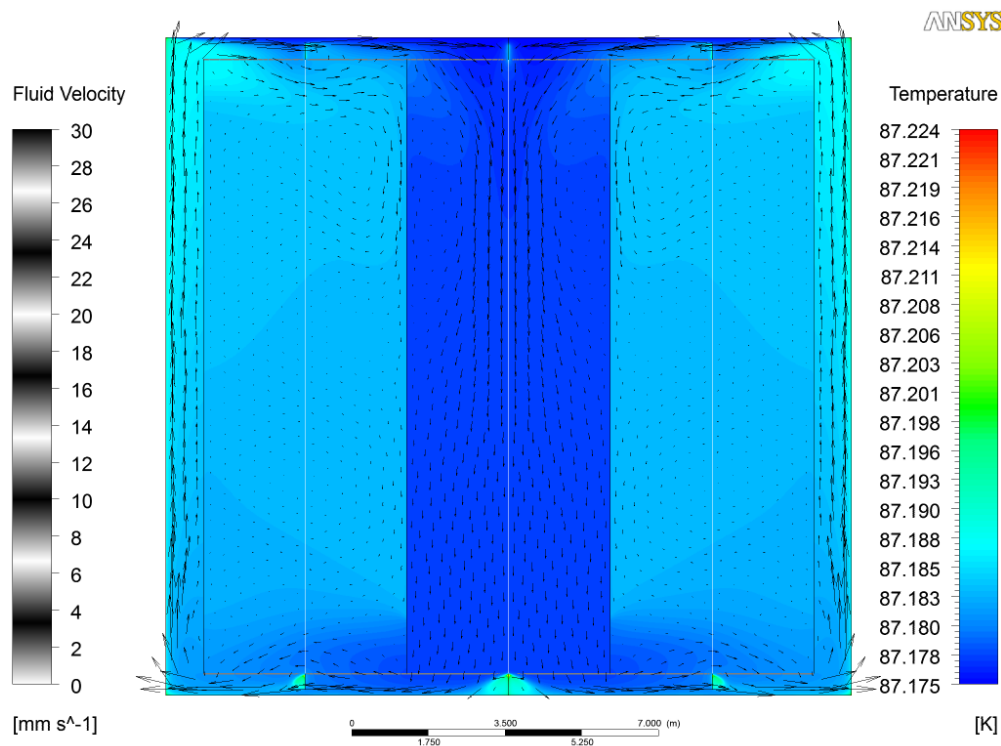
Figure 2–9: LAr temperature profile

exchange per day. The gaseous space in the insulation under the primary membrane is estimated to be 116 m³ which requires an argon gas flowrate of 16.3 m³/hr at standard temperature and pressure.

The insulation space between the primary and secondary barriers will be maintained at 30 mbarg, slightly above atmospheric pressure. This space will be monitored for changes that might indicate a leak from the primary membrane. The outer insulation space will also be purged with argon at a slightly different pressure. The pressure gradient across the membrane walls will be maintained in the outward direction. Pressure-control devices and relief valves will be installed on both insulation spaces to ensure that the pressures in those spaces do not exceed the operating pressure inside the tank.

The purge gas will be recirculated by a blower to a small purge gas dryer and reused as purge gas. The purge system is not safety-critical, and an outage of the purge blower would have negligible impact on LAr purity [16].

2.5   Cryogenic Systems Layout

Cyrogenic systems are located in three areas illustrated in Figure 1–5: the Detector Hall, the Cryogenics Equipment Building and the Purification Building. The design will be finalized with a focus on minimizing:

- the exposure of personnel to ODH

- passive heat ingress to the cryogenic system

- the potential for argon escape or contamination by minimizing the volume of the argon system external to the cryostat

The schematic in Figure 2–3 shows the layout of the cryogenic services. The compressor systems required for the LN2 refrigeration plants (Figure 2–10) will be housed in the Cryogenics Equipment Building. Each cryostat will have its own argon recondenser (Figure 2–11), argon-purifying equipment and overpressure-protection system for the cryostat it serves. The regeneration and purification systems will be housed in a second building ('Purification Building') to segregate the ODH risk and electrical noise of those systems from the Detector Hall. Gas analysis will take place in the Purification Building. The condensers and associated piping will be placed within the Detector Hall.

The outdoor facility, adjacent to the Detector Hall, will include a 50-m^3 LAr receiving dewar and two 50-m^3 LN dewars. Two 25-m^3/hr circulation pumps will be placed within each membrane cryostat to circulate liquid from the bottom of the tank through the purifier. Each pump adds about 5.2 kW of pump energy to the liquid (see Table 2–4). The refrigeration needs are dependent on the mode of operation within both detector modules (See Figure 2–14). The combined plant capacity of 165 kW (sum of three refrigerators) surpasses estimated loads during all modes of operation.

The following equipment will be placed directly on or within the cryostat:

- Circulation pumps to deliver LAr to purifiers

- LAr return/fill pipe

- Boil-off gas line

- Cryostat pressure-control valves

- Cryostat pressure-relief valves

- Purge pipework

- Cryostat-monitoring equipment (for pressure, temperature, density, depth, and so on)
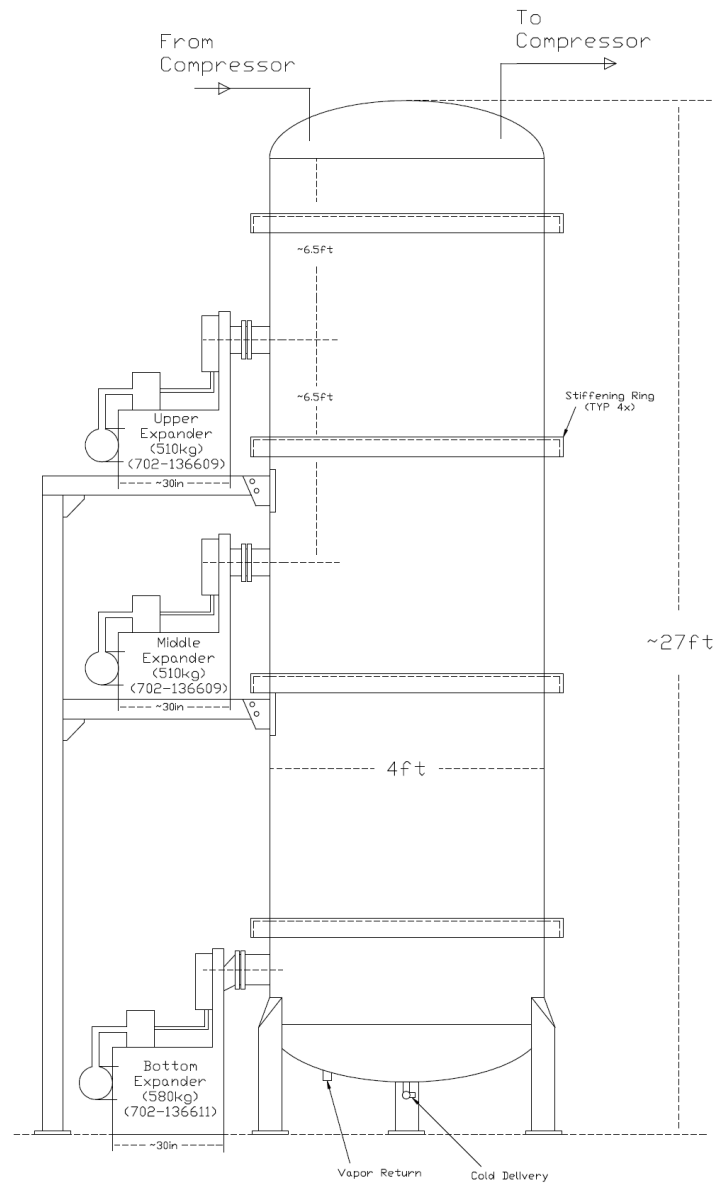
Figure 2–10: Nitrogen refrigeration plant
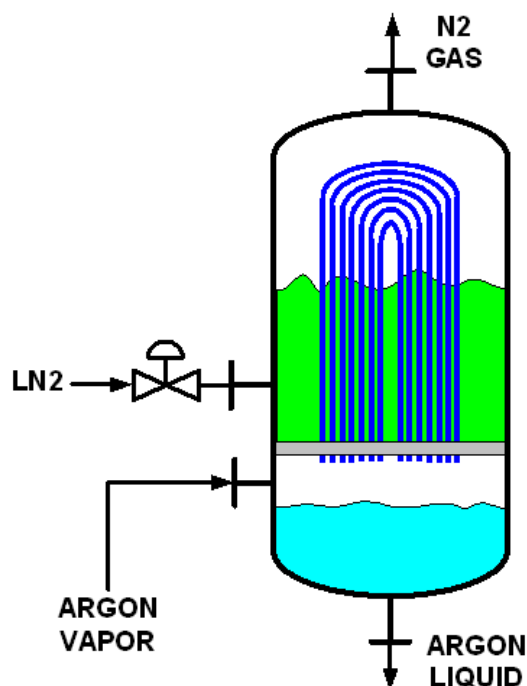
Figure 2–11: Liquid argon recondenser

2.6 Equipment Redundancy

Safety-critical equipment will be implemented, generally, on the basis of N+1 units. This will ensure continuity of operation and adherence to safety standards whenever a unit is unavailable, e.g., for maintenance. Items for short-term use and those already present in multiple units are exempted; a low probability of failure is assumed for the former and minimal impact to the performance of the overall system for the latter.

Where common-function equipment could be used for alternate systems, interconnections will be provided to increase flexibility during operation. An example of this would be an interconnection between the argon and nitrogen delivery lines between the cryoplant and the detector cryostat. Since the argon piping will only be used during the LAr delivery from the LAr storage dewar through purification to the cryostats, this cryogenic line can be designed as a backup for the LN transfer line which connects from the storage dewar to the condensers located near the cryostats. Later during the lifetime of the experiment, if the LN delivery system had a problem such as excessive heat leak due to a degradation of vacuum, the LAr piping could be used in its place.

2.7   Cryogenic System Processes

The functionality of the cryogenic system is shown in Figure 2–12. This diagram shows the interconnectivity between major functions of the cryogenic system. The details showing only major piping connections can be seen in Figure 2–3. The major functions serving the cryostat are cryogen supply for cool down and fill, gas filtration, condensing, liquid filtration and circulation, argon-purity analysis, and argon condensing. The methods presented in this section are motivated by experience from other LAr TPC cryogenic systems such as ICARUS and LAPD.

2.7.1   Cryostat Initial Purge and Cool-down

After cryostat construction and following installation of all scientific equipment, the cryostat will be purged of contaminants and cooled. Construction procedures leading up to this point will ensure that the completed cryostat does not contain debris and is free of all loose material that may contaminate the LAr.

2.7.1.1   Initial Purge

Argon piping will be isolated, evacuated to less than 0.1 mbar absolute pressure and backfilled with high-purity argon gas. This cycle will be repeated several times to reduce contamination levels to the ppm level in the piping. The reference-design choice for removing air from the membrane cryostat will be to flow/piston-purge argon, introducing the heavy argon gas at the bottom of the tank and removing the exhaust at the top. The bottom field cage (part of the TPC, described in Section 3.6), serves an additional role as a flow diffuser during the initial purge. A matrix of small holes in the field cage will provide a uniform flow, approximately 10-mm diameter at a 50-mm pitch.

The flow velocity of the advancing argon-gas volume will be set to 1.2 meters/hour. This is twice the diffusion rate of the air downward into the advancing argon so that the advancing pure argon-gas wave front will displace the air rather than just dilute it. A 2D ANSYS model of the purge process shows that after 20 hours of purge time and 1.5 volume changes, the air concentration will be reduced to less than 1%. At 40 hours of elapsed time and three volume changes, the purge process is complete with residual air reduced to a few ppm; see Figure 2–13. This simulation includes a representation of the perforated field cage at the top and bottom of the detector and heat sources due to the readout electronics. The cathode planes (Section 3.5) are modeled as non-porous plates although they will actually be constructed of stainless-steel mesh.

The computational fluid dynamics (CFD) model of the purge process has been verified with
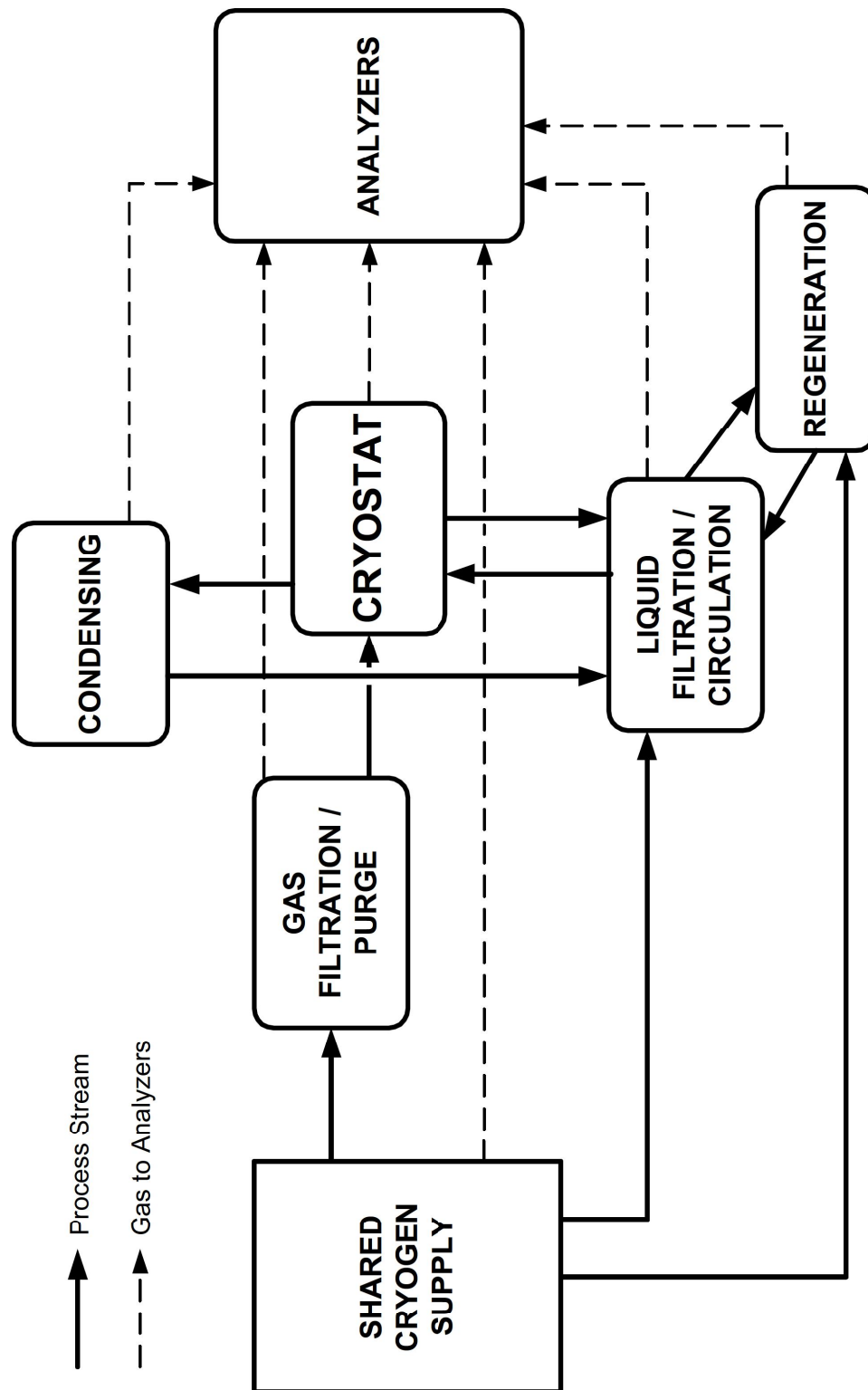
Figure 2–12: Block flow diagram of significant connections between cryogenic systems
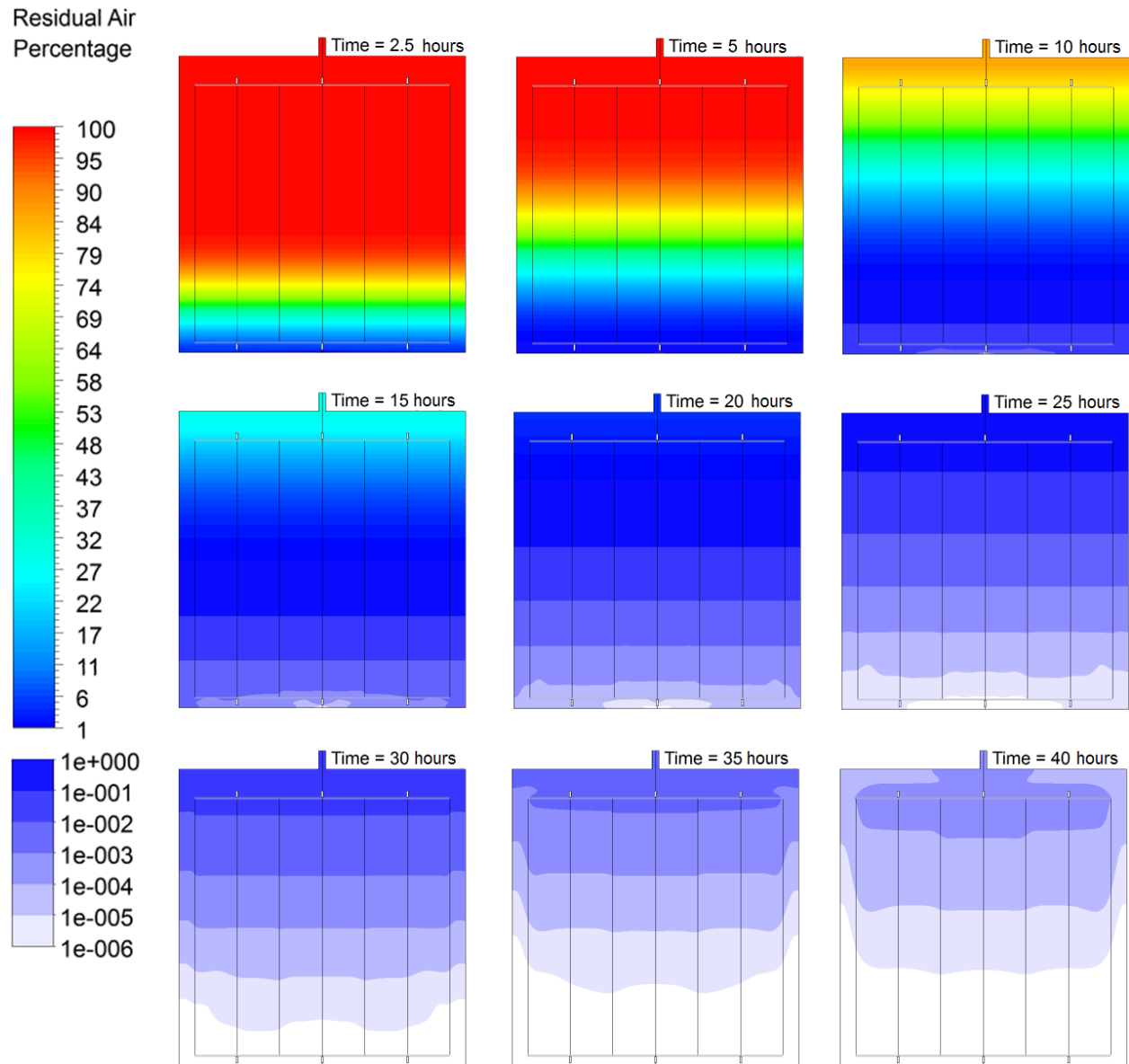
Figure 2–13: Residual air concentration during "argon piston" purge; original air concentration falls below 1 ppm in 40 hours.

purge tests in an instrumented 1-m-diameter by 2-m-tall cylinder. Recognizing that obtaining the required purity levels by the flow-purging method needs to be clearly demonstrated, a Liquid Argon Purity Demonstrator (LAPD) project is underway at Fermilab. The LAPD is a right-cylindrical vessel, 3 m in diameter and 3 m tall. LAPD took gas-sampling measurements at varying heights and times during the purge process. Experimental measurements taken by the Liquid Argon Purity Demonstrator (LAPD) have verified the previous modeling of this purge process. LAPD used nine volume changes to reach single-digit contamination levels (ppm by volume) for oxygen, water and nitrogen. Following the purge, the LAPD vessel was cooled down and filled with LAr.

On September 30, 2011, LAPD leaders presented initial results of this purge process in which purity levels of less than 100 ppt oxygen-equivalent were achieved. This confirms that the purge method works and it minimizes the risk to LBNE that an evacuable vessel will be required. This test will be repeated with a 35-ton membrane cryostat prototype.

2.7.1.2   Water Removal via Gas Flow

Water and oxygen will continue to be removed from the system for several days following the initial purge. Flowing gas will be used at the same rate. Each cryostat contains ∼1 ton of FR4 circuit-board material and a smaller inventory of plastic-jacketed power and signal cables. These somewhat porous materials may contain as much as 0.5% water by weight. Water-vapor outgassing from these materials will be entrained in the gas flow exiting the top of the cryostat and will be removed from the gas stream by filters. Adsorbed water will also be removed from the metallic inner surfaces of the cryostat and piping system. Water deep within porous materials will remain; after the cryostat is filled the FR4 outgassing is only a problem in the ullage where the temperature might exceed 120 K. Cabling in the gas ullage will be a source of water contamination but the quantity is less than ICARUS by volume and the gas exchange rate is higher. Tests at the LAr-Purity Demonstrator (Section 8.3.3) show that no measurable contamination occurs with FR4 in contact with LAr.

2.7.1.3   Alternative Water-Removal Method: Evacuation

The traditional method for removing water and oxygen from LArTPCs is to evacuate the tank to ∼10^{-4} mbar and then backfill it with pure argon gas. Although the primary membrane of the reference-design cryostat is not a vacuum vessel, it is possible to evacuate it. A membrane-cryostat vendor reports that evacuation of the insulation spaces (external to the primary membrane) is normally done during the construction and leak-checking phases. A vacuum pressure of less than 200 mbar absolute in the insulation spaces has so far been achieved in a membrane cryostat test section at Fermilab. As long as the pressure-differential direction across the walls is kept outward, it is possible to reduce the internal membrane-tank volume to these pressures as well.

2.7.1.4 Initial Cool-Down

Purified LAr will be distributed across the bottom of the cryostat to cool down the cryostat. The boil-off gas will flow through the volume of the cryostat, then routed to the recondenser and liquid-filtration system. Simulation has shown that the liquid cool-down method can be controlled to stay within the available recondenser capacity. The required cooling rate is determined by the maximum stress that detector components can tolerate. For example, the 150-μm APA wires will cool much more rapidly than the APA frames. A mass flow-control system with temperature-monitoring system will be used to control the temperature difference across the cryostat. The exact temperature difference required is yet to be determined; it will be based on input from the cryostat designer and the requirements of the TPC components and structure.

2.7.1.5 Initial Purge and Cool-Down Design Features

Internal piping is positioned within the cryostat to support the purge and cool-down procedure. Heavy argon vapor, which is a result of cooling down the membrane bottom with liquid, will promote purging after it rises from the base of the cryostat and is vented from the roof level. The argon gas supply pipework will have nozzles spaced along its length to distribute equal gas flow rates across the bottom of the cryostat. The flow nozzles will be directed downward or to the side so that the injection velocity will not cause local vertical gas plumes or turbulent mixing but rather will spread across the bottom of the tank and produce a stable, upwardly advancing argon wave front. The vertical velocity of 1.2 m/hr for the gas purge includes a contingency for some level of turbulent mixing.

Main gas returns, used for pressure control, will be distributed along the cryostat roof. All nozzles and dead-end (stagnant) volumes located at the top of the cryostat will have gas-exhaust lines for the initial purge and for continuous sweep-purge of those volumes during normal operations. The sweep-purge during the initial stage of purging will be vented through a pipe to the outdoors. After all but trace amounts of air have been expelled, the gas returns will be routed to the recondensers before being returned to the cryostat. When cool-down to 120 K is complete (and during steady state operations), the gas returns will be sent to the re-condensor to be liquefied by heat exchange with a liquid nitrogen stream. The recondensed liquid will be filtered and sent back to the cryostat to complete the cool-down operation. All purge gas will be contained and either vented outside of the detector pit, or recondensed and reused.

2.7.2 Liquid Argon Receipt

Each LAr detector module will hold an inventory of 9 kton of liquid argon. Initial purge operations are expected to consume and exhaust about 0.09 kton per module. Considering

that some product will also be lost in transit, approximately 19 kiloton of LAr will need to be procured. Planning the logistics and supply of LAr to the facility requires consideration of the following issues:

- total capacity of commercial air-separation plants within freight distance of the facility (the peak delivery potential)

- extent of boil-off that will occur in transit

- number of vehicle movements required and their impact on the local community

- costs and benefits associated with stockpiling LAr at the facility ahead of commencing the purge, cool-down and fill procedure

- provision of a temporary air-separation plant at the facility to generate liquid argon

- availability and cost associated with the delivery of high-purity LAr as opposed to lower-quality, commercial-grade argon combined with on-site, coarse purification

Total argon production in the United States is currently approximately 3.6 kton per day. Argon is normally co-produced along with large volumes of oxygen, so any project that requires large oxygen quantities may also spur additional argon production, enhancing the supply capacity. A 2013-2018 market-forecast report by the Freedonia group [17] indicates that the demand for argon will increase at a rate of 3.4% per year whereas the demand for oxygen will increase 4.8%.

The standard grade specification for argon is a minimum purity of 99.995%, allowing a maximum concentration of 5.0 ppm for O_2 and 10.5 ppm for H_2O. This is designated as Grade 4.5 in the gas-supply industry. Requiring higher-purity product would significantly reduce the volume of product available to the experiment, increasing cost and pushing out the schedule. Therefore, standard product will be procured from multiple vendors. The most efficient mode of argon delivery is over-the-road tank truck with a maximum capacity of 18.7 metric ton (MT). The expected number of such deliveries needed is 500 over two months to fill one cryostat. Rail delivery is not cost-effective as there are no rail spurs leading to the site. This mode would require transfer of product from rail tanker to a tank truck, introducing cost that exceeds the benefit.

Facilities are required for the offloading of LN and LAr road tankers. It will be necessary to procure approximately four trailer loads of liquid nitrogen (about 40 tons) for the initial filling of the LN refrigeration dewar and charging of a single refrigeration plant. Vehicle access and hard-surfaced driving areas are required adjacent to the LN dewar and LAr-supply piping. An interim LAr storage dewar will hold the contents of a road tanker in order to minimize off-loading time. Road tankers will connect to a manifold located close to the Cryogenics Equipment Building and will use their on-board pumps to transfer the LAr to the storage

Table 2–4: Estimated heat loads within the cryostat

Item	Heat Load (kW)
Insulation heat loss	17.3
Electronics power	2.9
Recirculation-pump power	5.2
Total	**25.1**

dewar. Each tanker will be tested to ensure that the LAr meets the purity specification. The LAr will be pumped to the from the storage dewar to the Detector Hall where it will be routed through the purification system prior to discharging into one of the cryostats.

2.7.3   Cryostat Filling

Liquid argon will be delivered via a manifold along the bottom of the cryostat to attain uniform cool down and filling. The filling process will take place over many weeks due to the delivery schedule of liquid argon described in the previous section. Liquid-argon purification can begin once the liquid depth reaches about 2 m in the cryostat. At this depth, the recirculation pumps can safely turn on and direct up to 51 m^3/hr (224 gpm) of liquid argon through the purification system.

2.7.4   Argon Reliquefaction and Pressure Control

High-purity liquid argon stored in the cryostat will continuously evaporate due to the unavoidable heat ingress discussed in Section 2.2.3. The argon vapor (boil-off gas) will be recovered, chilled, recondensed and returned to the cryostat. A closed system is required in order to prevent the loss of the high-purity argon.

During normal operation the expected heat load of approximately 29.7 kW (Figure 2–14, Scenario 3) into the argon system will result in an evaporation rate of 613 kg/hr. The argon volume changes by a factor of 200 in the transition from liquid to vapor. This increase in volume within a closed system will, in the absence of a pressure-control system, raise the internal pressure. In the LAr-FD, argon vapor will be removed from the top of the cryostat through the chimneys that contain the cryogenic feedthroughs. As the vapor rises, it cools the cables and feedthroughs, thereby minimizing the outgassing and sweeping contaminants up and out of the cryostat.

The gaseous argon leaving the cryostat will pass through a pressure control valve to maintain the cryostat at 0.013 MPa gauge +/- 0.003 MPa. The exiting gaseous argon will be directed to a heat exchanger (recondenser) in which it is chilled against a stream of liquid nitrogen and condensed back to a liquid. The liquid nitrogen stream (that provides the coolant for the

Heat Demand	Unit Loads (kW)	Scenarios						
		1	2	3	4	5	6	7
Recondenser Load, 1st Cryostat								
Cryostat (W) Heat Ingress	17.3	17.3	17.3	17.3	17.3	17.3	17.3	17.3
Recirculation Pump in cryostat W 1 pump	5.2		5.2	5.2	5.2	5.2	5.2	
Recirculation Pump in cryostat W 2 pumps	10.4	10.4	10.4					
Piping and Purification vessel Heat ingress (W)	2	2.0	2.0	2.0	2.0	2.0	2.0	
Detector Electronics in cryostat W	3			3.0	3.0	3.0	3.0	
Cryostat Cooldown load		42.3						
Condensers (W) in Operation		2	1	1	1	1	1	1
Condenser (W) Load		**72.0**	**29.7**	**27.5**	**27.5**	**27.5**	**27.5**	**17.3**
Recondenser Load, 2nd Cryostat								
Cryostat (E) Heat Ingress	17.3				17.3	17.3	17.3	17.3
Recirculation Pump in cryostat W 1 pump	5.2						5.2	
Recirculation Pump in cryostat W 2 pumps	10.4				10.4	10.4		
Piping and Purification vessel Heat ingress (E)	2				2.0	2.0	2.0	
Detector Electronics in cryostat E	3						3.0	
Cryostat Cooldown load					42.3			
Condensers (E) in Operation					2	1	1	1
Condenser (E) Load					**72.0**	**29.7**	**27.5**	**17.3**
LN Storage dewar recondenser	2	2	2	2	2	2	2	
Refrigeration Needed		74.0	31.7	29.5	101.4	59.1	57.0	
Refrigeration Plants in Operation		**2**	**1**	**1**	**2**	**2**	**2**	**0**
Actual Duty per plant		45	45	45	51	45	45	
electric trim heater load		16	13.3	15.5	0.0	30.9	33.0	
Total Refrigeration Load		**90**	**45**	**45**	**101.4**	**90**	**90**	**0**

Figure 2–14: Refrigeration loads; the Scenarios are described in Section 2.7.8.

recondenser) will be supplied from a closed-loop LN2 refrigeration plant. The commercial refrigeration plant uses compression/expansion and heat rejection to continuously liquefy and reuse the returning nitrogen vapor.

Each module of the detector has a dedicated nitrogen-refrigeration plant and a third plant will be on standby during normal operations. Further, each module will also have one operating and one standby argon recondenser. This will ensure high availability of the recondensing system, minimize the need to vent high-purity argon and allow down-time for maintenance of the recondensers and the refrigeration plants. The condensed stream of LAr will be combined with the circulating stream of LAr and purified prior to being returned to the cryostat.

The heat load introduced to the cryostat for the initial circulation rate will increase the total heat ingress significantly, in fact beyond the nominal 55 kW per refrigerator capacity. Therefore, additional refrigeration is required during the commissioning phase. However the refrigeration plant and recondenser have been provided on a fully redundant basis to ensure high availability. During the initial period the plants will be operated in parallel to provide the increased cooling capacity that will be required.

2.7.5   Argon Purification

Since the tank is designed without penetrations below the liquid level, pumps must be used to transfer LAr from the cryostat. Vertical submersible pumps will be inserted into pump wells extending down from the cryostat roof. The pump suction must be located a minimum distance (normally ∼1.5 to 2 m) below the lowest liquid level at which they are to pump in order to prevent cavitation and vapour-entrapment. The pumps and pump wells will extend to the bottom of the cryostat. They could also be staggered at different elevations to allow flexibility in drawing liquid from different elevations. Vertical, submersible, cryogenic pumps are supplied by manufacturers such as Ebara and Carter Cryogenic Products (see Figure 2–15). An example of a larger pump tower is shown in Figure 2–16.

The required flow rate of liquid argon to be sent for purification is expected to decrease over time. The initial maximum flow rate will be 51 m^3/hr (224 gpm). The liquid-argon volume in one cryostat will turn over every five days at this rate. Longer term, the rate will decrease to 25 m^3/hr with a turn-over rate of 10 days. As a point of comparison, ICARUS T600 has a maximum turn-over rate of eight to ten days. See Table 2–5 for a comparison of purification rates among other experiments and LBNE. To achieve the wide variance required between the short-term commissioning flow rate of 51 m^3/hr (224 gpm) and the long-term operational flow rate of 25 m^3/hr (112 gpm) through the purifiers, two removable 25 m^3/hr (112 gpm) pumps will be located at the end of the cryostat. Placing the pumps at this end of the cryostat will keep space clear for TPC installation. The purification skids are located in the Purification Building. The multiple-pump arrangement provides redundancy for uninterrupted cryostat operation even during pump maintenance.
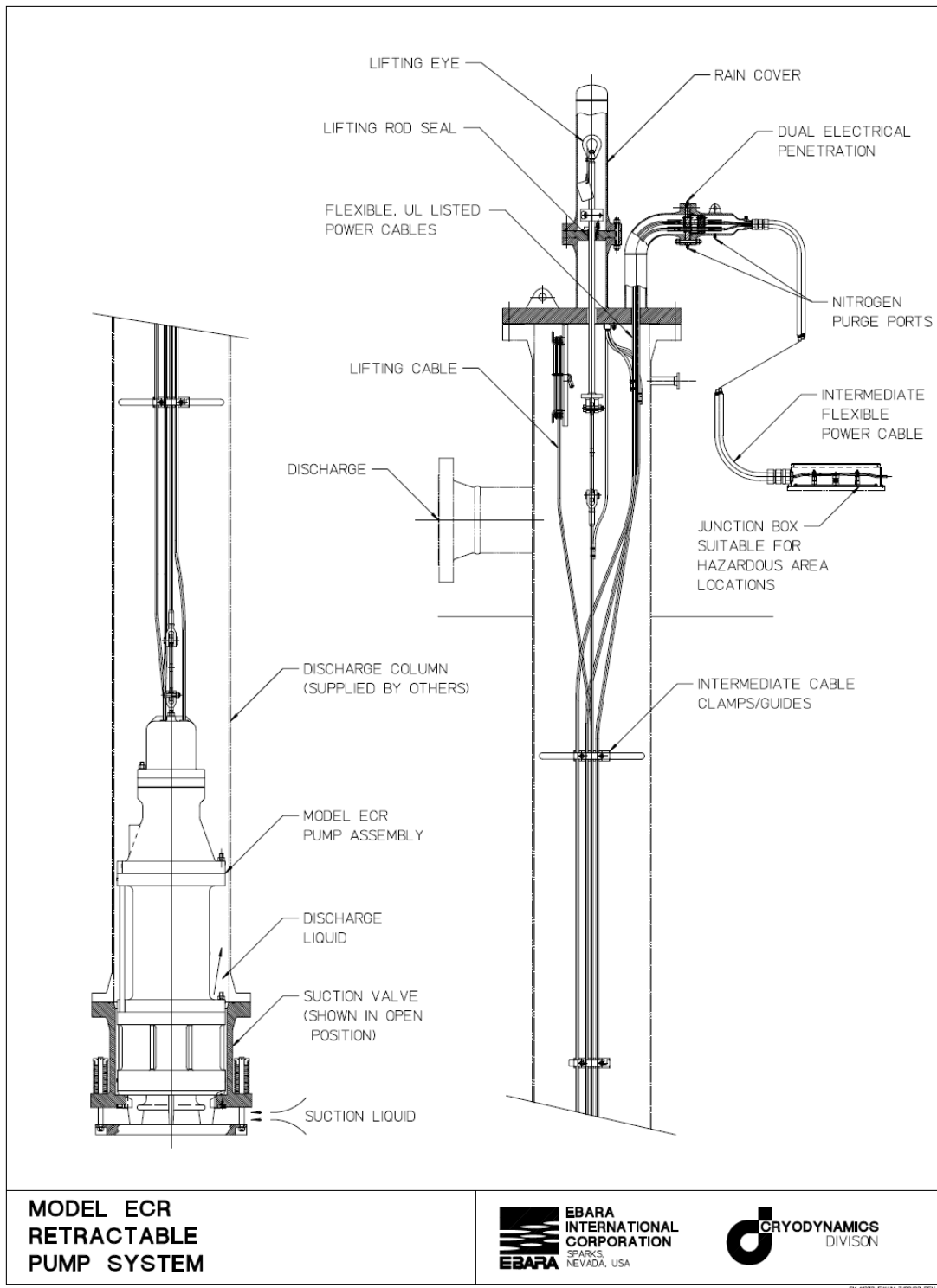
Figure 2–15: Vertical submersible cryogenic pump
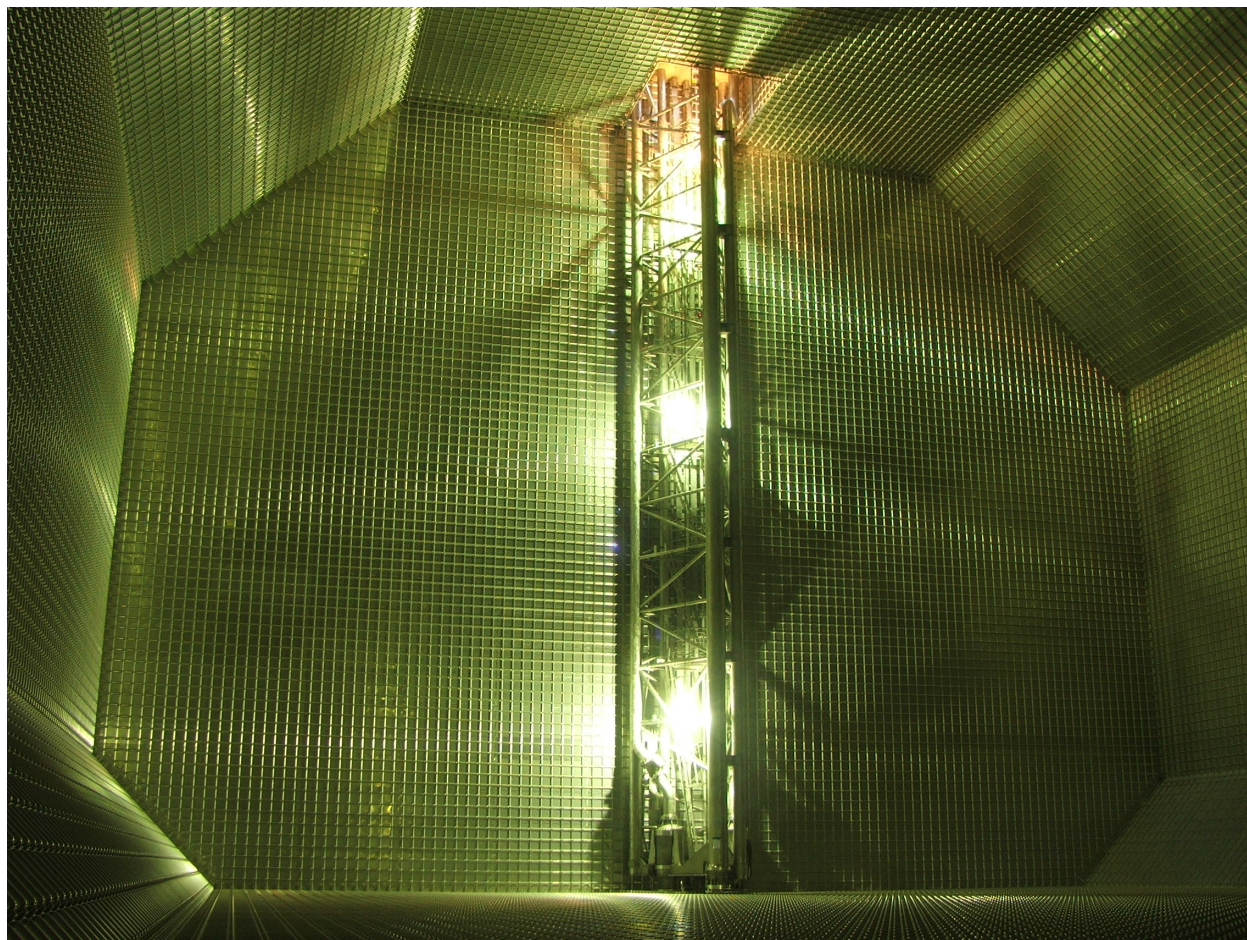
Figure 2–16: Pump tower in LNG membrane cryostat

The liquid purification system consists of three identical filter vessels, each containing molecular-sieve and copper media filters. Each bare filter vessel is 1.3 m in diameter by 3.5 m tall. The filters are sized to provide effective media usage at low pressure drop (2 kPa or 0.3 psi) over the expected range of flow rates. Only one filter will be in service at any time. For the initial fill and purification this redundant equipment will allow:

- Staggered filter regeneration and cool-down to lower the utility load (electric heating and LN2 cooling)

- Short turn-around time for regenerated filter (2 days)

- Maintenance of the purification beds

and for long-term operations it will allow:

- High available capacity at the reduced flow rate

- Relaxation of regeneration time to minimize utility swings

- Possibility of filter maintenance or filter media replacement without disruption

The cryostat liquid argon inventory is circulated through a purification filter to achieve and maintain the required purity. The purification filter, containing molecular sieve media to remove water and copper media to remove oxygen, will become saturated. The nearly saturated purification filter is regenerated to vent the contaminants. The liquid argon flow is switched to another purification filter for uninterrupted filtration. A purity monitor after the purification filter will monitor the filter effectiveness. (Purity monitors measuring electron lifetime will also be in the LAr bath and resident in the cryostat. It is a requirement that purity levels reach < 200 ppt oxygen equivalent to match the required electron lifetime of the detector).

The regeneration of a filter is done in several steps. A saturated purification filter is first warmed with heated argon gas to an elevated temperature driving the captured water into the gas. Hydrogen gas is generated and mixed with the circulating Argon gas up to 1.5% hydrogen by volume (below the explosive point) [18]. The hydrogen reacts with the oxygen and makes water that is also released into the circulating argon gas. Argon gas is vented to purge water from the hot circulating gas. The hot filter full of regenerated media is cooled by circulating chilled argon gas. The circulating argon gas is chilled first with a heat exchanger using a commercial R-404A refrigeration unit until the filter is cold. The commercial refrigeration unit accumulates the R-404A liquid and shuts down. The filter is next cooled down to cryogenic temperatures by circulating argon gas chilled by a second heat exchanger with a liquid nitrogen coolant. This completes the regeneration steps for a purification filter. The filter is now ready to be switched into service or held cold until

Table 2–5: Purification comparision data for LArTPCs

Experiment	LAr Vol (m^3)	LAr Mass (tons)	Liquid Purif Rate (kg/hr)	Gas Boil-off Rate (kg/hr)	Vol Change Rate (days)	Electron Life(ms)
ICARUS T600	550	761	2766	168	10.8	1.8
ICARUS prototype	10	13.9	692	0.69	0.8	1.1
MTS at FNAL	0.25	0.35	167	5.56	0.1	>5
ArgoNeuT	0.55	0.76	0	4.3	7.3	0.75
MicroBooNE	123	170	6875	83	1.0	TBD
LAPD	22.2	30.7	3791	46.7	0.3	4
LBNE LAr-FD	7,133	9,000	71,000	1058	5.5	1.4 req'd

needed. Two spare purification filters are used with separate heating and cooling loops to reduce the usage rate of electricity and liquid nitrogen.

2.7.6   Pressure Control

2.7.6.1   Normal Operations

The pressure control valves are sized and set to control the internal cryostat pressure under normal operating conditions to 130 mbarg. Ten percent excursions above or below this pressure will set off alarms to alert the operator to investigate and intervene. Fluctuations within the range of 50 mbarg and 200 mbarg will be allowed before automatic (executive) actions are taken. These actions may include stopping the LAr circulation pumps (to reduce the heat ingress to the cryostat), increasing the argon flow rate through the recondenser, increasing the LN flow through the recondenser vessel, powering down heat sources within the cryostat (e.g., detector electronics). Eventually, if the pressure continues to rise, it will trigger the pressure-relief valves to operate. Figure 2–17 gives important pressure values.

The ability of the control system to maintain a set pressure is dependent on the size of pressure upsets (due to changes in flow, heat load, temperature, atmospheric pressure, etc.) and the volume of gas in the system. The reference design has 0.96 meters of gas at the top of the cryostat. This is 6% of the total cryostat volume and is comparable to typical vapor fractions used for cryogenic storage vessels. Reaction time to changes in the heat load are slow, on the order of an hour. At the expected heat-load rate of 17.3 kW, and for an isolated, un-cooled cryostat, the rate of pressure rise would be 165 mbar (2.4 psi) per hour. We plan to provide two redundant pressure control valves to maintain the required pressure range, each sized to handle at least 1500 kg/hr of argon flow to the recondenser.

Figure 2–17: Important Cryogenic Pressure Parameters

Pressure Parameter	Gauge Pressure			Absolute Pressure @ Lead, SD, elevation*		
	mbar	MPa	psig	mbar	MPa	psia
Cryostat min. operating	50	0.0050	0.73	896.7	0.0896	13.00
Cryostat normal operating	130	0.0130	1.89	976.7	0.0976	14.17
Cryostat max. operating	200	0.0200	2.90	1046.7	0.10467	15.18
Cryostat design pressure	250	0.0250	3.63	1096.7	0.10967	15.91
Max. overpressure, other than fire**	275	0.0275	3.99	1121.7	0.1121.7	16.27
Max. overpressure, fire**	302.5	0.03025	4.387	1149.2	0.11402	16.67
Roof truss design working pressure	350	0.0350	5.08	1196.7	0.11967	17.36

* Lead, SD atmospheric pressure of 846.7 mbar at 1511.8 meters.

**Maximum code allowable 10% and 21% overpressures listed for reference.

2.7.6.2 Overpressure Protection

In addition to the normal-operation pressure-control system, it is planned to provide a cryostat overpressure-protection system. This will need to be a high-integrity, automatic, failsafe system capable of preventing catastrophic structural failure of the cryostat in the case of excessive internal pressure.

The key components of the planned system are pressure-relief valves (PRVs) located on the roof of the cryostat that will monitor the differential pressure between the inside and the outside of the cryostat and open rapidly when the differential pressure exceeds a preset value. A pressure sensing line is used to trigger a pilot valve which in turn opens the PRV A pressurized reservoir of power fluid is provided to each valve to ensure that the valves will operate under all upset and/or shutdown scenarios. The PRVs are self-contained devices provided specially for tank protection; they are independent of the control system.

The installation of the PRVs will ensure that each valve can periodically be isolated and tested for correct operation. The valves must be removable from service for maintenance or replacement without impacting the overall containment envelope of the cryostat or the integrity of the over-pressure protection system. This normally requires the inclusion of isolation valves upstream and downstream of the pressure-relief valves and at least one spare installed relief valve ($n + 1$ provision).

When the valves open, argon is released, the pressure within the cryostat falls and argon gas discharges to the outside. The valves are designed to close when the pressure returns to below the preset level.

2.7.6.3   Vacuum-Relief System

The membrane cryostat has integral to its design a relief system (vacuum-relief) which is a high-integrity, automatic, failsafe system designed to prevent catastrophic structural failure of the cryostat should the cryostat experience a negative pressure. The vacuum-relief system protects the primary membrane tank. Activation of this system is a non-routine operation and is not anticipated to occur during the life of the cryostat.

Potential causes of reduced pressure in the cryostat include operation of discharge pumps while the liquid-return inlet valves are shut, unregulated gaseous argon condensing in the recondenser or a failure of the vent system when emptying the cryostat. Vacuum-relief valves are provided on LNG/LPG storage tanks to protect the structure from these types of events.

The key components of this additional protection system are vacuum-relief valves located on the roof of the cryostat that will monitor the differential pressure between the inside and the outside of the cryostat and open when the differential pressure exceeds a preset value, allowing ambient air to enter the cryostat to restore a safe pressure.

2.7.7   LN Refrigeration System

Three commercial LN-refrigeration plants will be procured for LAr-FD. Each cryostat will have a dedicated LN plant for steady-state operations. A third plant will be used as a stand-by unit. The plants will be located in the Cryogenics Equipment Building. The LN plants are part of a closed-loop system that supplies LN to the argon condensers. The nominal rating of the quoted refrigerators is in the range of 55 kW.

Two-phase nitrogen is delivered from the cold end of the refrigerator into two 50 m^3 LN dewars. Pure liquid is withdrawn from the dewars and is supplied via transfer line to a pressure-reducing valve and phase-separator tank also located in the Detector Hall. LN is then withdrawn from the bottom of the phase-separator tank, at a pressure of 2.0 bar and temperature of 84K, and directed to the recondenser. This results in a 5 K temperature difference relative to the 87 K argon recondenser temperature. The dewar size was chosen because it is one of the largest available vertical dewar volumes available. The chosen 50 m^3 size will allow for greater than forty hours of refrigeration time. This time window is adequate to cover most power outages, refrigerator performance problems and refrigerator switch-overs.

The refrigeration system operation, illustrated in Figure 2–18, is based on a screw compressor package and coldbox with three turbo expanders. This system is expected to be capable of running continuously for at least a year, and then require only minor servicing. The system will be equipped with automatic controls and a remote monitoring. Estimated maximum power requirement is 522 hp (390 kW), not taking into account the option of power gen-
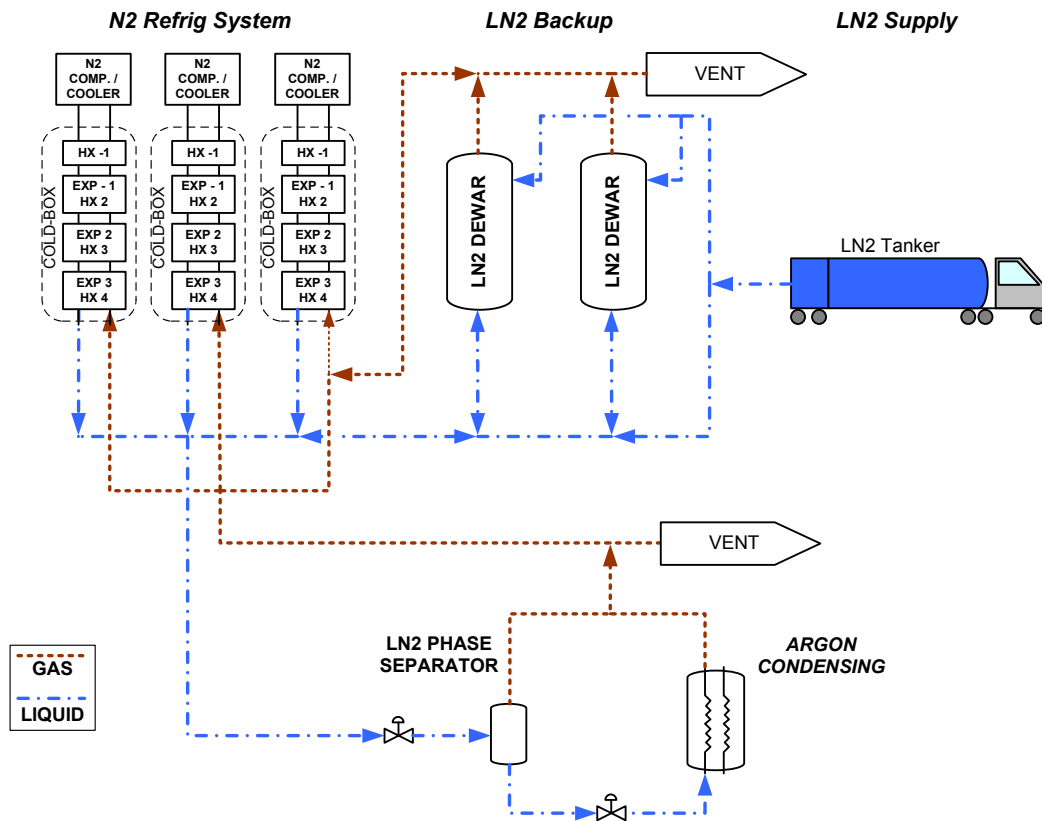
Figure 2–18: Nitrogen refrigeration-plant flow diagram. The nitrogen refrigeration plant consists of 50 m^3 of liquid storage, three cold-boxes, each with four stages of heat exchangers and expanders.

eration with the expanders. The LAr-FD reference design places the nitrogen compressor in a Cryogenics Equipment Building. A closed-loop water system with evaporative-cooling tower removes heat from the compressor. Compression is carried out at close-to-ambient temperature. A compressor aftercooler is provided to reject heat.

The fluid is next routed to a 'cold box' consisting of four heat exchangers. This series of exchangers provides staged heat transfer from a cooling nitrogen stream to a warming one. The expanders are connected between the heat exchangers to progressively reduce the pressure of the cooling nitrogen stream to isentropically reduce the pressure and temperature of the nitrogen stream, eventually leading to a large liquid-nitrogen fraction at the coldest end of the cold box.

The main cold box shell is 1.22 m (4 ft) in diameter and 8.2 m (27 ft) tall. The expanders are adjacent to the cold box at three elevations and extend about 1 m to the side of the cold-box shell. The cold box will weigh 5670 kg. The compressors are located inside the cryogenic equipment building. The compressor skid (frame) is 4.3 m long, 1.8 m wide and 2.7 m tall and will weigh approximately 3630 kg.

2.7.8   Refrigeration Load Scenarios

In order to determine the optimal plant capacity and number of plants required, a plan has been develop which forecasts the LN refrigeration loads and plant capacity needed over seven scenarios. Those scenarios are described below and summary tables taken from Arup Concept Report LAr-FD at 800L are shown in Figure 2–14. The conclusion points to the requirement of three 55-kW plants. Each of these plants can achieve a 20% turn up or turn down thereby allowing a minimum single-plant capacity of 66 kW. Scenario 4 imposes the most severe requirement. In this scenario, all three plants will be required to operate at a duty cycle of approximately 59%. This scenario includes one completely filled and purified cryostat while the second is being purified and requiring frequent filter filteration.

Scenario 1 The initial operation will be the purging, cooling and filling of the first cryostat. The surface LAr and LN dewars will be operational and the cooling load for the dewars will come directly from the refrigeration plant. The pipework and vessels will be cold, the LAr in the cryostat will be circulating at high flow rate through the purification plant, and the cryostat will be cold. Both recondensers on the cryostat being filled will be in service to remove this heat. The LAr-FD L2 Project has assumed that the cryostat cool-down rate will be governed by the residual capacity of the two recondensers operating at 110% of their rated load where 110% is the absolute maximum GAr which could be recondensed. Each recondenser has been sized to accommodate the long-term refrigeration load associated with the cryostat. As the LAr is circulated to achieve the operational purity the filtration plant will need to be regularly regenerated. This will mean that the associated refrigeration load will normally be present.

Scenario 2 Once the first cryostat is filled with LAr the cool-down load will reduce to zero and the cryogenic plant will run for several months purifying the LAr inventory.

Scenario 3 When the LAr in the cryostat reaches the required purity level, the circulation flow rate will be reduced and the detector electronics will be turned on. At this stage the recondenser refrigeration load falls such that only one recondenser is required and the second unit can operate as a spare unit.

Scenario 4 The first cryostat continues to operate in normal experimental mode while the second cryostat is being purged, cooled down and filled with LAr.

Scenario 5 The second cryostat is full and LAr is circulated at high flowrate through the purification plant. The first cryostat continues to operate as normally.

Scenario 6 Both cryostats are operating in normal experimental mode. A spare recondenser is available on each cryostat to facilitate maintenance.

Scenario 7 It is assumed that a total failure of the refrigeration plant has occurred. All non-critical heat sources are isolated and liquid nitrogen from the LN dewars is utilized to recondense the inventory of high purity LAr. When the liquid nitrogen reservoir is exhausted an additional supply will be required or the high purity argon will need to be vented. In the locked-down state the circulation pumps and the purification plants are shut down.

2.8   Prototyping Plans

The development of the LAr-FD from conceptual to preliminary design will include a prototyping program. The most significant issue to resolve is whether a membrane cryostat the size of LAr-FD can achieve the required electron-drift lifetime. The Liquid Argon Purity Demonstrator (LAPD), already in progress and discussed in Section 8.3.3, is an off-project prototype being built as part of a development program at Fermilab to study the scaling of LArTPCs to kiloton sizes. In addition, a 35-ton membrane-cryostat prototype, discussed in Section 8.3.7, is being developed as an LBNE effort to confirm, among other things, that at larger scales the required LAr purity can still be achieved. The prototype will be used to repeat the purge process accomplished in the LAPD to confirm that initial evacuation of the cryostat is unnecessary. It will also seek to confirm that an LAr purity level sufficient to enable the required drift times in a membrane cryostat can be achieved.

2.9   ES&H

During all phases of LAr-FD and the proposed protoypes, Fermilab ES&H standards and SURF ES&H codes and standards will guide the design, procurement and installation phases

of the project. Particular attention will be paid to critical sections of FESHM Chapter 5000 [19] relating to ODH, standards for piping construction and vessel design. The planned work process will provide for reviews throughout all phases of the project to guarantee stringent adherence to the safety requirements. Requirements on the membrane-cryostat materials and their fabrication will be strictly outlined in the specification documents. Close communication between the vendors, Fermilab's cryogenic and process engineers, and Fermilab and SURF ES&H personnel will be maintained at all times.

3   Time Projection Chamber and Electronics (WBS 130.05.04)

The scope of the Time Projection Chamber (TPC) subsystem includes the design, procurement, fabrication, testing, delivery and installation of the mechanical components of the TPC:

- anode plane assemblies

- cathode plane assemblies

- field cage

and the high voltage system connected to the cathode planes. This chapter describes the reference design for the TPC that meets the required performance for charge collection in the LBNE liquid argon detector, LAr-FD.

3.1   Introduction

The Time Projection Chamber (TPC), with its integrated front-end readout readout electronics (described in Chapter 4, and its embedded photon detectors (described in Chapter 6, are the active detector elements of LAr-FD. The TPC is located inside the cryostat vessel and is completely submerged in liquid argon at 87 K. The TPC consists of alternating anode plane assemblies (APAs) and cathode plane assemblies (CPAs), with field-cage panels enclosing the four open sides between the anode and cathode planes. A uniform electric field is created in volume between the anode and cathode planes. A charged particle traversing this volume leaves a trail of ionization. The electrons drift toward the anode plane, which is constructed from multple layers of sense wires, inducing electric current signals in the front-end electronic circuits connected to the wires.

The TPC subsystem interfaces with the following subsystems:

- Cryostat and Cryogenics provides mechanical anchors to support the TPC

- Cold Electronics are directly installed into the APAs

- DAQ controls and monitors the HV power supplies

- Photon Detectors are directly installed into the APAs

- Installation assembles all TPC components inside the cryostat

The TPC's active volume (Figure 3–1) is 14 m high, 13.9 m wide and 25.3 m long in the beam direction. This large volume can be visualized as being constructed from a 3D array of TPC cells. Each TPC Cell (outlined in the upper left in Figure 3–1) has one double sided APA in the middle, two CPAs on each side with a 2.3-m anode-cathode separation. Both APAs and CPAs are 2.5 m wide (in the beam direction) and 7 m high. Each TPC cell operates as an independent detector. It occupies an active volume of 4.6 m × 7 m × 2.5 m, or 112 tons of LAr mass. Sixty such TPC cells stack together (2 high, 3 wide and 10 deep) to form the entire TPC.

Each cryostat houses a total of 60 APAs and 80 CPAs. Each facing pair of cathode and anode rows are surrounded by a "field cage," assembled from panels of FR-4 sheets with parallel copper strips connected to resistive divider networks.

On each APA, four planes of wires cover each side of a frame (the "wire frame"). See Figure 3–2. The inner three planes of wires are oriented, going from the inside out: vertically, and at $\sim \pm 45°$ to the vertical, respectively. Each wire is connected to a front-end readout channel. These three planes of sense wires provide redundancy against the occasional dead channels and ensure reliable 2D position reconstruction regardless of track angles. The wires on the outermost plane are oriented vertically. They shield the inner sense wires and are not connected to the readout electronics. At a nominal wire pitch (center-to-center separation) of 4.5 mm, the total number of readout channels in an APA is 2560, for a total of 153,600 in each cryostat.

3.2 Design Considerations

The requirements for the TPC can be found in the requirements documentation [13]. The most significant ones are the following:

- Provide the means to detect charged particles in the detector and transmit the detector signals to the Data Acquisition System (DAQ)
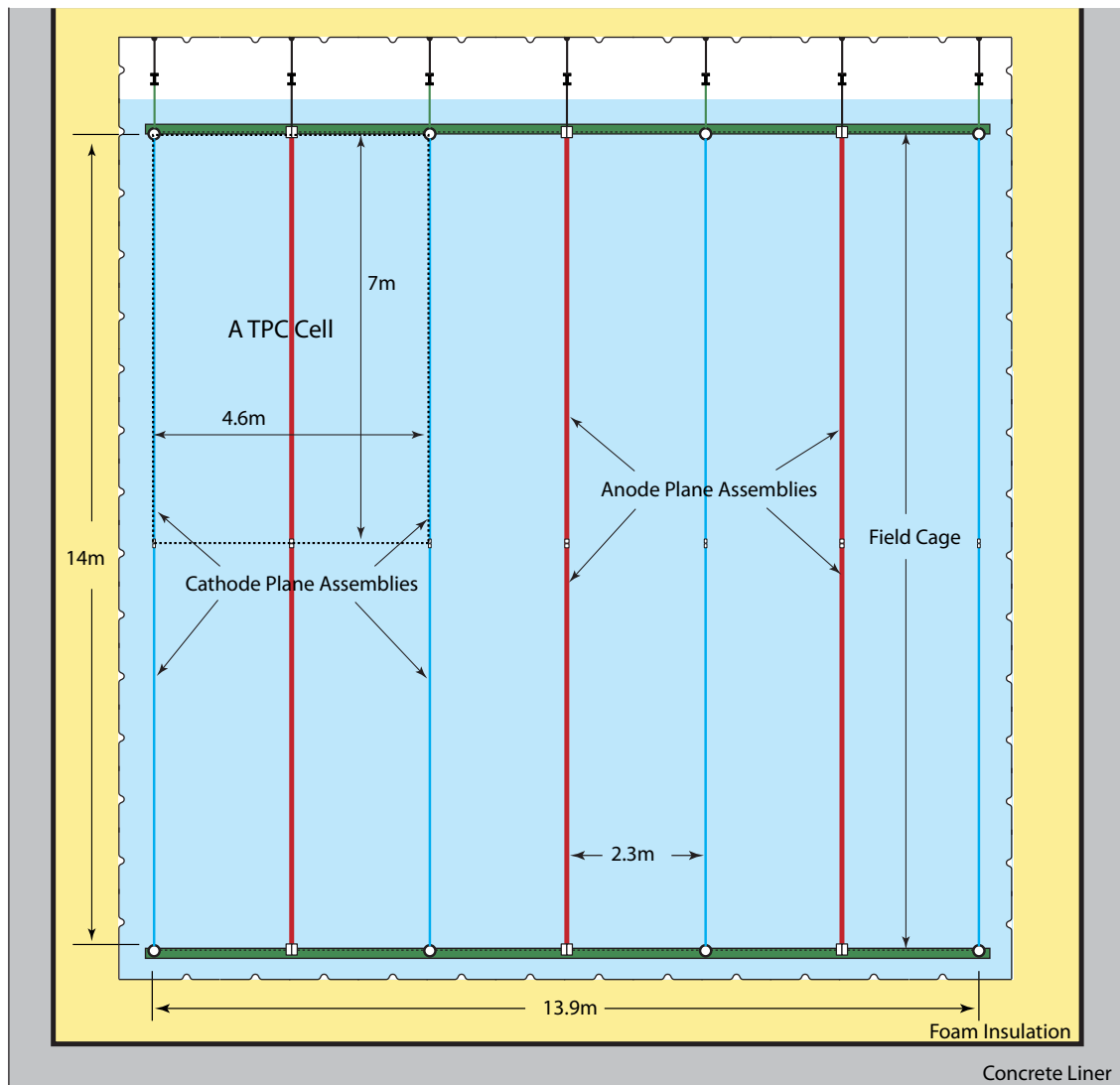
Figure 3–1: Cross section of the TPC inside the cryostat. The length of the TPC is 25.3 m, along the direction of the neutrino beam (into the paper).
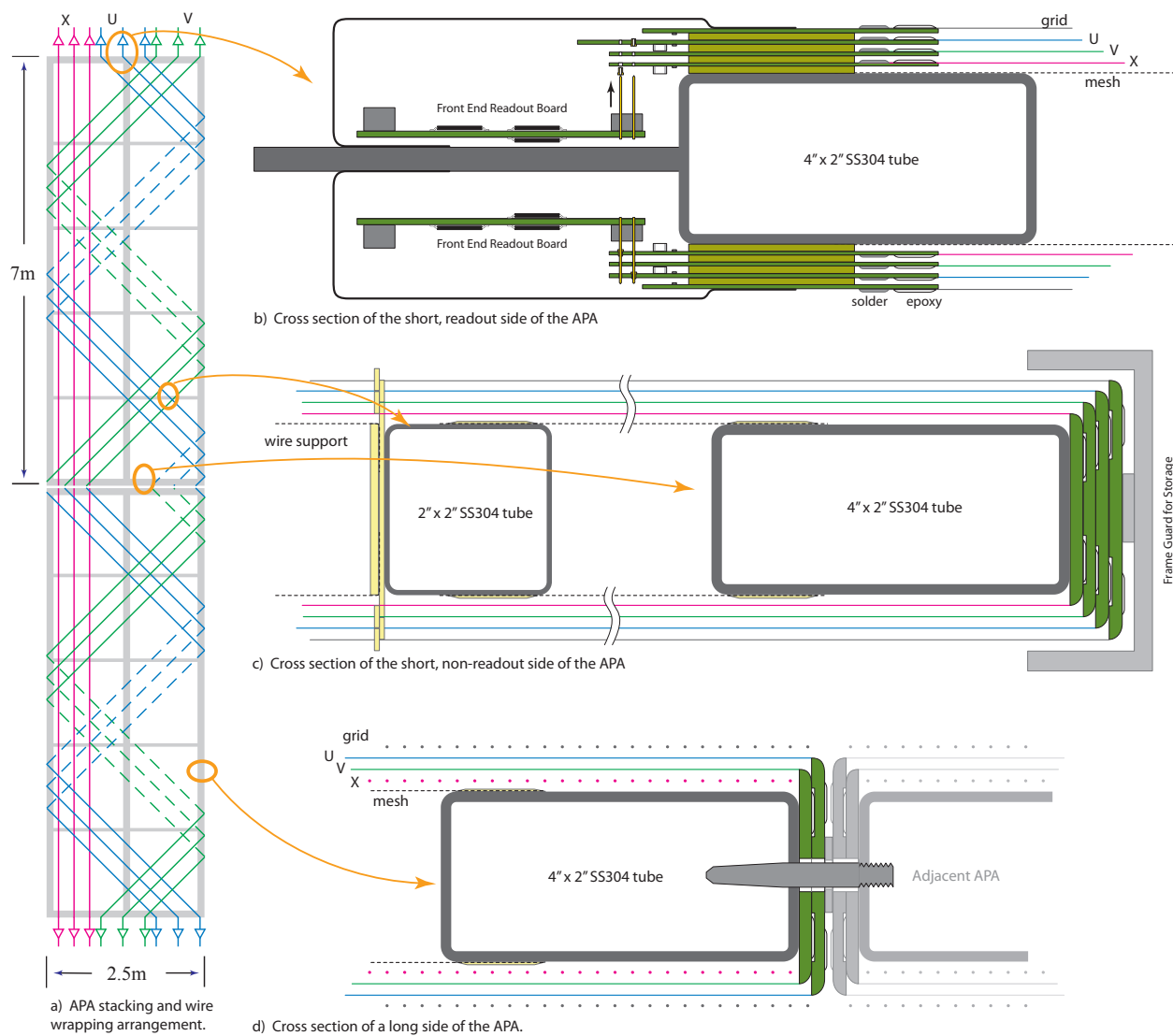
Figure 3–2: Illustration of the APA wire wrapping scheme, and three cross sectional views.

- Meet the physics requirement for electron/photon discrimination; the TPC wire spacing will be < 5 mm

- Limit variation in the wire sag to < 0.5 mm such that it does not significantly impact the position and energy resolution of the detector

- Provide redundancy in the discrimination of electrons from photon conversions and ensure long-term reliability over the life of the experiment; configuration will use three instrumented wire planes

- Optimize the measurement of high-energy and low-energy tracks from accelerator-neutrino interactions; the wire-plane orientation is optimized for neutrinos in the LBNE energy range

- Enable the detector to distinguish a Minimum Ionizing Particle (MIP) from noise with a signal-to-noise ratio > 9:1

- Enable the detector to measure the ionization up to 15 times that of a MIP particle; this is necessary to perform particle identification of stopping kaons from proton decay, a goal to pursue in case the opportunity arises to locate the detector deep underground

- Use only materials that are compatible with high-purity liquid argon

3.3   Anode Plane Assemblies (WBS 130.05.04.02)

The APAs are 2.5 m wide, 7 m long, and ~ 9 cm thick. The 7-m length is chosen to limit the maximum wire length to 10 m (which caps the input capacitance to the preamps to $\sim$200 pF) at a 45° wire angle, and the 2.5-m width is set to fit in a standard HiCube container for storage and transport. Each APA is constructed from a framework of light-weight, stainless-steel rectangular tubing, with four layers of wires wrapped over both sides of the frame. The front-end electronics boards are mounted on one end of the wire frame and protected by a metal enclosure.

3.3.1   Wires

The wires used in the TPC must provide:

- High break load to withstand the applied tension

- Good conductivity to minimize noise contribution to the front-end electronics

- Comparable thermal-expansion coefficient to that of the stainless-steel frame to avoid tension change after cool-down

Both stainless-steel and copper-beryllium (CuBe) wires are potential candidates. Stainless steel was the choice of ICARUS, while a copper-plated stainless-steel wire was chosen by MicroBooNE (to reduce resistance). Both experiments use a wire-termination technique that is labor-intensive and impractical for LAr-FD. Previous experience from FNAL [20] has shown that a CuBe wire under tension can be reliably bonded to a copper-clad G10/FR4 (glass epoxy material) surface by a combination of epoxy (mechanical bonding) and solder (electrical connection). This bonding technique greatly simplifies the electrical connection to the readout electronics and it can be easily automated with commercial equipments (soldering and adhesive dispensing robots). Therefore CuBe wire is selected as the reference design wire of choice.

At 150 μm diameter, the breaking tension of a hardened CuBe wire is $\sim$30 N. To ensure no wire breakage in the TPC, e.g. during cryostat cool-down, the nominal operating tension of the wire will be set at 5 N. Periodic support structures on the wire frame will limit the unsupported wire length to less than 2 m, resulting in less than 0.2 mm deflection due to gravitational or electrostatic forces. Wire ends will be glued and soldered (if electrical connection is needed) onto printed circuit boards attached to the wire frame.

3.3.2   Wire Planes

Four planes of wires are installed on each side of an APA as shown in Figure 3–2. A nominal wire pitch of 4.5 mm is selected to meet the position resolution and signal-to-noise ratio requirement. The distance between wire planes is set to 4.8 mm (3/16 in) to use standard printed circuit board thickness, while maintaining optimal signal formation. These four planes (along the direction of electron drift) are labeled as: the *grid plane*, the *first induction plane* (U), the *second induction plane* (V), and the *collection plane* (X). The wires on the grid and the collection planes are vertically oriented, while the two induction planes are oriented at $\sim \pm 45°$ to the vertical. This wire layout is shown to be the best for reconstructing beam-neutrino events [10]. The wires on the grid plane are not connected to the readout electronics; they shield the first induction wire plane from being influenced by distant ionizations. The four wire planes will be electrically biased so that electrons from an ionizing-particle track completely drift past the first three planes and are collected by the fourth plane. Calculations show that the minimum bias voltages needed to achieve this goal are $V_G = -665$V, $V_U = -370$V, $V_V = 0$V and $V_X = 820$V respectively. It is convenient to set one of the wire planes to ground so that the wires can be DC coupled to the front-end readout electronics. In this instance, the V wire plane is set to ground potential to reduce the maximum bias voltages on the other wire planes, and enable the use of lower voltage rated AC coupling capacitors. A grounded mesh plane, located 4.8 mm behind the collection plane, prevents the electric field around this set of wires from being distorted by the metal frame structure and the wires on the opposite side of the frame. It also shields the sensing wires from potential EM interferences from the photon detectors mounted within the frame. The mesh should have a wire pitch less than 2 mm to ensure a uniform electric field while

maintaining a high optical transparency. Figure 3–3 shows the electric potential distribution near the APA frame with the wire planes biased with the appropriate voltages.
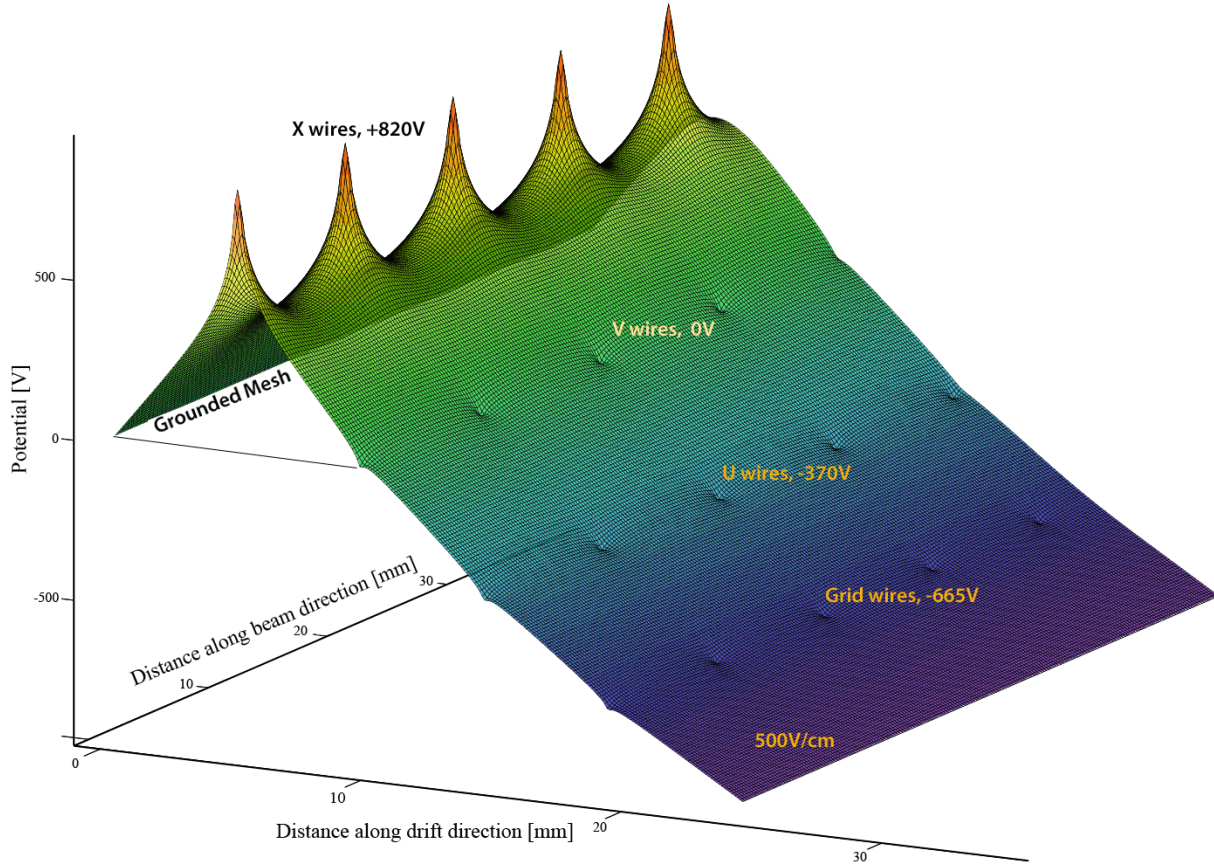
Figure 3–3: A surface plot of the electric potential distribution near the wire planes. The voltages on the wire planes are biased to provide complete electron transparency through the first three planes, and complete collection on the fourth plane.

The wires on the two induction planes (U & V) are wrapped in a helical pattern around the long edges of the wire frame (Figure 3–2a). This technique makes it possible to place readout electronics only at one short edge of a wire frame, enabling joining the APAs on the other three sides with minimal dead space. It slightly complicates the track reconstruction because the U & V wires are sensitive to tracks on both sides of the APA. The upper APAs in the cryostat will have their readouts at the top edge of the frame (as shown in Figure 3–2), while the lower APAs will mount their electronics at the bottom edge.

If the wire angles of the U & V planes are equal to 45°, both wires wrap around the frame one complete cycle, covering a 5-m height, then repeat the same pattern for another 2 m. An ambiguity problem arises when wire pattern of all three sensing planes in the top 2-m section is identical to that in the bottom 2-m section. The detector will not be able to tell if a track is in the top or the bottom section of an APA (see Figure 3–4). To resolve this ambiguity, the wire angles of U & V planes are set slightly differently: $45° \pm \delta$, such that the
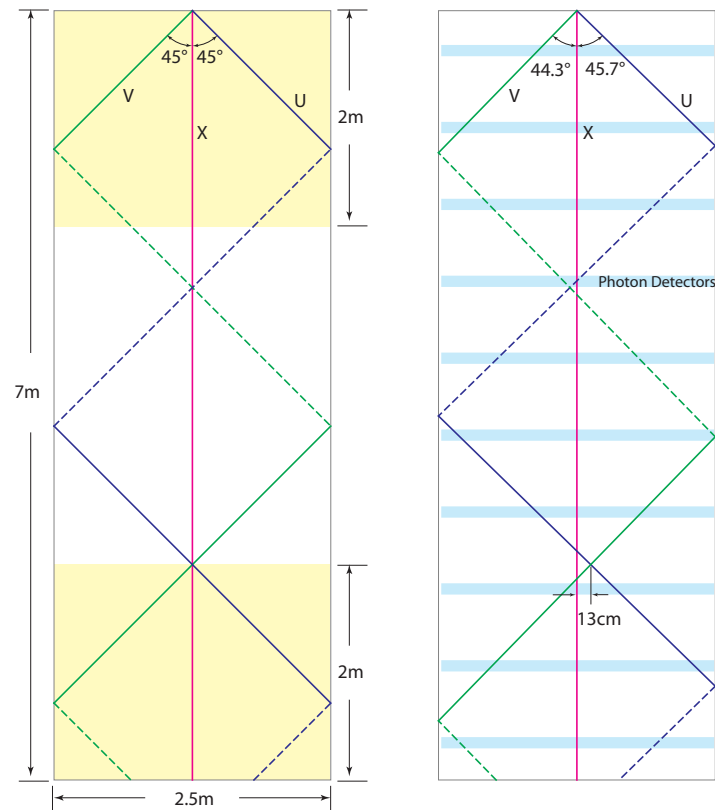
Figure 3–4: Left: illustration of the ambiguity problem if the U & V wire angles are equal; Right: slightly changing the wire angles and photo detectors help to resolve the problem.

same three wires do not cross again. In addition, the multiple photon detectors embedded in the APA frame will help to identify the vertical location of an ionizing track.

The angles and pitches of the U & V wires are chosen such that (1) a modularity of 128 channels forms at the readout end of the APA, with the X wire pitch at 4.5mm; (2) a modularity on the side wrapping boards forms with a module length similar to that of the readout board. The current configuration has the U wires at 45.7° from vertical, at a 4.9-mm pitch, while the V wires at 44.3° from vertical, and 5.0-mm pitch.

The APA readout electronics are divided into 20 identical modules. Each module covers 128 readout wires, consisting of 56 X, 36 U and 36 V wires. These 128 readout wires span a width of 252 mm. Using this modularity, the APA's active width is set to 2520 mm. There are 1120 X wires, 720 U wires, 720 V wires, and 1120 grid wires for each APA. The total number of readout channels is 2560 per APA. The total number of wires per APA is 3680.
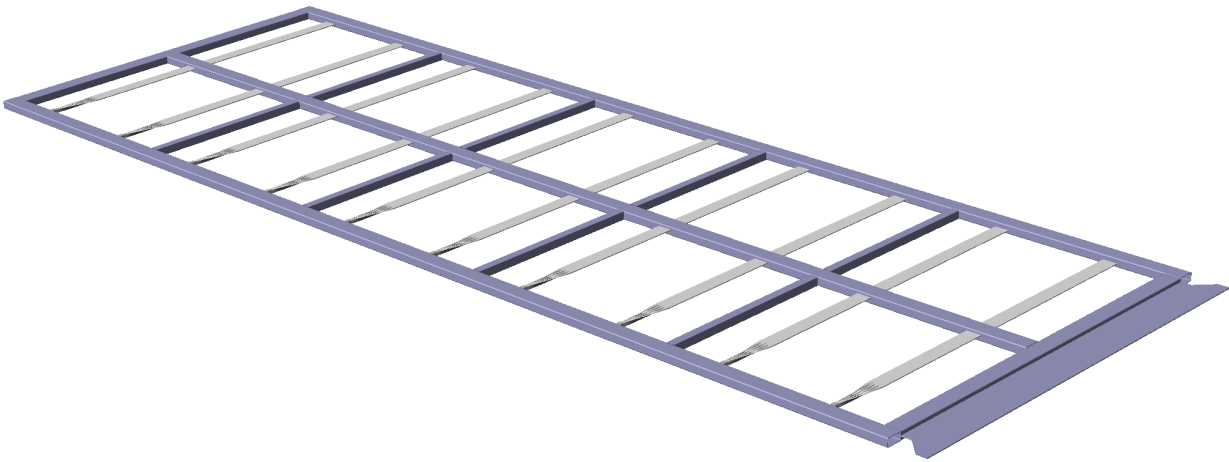
Figure 3–5: Conceptual design of a wire frame (shown without wires). The photon detectors are shown installed on the APA frame.

3.3.3   APA Frame

At a nominal wire tension of 5 N, the 3680 wires exert a force of $\sim$ 6.4 kN/m on the short edges of the APA, and a $\sim$ 2 kN/m force on the long edges. The wire frame must be able to withstand the wire tension with a minimal distortion, while minimizing the thickness of the frame to reduce the resulting dead space. A conceptual design of the wire frame is shown in Figure 3–5. It is constructed from all stainless-steel tubes welded in a jig. Finite element analysis has shown that the maximum distortion of the frame due to wire tension is under 0.5 mm. The total mass of a frame is $\sim$ 250 kg. All hollow members of the frame are vented to prevent the creation of trapped volumes. The two long outer members of the frame are open-ended, so that signal and power cables can be threaded through them to reach the readout end of the lower APA.

3.3.4   Wire Wrapping Around an APA

Figure 3–2b-d shows three major cross sections of an APA. The top figure is the cross section of the readout end of an APA. The four planes of wires are attached to their respective wire-bonding boards through a combination of epoxy and solder. Figure 3–6 shows both sides of the board for the x wires. The wires are wound on the top surface of the board (left) using a winding machine. The wires are then glued down with a bead of epoxy at the leading edge of the board. After the epoxy has cured, the wires are soldered onto the copper pads under each wire, and the wires are cut beyond the pads. On the bottom of this board, the copper traces connect the wires to the bias voltage supply through an RC network. The resistors in this network have values about 20 MΩ, such that in the event that a wire from a different plane breaks and is shorted to these wires, the bias voltages on the rest of the wires will not be affected. The AC-coupled signals from the wires are connected to sockets that will mate with the front-end readout boards.
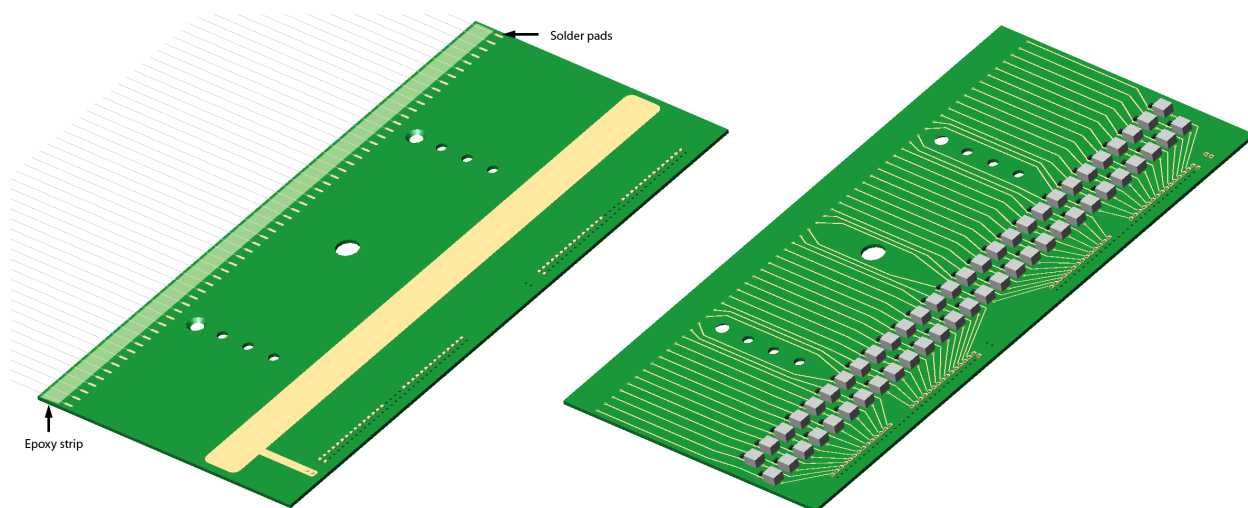
Figure 3–6: Conceptual design of a wire bonding board for the x wires. Left: An array of wires are glued on the leading edge of the top surface, and then soldered onto the soldering pads; Right: the bottom side of the board has the RC network for the bias voltage.

Similar boards for the U & V planes are aligned and stacked above the X boards. An array of pins on the front-end readout boards is pushed through the mating through-hole sockets on the stack of wire bonding boards, making electrical connection between the readout electronics and the matching wires (Fig.3–7). These readout boards, as described in Chapter 4, process the analog signals from the wires and transmit the digital information through feedthroughs to the DAQ system outside the cryostat. The electronics on the readout boards dissipate an estimated ∼40 W of heat per APA and may generate a small quantity of argon bubbles. Two stainless-steel covers are placed over the readout boards to contain the bubbles and direct them to the gas volume of the cryostat. In the case of the lower APAs, the bubbles, if not already re-condensed, will be funneled through the vertical hollow frame members to the top of the cryostat.

U top board

V top board

X top board

Front-end Readout Board
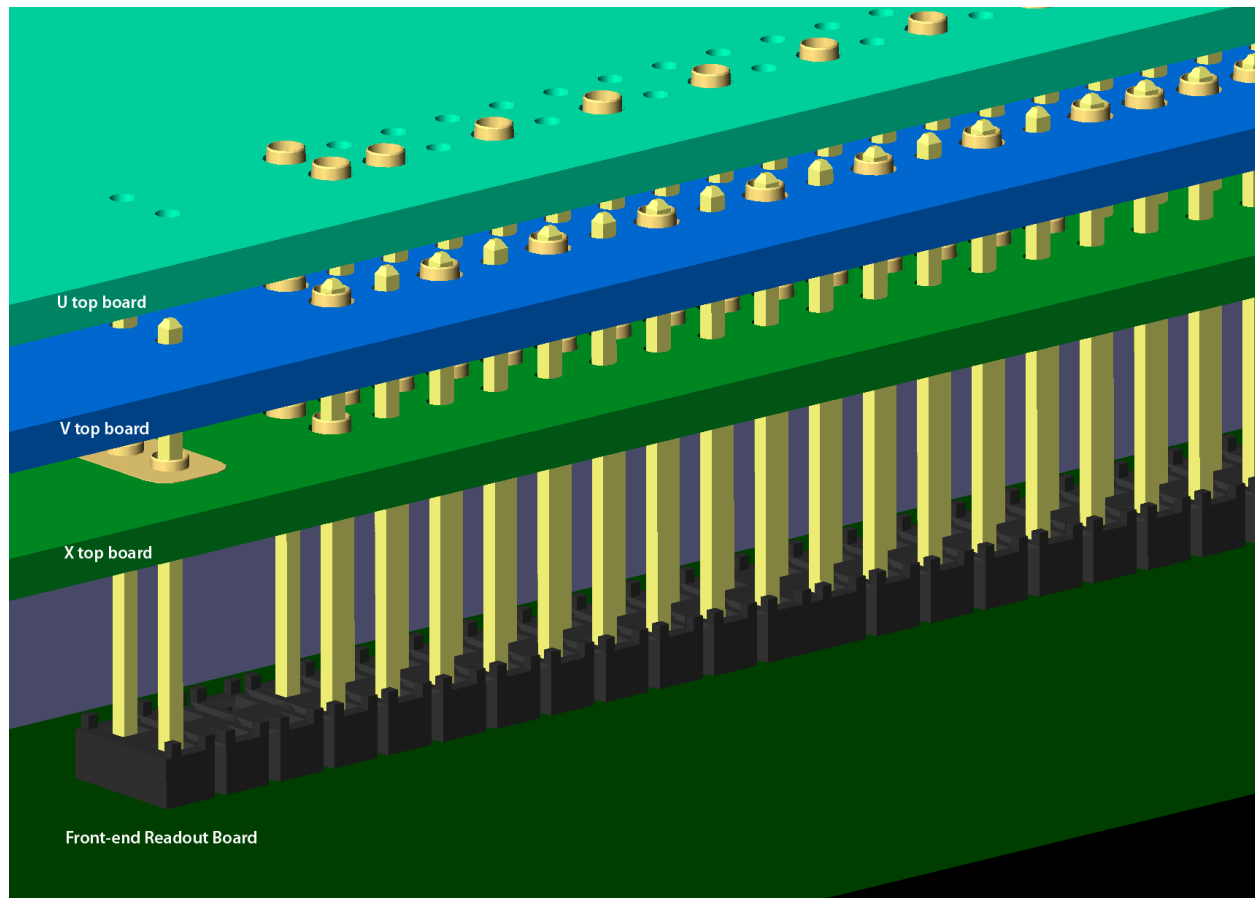
Figure 3–7: Conceptual design detail of the interconnect between the three wire bonding boards and the front-end readout board. A similar technique is used in MicroBooNE to connect the wire carrier boards and the preamp motherboards.

Figure 3–2c shows the cross section of the short, non-readout end of an APA. All wires are mechanically terminated on this end on the four layers of wire-wrapping boards. No electrical connections are needed.

Figure 3–2d shows the cross section of a long edge of an APA. Only two layers (U & V) of wire wrapping boards are needed here. The wire-wrapping boards are made from printed circuit boards, shown in Figure 3–8. The boards are attached to the APA frame, and then a winding machine wraps a wire around the APA in a helical fashion, placing the wire into the grooves on the edges of each board. After winding, the wires are glued down to the wire-wrapping boards near the grooved edges. To clear the mounting holes on the board, a few wires are soldered onto the copper pads, and cut, leaving the copper traces to bridge the connection.

Figure 3–9 is a closeup view of a corner of an APA frame with some wires and various wire bonding boards to demonstrate the assembly.

After the grid plane wires are placed on the APA, metal guards are placed along the three wrapped edges of an APA. These guards protect the fragile wires during APA handling, storage and transport.
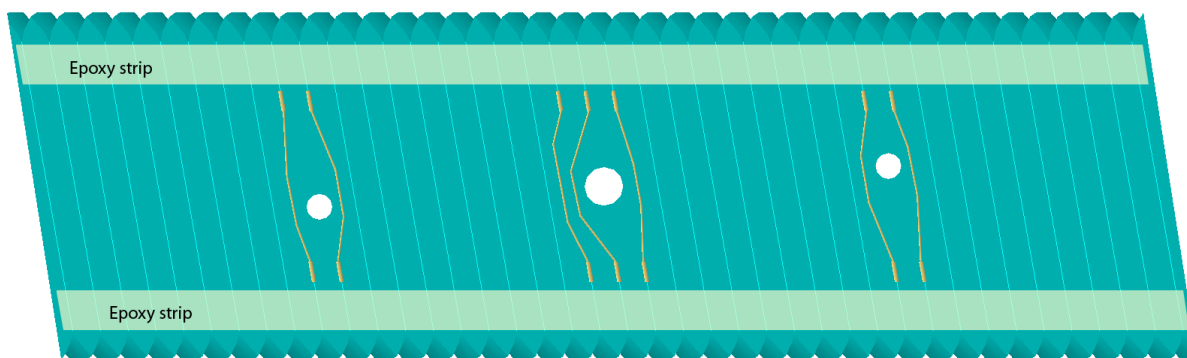
Figure 3–8: Conceptual design of a wire wrapping board for the U wires on a long edge of an APA. The light cyan colored lines represent the wires wrapped over the board surface. Some wires near the mounting holes must be soldered to the copper traces and then cut.

3.3.5   Wire Supports on Inner Frame Members

The left of Figure 3–2b also shows the wire-support structure mounted on one of the inner horizontal frame members. A detailed rendering of this concept is illustrated in Figure 3–10. The support structure is composed of strips of thin fiberglass boards, with notches machined at specific intervals. The support strips for X plane is directly mounted on the inner frame members. After all X wires have been placed into the slits, the V support strip (shown in
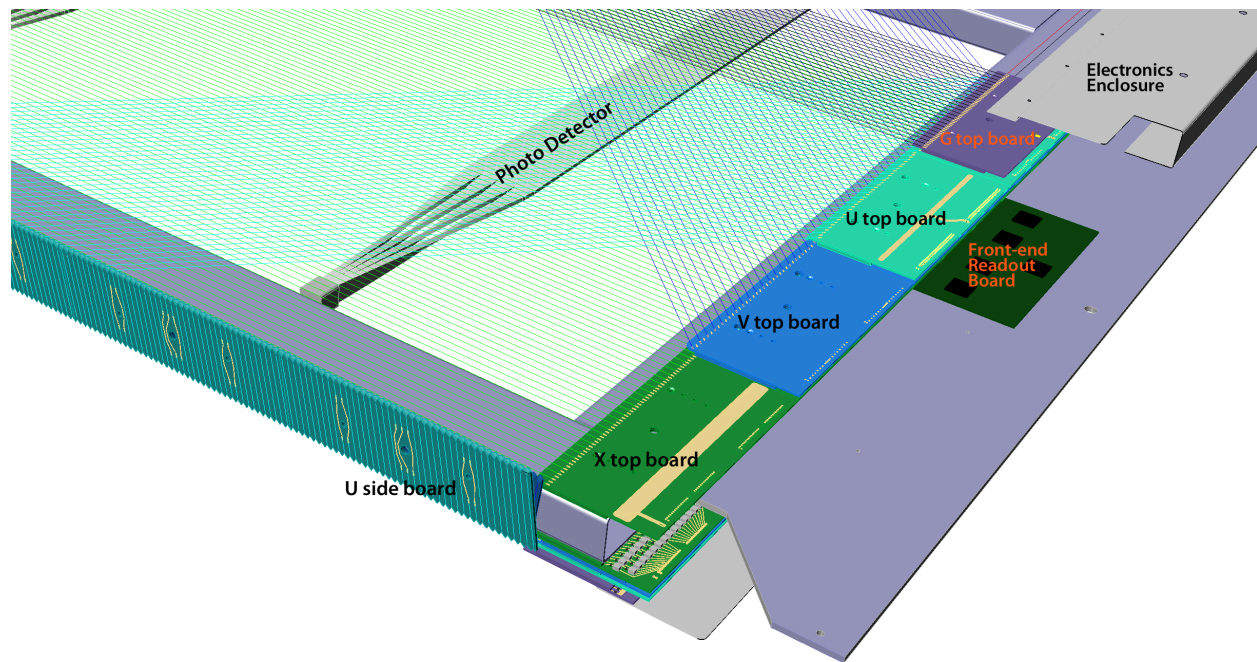
Figure 3–9: A closeup view of a partially assembled corner of an APA. For clarity, only every other wire is shown in this illustration.

green) is glued onto the tips of the X strips, trapping the X wires in position. After the V wire are placed into the slits, the U support strip (identical to the V strip) is glued to the V strip, trapping the V wires. These structures are repeated four times along the 7-m length of an APA, limiting the unsupported wire length on any wire plane to < 2 m, while introducing only millimeter-scale dead regions. These wire supports play a key role in minimizing wire deflection due to gravity and electrostatic force, enabling the use of a moderate wire tension and reducing the risk of wire breakage. They also help to maintain the proper wire plane spacing in frames with minor warps. In the unlikely event of a broken wire, the wire supports will also reduce the risk of the loose wire touching the high voltage cathode plane.

3.3.6   Wire-Winding Machines

Two winding machines will be constructed to lay the 3680 wires on each APA. Their working concepts are illustrated in Figure 3–11. For the X and the grid wire planes, (left figure), the wire frame will be standing on one of its long edges, while a wire is wrapped around the frame using a commercial 3-axis gantry robot. A wire-tension controller maintains the wire tension and feed rate of the wire off the spool. Although the entire plane of wires can be wound in one pass, a more fault-tolerant procedure is to pause the winding machine periodically and solder the last wire onto the frame. This intermediate soldering step will prevent the unraveling of a large section due to an accidental broken wire. The winding machine for the U & V planes will wrap a group of wires (~ 10) as a band in each pass. An automatic soldering robot will
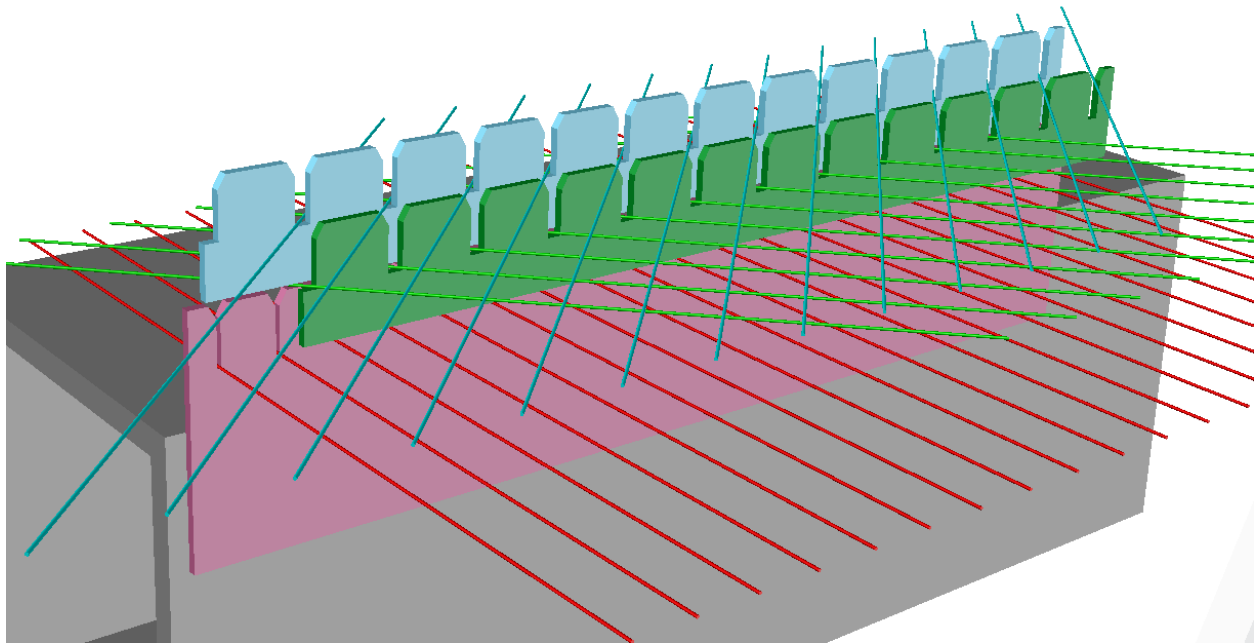
Figure 3–10: Conceptual design of the wire support for the U, V & X wires. Similar structures will be used to support the grid wire plane.
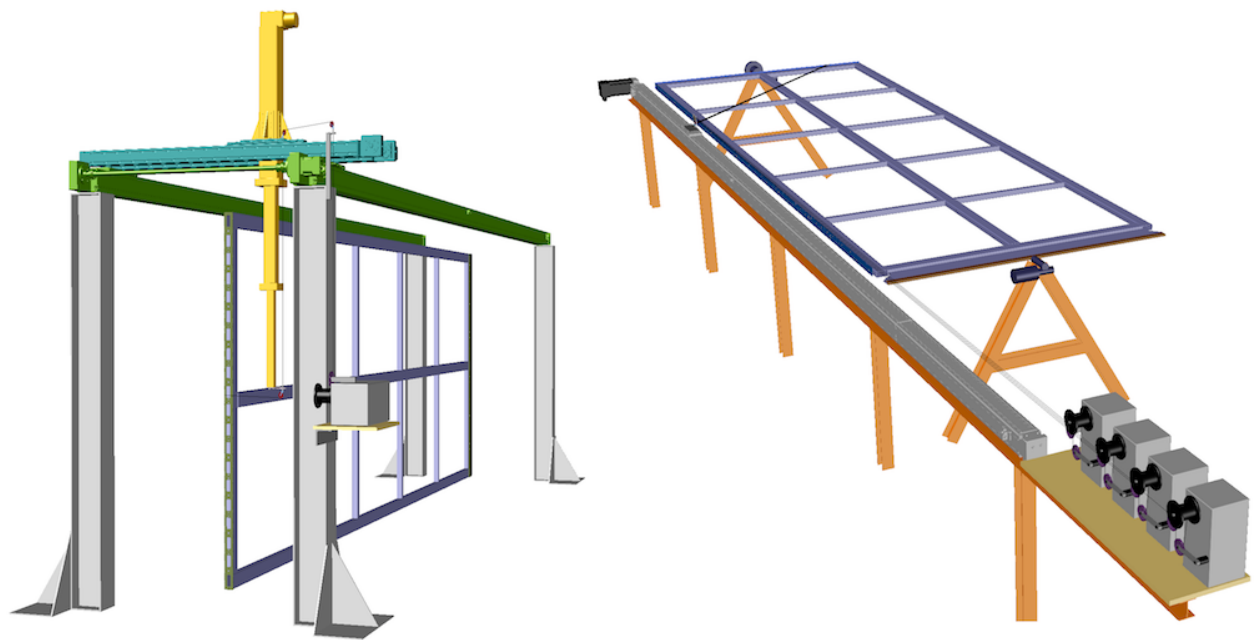
Figure 3–11: Two winding machine concepts. The left figure is for the X and grid wires. The right figure is for the U & V wires.

solder the wire ends after the group of wires has been laid down on one side of the frame. A wire-tension measuring device will scan the newly placed wires and record the wire tension of each wire. Any wires with abnormal tension will be replaced manually.

3.4   Alternative APA Construction

The APA design described above requires two customized machines capable of placing wires directly on the 2.5 m × 7 m APA frame with a precision of the order of 1 mm. Cleaning the solder flux off the APA after wire bonding also poses a challenge on an object this size. An alternate APA design is under development to alleviate these difficulties. In this design, the APA frame dimensions and the wire geometry remain approximately the same, but the wires are attached to the APA frame in a two-step process.

The first step is to bond a group of wires (∼64) with epoxy and solder on two FR-4 boards to form a wire module. The second step is to mount all the assembled wire modules onto an APA frame using a stretching table. The wire lengths in each wire module are determined in such a way that when a module is mounted on the frame, all wires will reach a uniform tension of 5 N. Jumper cables interconnect the corresponding U or V wire modules along the two long edges of an APA to complete the helical wire wrapping pattern electrically. The assembly of an APA frame using prefabricated modules will be easier and faster than direct winding on the big frame. If a wire is broken while being attached to the frame, it is relatively straightforward to replace the affected wire module. The details of APA assembly are shown in Figure 3–12.
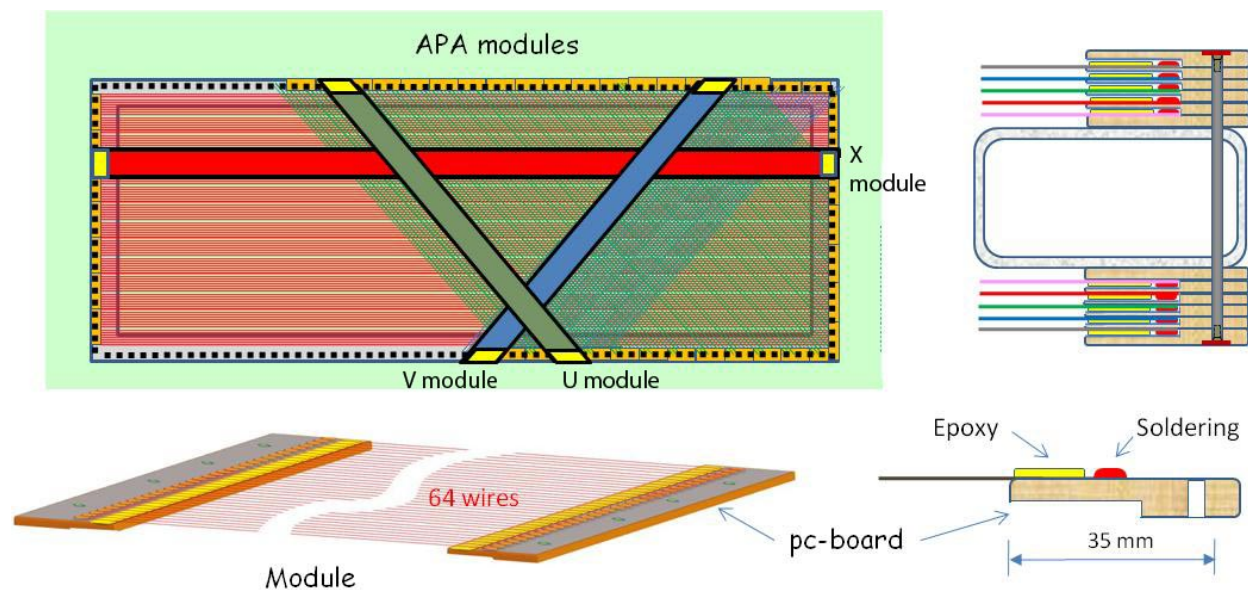
Figure 3–12: Concept of the alternative APA wiring scheme using pre-assembled wire modules

One major drawback of this alternative design is a relatively large dead space between any APA joints ($\sim 2 \times 35$ mm) due to the FR-4 board size. The electric field in the drift region directly above the FR4 boards will have some irregularities, causing minor distortion to the track trajectories. To eliminate these problems, additional special wire modules could be placed over the dead region at the APA edges. For example, a module with two layers of 18 wires ($\sim$90 mm wide) would completely cover the FR-4 boards between two APA frames. The upper layer wires maintain the uniform drift field, collect the electrons, and provide the X position information, just like the regular X readout wires. The obtained X coordinates and charge information partially restore the detector sensitivity at the APA joints. The scheme with additional wire modules is shown in Figure 3–13.
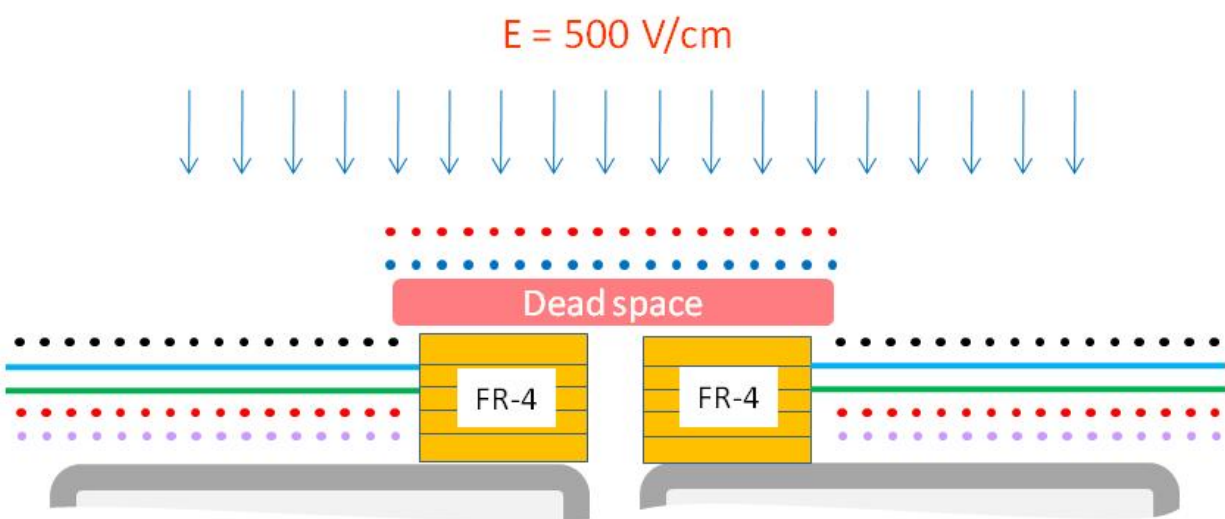
Figure 3–13: Illustration of dead space above FR-4 boards for alternative APA design, and possible solution with installation of two additional wire planes above.

Using the wire geometry shown in Figure 3–13 the bias voltages for wire planes have been defined and electric field strength calculated in 2D. The calculation confirmed that the drift field above the FR-4 boards is uniform, and full collection of electrons can be achieved on the additional wire modules. From past experience, the electric field is not expected to change very much in a 3D simulation. Nevertheless, it is necessary to develop a full 3D model for more accurate field calculations and simulation of electron drift in real APA geometry.

One of the advantages of this alternative design is the modularity of wire planes that will simplify the wire placement and APA assembly. The winding procedure becomes simple and reliable and a simple winding machine with replaceable wheels is required. The module production could be done at several sites to accelerate the APA assembly schedule. The completed modules will be cleaned in an ultrasonic bath, dried in a vacuum oven and stored in dry air. A set of tests will be performed to ensure that modules meet the technical specifications. The winding scheme for module fabrication is presented in Figure 3–14.
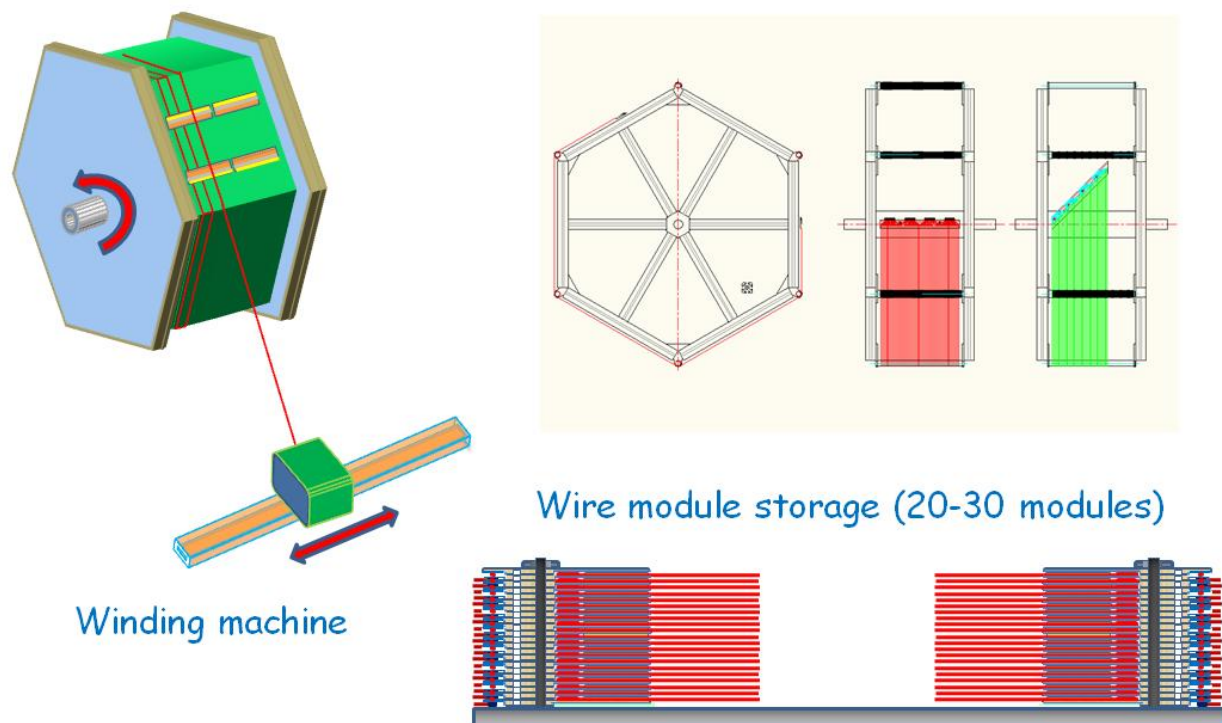
Figure 3–14: Conceptual designs of the alternative APA wire winding machine and wire module storage fixture. Upper left: the fabrication of the wire modules are accomplished by attaching the wire module boards on to a large drum with specific circumference, and laying the wires over the boards at a constant pitch. Upper right: placement of the wire module boards for the X and grid wires (red), and U, V wires (green). Bottom: completed wire modules are stacked on a storage fixture.

For the assembly of the wire modules onto APA frames, a special assembly table will be used. The table will allow frame rotation in order to allow access to both sides of an APA frame. A special movable, stretching mechanism will be mounted on the table edge for installation of wire modules. After assembly of each plane the final wire tension and wire spacing will be measured. If some wires' tension or spacing are out of specifications, their corresponding wire modules will be replaced. A schematic design of a wire-stretching table is shown in Figure 3–15.
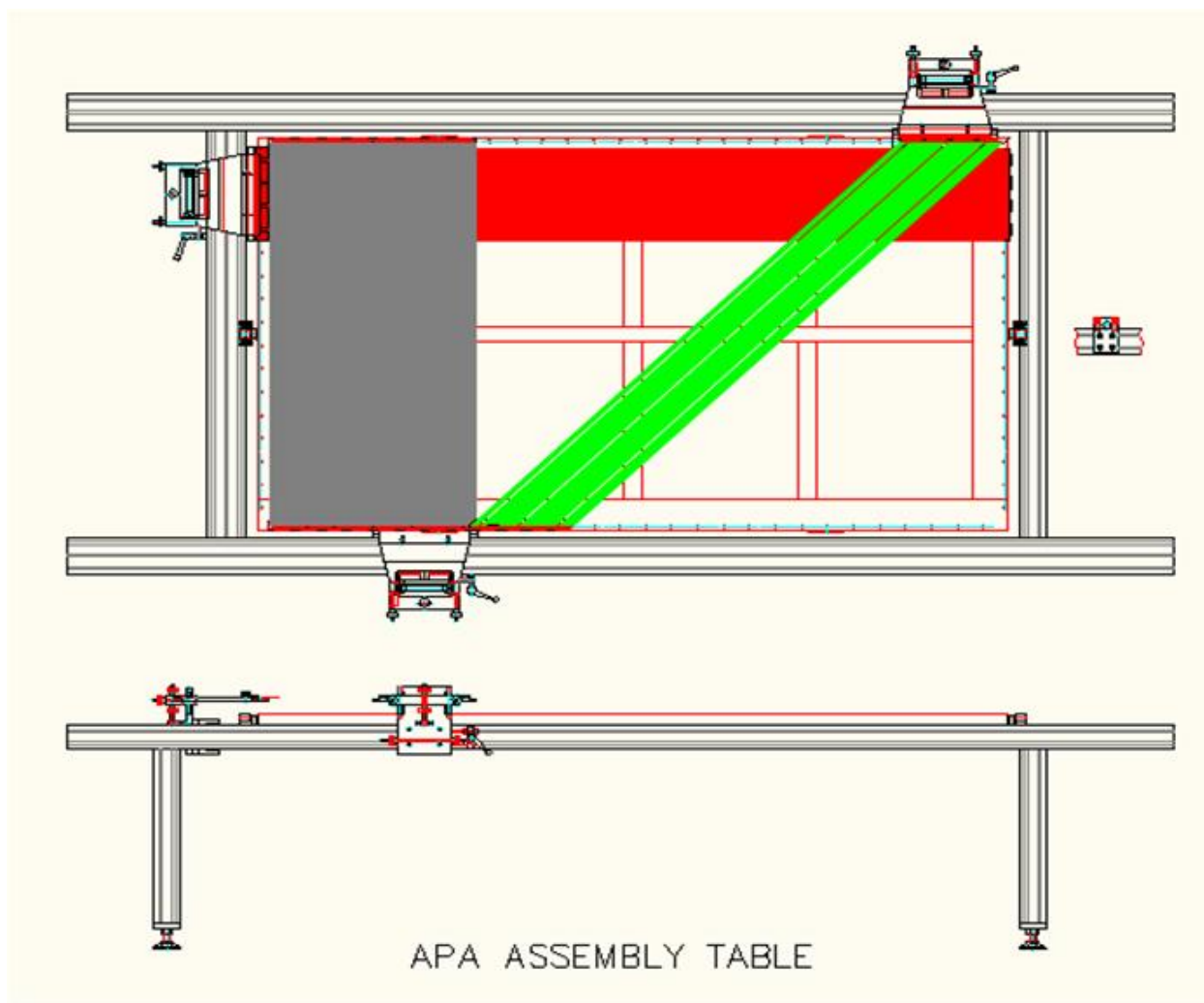
Figure 3–15: Assembly table with equipment for stretching wires (alternative APA design)

Demonstration modules of both the reference APA design (Section 3.3) and this alternative design are being constructed. They will be evaluated to determine which design will move forward in the preliminary design phase. ^{bo:}The cost estimate for the APA design and construction is based on the reference design.

3.5 Cathode Plane Assemblies (WBS 130.05.04.04)

The cathode plane assemblies (CPAs) have similar dimensions to the APAs, 2.5 m wide and 7 m high. Each CPA is made of a stainless-steel framework, with a layer of conductive material stretched over one side of the frame. To reduce drift-field distortion, all surfaces that rise significantly above the mesh, including the stainless-steel frame structure on the other side of the mesh, are covered with field-shaping electrodes biased at appropriate voltages. Figure 3–16 illustrates the concept of the CPA.

Due to the relatively high cosmic ray flux in the surface detector, it is preferable to prevent the scintillation light emitted by a cosmic ray in one drift volume from entering another through the cathode plane. The cathode plane, either wire mesh or sheet, will be nearly opaque to achieve light isolation. The permeability of the cathode surface will be determined by analyzing the LAr flow pattern in the cryostat. Preliminary CFD analysis [21] have shown that solid cathodes in the cryostat result in LAr flow pattern that neither causes excess positive ion buildup, nor degrades the LAr purity.
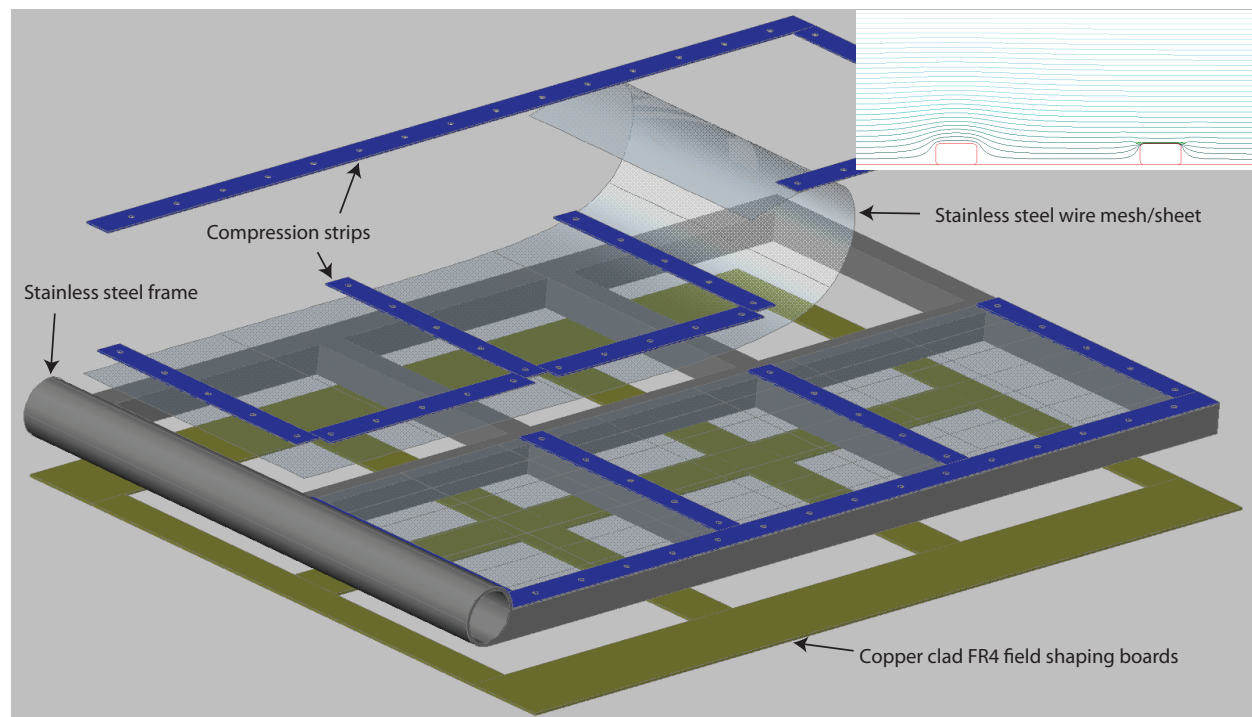
Figure 3–16: Conceptual design of a cathode plane assembly (not to scale). The assembly is 2.5 m wide and 7 m tall, similar to the APAs. The inset illustrates the field uniformity near two cathode frame members with (right) and without (left) the field shaping boards.

To achieve a 500 V/cm drift field over a 2.3-m distance, the bias voltage on the cathode plane must reach −115 kV. The reference design calls for four high-voltage (HV) power supplies, one for each CPA row in the cryostat. Further partitioning of the CPA row and

the field cages is being considered to reduce the loss of active volume in the event of HV failure inside the cryostat. For example, an eight-zone configuration will require that a gap of several centimeters be maintained in the middle of each CPA row and field cage. Failure to maintain HV in one zone will result in the loss of no more than 20% of the active volume.

3.6   Field Cage (WBS 130.05.04.05)

Each pair of facing cathode and anode rows forms an electron-drift region. A field cage completely surrounds the four open sides of this region to provide the necessary boundary conditions to ensure a uniform electric field within, unaffected by the presence of the cryostat walls.
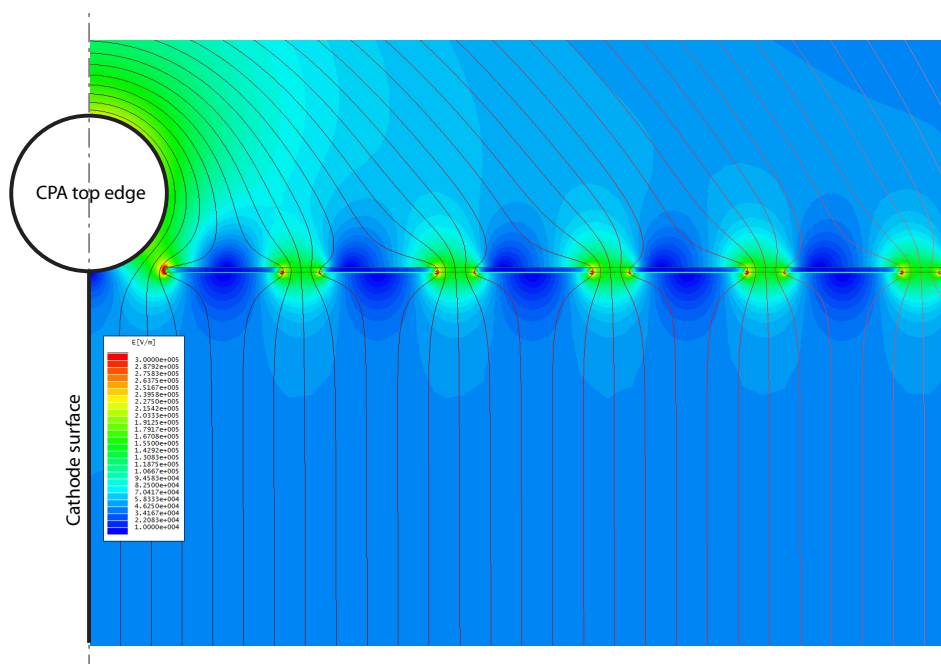
Figure 3–17: Electrostatic simulation of the electric field near a section of the field cage. The filled color contours represent the electric field strength. The line contours represent the electric potential at 500 V intervals. The pitch of the electrodes is 5 cm in this model.

The entire TPC requires ~ 1100 m^2 of field cage material. The field cages are constructed using copper-clad FR4 sheets reinforced with fiber glass I-beams to form panels of 2.5 m $\times$ 2.3 m in size. Parallel copper strips are etched/machined on the FR4 sheets. Strips are biased at appropriate voltages provided by a resistive-divider network. These strips will create a linear electric-potential gradient in the LAr, ensuring a uniform drift field in the TPC's active volume. Figure 3–17 shows the results from an electrostatic simulation of a particular strip

pattern. The drift-field non-uniformity quickly drops below 1%, roughly a strip pitch away from the field-cage surface. Since the field cage completely encloses the TPC drift region on four (of six) sides, the FR4 sheets must be frequently perforated to allow natural convection of the liquid argon. The "transparency" of the perforation will be determined by a detailed LAr computerized fluid dynamic (CFD) study.

The resistor-divider network will be soldered directly onto the field-cage panels. Multiple resistors will be connected in parallel between any two taps of the divider, in order to provide fault tolerance. The resistance between taps is of the order of 1 GΩ. One end of the divider chain is connected directly to the cathode, while the other end is connected to ground at the APA through resistors of the appropriate value.

3.7   TPC Assembly in the Cryostat
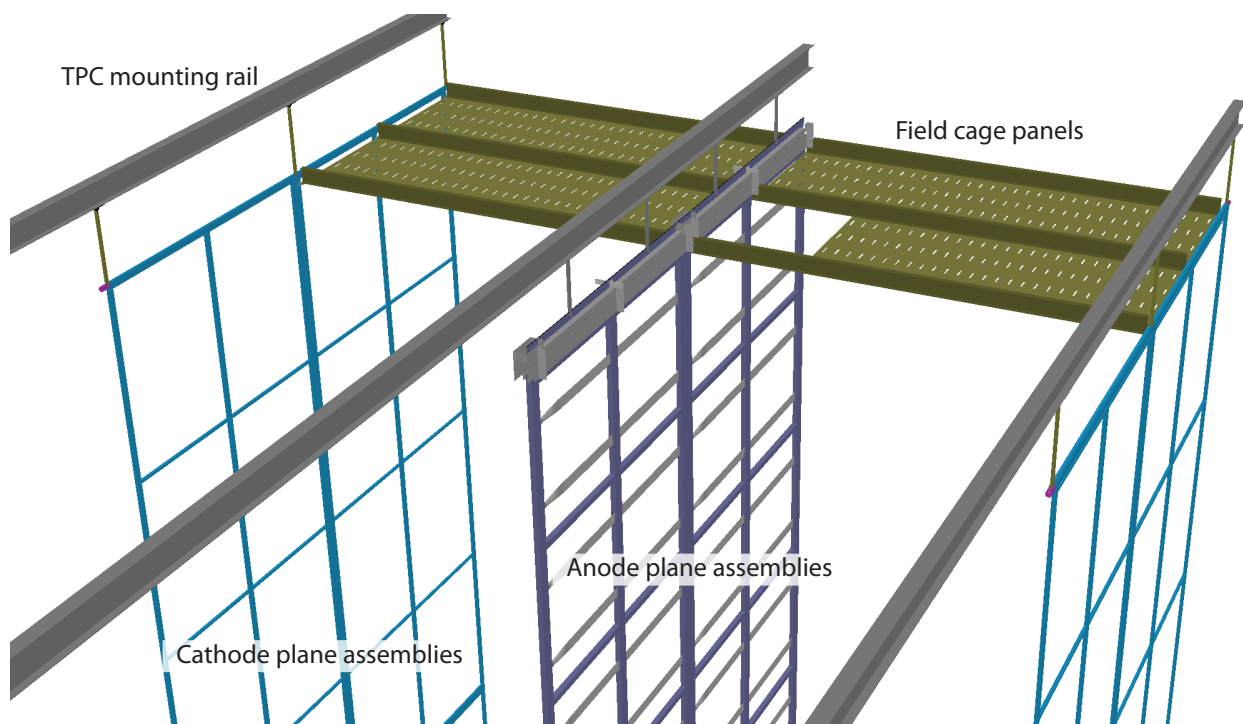
Figure 3–18: A partial assembly of the TPC showing all major components

Figure 3–18 shows a partial assembly of a section of the TPC. The finished cryostat has seven rows of anchor points distributed along the ceiling (not shown in the figure). A mounting rail is suspended through stainless-steel rods to each row of the anchor points. Under these seven mounting rails, rows of CPAs and APAs are suspended in an interleaved fashion. Because the cathodes are at a high voltage, the CPAs are attached to their mounting rails through G10 rods. The distance between the facing anode and cathode is maintained by

the pultruded fiberglass I-beams holding the FR4 sheets forming the field cage. The TPC installation procedure is discussed in Chapter 7.

3.8 Cathode High-Voltage System

The cathode high-voltage system consists of high-voltage power supplies, high-voltage cables and filtering networks, and the high-voltage feedthroughs.

3.8.1 Design Considerations

*anne:*The system must be designed to supply adequate current, control the voltage ramp rate and keep from introducing unacceptable noise. It will need to operate in a cold environment.

- The power supplies for the TPC cathode planes must be able to provide 150 kV at 1 mA current.

- The filtering network must ensure the output voltage ripple at the cathode surface must not introduce more than 10% of the equivalent thermal noise from the front-end electronics.

- The power supplies must be programmable to trip (shutdown) their output at a certain current limit. During power on and off, including output loss (for any reason), the voltage ramp rate at the feedthrough must be controllable to prevent damage to the in-vessel electronics through excess charge injection.

- High-voltage feedthroughs must be able to withstand -250 kV in 1 atm air or argon gas environment with their cold tips submerged in liquid argon.

3.8.2 Reference Design

The cathode planes are biased at -115 kV to provide the required 500 V/cm drift field. At a minimum, four high-voltage power supplies, each connecting through its own feedthrough, will be used. Each supply will provide high voltage to one of the four rows of the cathode plane assemblies.

The current candidate for the high-voltage power supplies is the Heinzinger PNC*hp* series, which is used by the ICARUS experiment. Additional filtering of the voltage ripples is done through the intrinsic HV cable capacitance and series resistors. Established techniques and

practices will be implemented to eliminate micro-discharges and minimize unwanted energy transfer in case of an HV breakdown.

To ensure safe and reliable operation, the feedthroughs will be tested at a much higher voltage than expected in routine operation (~ 250 kV) in liquid argon. The feedthroughs will be mounted on the ceiling of the cryostat, their cold ends reaching through the gas ullage space and submerging into the liquid argon. The center conductor on the cold side of a feedthrough will be insulated and shielded by a grounded shroud at least 50 cm below the surface of the LAr. Connections between a feedthrough and a CPA row is made through a specially designed high voltage receptacle attached to the end of a CPA row. A redundant feedthrough will be installed on the opposite end of each CPA row as backup. Figure 3–19 shows an example of a feedthrough made by the UCLA group for the ICARUS experiment, as well as the conceptual design of a feedthrough suitable for the LAr-FD TPCs. Figure 3–20 shows a corner of the cryostat where the feedthrough is connected to a CPA through a HV receptacle.
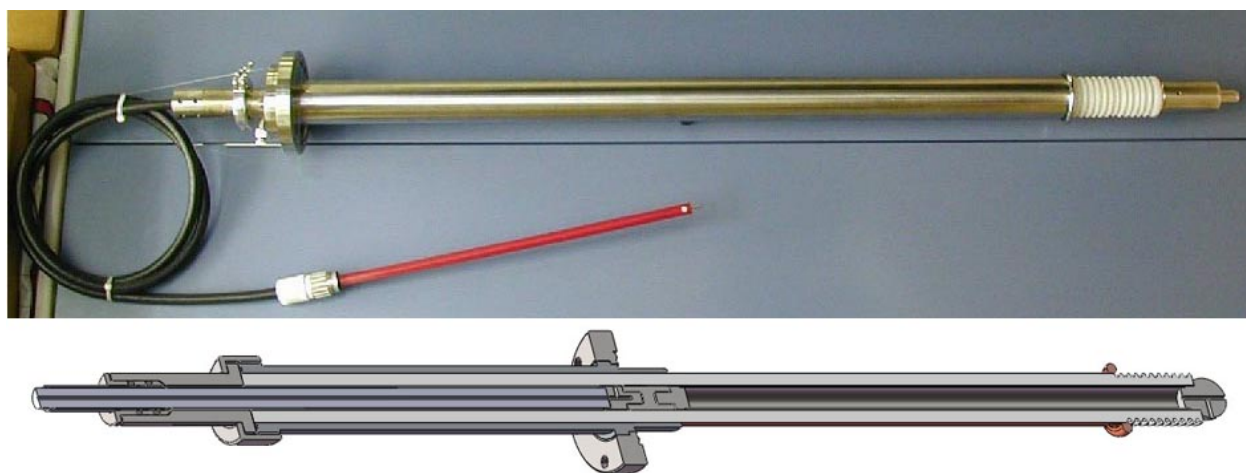
Figure 3–19: Top: A high voltage feedthrough developed by the UCLA group for the Icarus experiment. It was tested up to 150 kV. Bottom: a conceptual design of a new feedthrough for the LAr-FD.

3.9　TPC Prototyping, Test and Checkout

3.9.1　TPC Prototyping

Several prototype TPC modules will be constructed during the design phase. The initial prototypes will be fraction scale or partial models of the APA, CPA and field cage. The CPA prototype will be used to evaluate the wire-mesh tension and field-shaping electrode attachment techniques. The APA prototype will be used to study the placement of the wire-
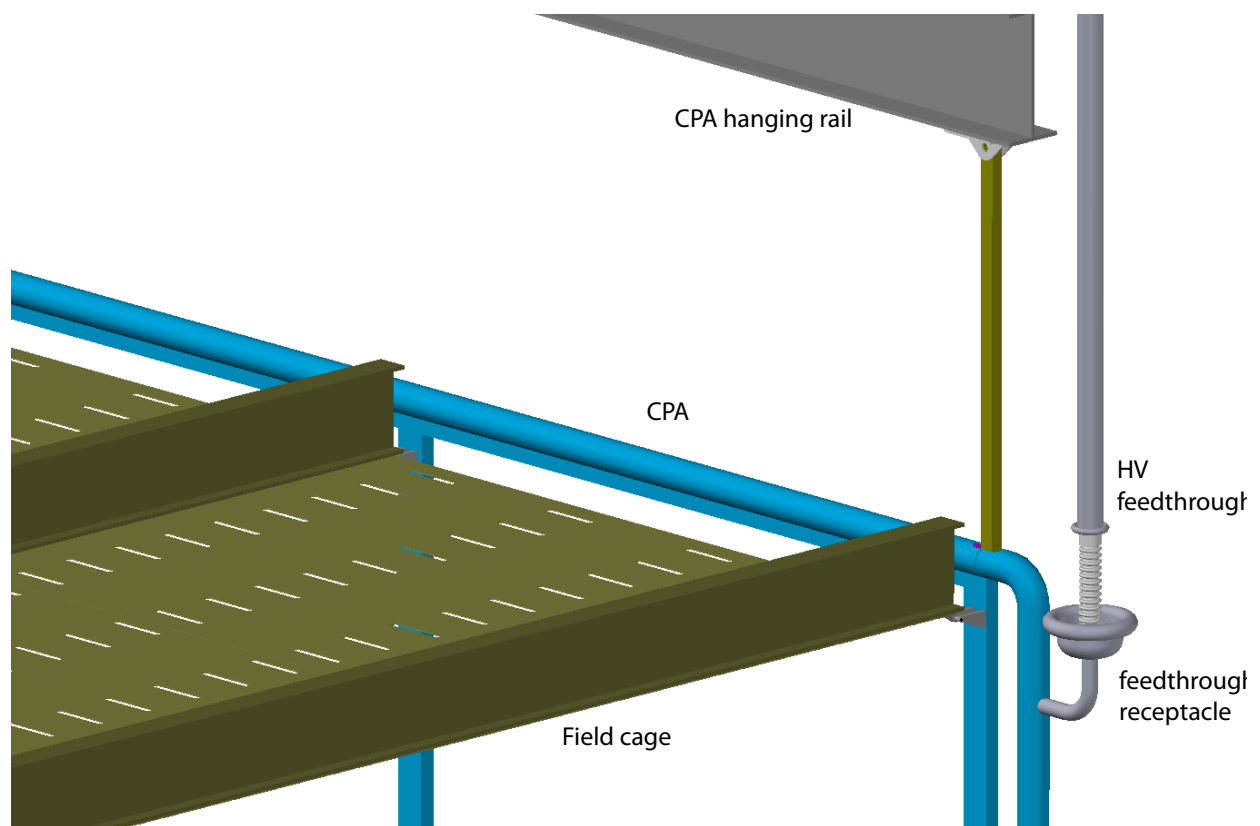
Figure 3–20: A closeup view of a corner of the TPC showing the connection between the HV feedthrough and the CPA

wrapping boards and wire-support structures. It will also be used to develop the prototype winding machines. The prototypes will undergo numerous thermal cycles down to liquid-nitrogen temperature to test the integrity of the wire-to-board and board-to-frame bonds.

These small prototypes, or revised versions of them, are planned to be installed into the 35-ton cryostat as part of its "Phase II" development. See Section 8.3.8 for details.

The final set of prototypes will be the pre-production prototypes. These are full scale APA, CPA and field cage modules using the final design. They will be constructed using pre-production toolings with less automation. These prototypes will be used to validate the final design, evaluate production and testing procedures, refine production cost estimates, and develop installation tooling and procedures.

Every APA will undergo a series of tests as part of the QA process.

- The tension and electrical continuity of each wire will be measured after the plane of wires is bonded to the frame.

- After the front-end electronics boards have been installed on the APA, an initial calibration of all electronic channels will be performed. The electronic gains and noise levels of all channels will be recorded in a database.

- A cool-down stress test will be performed on each completed APA in a liquid-nitrogen environment. Electronic calibration on all channels will be performed while the APA is cold and again after it is warmed up. Significant differences in the cold and warm calibration results will be investigated and rectified.

- The embedded photon detectors will be tested using procedures developed by the photon detection subsystem.

For the CPAs, a cool-down stress test will be performed on each completed CPA in a LN_2 environment. The flatness of the cathode surface will be monitored while cold. Units with excess distortion will be reworked.

For the field cages, the resistance will be measured along each copper strip, and between strip pairs. The resistance between two strips should exceed 50 GΩ in LN_2, without the resistive divider.

3.9.2   Checkout (WBS 130.05.04.07)

The Checkout of the TPC components is a set of testing procedures performed between the completion of the TPC components at the fabrication site, and the final installation of

the TPC inside the cryostat. The detailed testing protocol and equipments of the completed APAs will be developed in a joint effort with the Cold Electronics, DAQ, and Photon Detector subsystems.

These tests will be performed at these points in time:

- At the component assembly site, before the component is to be put into storage $^{bo:}$(part of the fabrication procedures)

- Before the component is shipped to the FD site $^{bo:}$(electronic test of APAs)

- After the component is received at the FD site $^{bo:}$(electronic test of APAs)

- After the component is removed from the storage at FD site and before moving to the Detector Hall.

The following tests are planned for the assembled APAs:

- visual inspection of all wires

- removal of broken wires or wires with very low tension

- inspection of the integrity of the wire support structure and wire wrapping boards

- verification that all fasteners and join mechanisms are tightened

- measurement of the leakage currents on the wire bias terminals

- connection of the readout cables to a mini DAQ station to run electronics calibration to identify bad channel/wire connections

- testing of the photon detectors in a dark enclosure

For the CPA and Field Cage assemblies, the following tests are planned:

- visual inspection of the cathode surface

- verification that all fasteners and join mechanisms are tightened

- removal of any broken wire ends protruding above the wire mesh surface

- a check of the resistivity between the bias electrodes and the frame

- a check of the integrity of the resistors on the field cage

- measurement of the resistivity between each field cage strip

- verification of the electrical connection between the field cage and the cathode, and between the field cage and the attachment mechanism to the APA

In the Detector Hall, further testing procedures of the TPC at component and system level during and after installation are described in detail in Section 7.5.

4   In-Vessel Front-End Electronics (WBS 130.05.08)

The scope of the Vessel Front-End Electronics subsystem includes the design, procurement, fabrication, testing, delivery and installation of the in-vessel electronics, signal and power cables, their feedthroughs, as well as the low- and high-voltage power supplies feeding the electronics. This chapter describes the reference design for the Front-End Electronics that, together with the TPC design, meets the required performance for charge collection in the LBNE liquid argon detector, LAr-FD. The front-end electronics will operate at cryogenic temperatures. This system provides amplification, shaping, zero supression, digitization, buffering and multiplexing of the signals. All functions of the readout chain will be programmable or selectable through a register on the ASICs. The APAs will be self triggering. $^{anne:}$ ~~so that they can accomodate both neutrino-oscillation measurements (which provide a beam trigger), and other measurements which do not, such as proton decay and supernova bursts, that would be important in LBNE Phase 2.~~ The electronics inside the cryostat vessel will be designed to operate continuously, without access, for 20 years.

4.1   Architecture

The large number of readout channels (153,600) required to instrument the LAr-FD TPC dictates the use of CMOS ASICS for the electronics. Requirements of low noise (less than 1000 rms electrons for a wire capacitance of 220 pF) and for achieving extreme purity of the LAr dictate that the front-end electronics be located at the signal wires in the LAr. Close proximity of the electronics and sense wires reduces the signal capacitance and hence the noise. A significant degree of digitized signal multiplexing can then also be used, minimizing the number of cables in the ullage gas and the attendant outgassing of electronegative impurities. This electronics architecture, combined with the modular TPC elements, also leads to a TPC implementation that can be readily scaled to any detector size or geometry.

Figure 4–1 shows the architecture of a front-end electronics design that meets the requirements for the LAr-FD TPC. The entire electronics chain is immersed in the LAr and thus operates at the local argon boiling temperature of approximately 87K. It is composed of a 16-channel front end implemented as a mixed-signal ASIC providing amplification, shap-
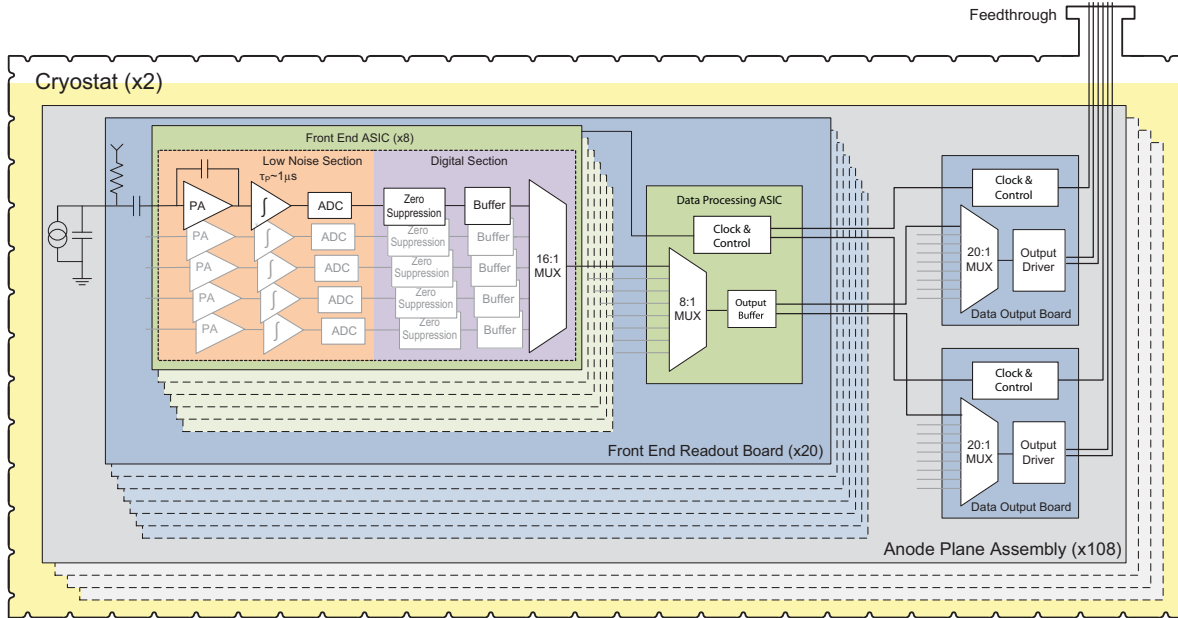
Figure 4–1: Conceptual architecture of the front-end electronics operating in LAr

ing, digitization, buffering, a 16:1 multiplexing stage, a driver and voltage regulators. Eight front-end ASICs plus a single digital ASIC implementing an 8:1 multiplexer, clock and control circuitry comprise a single 128-channel front-end readout board. A third digital ASIC containing a multiplexing stage (20:1) and driver is used for each APA module to serialize all of the data from the 20 readout boards on a single APA (for a total of 2,560 channels per APA) and transmit it out of the cryostat on either a twisted copper pair or an optical fiber. The choice between twisted-pair copper and optical fiber will be postponed until further work is completed to evaluate the long-term reliability of optical drivers at LAr temperature. The data rates per APA are not expected to be high enough to require the use of optical fibers. For either choice, a least a two-fold redundancy per APA will be implemented to minimize the probability of the loss of an entire APA.

Figure 4–2 shows a block diagram of the proposed 16-channel front-end ASIC. Each channel includes a charge amplifier with a selectable gain of 4.7, 7.8, 14 and 25 mV/fC (full scale charge of 55, 100, 180 and 300 fC), a high-order anti-aliasing filter with adjustable time constant (peaking time 0.5, 1, 2, and 3 μs), an option to enable an AC coupling stage, baseline adjustment for operation with either the collecting or the non-collecting wires, a 12-bit 2 MS/s ADC and a zero-suppression/data compression stage. Shared among the 16 channels are the bias circuits, programming registers, a temperature monitor, the digital multiplexer (16:1), an analog buffer for signal monitoring, and the digital interface. A 600-kb buffer will be included in this design, capable of storing a 1.5-ms event sampled at 2 MS/s in each channel assuming no compression. Two or more events can be stored with compression. The layout size is on the order of 10×5 mm^2, which would provide a yield in excess of 90%.

The estimated power dissipation is below 15 mW per channel at 1.8 V supply.
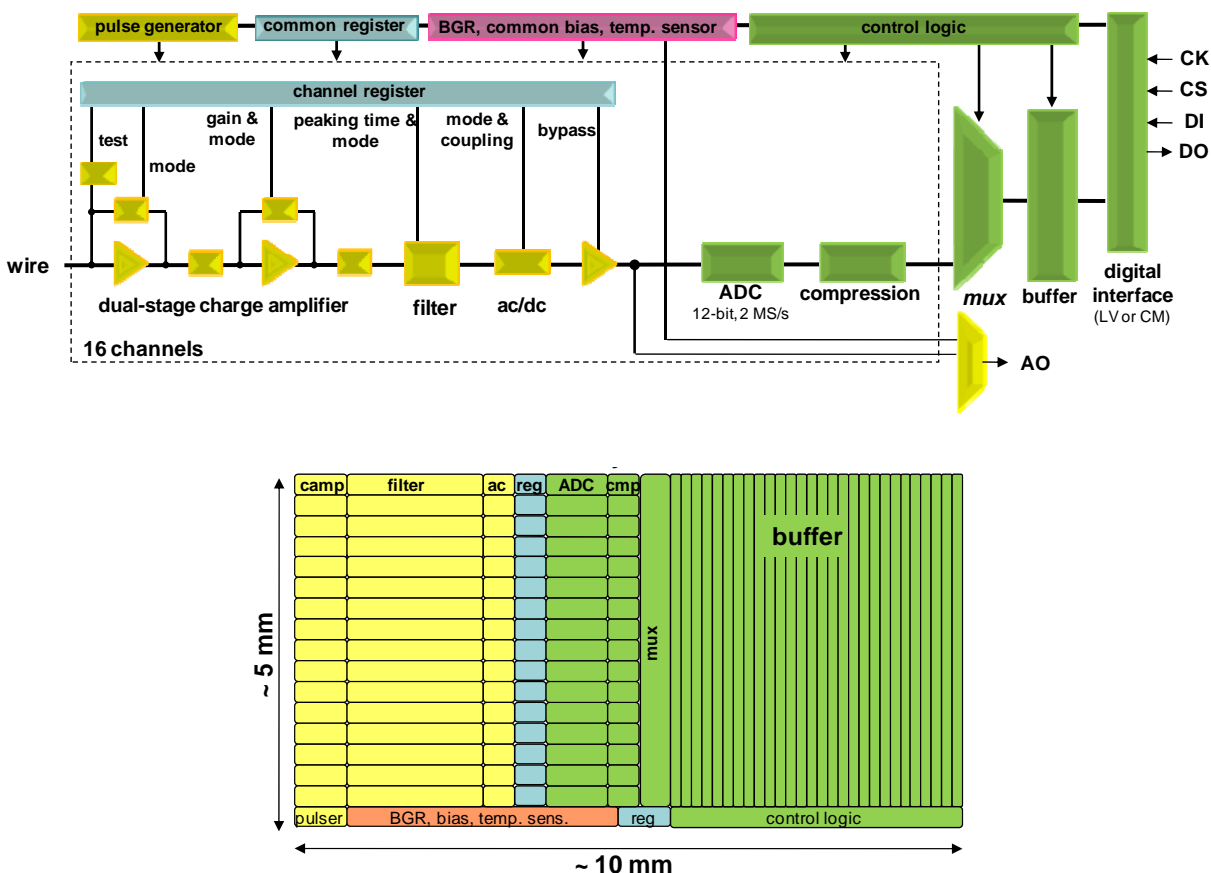
Figure 4–2: Architecture and layout of the 16-channel front-end mixed-signal ASIC

4.2   Data Rates

For neutrino-oscillation measurements the pulsed beam can provide a trigger for readout, but for other measurements, such as proton decay and supernova bursts (if enabled by future scope opportunities), no trigger would be provided. Therefore the APAs will be self triggering.

Data rates for the detector on the surface will be dominated by cosmic muons. In order to reduce the rate (and volume) of recorded data to tolerable values, zero suppression and data buffering must be provided. The simplest scheme is to do this at the APA level, deriving a write-enable from the logic OR of discriminators on all the charge collecting (Y) wires in an APA, and then writing all data to a buffer while the write-enable is true. This mode would still record large volumes of data without useful information, particularly for simple event topologies and from low-energy events (radioactive decays) and noise.

An effective zero-suppression can be implemented at the chip level with a dedicated buffer with a write-enable consisting of the OR of channel with charge above threshold and its nearest neighbors. A few samples before and after the write-enable will also be recorded to capture the below-threshold leading and trailing edges of the signal waveform. Baseline samples would be recorded with reduced range (4 bits) and compacted into full words. This mode provides maximal zero-suppression that is insensitive to localized low-energy events and noise, while still retaining all of the charge in the signal.
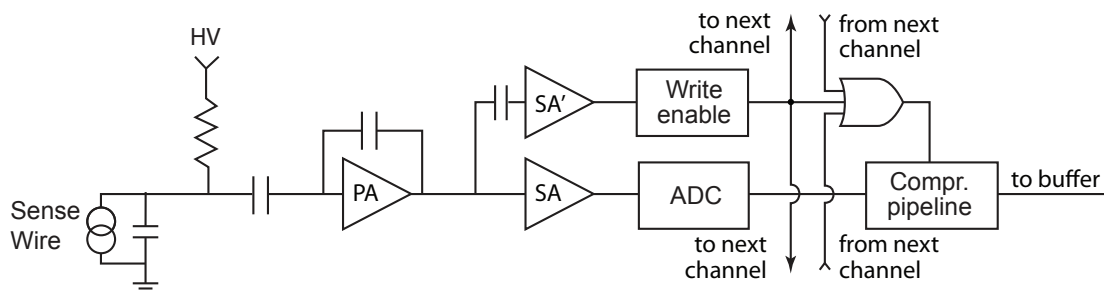
Figure 4–3: Conceptual architecture of zero-suppression using a write enable using separate analog shaping

A conceptual diagram of this zero-suppression implementation is shown in Figure 4–3. The write-enable for each channel is derived from a separate shaping amplifier with AC coupling to remove low-frequency, baseline fluctuations. Multiple programmable discriminators in the "write-enable" logic are needed to sense both unipolar (collection wire) and bipolar (induction wire) waveforms. The write-enable gate passes to, and is OR-ed with, channels of a (programmable) number of adjacent wires to record the below-threshold portion of charge shared with these wires. The "above threshold" signal will pass into and out of the gate logic for the first and last channels of each chip. A channel number and time stamp prepended to each block of contiguous data allows a single common buffers to serve all 16 channels on one chip. The operating parameters of the zero-suppression system will be programmable through a register. An option to disable all suppression will be provided to read signals continuously.

4.3   CMOS Circuit Design

To successfully design CMOS circuits that will operate at cryogenic temperatures, two critical issues must be addressed and resolved. The first is the requirement for realistic models at the operating temperature of active devices, interconnects and passive components (resistors and capacitors) in order to reliably predict operating points, signal response and noise during the design process. The second critical requirement is that the design must ensure a long operational lifetime, since once the TPC is filled with LAr, the detector must operate $^{anne:}$~~for about 20 years~~ without any access to the electronics for repair or replacement. Concerning the

availability of realistic models, our preliminary results from the cryogenic characterization (down to 40 K) of a complete mixed-signal ASIC [22] in a commercial CMOS 0.25 μm technology, originally developed for room-temperature applications, indicates that the models are useful to first order. To refine these models, several single-transistor test structures were fabricated on the first prototype of the 0.18 μm device. Measurements of the properties of these structures at cryogenic temperatures have been used to refine the device models at 87 K.

The lifetime of CMOS circuits is limited by several mechanisms which degrade the performance over time, eventually causing the circuit to fail to perform as specified. The rates of most degradation mechanisms in CMOS, such as electro-migration (EM), stress migration (SM), time-dependent dielectric breakdown (TDDB), thermal cycling (TC), and negative bias-temperature instability (NBTI), all scale with temperature such that cryogenic operation is favored [23][24]. The only mechanism that could affect the lifetime at cryogenic temperature is the degradation due to impact ionization, which causes charge trapping in the MOSFET gate oxide at large drain-current densities (the "Hot Carrier" effect). Results from a CMOS reliability studies in the literature [25] provide general design guidelines (for device geometry, bias and current density) that should guarantee a lifetime well in excess of $^{anne:}$20 years the planned period of detector operations, assuming continuous cryogenic operation. These design guidelines also provide information for designing test conditions to observe the deterioration mechanism and to extrapolate from accelerated deterioration rates, measured under stressed conditions within practical times, to the ultimate lifetime under normal operation.

A monitor of the impact ionization is the bulk current, which reaches a maximum at $V_DS = V_DD$ and at $V_GS = 0.5V_DD$. When operating constantly in this condition at room temperature, a properly designed device will typically have a lifetime (defined as a 10% degradation in g_m) of about 10 years. The bulk current (i.e., the impact ionization) increases by roughly a factor of four from 300 K to 77 K [25] and a circuit designed for operation at room temperature would have a proportionately shorter useful life at cryogenic temperature. As stated above, in order to guarantee the required lifetime at cryogenic temperatures, design guidelines must be modified for both analog and digital circuits. For analog circuits, this is done by operating the devices at moderate-to-low drain current densities, where impact ionization becomes negligible. For digital circuits, operating the devices with reduced V_DD (about 20%) and using non-minimum channel length L, which is easily accommodated since at cryogenic temperature the speed of the digital circuit increases, compensating for the increased L. These guidelines will be verified with accelerated aging tests, at increasing values of V_DD, on dedicated structures. Such tests also will be conducted on prototype samples throughout the development process to verify the long-term reliability of the final ASICs.

The development of the readout ASIC has begun by designing and fabricating in a commercial CMOS process (0.18 μm and 1.8V) a 16-channel ASIC implementing the complete analog front-end section of the scheme shown in Figure 4–2. This process is expected to be available for at least another 10 years. The charge amplifier input MOSFET is a p-channel biased

at 2 mA with a L/W (channel length/width) ratio of 0.27 μm / 10 mm, followed by dual cascade stages. The charge amplification and shaping filter have digitally programmable gain and peaking time as described above. Each channel also implements a high-performance output driver which, in the final version, will be replaced with a sample-and-hold stage preceding the ADC. The ASIC integrates a band-gap reference (BGR) to generate all the internal bias voltages and currents. This guarantees a high stability of the operating point over a wide range of temperatures, including cryogenic. The ASIC is packaged in a commercial, fully encapsulated plastic QFP 80 package.

This ASIC has now been through four design/fabrication/testing revision cycles. Prototypes from each cycle have been evaluated and characterized at room (300 K) and liquid nitrogen (77 K) temperatures. During these tests the circuits have been cycled multiple times between the two temperatures and operated without any change in performance. In fact, the observed performance of the circuit is almost identical at all temperatures between room temperature and 77K, with the exception that the noise decrases by more than a factor of two from room temperature to 77K. Figure 4–4 shows the measured pulse response, along with details on the adjustability of the gain, peaking time and baseline. These results are in close agreement with the simulations and indicate that both the analog and the digital circuits and interface operate as expected in a cryogenic environment. Simulations and experimental results show that the pole-zero cancellation needs to be optimized, which will be done in the next revision of the design. Also reported in Figure 4–4 are the outputs of the BGR and temperature sensor, which are in close agreement with the simulations as well.

Figure 4–5 shows the measured Equivalent Noise Charge (ENC) versus filter-time constant (peaking time). At 1 μs about 650 e$^-$ was measured, to be compared to the simulated value of 500 e$^-$. The difference is mainly due to the dielectric loss from the capacitor (220 pF) used to simulate the wire. This contribution would not be present with the input connected to a sense wire in the TPC.

Each channel is equipped with an injection capacitor which can be used for test and calibration and can be enabled or disabled through a dedicated register. The injection capacitance has been measured using a calibrated external capacitor. The measurements show that the calibration capacitance is extremely stable, changing from 184 fF at room temperature to 183 fF at 77 K. This result and the measured stability of the peaking time demonstrate the high stability of the passive components with the temperature. Channel-to-channel and chip-to-chip variation in the calibration capacitor are typically less than 1%. Measurements are being carried out on the individual test structures fabricated on this ASIC to confirm device models and design guidelines.

All data, control, bias and power supply lines will be duplicated to provide redundancy to avoid the loss on an entire APA. Four APAs will be cabled to warm feedthroughs in "chimneys" in the roof of the cryostat that contain the support rods for the TPC modules. A design for the feedthrough is shown in Figure 4–6.
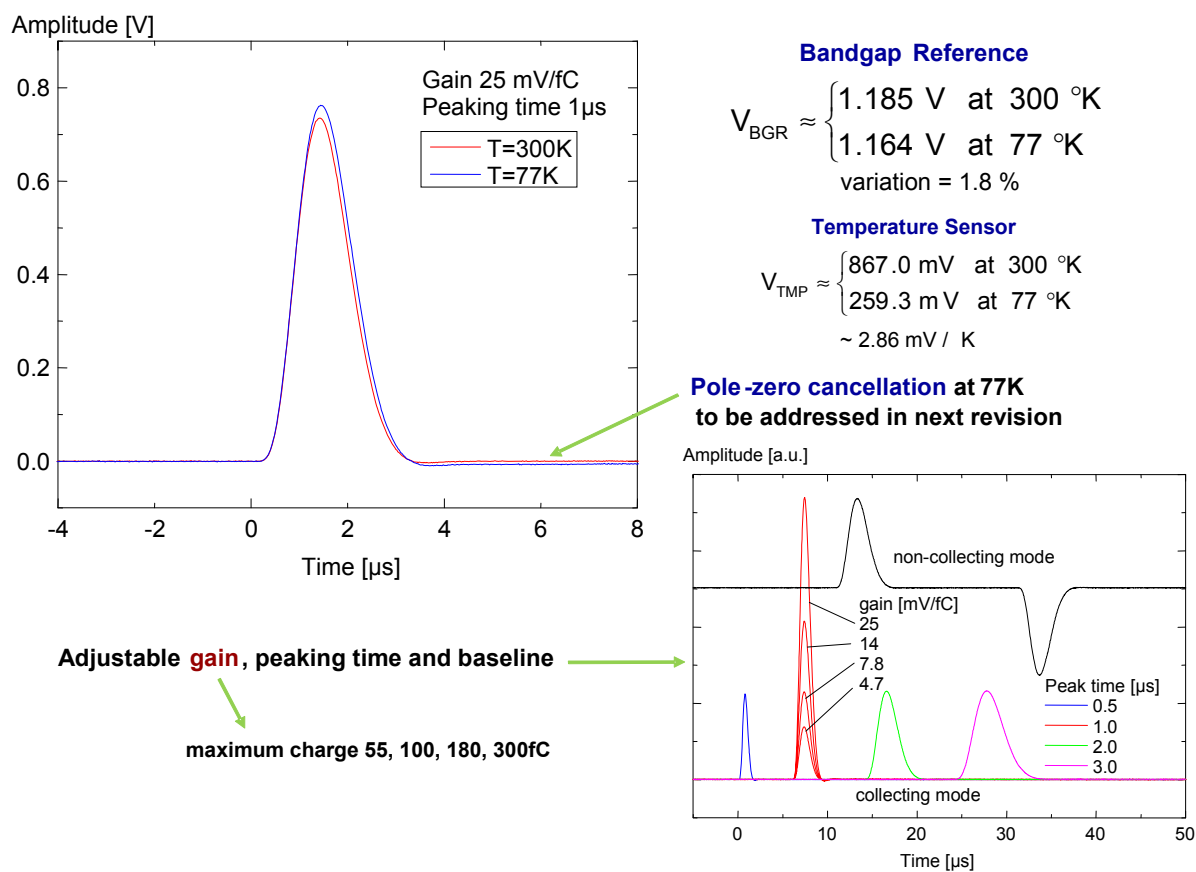
Figure 4–4: Measured pulse response with details on gain, peaking time and baseline adjustments
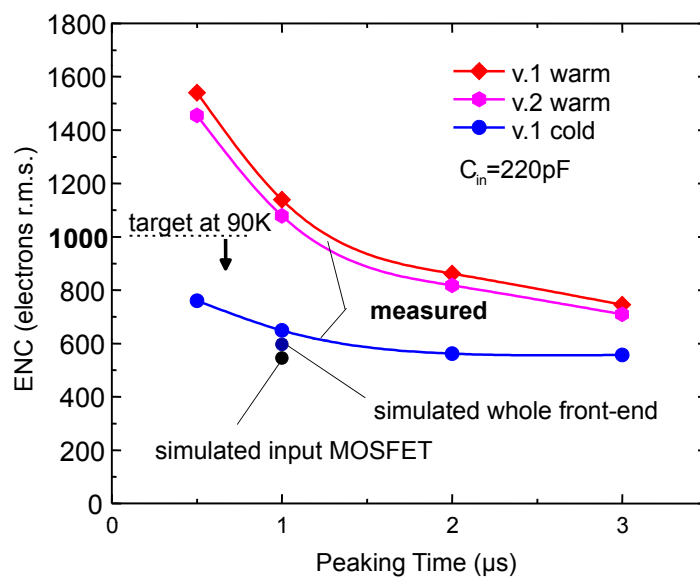
Figure 4–5: Measured ENC vs filter time constant from the first two versions of the analog front end ASICs
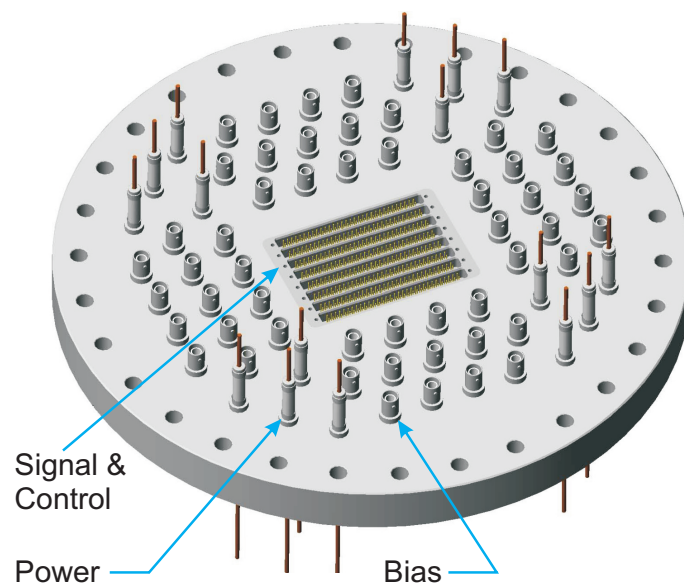
Figure 4–6: Mechanical model of the signal, control, bias, and power feedthrough for the cold electronics serving four APAs

5   Data Acquisition (WBS 130.05.05)

The scope of the data acquisition (DAQ) subsystem includes the design, procurement, fabrication, testing, delivery and installation of a combination of custom and commerical electronics modules, (including commodity computing and networking hardware), as well as both commercial and internally developed software.

5.1   Introduction

The DAQ subsystem will perform the primary functions of:

- Configuration, online calibration/checkout, and control of operations of detector subsystems, including the generation and distribution of timing and control signals,

- Readout of raw data from the TPC and other detector subsystems,

- Filtering the data and constructing event records to be logged to persistent storage media,

- Control of, and readout of data from, devices providing real-time information on detector, subsystem and environmental conditions,

- Providing user/operator interfaces for these functions via a run control system, and

- Receiving and handling the LBNE beam-spill signal.

In this chapter, a reference design for the DAQ subsystem is presented. The development of this design is guided by recent experience gained in the development of relevant systems for the NOνA [26] and MicroBooNE [27] experiments, as well as from running experiments with comparable channel counts and/or experimental conditions, such as D-Zero, CDF, MINOS and ICARUS.

The DAQ subsystem is to be located external to the cryostat vessel, with components in the Detector Hall and in an on-site control room. The primary interface is with the TPC front-end electronics. Additional interfaces are with the front-end electronics systems for the photon-detector subsystem, with the Fermilab Accelerator complex (the beam-spill signal), and with the cryogenics subsystem (for logging of conditions).

The DAQ subsystem reference design described in this chapter consists of the following components:

- custom 'Data Concentrator' modules located in the Detector Hall to receive data from the TPC (transmitted via redundant LVDS or optical lines) and to carry out low-level data processing operations (these connect to the network, listed next)

- a network consisting of commercial ethernet switches located in the Detector Hall and a commercial router located in the counting house/control room (for the transmission of data to the farm, listed next)

- a local farm of commodity computers that provide trigger event-building and real-time processing/event reconstruction functions

- a custom timing system consisting of a master unit that locks onto a GPS clock and distributes timing signals to the data concentrator modules via slave units

- dedicated computer nodes that host run control, routing control, node supervisor and slow controls processes

The DAQ subsystem does not include power-supply hardware for the TPC or front-end electronics, nor does it include the cryogenics subsystem process-control and monitoring functions.

5.2   Design Considerations

Physics considerations determine the scale of the primary tasks of digitized TPC data read-out, event building and online processing. The requirements on the DAQ system are listed in the requirements documentation [13].

In addition to rates for processes of interest, the DAQ subsystem design depends critically on the specifications for the TPC and front-end electronics systems, chosen to satisfy the LBNE physics requirements. As described in Chapter 3, obtaining sensitivity to signals that occur independently of the LBNE beam spill, together with the anticipated latency in arrival of a beam spill signal motivate a free-running transmission of data from the TPC front-end

electronics. The sampling rate of 2 MHz has been chosen so as to achieve the required position resolution along the ionization drift direction.

The task of data transfer is facilitated by multiplexing and data compression/zero-suppression capabilities in front-end ASICs located within the liquid argon volume, and by redundant data lines that provide connection to data-acquisition hardware located outside the cryostat. With these specifications, event building and triggering/filtering can be accomplished outside the cryostat. The LBNE beam-spill signal and data from the photon-detection system are considered part of the data stream, and can be used at this stage to select events for processing and storage through physics-specific data streams, as desired.

As suggested above, the DAQ system will have to contend with irreducible backgrounds from cosmic ray muons and contamination of detector materials by radionuclides that will generate signals in the detector at a much higher rate than the physics rate. With the present plan to site the detector at/near the surface, the muon rate will dominate. Some of this background rate will be useful for calibration purposes. Details on expected rates and timing issues and their implication for the DAQ system are discussed below in Section 5.2.1.

From a systems design point of view, DAQ design goals include minimizing the impact of single-point failures and maximizing the use of commercial components.

Together, the above considerations motivate a DAQ system conceptual design that involves moderately-high-bandwidth signal input and network components, channeling blocks of data to commodity computers that can carry out triggering, event-building and online-analysis functions. Alternate DAQ system models have not been excluded at this time. In one direction, implementation of a system with higher bandwidth transmission capabilities continues to be under investigation. Such an approach would rely less on zero compression in the front-end electronics, and thereby be less sensitive to uncertainties in background rates at a cost of additional network, computing and data storage loads within the DAQ system. There is no hardware trigger for the detector so the DAQ system has adopted a "data push" architecture. This is a free flowing data architecture where the data gathered from the front end ADCs in a given time window is routed to a node in the computer farm. The node then decides whether or not to keep the data, i.e., it is a software generated trigger. Saved events are then sent to various data streams for online data checking and to persistent storage.

This type of trigger is made possible by local zero suppression and data buffering in the front end ASICs. Additional data buffering in the external hardware and in the commercial internet switches is also required.

5.2.1   Event Rates and Timing

Cosmic-ray muons will dominate the rate of signals pushed out of the front end electronics. An accurate estimate of the muon rate has not yet been made for the currently envisioned detector location and shielding plan. A crude and conservative model incorporating a flat 3-meter overburden yields a muon rate of 44 kHz over the full detector. Beginning with this rate, and together with some consideration for the site/shielding conditions currently imagined, it is estimated that within a single 1.4-ms maximum electron drift time interval, each APA will be traversed by a handful of muons. The average data rate from muons, including those out of time with respect to the beam spill, is estimated to be approximately 300 Mb/s.

As described earlier in this report (see Figure 4–1), the cold electronics for a single Anode Plane Assembly will consist of twenty 128-channel Front-End Readout Boards, each providing a single digital input to a 20-channel Data Output Board, which nominally includes a 20× MUX stage into a driver for redundant LVDS outputs.

The Front-End Boards will generate zero-suppressed data: worst-case instantaneous rate scenarios (i.e., $> 10\,\mathrm{GeV}$ EM showers contained within a single APA) indicate roughly a factor of ten reduction in the number of samples read out with respect to the maximum (2560 wires × 2840 0.5-μs samples per wire). For cosmic-ray muons, the rejection factor is estimated to be ~ 200. The rejection factor is of course much higher in APAs not containing any portion of a physics event. Radioactive decay from ^{39}Ar and ^{85}Kr in the LAr, and to a lesser extent from detector materials (U/Th/Co/K), is estimated to provide a 44-kHz/APA rate of activity of energy above about 300 keV (0.3 MIPs) but less than $\sim 5\,\mathrm{MeV}$, while electronics noise (assuming 10:1 S/N for 1 MIP, and a threshold of 0.3 MIPs) will contribute a relatively low rate per APA of singles. Table 5–1 provides a summary of these rate estimates. Work is ongoing to further refine them.

From the table, we conclude the average per APA data rate out of the front-end electronics system is manageable: about 300 Mbps of muon tracks, plus 20 Mbps of 'salt and pepper' due to radionuclides in the Ar and TPC materials. Large beam- or atmospheric-neutrino interactions or showering ultra-high-energy cosmic-ray muons will result in high (Gbps-level) instantaneous rates on the scale of the maximum ionization drift period, but contribute negligibly to the average rate. With sufficient buffering in the front-end ASICs, as described in Chapter 3, the plan of having a single output channel per APA (plus redundant lines) appears to be feasible. However, to be conservative, and to provide opportunities for collecting data with relaxed zero-suppression, the DAQ reference design described below considers 20 output lines per APA (one per front-end board), each operating below 20 Mbps.

Table 5–1: Per-APA estimates of rates and data sizes/rates for various processes. Unless otherwise stated, estimated numbers of samples and data rates assume suppression of signals below 0.3 MIP. A 12-bit ADC is assumed, and no allowance is made for data items such as time-stamp, channel identifier, etc.

Process	Rate (kHz/APA)	Samples (per APA)	Avg. Data Rate (Mbps)
Generic 1.4 ms interval (not zero-suppressed)	0.70	7.3×10^6	61,000
Cosmic ray muons (Surface)	~ 1	2.5×10^4	~ 300
Radioactivity: U/Th (γ's)	~ 1	40	0.48
^{39}Ar/^{85}Kr (β's)	40	24	12
Electronics noise (not common mode)	~ 1	15	0.2

5.3   Architecture Summary (WBS 130.05.05.02)

The reference design of the DAQ system is summarized in block diagram form in Figure 5–1. Component counts are given in Table 5–2. The main elements of the design are described in the following sections.

5.4   Data Concentrator Module (WBS 130.05.05.03)

The LBNE/LArTPC Data Concentrator Module (DCM) serves as the primary interface between the cold TPC electronics and the DAQ subsystem, with the main tasks of receiving serial data pushed out of the front end and timing information from the global timing system. It also packetizes and transmits the data to 'data farm' computers for event building via an ethernet switch array, described in Section 5.5. Finally, it will provide the interface for transmitting timing and control signals to the cold electronics. As such, it is envisioned to provide the functionality of NOνA's custom electronics module of the same name, and similarly, the digital portion of MicroBooNE's "Front End Module" (FEM) cards.

For the purposes of this conceptual design, the NOνA DCM is considered largely as is. Several NOνA prototype modules are shown in Figure 5–2. The NOνA DCM consists of 64 input ports (RJ45 sockets) with input bandwidth of 24 Mbps per channel, and a single 1 Gb (640 Mbps) output line. A large FPGA provides preliminary data processing capability. A processor (running Linux) provides local control for configuration, buffering and routing functions.
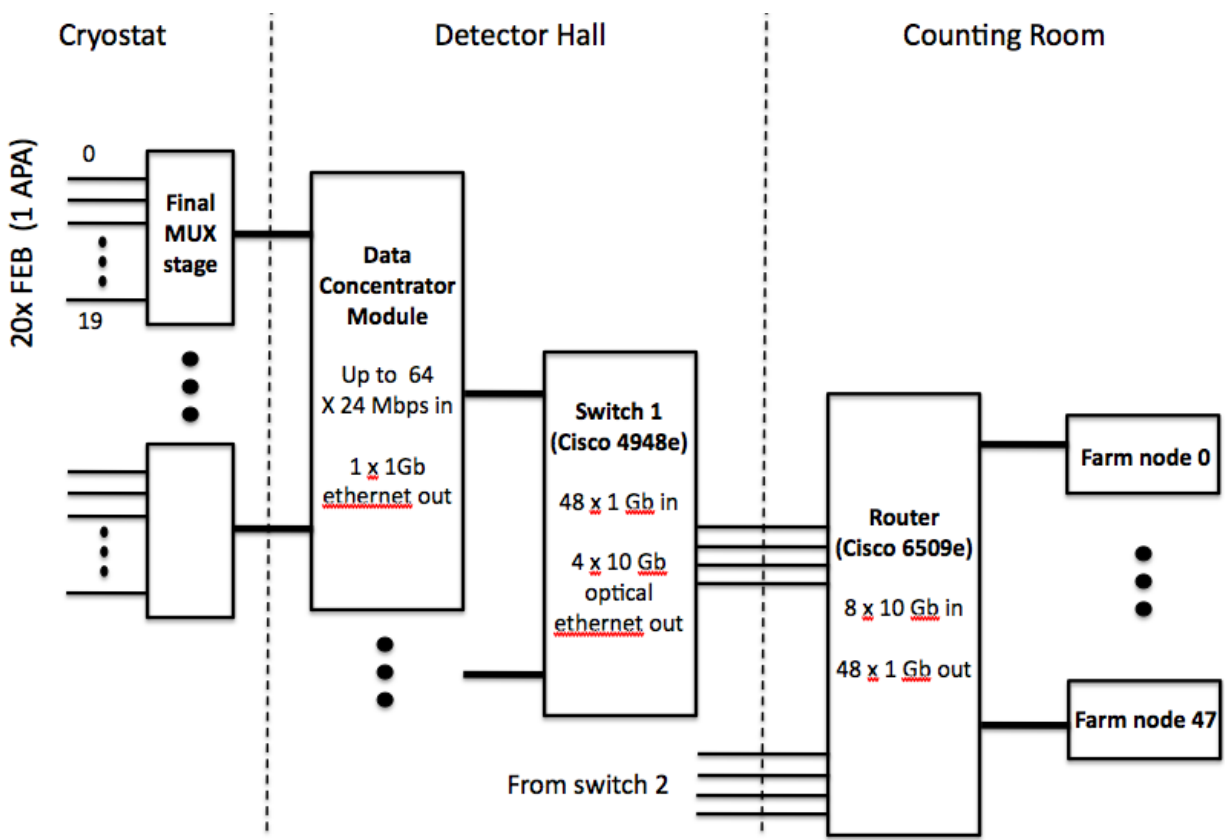
Figure 5–1: Block diagram depicting the DAQ reference-design architecture

Table 5–2: DAQ subsystem component counts for one 5-kton module/cryostat. The total component count for the two-cryostat LAr-FD will be twice what is shown.

Quantity	Description
30	Data Concentrator Modules
2	Ethernet Switches (Cisco 4948E or similar)
1	Ethernet Switch Chassis (Cisco 6509E or similar), with
1	8-port input optical 10-GB ethernet interface module, and
1	48-port output 1-GB ethernet interface module
48	Data Farm compute nodes
1	Readout Supervisor compute node (not shown in Figure)
1	Routing Master compute node (not shown in Figure)
1	Master timing unit + GPS receiver (not shown in Figure)
5	Slave timing units (not shown in Figure)
1	Run Control compute node (not shown in Figure)
1	Slow Controls compute node (not shown in Figure)
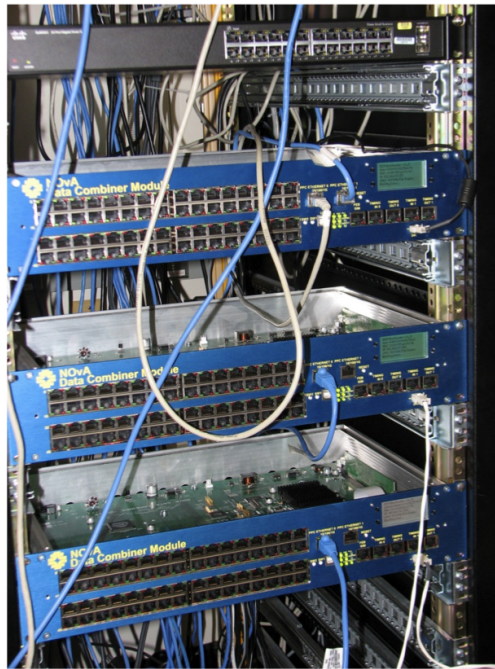
Figure 5–2: Photograph of several prototype NOνA Data Concentrator Modules.

Considering data rates of order 300 Mbps per APA (see Table 5–1), the bandwidth of a single NOνA DCM would be saturated by data from two APAs. The LBNE DCMs would have to be designed for higher bandwidth, to provide sufficient headroom to accommodate unforeseen sources of excess rate, and to permit special operating modes where data-compression/zero-suppression in the front ends is loosened. Estimates have been made assuming two APAs per DCM, utilizing known production costs from the NOvA project.

5.4.1 Data Processing/Handling

As currently imagined, buffers in the front-end electronics will constitute a source of variable-length (i.e., zero-suppressed) time-ordered sequence of samples for each channel (wire) registering activity, along with a channel address and time stamp. Although this format is likely to be suitable for transmission to the data farm, the DCM's task of generating ethernet packets also provides an opportunity for additional data processing. If re-formatting or additional zero suppression is desired, it could be done here.

5.4.2 Timing, Control and Configuration Signals

The DCM will provide the interface for the transmission of timing, control and configuration signals to the TPC/front-end electronics. More detail on these signals is given in following sections.

5.5   Ethernet Switch Network (WBS 130.05.05.04)

The network accomplishing transmission of data from DCMs to the data farm will consist of two layers of ethernet switch arrays. The first level will reside in the Detector Hall, and is imagined to be able to operate with little external control. Commercial switch modules such as the Cisco 4948E are well suited for this application. The 4948E has 48 1-GB input ports and four 10-GB optical output ports, as well as 175 MB of buffer memory. Two modules will support the required data throughput for the entire detector.

The second level will be deployed in the control room and will serve as a router to the data farm nodes located there. For this application the Cisco 6509E switch chassis provides a possible implementation. This would be loaded with a single 8-port 10 GB blade for input data from the 4948E's, and a single 48-port 10/100/1000 MB blade for 1-GB output to farm nodes.

Routing information will be provided to DCMs by a Routing Master. This task will run on a computer located in the counting room. It will monitor the state of data farm nodes, and provide routing information to DCMs.

5.6   Event Building and Triggering (WBS 130.05.05.05)

The event building and triggering function of the LAr-FD DAQ system will be performed by the data-farm computers. Event data will be staged locally before being transmitted in quasi real-time (nominally to Fermilab) for archival to persistent storage.

5.6.1   Event Building

At present it is imagined that an event will consist of raw data from the entire detector, spanning a time interval yet to be determined. To construct such an event, DCM packets corresponding to data with a common (range of) timestamp value(s) will be routed to a particular data-farm node.

An alternate scenario considers events as being localized to individual APAs, or possibly small APA clusters. Individual farm nodes would work only on the corresponding data to generate event records. This concept is attractive in that event record sizes are kept as small as possible for convenient utilization offline. The main drawbacks are that (1) offline processing/analysis of these event records for physics events with activity spanning geographical boundaries would become more cumbersome; (2) certain physics studies might benefit from simultaneous access to data-registering activity in disparate geographical regions of the detector; and (3) auxiliary data would either be unnecessarily duplicated or would have to be stored in its

own event record, again adding complexity to the data-analysis process. Evaluation of this alternative is ongoing.

5.6.2   Event Data Model

An Event Data Model (EDM) is required. It may be advantageous to implement the raw data EDM in a custom format, as opposed to one based on ROOT. Experience with MicroBooNE will be helpful in optimizing the design for this.

5.6.3   Triggering and Selection for Output Streams

Significant work remains to understand how data-farm nodes will carry out event filtering and creation of separated physics/task-specific data streams. Use of the LBNE beam-spill signal to identify events recording beam-induced activity is expected to be straightforward. However, identifying events of interest that lack such a signal requires study. Is it sufficient to find a suitable way to generically veto data from geographic regions of the detector, corresponding on one hand to the presence of a cosmic ray muon, or on the other hand to a lack of coherent detector activity? Or, must 'positive' signatures for each of the physics processes of interest be identified for triggering? To indicate the range of signatures, these processes of interest include, for example, (1) beam-induced events for which the corresponding beam-spill signal is missing due to network failure or other malfunction, (2) atmospheric-neutrino interactions, (3) supernova-neutrino bursts, (4) proton decay, and (5) magnetic-monopole incidence. (While the sensitivity of a surface detector to some of these processes is under study, all are listed here at the present time for completeness, and to accommodate the possibility that the detector would be sited at depth.)

5.6.3.1   Rejection of Event Records

During every canonical 1.4-ms interval, roughly 20 cosmic ray muons will traverse each 5-kt detector module, corresponding to one or more track fragments generating signals in each APA. Fast reconstruction algorithms will allow identification of such muons or muon fragments. Both stopping and through-going muons will be useful for different calibration and detector monitoring functions: they can be identified and selected via prescaling or other criteria.

5.6.3.2   Event selection for Physics-Specific Streams

Even given the above statements about event rejection, it is desired to perform some type of high-level event reconstruction to identify candidates compatible with specific physics signatures. This level of analyses is essential both for online detector performance diagnostics as well as for the case where candidate event records of particular types are to be written to parallel output streams. For the former application, an unanticipated shortfall in the DAQ data farm computing capacity could be easily addressed through establishment of a separate computer farm for online analysis. For the latter application, it would be necessary to adjust the size of the data farm depending on the processing requirements. These are not known at this time. However, with anticipated costs for commodity computing systems, it is not expected that the overall cost of the DAQ/online computing systems would increase significantly relative to the currently budgeted system.

5.7   Timing System (WBS 130.05.05.06)

Comparable requirements and conditions suggest a timing system similar to that being implemented for NOνA. That system meets the requirements of deterministic timing and coherence of signals distributed across the entire detector. It consists of a Master Timing Unit (MTU) whose main task is generation of GPS-based timing packets, and an array of Timing Distribution Units (TDUs). The TDUs are geographically distributed: they compensate for propagation delays before transmitting timestamp packets to the front ends via DCMs. Such a system could work well for LBNE and may be able to be adapted with only minor design modifications. For NOνA, each TDU is associated with 12 DCMs; for LBNE a reasonable distribution could be achieved with 5 TDUs, providing one for every 6 DCM's/12 APA's. These would be spaced at intervals of 5 m along the length of the detector.

5.8   Run Control (WBS 130.05.05.07)

The scope of functionality of the Run Control system includes operation of DAQ subsystem components, configuration of front-end electronics, control of power supplies and other auxiliary equipment, and control of data collection. Development of a user interface for experimenters during data-taking and for technical personnel to assist with commissioning and debugging activities is key. To date, limited effort has been put forth in the design of the Run Control system. To the extent that the challenges faced are similar to those that have been addressed at MINOS and ICARUS, no technical obstacles are foreseen. As the designs of the DAQ and other subsystems continue to develop, specifications of the Run Control system will become more concrete.

5.9 Slow Control Systems (WBS 130.05.05.08)

The Slow Control system is a critical element of the DAQ, providing the main interface to power supplies for the detector and electronics as well as to equipment used to monitor the operational status of the detector and supporting systems. As in the case of the Run Control system, the development of the conceptual design for the Slow Control system is in its early stages. Again, based on experience from other experiments, no obstacles are foreseen with regard to the development of a robust system.

5.10 DAQ Infrastructure (WBS 130.05.05.09)

5.10.1 Wide Area Network

As in the case of MINOS and NOνA, it is expected that event data can be transmitted over the network to Fermilab. Although rates for events of interest are comparable, data throughput for the LBNE LArTPC is expected to be at least an order of magnitude higher. A detailed analysis of the requirements of SURF for the appropriate level of connectivity within and off the lab site will need to be carried out.

5.10.2 Online Data Storage

To protect against signficant periods of absent network connectivity, it is desired to store a significant amount of the data emerging from the DAQ to local storage. A local data storage facility of $\sim 100\,\mathrm{TB}$ is expected to be more than adequate for five days worth of detector data, even without prescaling cosmic-ray muon events.

5.10.3 Power and Cooling

Power and cooling requirements for the DAQ system described here are modest. DCMs operate at below 50 Watts each, while the maximum power consumed by each of the two Cisco 4948Es is 275 Watts. Assuming power supplies that operate at 75% efficiency, and accounting for other components, the total DAQ subsystem budget for power in each detector/cryostat hall is expected not to exceed 10 kW.

6   Photon Detector (WBS 130.05.07)

6.1   Introduction

The scope of the photon detector system includes the design, procurement, fabrication, testing, delivery and commissioning of a subsystem that meets the performance requirements for photon collection in the LAr-FD. This subsystem will provide absolute event timing, thereby enhancing the detector's event localization and particle-identification capability. Absolute event timing also makes possible time-of-flight measurements.

6.2   Physics Motivation for Photon Detection

6.2.1   Photon Production in Liquid Argon

Photons are produced in liquid argon by scintillation and by Cherenkov radiation induced by charged particles. The former dominates by a factor of five. The Cherenkov light is directional, while the scintillation light is isotropic. Twenty-three percent of the scintillation signal is in prompt 6 ns light and 77% of the signal is in late 1.6 μs light. The decay photons are in the VUV and have a wavelength $\lambda = 128$ nm. The photon-detector system is designed to detect these 128-nm scintillation photons.

Identification of the different charged-particle types depends on accurate measurements of ionization along tracks. Some drifting ionization electrons are lost due to impurities in the LAr. The measured ionization charge, Q, is therefore lower than the true ionization charge, Q_0, and is expressed as $Q = Q_0 e^{-t_{drift}/\tau} = Q_0 e^{-(t_{arr}-t_0)/\tau}$, where t_{drift} is the measured drift time and τ is the lifetime of the drifting ionization electrons, measured by purity monitors in the cryostat (Section 2.7.5). The drift time is the time difference between the time of occurrence of the event, t_0, and the arrival time of electrons at the anode plane, t_{arr}. The photon-detector system detects the arrival time of the event, t_0, which allows one to both correct for recombination and locate the event in the detector.

6.2.2 Impact on Physics Analyses for a Surface Detector

Photon detection is important for mitigating the effects of the significant cosmic ray backgrounds expected for a detector at the surface. Beam spills are a few μsec in length and the subsequent drift times to the APA planes take a few msec. Since the cosmic ray background rate is $\sim$10 kHz, a handful of cosmic ray muons will fall within the drift time window. Accurate t_0 determination delivered by the photon-detection system will reliably identify events falling outside the beam-spill window. In addition, with dE/dx corrected by t_0, particle identification will further improve the background rejection.

6.3 Reference Design

The reference design employs adiabatic light guides, demonstrated by Bugel *et al.* [28]. These light guides are bars that consist of extruded polystyrene cores with a co-extruded layer of polystyrene around the outside that is infused with the waveshifter tetraphenyl butadiene (TPB [2]). The TPB converts the 128-nm incoming scintillation photons to visible light. The optical photons propagate into the polystyrene core, where they are transported to the end by total internal reflection to a photomultiplier tube (PMT) modified to work efficiently at LAr temperatures.

Four light guides are ganged together into a "paddle" held by a frame that mounts onto an APA (described in Chapter 3 and illustrated in Figures 3–9 and 6–1). An APA holds ten paddles and each paddle includes a PMT mount with a custom cryogenic base. The same cable is used to bring HV into the base as to carry out the readout signals, resulting in a total of ten cables per APA for the photon-detection system. There are 120 APA frames in the reference resign. Four light guides per paddle × ten paddles per APA frame × 120 APA frames comes to 4,800 adiabatic light guides.

Figure 6–2 shows the details of the light-guide design. The dimensions have been chosen so that four light guide bar cross sections completely cover the photocathode area of the PMT.

The readout electronics are warm (located outside the LAr) and set to trigger at 0.5 PE. The readout is based on the MicroBooNE 60-ns shaper and commercial electronics, where possible, to minimize cost. The signal is digitized at 65 MHz and the integration time is 3.2 μs, or twice the lifetime of the late light. The digitization gives four samples for the 60-ns shaped pulse; there are 208 samples per trigger. Once a trigger is received, a signal is sent to adjacent PMTs to begin recording.
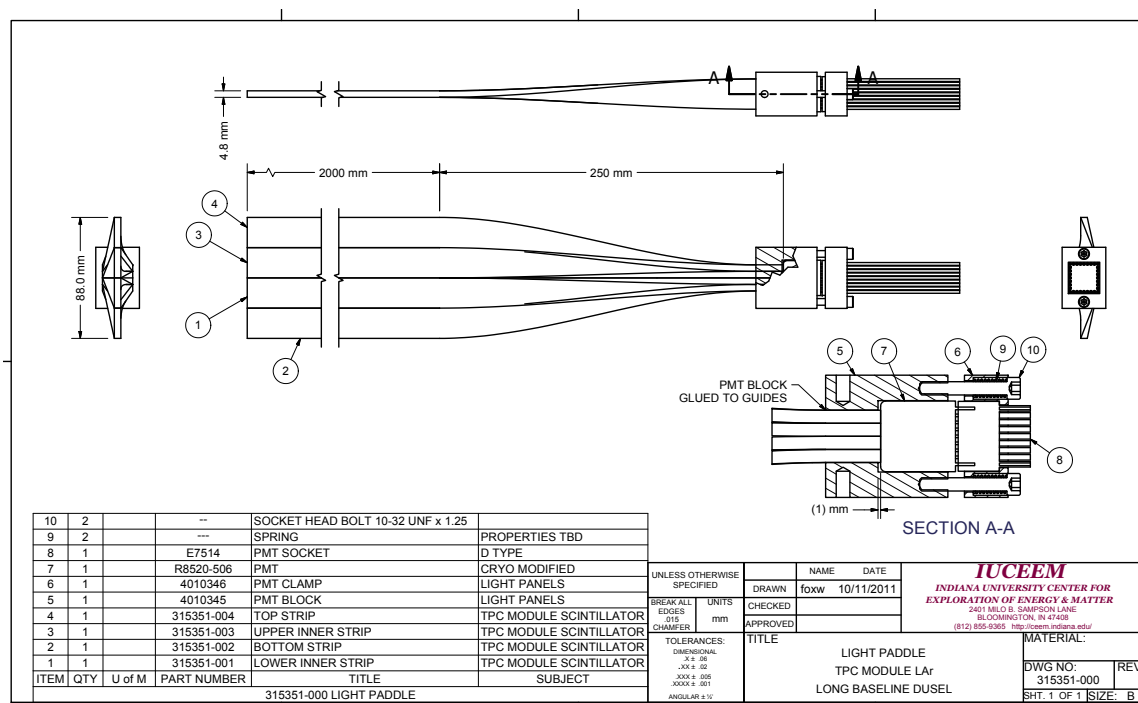
Figure 6–1: Four adiabatic light guides bent through 90° and clamped onto an R8520-MOD PMT.
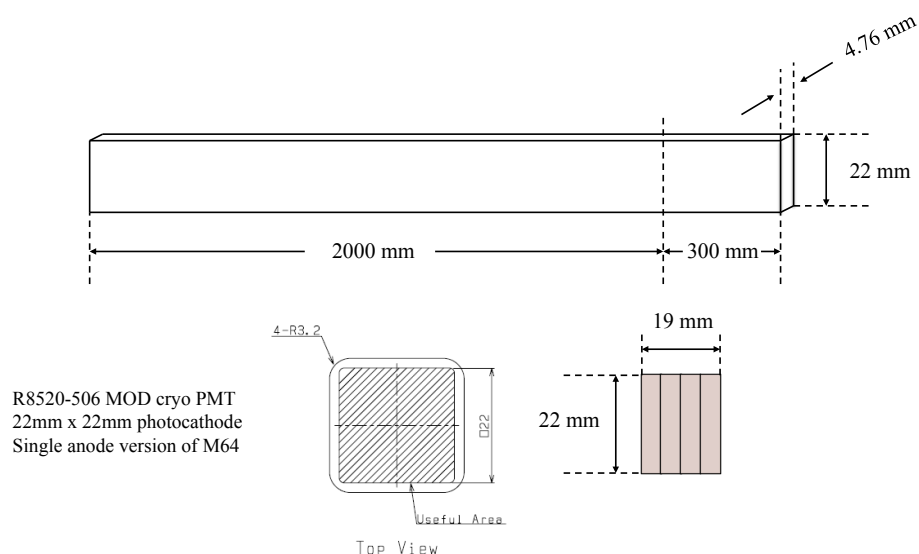
Figure 6–2: *top*: Dimensions of adiabatic light guide bar. *bottom*: Four light guides are ganged together to fill the photocathode area of a Hamamatsu R8520-MOD PMT.

6.3.1 Photon Production and Detection

For a MIP particle the number of photoelectrons detected in the the LAr-FD detector calculated for a MIP particle, N_{PE}, per MeV of energy of the ionizing particle can be written

$$N_{PE}/\text{MeV (MIP)} = (N_{128}/f) \times \epsilon_E \times (N_{420}/N_{128}) \times DQE \times \Omega$$
$$= 0.2 \ \text{PE/MeV}$$

where (N_{128}/f) is the number of prompt 128-nm photons/MeV, corrected by $f = 0.23$ to the total (prompt + late) light signal $= 3.3 \times 10^4$ for a MIP particle [29]; ϵ_E ($= 0.6$) is the reduction in light due to the 0.5-kV/cm electric field [30]; (N_{420}/N_{128}) (≈ 1) is the number of 420-nm photons emitted by the waveshifter for every absorbed 128-nm VUV photon [2]; DQE = detector efficiency $= 2.7 \times 10^{-3}$ [30] and includes first estimates of the light-system design parameters for the baseline detector described here; and $\Omega = 0.0036$ geometric acceptance, including photon transmission past the wires [30]. For particles of lower energy than MIPs, there would be more photons.

Backgrounds in LAr were studied in the 2.3-liter WARP detector [1]. The energy spectra for these backgrounds are shown in Figure 6–3.
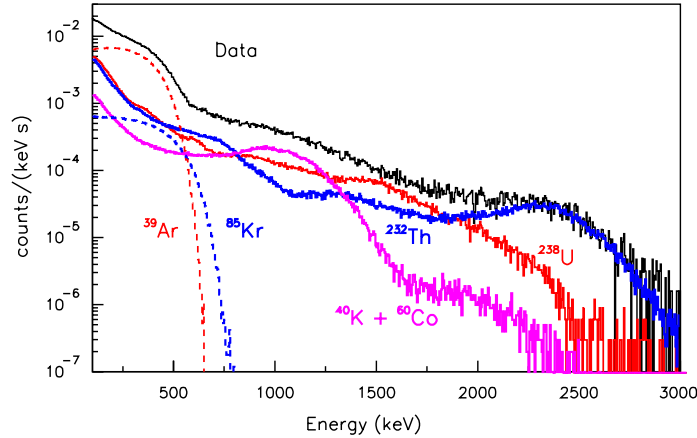
Figure 6–3: Backgrounds measured in the WARP detector [1]

The dominant internal background is from Ar^{39} beta decays. The dominant external background comes from Co^{60} contamination in the stainless steel. For a typical 0.5-MeV β from Ar^{39}, $N_{prompt}(Ar^{39}) = 0.05$ PE; $N_{tot}(Ar^{39})$ equals 0.2 PE and does not present a problem. For the Co^{60} in the stainless steel, the 1.2/1.3 MeV γ's give $N_{prompt}(Co^{60}) = 0.06$ PE and $N_{tot}(Co^{60}) = 0.3$ PE. But this background has a rate that is an order of magnitude lower at 0.5 MeV and two orders of magnitude lower at 1.25 MeV than the Ar^{39} background, thus not presenting a problem.

6.3.2 Adiabatic Light Guides

6.3.2.1 Extrusion Technology

The technology for extrusion of particle-detection scintillators is quite mature. MINOS has demonstrated that co-extruded solid scintillator with embedded TiO_2 can be manufactured with excellent quality control and uniformity in an industrial setting. The co-extruded scintillator elements required for the LAr-FD can be produced at Fermilab using the extrusion line jointly operated by Fermilab and the Northern Illinois Center for Accelerator and Detector Development (NICADD) at Northern Illinois University (NIU). This facility ensures that the High Energy Physics community has access to high-quality extruded scintillator. Fermilab and NICADD personnel have been responsible for commissioning the extruder, for simulations, production and prototyping of dies associated with specific detectors, and for productions of extrusions for prototypes and detector construction.

Scintillator strips (bars) are composed of a polystyrene core and a co-extruded, 0.25-mm thick polystyrene layer (around it on all four sides) infused with TPB. This layer is introduced in a single step as part of a co-extrusion process. The layer is rugged enough to allow direct gluing of the bars to each other to form paddles.

6.3.2.2 Waveshifter (TPB)

The detection of 128-nm UV photons emitted by Ar is challenging. Short wavelengths are ordinarily strongly absorbed by nearly all materials used for visible optics, such as quartz or glass windows of PMTs, but they are not energetic enough to be treated calorimetrically like x-rays or γ-rays [2]. This obstacle can be overcome by down-shifting the VUV photons into visible photons with a waveshifter such as TPB, which is well-studied for this application [2,31].

The re-emission spectrum of TPB when illuminated by 128-nm photons is shown in Figure 6–4 [2]. The efficiency for TPB to convert input VUV photons is shown in Figure 6–5 [2]. The photon conversion efficiency $(N_{420\,nm}/N_{128\,nm}) \sim 1$ used in the calculation of photon production has been taken from this figure.

6.3.3 Light Guide Paddles

6.3.3.1 Design

As discussed in Section 6.3, four adiabatic light guides are ganged together into a "light guide paddle" to maximize photocathode coverage. This is illustrated in Figure 1–11.
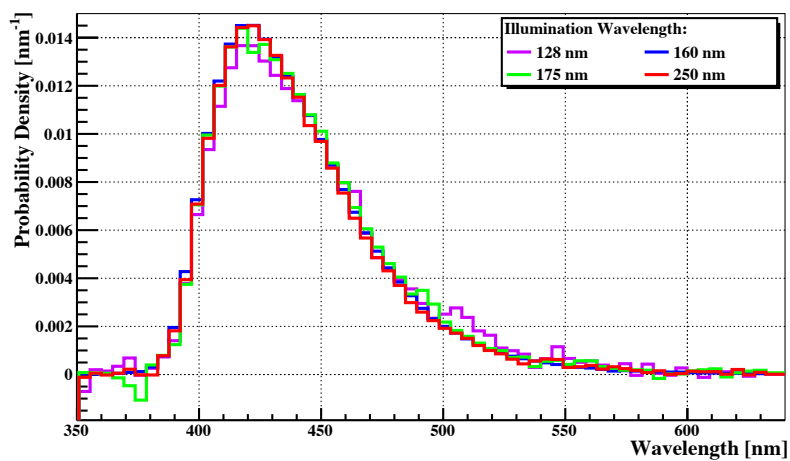
Figure 6–4: TPB re-emission spectrum from Gehman *et al.* [2].
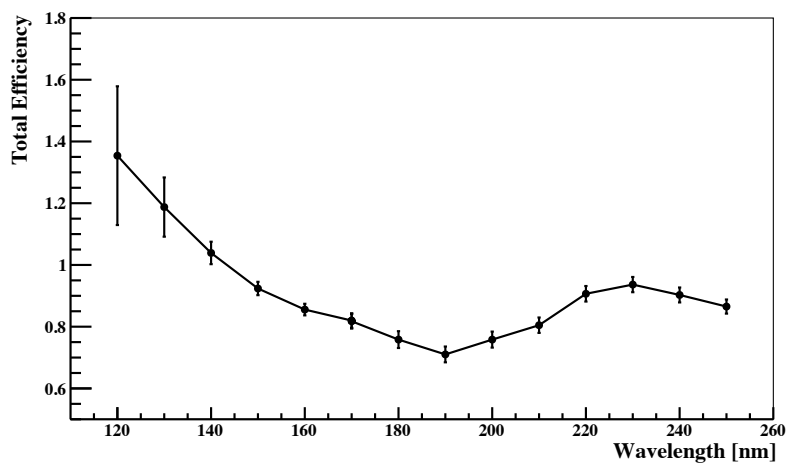
Figure 6–5: TPB efficiency as a function of VUV photon wavelength from Gehman *et al.* [2].

Figure 6–1 illustrates the assembly of four light guides into a paddle. The two center drawings show how the light guides are bent through 90° to fit onto the PMT.

The figure also shows how the light guides are held and clamped onto the PMT. To minimize feedthrough holes in the APA frame, the light guides are all bent in the same sense. The details of the design for the PMT holder and the PMT clamp are shown in Figure 6–6.

6.3.3.2   Assembly

The procedures for assembling the paddles will be developed during the development phase (Section 8.3.4). Once the light guide bars are extruded, they will be heated in an oven and then bent through 90° into the proper shape. As seen in Figure 6–1, each of the four light guides in a paddle requires a somewhat a different shape, depending on its position in the paddle. The bent light guides will then be set into a custom-designed fixture and glued. It is important that the four ends of the light guides be clamped in the fixture during this gluing assembly step to assure that they are properly aligned for flycutting. Once the glue sets, the ends will be flycut and set into a PMT block. Finally, the paddle assembly will undergo quality control testing, most likely with an LED in a dark box.

6.3.4   Photomultiplier Tubes

The PMTs in the reference design photon-detection system are Hamamatsu R8520-MOD cryogenic tubes, shown in Figure 6–7.

These 1-in tubes are single-channel, cyrogenic versions of the Hamamatsu M16 tubes used in the MINOS far detector. General information on these tubes is given in Figure 6–8. The PMT characteristics are given in Figure 6–9.

6.3.5   Electronics

Scintillation light from LAr comes from two different excited states with lifetimes of 6 ns and 1.6 μs. Only a limited amount of light is collected by this system, so the electronics is designed to collect the light from both excited states. The basic architecture is shown in Figure 6–10.

Signals from the PMT are transmitted from the LAr to electronics racks located near the ports on top of each cryostat. The signals on the HV cable are picked off using a blocking capacitor and then sent to a pulse shaper with a 60-ns shaping time. From there, the shaped signals are sent to a commercial 32-channel wave-form digitizer module and digitized to 12 bits at a frequency of 62.5 MHz. One channel of the digitizer is used to digitize the

Figure 6–6: *top*: PMT holder. *bottom*: PMT clamp.
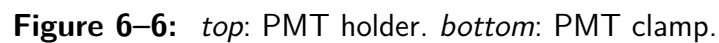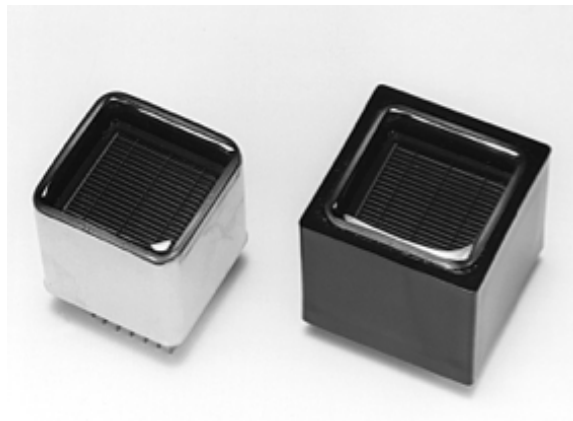
Figure 6–7: Hamamatsu R8520-MOD PMT.

General

Parameter		Description / Value	Unit
Spectral Response		300 to 650	nm
Window Material		Borosilicate Glass	-
Photocathode	Material	Bialkali	-
	Minimum Effective Area	22 x 22	mm
Dynode	Structure	Metal channel Dynode	-
	Number of Stages	10	-
Weight		Approx. 28	g
Operating Ambient Temperature		-186 to +50	deg. C
Storage Temperature		-186 to +50	deg. C

Figure 6–8: Hamamatsu M16 tubes, general information

experimental clock which has both the 32-MHz clock and special time markers encoded on it that are identical to those generated in the DCMs used to read out the TPC data. This allows the onboard FPGA to determine the time that an event occurred and also to determine when a time slice has ended so that data from the last time slice can be sent to the host PC. The FPGA is also used to zero-suppress the PMT data, time-stamp it and send the time-stamped data to the host PC. A simplified diagram of the FPGA logic is shown in Figure 6–11.

The host PC then groups the data into time blocks (which may contain multiple time slices) and sends the data to the farm node that is processing the APA data for a given time block.

The photocathode is located close to the APA wire planes, which are at or near ground potential. In order to eliminate any possibility of HV breakdown, the photocathodes are also run at ground potential. The PMT output signal is then offset from ground by the full DC bias voltage. This has the advantage that only one cable per PMT is required, but the signals must be AC-coupled into the readout electronics.

Characteristics at 25 deg. C

Parameter		Min.	Typ.	Max.	Unit
Cathode Sensitivity	Luminous (2856K)	-	100	-	uA/lm
	Quantum Efficiency at 340 nm	-	25	-	%
Anode Sensitivity	Luminous (2856K)	-	100	-	A/lm
Gain		-	1.0×10^6	-	-
Anode Dark Current (after 30 min. storage in darkness)		-	2	20	nA
Time Response	Anode Pulse Rise Time	-	1.8	-	ns
	Transit Time Spread (FWHM)	-	0.8	-	ns
Pulse Linearity at +/-2% deviation		-	30	-	mA
P/V Ratio		1.1	-	-	-

Figure 6–9: Hamamatsu M16 tubes characteristics

Since the electronics are outside the cryostat, there must be a HV-feedthrough connector. There are a total of 600 connections per cryostat, assuming 120 APAs with ten PMTs per APA and two PMTs per HV power supply. The connector must be very reliable and occupy little space. The current plan uses the Reynolds 8-channel HV connector in which the channels are in a round configuration. The connector is 1.187 inches in diameter and can withstand 10 kV. This connector has been used in D-Zero for the LAr calorimeter. It was mounted in the ullage and was operated at 2 kV for nearly 25 years.

The D-Zero system has eight tefzel-insulated cables inside an overall braided shield. This cable is ∼0.25 cm in diameter. Since the signals are also on this cable, the lack of individual shields may lead to unwanted crosstalk and poor signal propagation. The best solution is to add a braided or foil shield to the individual wires in the assembly. This will significantly increase the diameter of the cable, but its diameter should still be much less than that of the connector. If the individual coax cables have too small a diameter, the impedance will be less than 50 ohms, which effectively sets the lower limit on the cable size.

The Reynolds connector has a common ground so all the braids will be connected together at the feedthrough. The connector is less than 1/40 of a wavelength for frequencies up to 100 MHz so this interruption in the coaxial cable should not be a significant problem.

The interior cryostat cables will be terminated at the PMT end with a coaxial HV connector such as SHV or LEMO and be plugged directly to the PMT base. This will minimize the number of connections in the cryostat. It also allows the cable to be threaded through the 1-by-3 inch openings in the cryostat frames.

There are two candidates for the HV system. The reference design candidate is a custom system manufactured by Weiner corporation. The alternative is a VME-based system designed by Fermilab and manufactured by BiRa corporation. The BiRa system would allow most of the supplies to be recovered from the D-Zero and CDF experiments. However, since the purchase price of the Weiner system is less than the BiRa system (assuming no recovery from completed experiments), it was selected for costing. Each port will require 20 channels
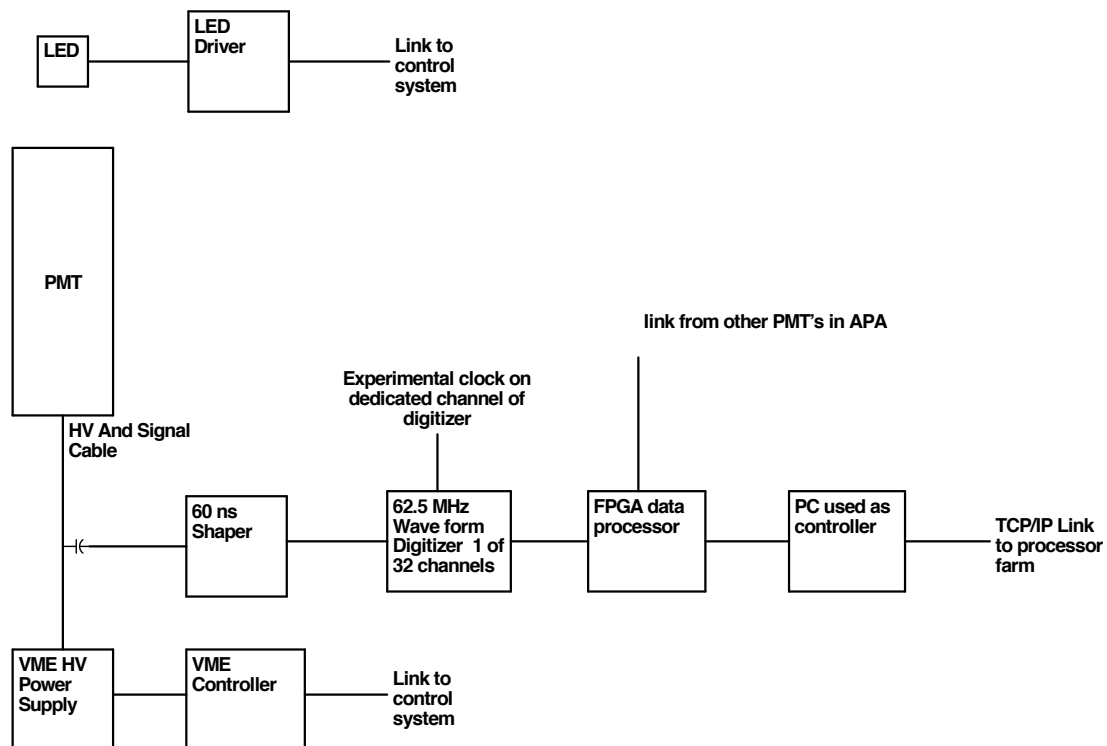
Figure 6–10: Block diagram of the electronics chain for the PMT system.
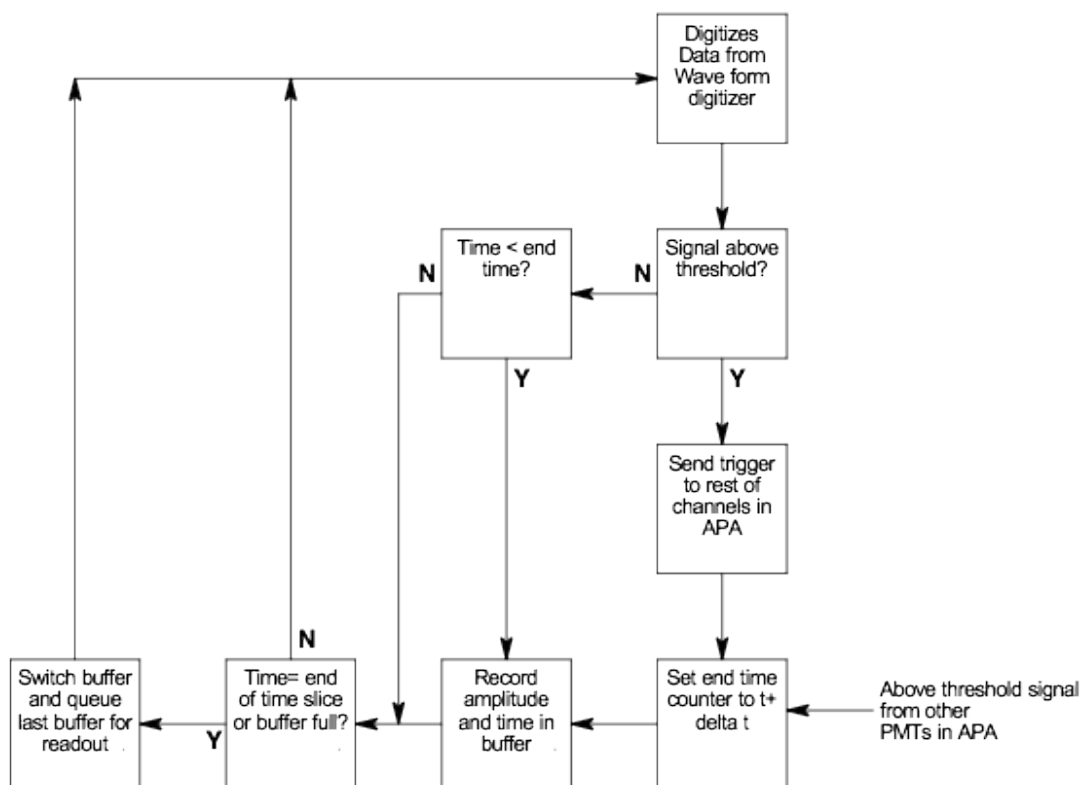
Figure 6–11: FPGA logic diagram. The time information will come from a dedicated channel in the digitizer. This logic will actually be implemented as a finite-state machine.

(40 tubes). Both systems have more than 20 channels per crate, so the crates will be located at the the end of each row of racks (for the reference design) or at every other port if the VME-based alternative is used.

The signal splitter will house a HV-blocking capacitor and a 60-ns shaper that is identical to the one designed for the MicroBooNE experiment. The shaper is shown in Figure 6–12. Output from the splitter will be fed into a commercial waveform digitizer.
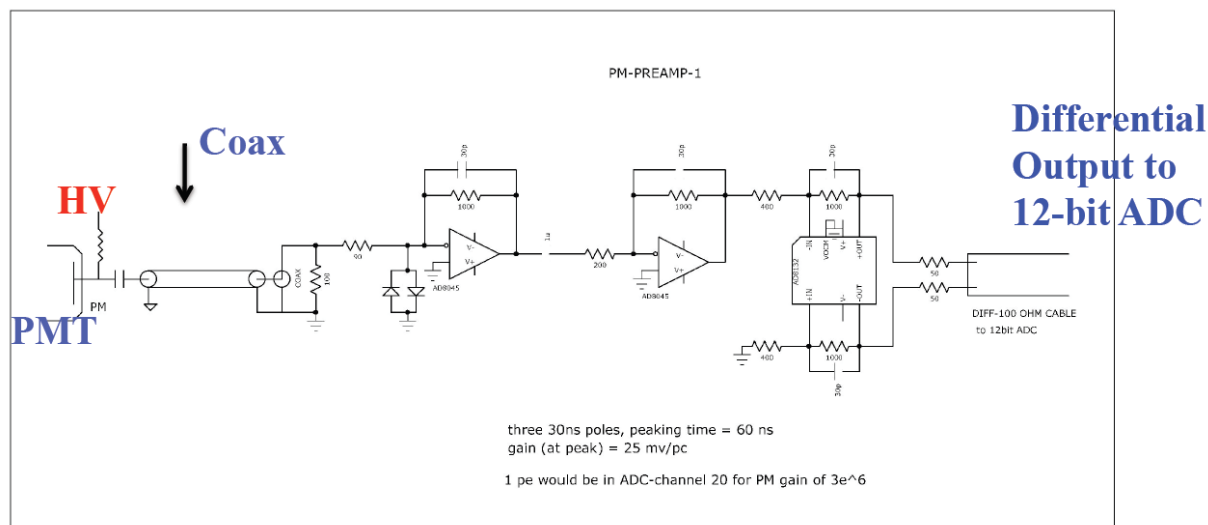
Figure 6–12: Shaper circuit designed for the MicroBooNE experiment. This figure has been taken from the MicroBooNE CDR.

LBNE needs continuous digitization followed by zero suppression and time stamping, unlike what a digital oscilloscope or many commercial digitizers can do. The zero suppression is controlled by a user-programmable FPGA.

All of the commercial digitizers under consideration send data to a PC over a PCI or USB bus. The digitizer FPGA will be programmed to provide appropriate timing information to the PC so that it can assemble the PMT data into packets spanning time periods that are identical to those generated in the DCMs first for the drift-chamber data. These packets will be sent to the appropriate farm node using an algorithm similar to the one in the DCMs.

Time-stamping can be done either by internal timing or by using one channel of the digitizer to digitize the experiment clock. At least one vendor has a product that uses a GPS signal to derive the time stamp. A second vendor who makes a similar product has been identified. No difficulty is anticipated in finding a commercial product that will meet the requirements.

6.4   Alternatives

6.4.1   Waveshifters

Two different waveshifters are being explored as more cost-effective alternatives to TPB, bis-MSB and p-Terphenyl. Studies are underway to extrude light guides at Fermilab with co-extruded layers doped with the same concentrations of TPB, bis-MSB and p-Terphenyl. The purpose of these studies is to quantify the relative light output of these three waveshifters. To make these comparisons, a NIST-calibrated photodiode will be used to calibrate the VUV vacuum monochromator at Fermilab.

6.4.1.1   bis-MSB

The waveshifter bis-MSB is widely used to convert the UV emission from primary scintillants like pseudocumene or doped polystyrene to wavelengths that can be absorbed by WLS fibers (used by MINOS, NOνA, MINERνA). Bis-MSB is inexpensive relative to TPB. Figure 6–13 shows the typical emission spectrum of bis-MSB in the range 360-500 nm which is well-matched to the R8520-MOD PMT. In this figure, the absorption spectrum is also shown for the typical range of interest down to 280 nm.
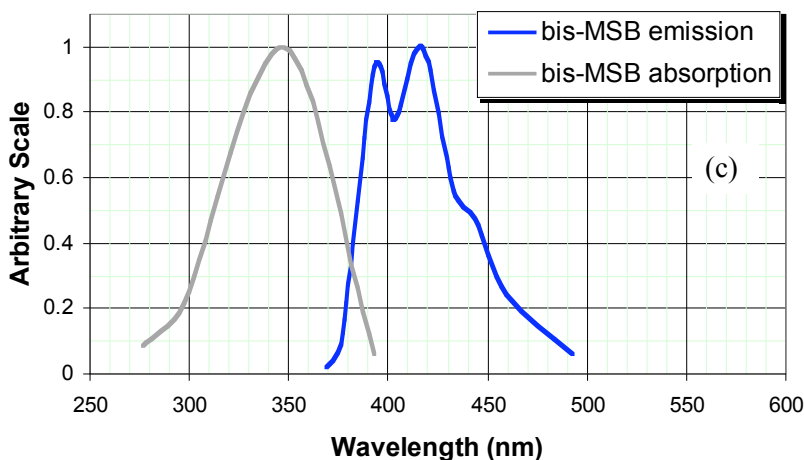
Figure 6–13: Absorption and emission spectra of bis-MSB. The absorption below 280 nm has not been found in the literature.

The group at Indiana University did an exploratory study on light guides extruded at Fermilab having a co-extruded layer doped with different concentrations of bis-MSB. Figure 6–14 shows the results of this preliminary study. The spectra in this figure have not been corrected

for the spectrum of the deuterium lamp. The figure shows that there is clear absorption of 128-nm photons with re-emission at 420 nm when compared with an undoped bar. The current effort is aimed at comparing the 420-nm light output of bars doped with bis-MSB to bars doped with TPB when illuminated at 128 nm.
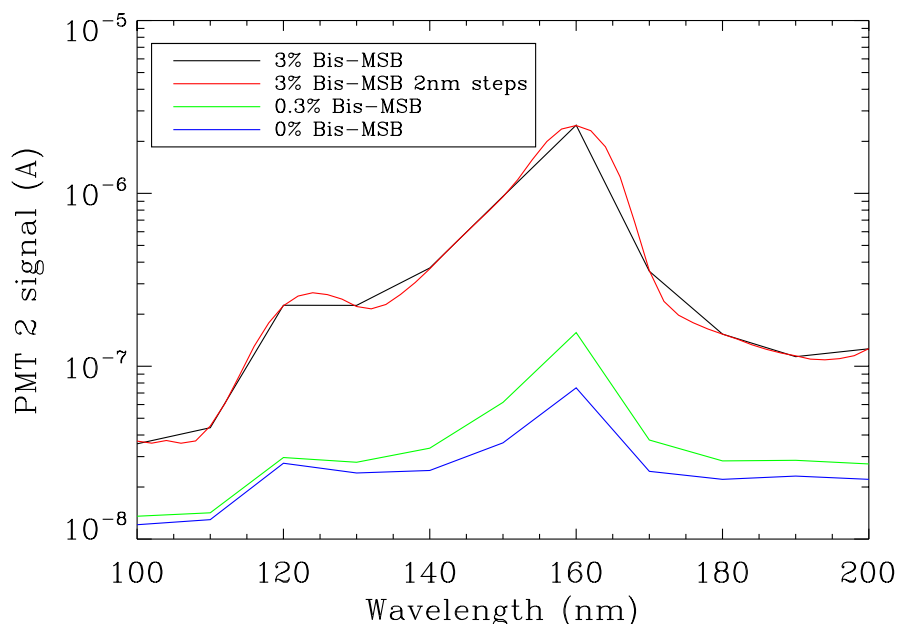
Figure 6–14: Relative emission at 420 nm for co-extruded bars doped with bis-MSB as a function of illuminating wavelength in the VUV monochromator at Fermilab. The co-extruded bars, doped with different concentrations of bis-MSB, are compared with an undoped bar. The spectra are not corrected for the deuterium-lamp spectrum.

6.4.1.2   p-Terphenyl

Another cost-effective waveshifter that may prove to absorb at 128 nm and re-emit at 420 nm is p-Terphenyl. The absorption and emission spectra are shown in Figure 6–15. Bars doped with p-Terphenyl will be compared to bars doped with bis-MSB or TPB.

6.4.2   Cast-Acrylic Light Guides

As a test of the technology, several cast-acrylic bars were obtained from a commercial vendor to compare with the extruded polystyrene bars. Work at MIT suggests that cast acrylic may prove to be a superior method producing light guides. The first tests of the commercial
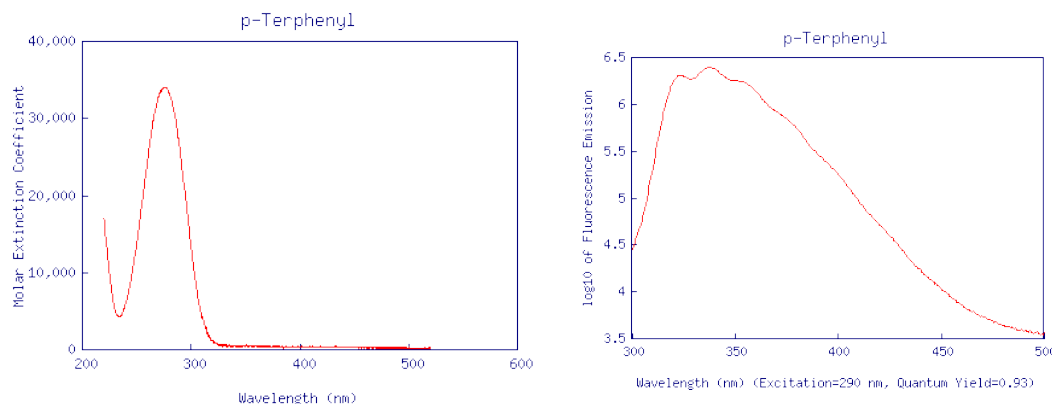
Figure 6–15: p-Terphenyl absorption (*left*) and emission (*right*) spectra. The absorption below 200 nm appears to be rising.

cast-acrylic bars compared their attenuation lengths to those of extruded polystyrene bars. In addition, comparisons were done between the cast-acrylic bars and extruded-acrylic bars produced at the Fermilab extrusion line.

As seen in Figures 6–16 and 6–17, cast acrylic offers great promise because its attenuation length at 420 nm is significantly longer than that of extruded acrylic and extruded polystyrene. In addition, it might be possible to cast the light-guide paddle in one piece, which would significantly improve the efficiency of paddle construction. Clearly, cast-acrylic adiabatic light paddles show great potential.

However, as also seen in Figure 6–16, fluctuations in the cast acrylic are much larger than in the extruded parts shown in Figure 6–17. The cast acrylic clearly shows potential but the production of acceptable light guides with this technology requires improvement in uniformity. In addition, techniques for coating the cast acrylic with waveshifter for the large number of required paddles would need to be developed.

6.4.3   Silicon Photomultipliers

Over the last decade a new type of photon detector has been developed, generically called Silicon Photomultipliers (SiPM), which may provide an attractive alternative to PMTs as detectors for the photon-detector system in the LArTPC.

An SiPM is a photon-counting multi-pixel device, consisting of silicon-based avalanche photodiodes (APD) operating in Geiger mode. The characteristics that make them attractive for this task are their high photon-detection efficiency (PDE), high intrinsic gain (10^5 to 10^7), lack of need for an HV system, increased performance in cryogenic environments, low cost per sensitive area and low peripheral costs. There are now many manufacturers of SiPMs
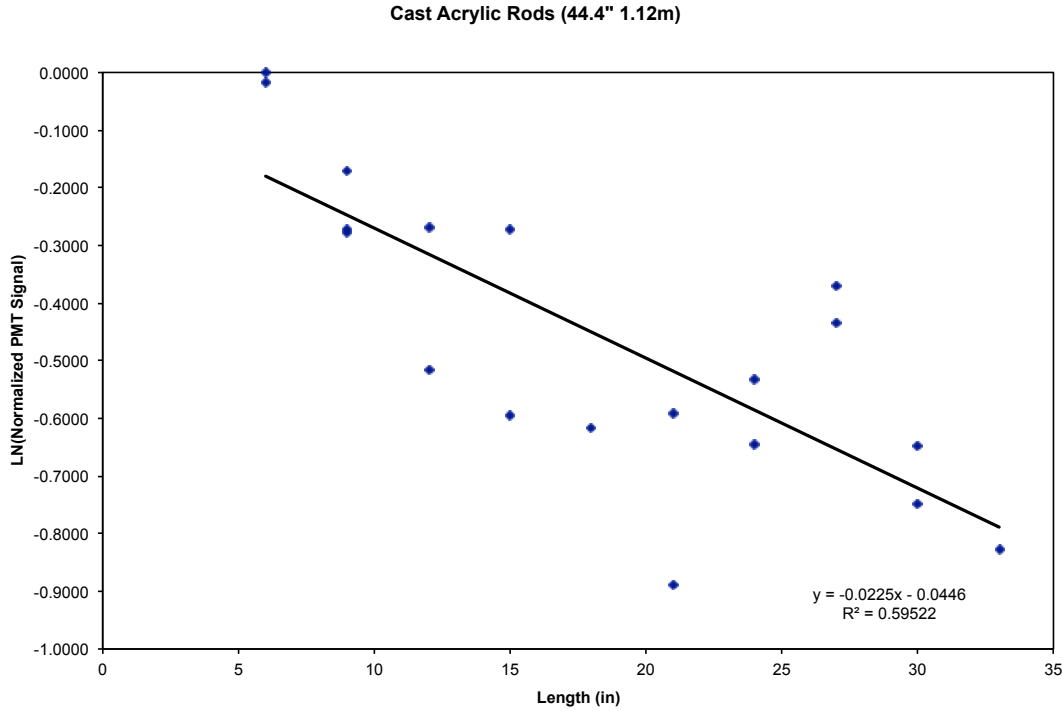
Figure 6–16: Attenuation lengths at 420 nm for cast acrylic, $l = 44.4''$

(Hamamatsu, CPTA, SensL, MEPhI/Pulsar, and AdvansID, amongst others).

Figure 6–18 shows the PDE for the Hamamatsu's S11064, a 4×4 channel array, in which each channel is a 3×3 mm^2 SiPM. The PDE has been corrected for crosstalk and afterpulses, as measured by the manufacturer. This device is being studied at Fermilab.

In the particular case of the above device, the effective active area-per-channel is 9 mm^2 and for 16 (4×4) channels, the photosensitive area is 144 mm^2. The fill factor is 0.308, reducing the effective photon-collection area to 44.35 mm^2.

The Indiana University group is studying the Hamamatsu S10985-100C, a 2×2 channel array in which each channel is 3×3 mm^2. There are 900 pixels per channel with a pixel size of 100 μm^2. There is an effective active area-per-channel of 9 mm^2, giving a total area of 33 mm^2 for the four channels. The fill factor is .785, reducing the effective collection area to 28.26 mm^2. At peak sensitivity of 440 nm, the PDE is 50%.

6.5   Preliminary Engineering Design and Prototyping

The preliminary engineering design studies will concentrate on production of prototype light-guide paddles with the goal of producing the paddles needed for the integrated system tests in the 35-ton membrane-cryostat prototype detector, discussed in Sections 8.3.7 and 8.3.8. These prototype light guides will be based on the reference design. The light guides will be tested in an apparatus at Indiana University that is based on the MIT design [28]. The paddle assemblies and their associated photodetectors will first be tested at a more appropriate facility like Fermilab's LAPD facility, discussed in Section 8.3.3.

As the prototypes are developed, three areas will be investigated as potential paths to improve the light guide/paddle performance and cost. As described above, these include (1) alternative production technologies for light guides; (2) alternative, more cost-effective waveshifters; and (3) SiPM photodetectors.

Efforts that contribute to development of the LBNE photon-detection system design are described in Section 8.3.4.

Extruded Acrylic Attenuation Length (16.75" 0.42m)

y = -0.0597x + 0.3713
R² = 0.882

Extruded Polystyrene Attenuation Length (11.64" 0.296m)

y = -0.0859x + 0.4731
R² = 0.99432

,
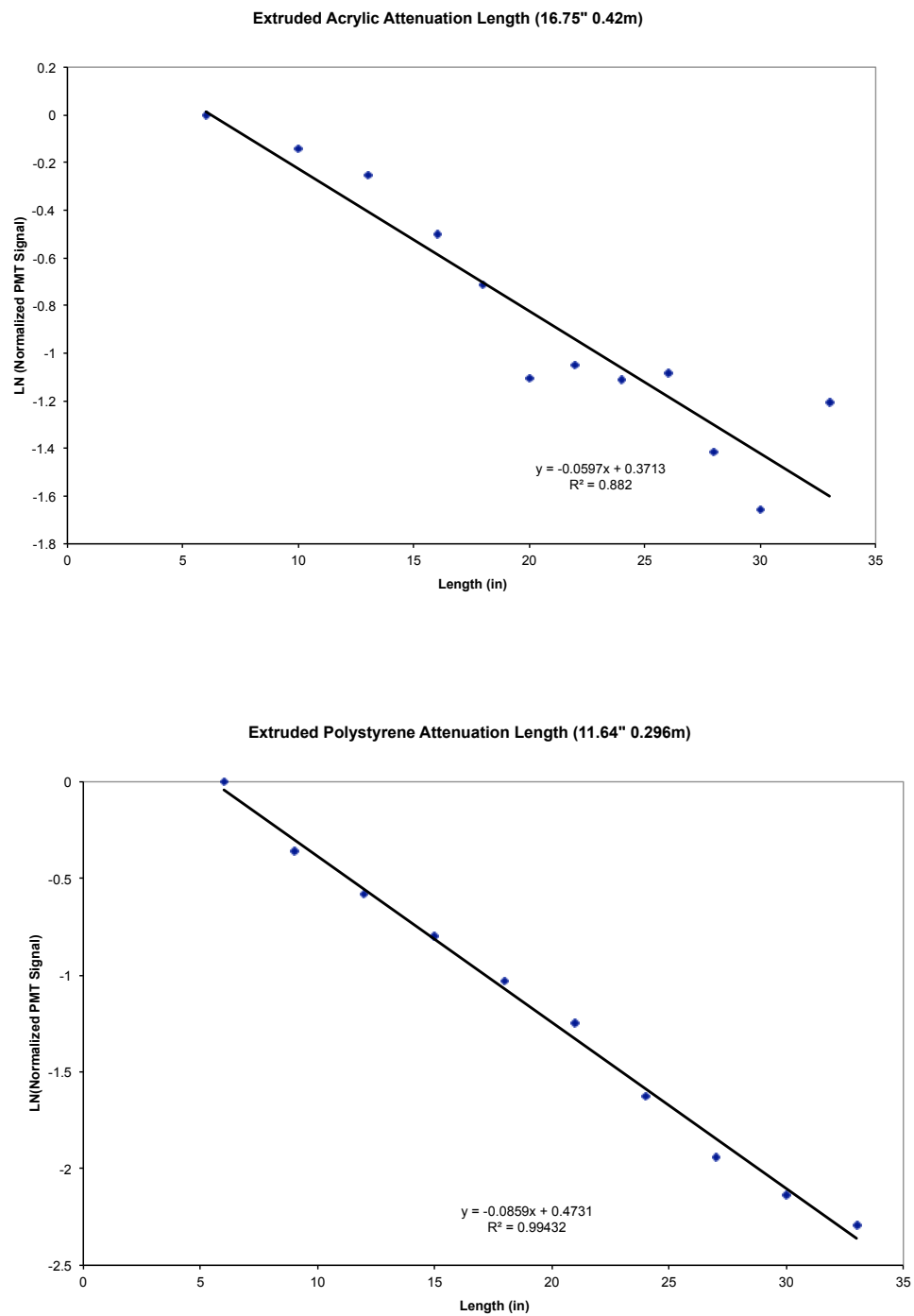
Figure 6–17: Attenuation lengths at 420 nm. (*top*): extruded acrylic, $l = 16.8''$); and (*bottom*): extruded polystyrene, $l = 11.6''$.
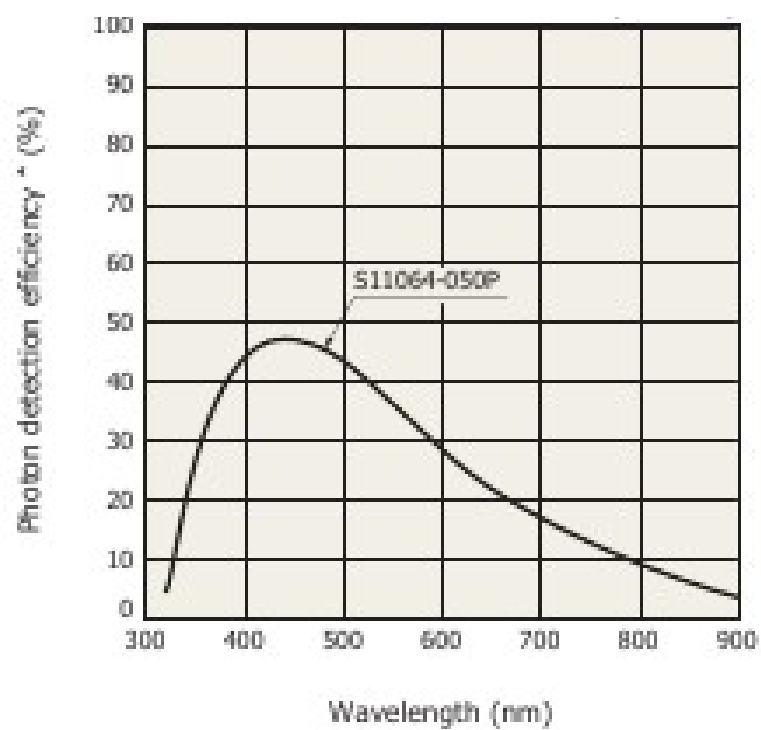
Figure 6–18: PDE for the Hamamatsu S11064 SiPM.

7   Installation and Commissioning (WBS 130.05.06)

7.1   Introduction

The scope of the Installation and Commissioning task is the installation of the detector systems and the startup and commissioning of the detector. The task also includes the design, and procurement of any special equipment required for detector installation. The Installation and Commissioning task interfaces with the detector subsystems and the far site Conventional Facilities.

LAr-FD construction and installation will occur in a series of distinct phases (those items under the control of this WBS are shown in italics):

- *installation planning and prototyping*

- *storage set-up and operation of receiving area for detector components*

- excavation and outfitting of the Detector Hall at the Far Site; this activity is the responsibility of the Conventional Facilities L2 Project (CF), WBS 130.06

- construction and installation of the cryogenics system and cryostats by a construction management firm; this activity is the responsibility of the cryogenics system (WBS 130.05.02)

- construction of LAr-FD components at collaborating institutions and shipment to the Far Site; this activity is the responsibility of the detector sub-systems and will occur in parallel with the Far Site outfitting and cryogenics construction

- *installation of detector components and installation management*

- delivery of LAr and *transfer of LAr to the cryostats*

- *commissioning activities leading to CD-4*

The Installation and Commissioning group will begin work on infrastructure and other LAr-FD facilities upon receipt of Beneficial Occupancy of the Detector Hall. The following items will have been put in place at that time:

- ventilation in accordance with OSHA standards

- electrical power sufficient for the HVAC, cryogenics plant cooling and general electrical services

- quiet power for the electronics with a double Faraday-shielded transformer connected with long cables to the Detector Hall to take advantage of the inductance of the power lines. The primary shield will be connected to the main substation via a grounded feed wire and the secondary shield will be connected to the Ufer ground.

- communications consisting of telephone lines and computer network

- Detector Hall lighting in accordance with OSHA regulations for industrial use

- lighting with battery-powered backup or emergency circuit backup

- environmental monitoring of oxygen, carbon monoxide, smoke and temperature

- sump pumps for groundwater removal

- a 15-ton bridge crane in the Detector Hall

- truck docking stations with drive through option

The cryostat and cryogenics contractor will retain responsibility for the site during construction of the cryostat and cryogenics system with that L3 WBS system providing oversight. Upon completion of this contract, the cryostat and cryogenics L3 WBS system will have completed the following tasks:

- the LN2 refrigeration system will be complete and tested

- the LAr systems will be constructed and tested without the introduction of cryogens into the cryostat

- the cryostat will be leak tested and cleaned

- the access hatches on the cryostat and the cryostat feedthroughs will be temporarily sealed

- the APA- and CPA-installation support beams will be in place

- the cryostat will be electrically connected to the steel roof structure thus connecting the detector ground to the "Ufer" ground

In the Ufer grounding scheme, the detector will utilize the cryostat pit rock bolts. The rock bolts in the pit will extend through the concrete that lines the pit and be attached to the reinforcing steel network within the cryostat concrete liner, thus forming an Ufer ground. The reinforcing steel will be connected to the steel truss cover. The Ufer ground will be connected to the detector ground (the cryostat SS liner) through a low-impedance connection.

The responsibility and authority for the design, installation and use of the detector quiet-power distribution and detector-grounding system is held by the L2 project electrical engineer. This engineer has oversight responsibility for all electrical and electronics design and installation tasks, including all attachments to the detector that create an electrical connection.

The Installation and Commissioning group will be responsible for all LAr-FD-related activities at the Far Site from this point in time until the end of the LAr-FD project. Close coordination is clearly required between this group, system groups that provide components and other Far Site construction activities.

On-project commissioning activities include the coordination of system-checkout activities, culminating in the approval to introduce LAr into the detector modules, and managing the steps required to meet the CD-4 goals.

7.2   Material Receiving and Storage

Detector components will be delivered to the Far Site over a period of many months and will need to be stored in a storage facility. This will allow the supply of material to be maintained ready for installation. A facility for this purpose will be identified and an agreement will be made for its use during LAr-FD construction.

The initial storage plan includes three facilities: a 4,000 ft^2 warehouse structure for material receiving and unpacking, an on-site hardstand for storage of a small number of cargo containers and an off-site hardstand area for the storage of a larger number of cargo containers. Material will be transferred from these areas to the Detector Hall for installation, as required. Each system group is responsible for delivery of its components to any of the three facilities. The Installation and Commissioning group will provide the management and labor resources for inventory control, material handling and transport from the off-site and on-site storage facilities to the Detector Hall.
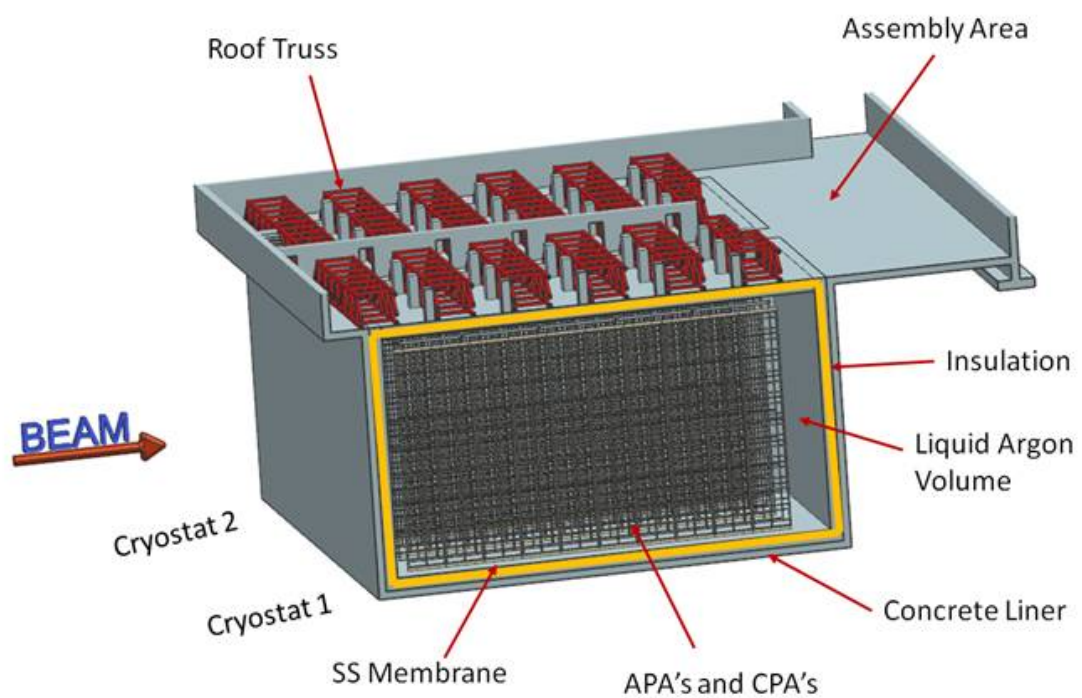
Figure 7–1: Cutaway view of detector with TPC detectors installed

7.2.1   Cryostat Materials

The warehouse storage space will initially be made available to the cryogenics system contractor who will construct the cryostats. The cryostat insulation will comprise the largest bulk of material; approximately 2000 m^3. Figure 7–2 shows membrane-cryostat components staged in the hull of an LNG tanker under construction.

Figure 7–2: Membrane cryostat components staged in a LNG transport ship under construction.

Cryostat materials will come from overseas in approximately 35 shipping containers that will be stored off-site. The containers will be brought to the Detector Hall.

Control of the storage area will revert to the Installation and Commissioning group when the cryostat-construction contract is completed.

7.2.2 TPC Materials

APAs and CPAs, referred to as "TPC panels" in this chapter, will be constructed before arrival at the Far Site. The Photon Detector light guides will be installed in the APA panels. The electronics will already be installed and the cold-testing performed. They will be shipped in sealed shipping containers to either the on- or off-site hardstand area, depending on the TPC production rate. No significant preparation or extensive testing of these components is required after arrival and prior to installation. The entire set of TPC panels for the two-cryostat detector will require approximately thirty shipping containers. Figure 7–3 shows a group of TPC panels in a shipping container. The panels will be held in a rack that will also be used to hold the panels in the installation staging area in the Detector Hall. Each rack of panels will be sealed to maintain cleanliness.

TPC-panel containers will be transported to the Detector Hall and unloaded every few days to supply the TPC components for installation.

7.3 Detector Pre-Installation (WBS 130.05.06.06)

The detector pre-installation activities must be completed prior to the start of TPC installation into the cryostat. These activities include design, procurement and installation of detector-specific infrastructure such as man-lifts, lifting fixtures, ladders, tools, and so on. The major items include the support rails for the TPC panels, installation monorails for moving the panels inside and outside of the cryostat, the lower panel holding fixture for joining two panels, fixed scaffolds with stair towers at the cryostat hatches, and a mobile scaffold for providing access to the top and middle of stacked TPC panels. The equipment also includes a temporary floor for the cryostat and temporary ventilation and lighting inside the cryostat.

7.3.1 Rails for TPC-Panel Support and Transfer

The support rails are key elements of the TPC installation process. Segments of support rails will be included in the installation prototype. The rails will be designed to meet the requirements of the detector and compatible with LAr service. The rail installation can be completed most efficiently while the large scaffolding system used for cryostat construction is still in place, therefore that task will be part of the cryostat-construction contract.

A set of seven support rails, shown in Figures 7–4 and 7–11, permanently mounted in each cryostat, will provide the support for the APA and CPA panels and a track for moving the panels into position. Support rods spaced at 5-m intervals will support the rails. The rods will be hung from anchor points mounted in the top of the cryostat. The anchor points will
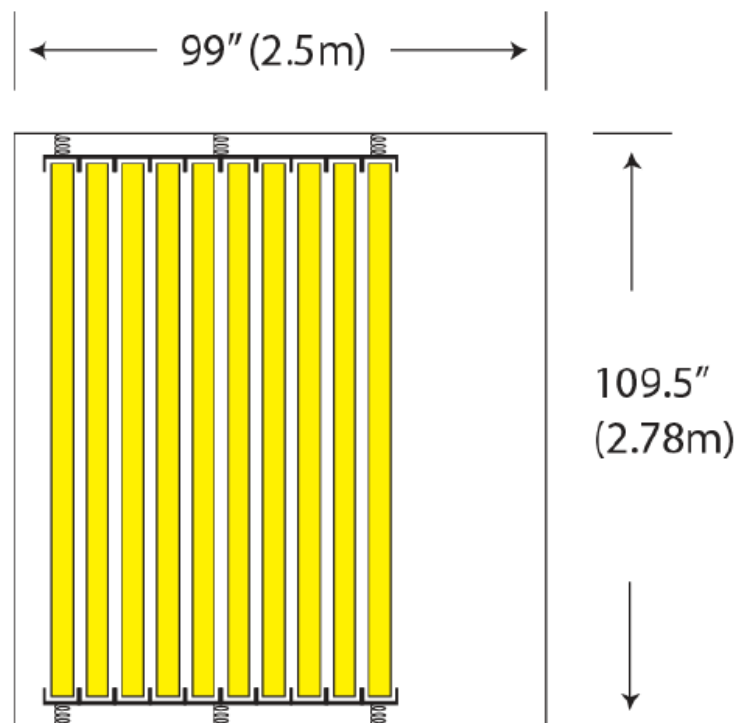
Figure 7–3: Concept for APA shipping containers - cross section view

be designed for a capacity of approximately 1,500 kg with an appropriate safety factor. The thermal load through the anchor points should not be a significant load on the cryogenic system. The rods will be adjustable to enable level installation of the rails, which will be done in rail segments with the aid of a laser level. The rails shrink approximately 7 cm along their entire length during cooldown. The rods will be installed with an angle bias that allows the rails to return to level after the cryostat and TPC is cooled.

The mass of each stacked set of APA panels is 600 kg and the mass of each stacked set of CPA panels is 250 kg. The load of the TPC on the support rails comes to 200 kg/m for the APA rails and 100 kg/m for the CPA rails. The rail segments will be constructed from 20-cm-deep laser-welded, W-shaped, stainless steel beams. The rail segments will be joined end-to-end with large pin connections. The upper support rods will be made from 15-mm-diameter stainless steel.
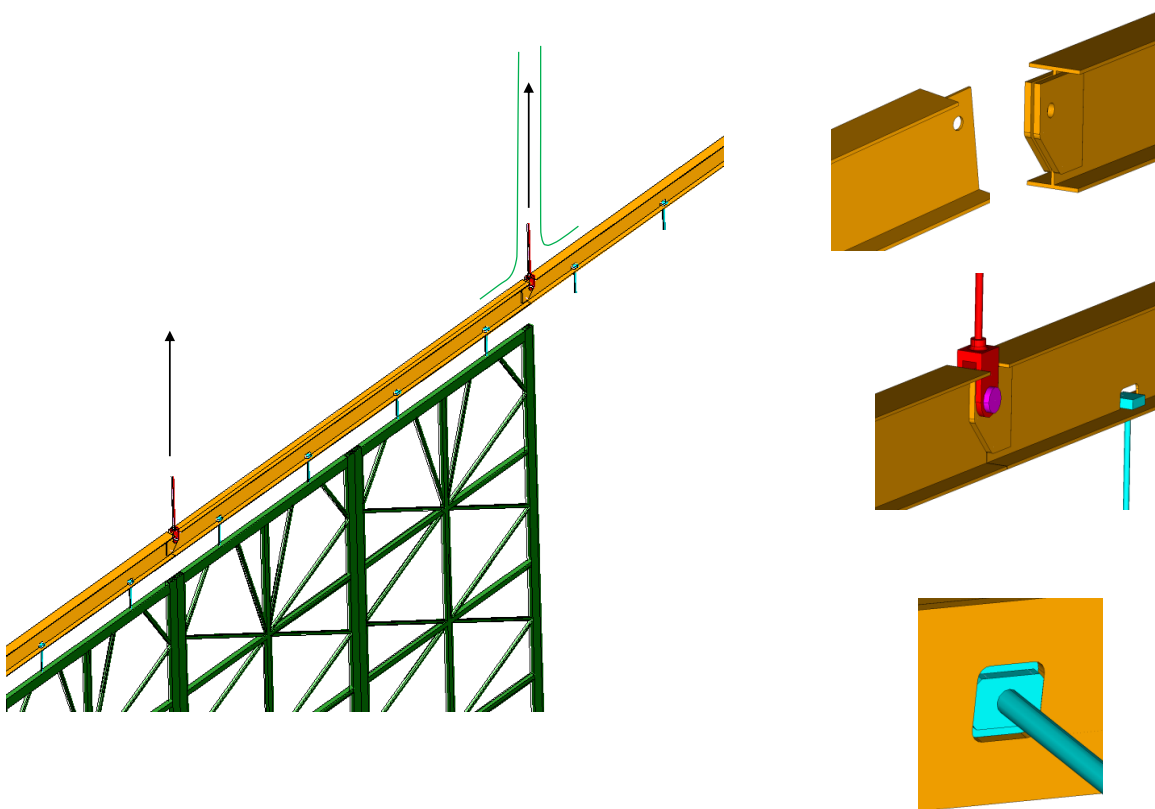
Figure 7–4: Support rails inside cryostat

Signal and power cables will be installed from the cryostat feedthrough ports next to the APA support rods, shown in Figure 7–5, along the rails to the point where the connection to the APAs will be made. The cables will be preplaced and tested before APA installation

begins.
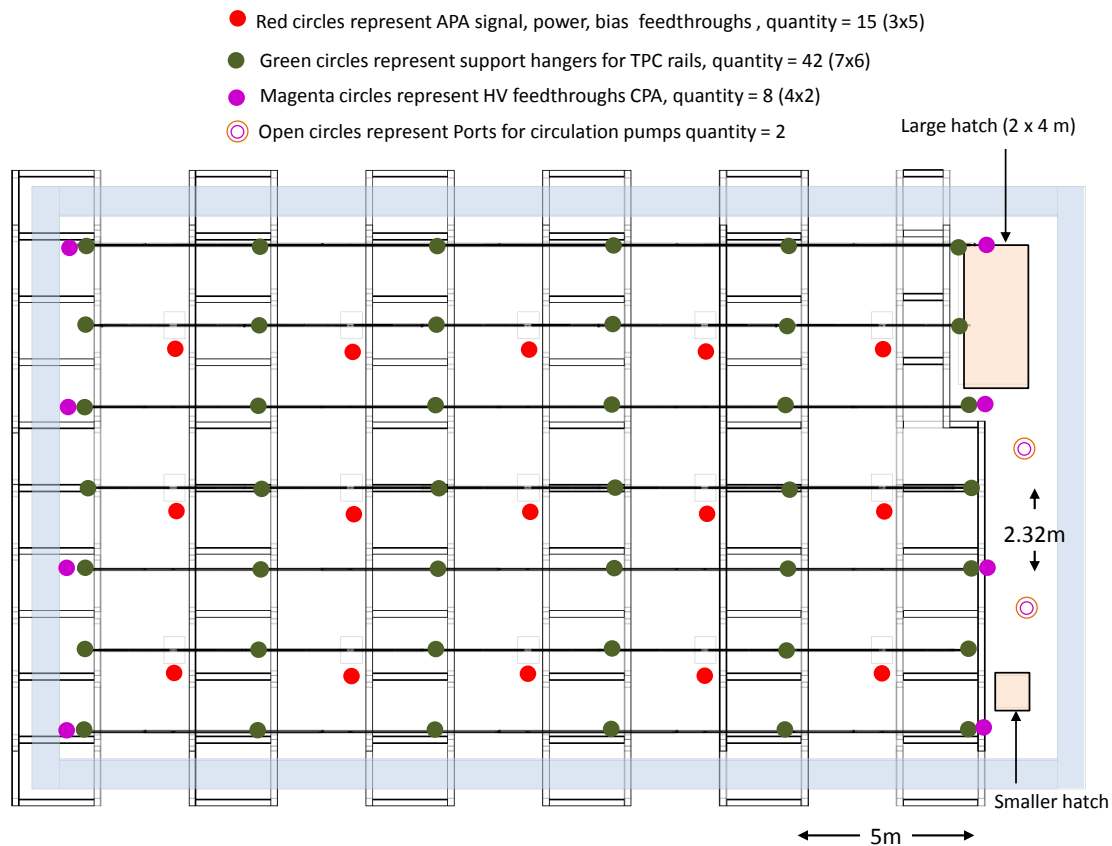
Figure 7–5: Feedthroughs

A transfer rail with motorized trolleys will move TPC panels inside the cryostat. After top and bottom panels are connected, a motorized trolley will move the stacked panels from the hatch area to the final position. Since the duty cycle of the trolley is rather low, the trolley could be battery-powered to avoid the need for cable festooning. The trolley initially moves along a transfer rail until it reaches the end of the final support rail where the stacked panel will be permanently mounted. An arrangement of transfer switches is used to connect the transfer rail to the final support rail. See Figure 7–6 for an example of a transfer rail. The trolley and transfer rail are removed when TPC installation is complete. The trolley and transfer rail do not need to compatible with LAr service but they will be constructed of materials appropriate to prevent contamination of the detector.
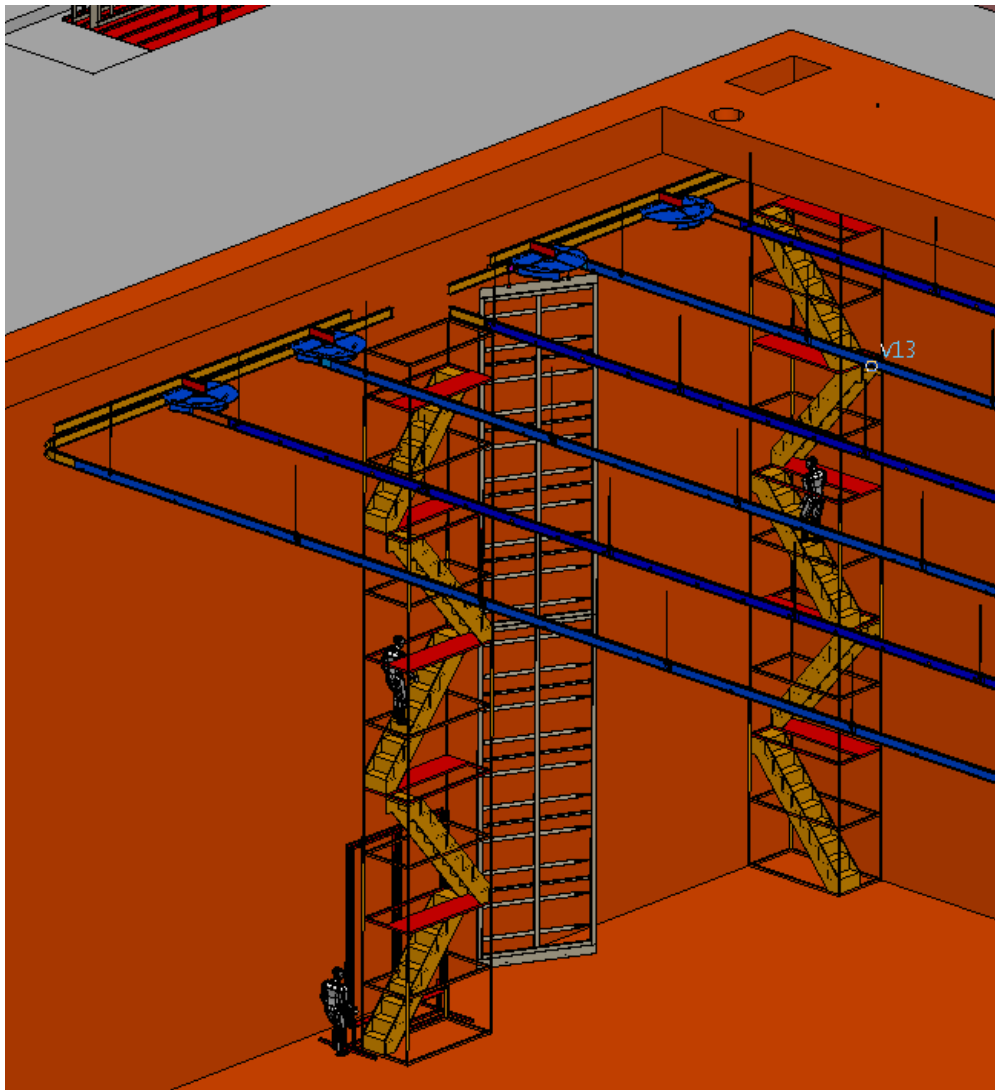
Figure 7–6: TPC installation monorail with APA moving to support rail

7.3.2   Equipment Required Inside the Cryostat for Detector Installation

Several items will be installed in the cryostat for use during TPC installation, and removed before the cryostat is filled with argon.

- A temporary lighting system inside the cryostat with emergency backup lighting will be in place for TPC installation and removed in sections as the TPC is installed and be completely removed before filling the crysotat with Argon.

- A ventilation system and air-monitoring sensors with alarms will assure adequate air quality for the personnel working inside the cryostat. The system will also include a high-sensitivity smoke-detection system that is interlocked to the power for all devices inside the cryostat. The blowers and temperature control will be located outside of the cryostat and polyester ducts will be located inside the cryostat to distribute the air properly.

- A raised-panel floor to protect the cryostat floor; see Figure 7–7. The raised-panel floor will have support spacers located between the convolutions in the stainless-steel primary membrane to provide a flat surface for moving equipment around within the cryostat. The pressure limit for the insulation in the floor is 0.5 MPa and the load of the vacuum that will be used to monitor leakage during installation reduces the effective limit to 0.4 MPa. The stock round spacers in the raised-panel floor are 10-cm diameter and would support a load of 310 kg. The load can be increased by adding larger-diameter plates under the standard spacers. Since the raised floor is modular, it can be removed in sections as the TPC installation progresses. A perforated pipe manifold will be located on the cryostat floor to distribute the argon during the gas piston purge and during liquid recirculation. Depending on the details of the membrane cryostat corrugation height, the distribution piping may fit under the temporary floor or be installed in sections as the floor is removed.

- Tooling for APA and CPA panels including fixtures to insert the lower APA and CPA panels. The top and bottom TPC panels of a stacked pair will be moved into the cryostat separately and connected together below the cryostat equipment hatch. A lower panel holding fixture will temporarily hold the bottom APA and CPA panels when they are inserted into the cryostat. See Figure 7–8.

- Two fixed scaffolds with integral stair towers will be installed temporarily inside the crysotat. One tower will be located in the work area of the large hatch. This tower will provide access for personnel to make the connections between stacked panels and to connect stacked panels to the motorized trolley inside the cryostat. The second fixed tower will be located near the smaller hatch and will provide a second route of egress from the crysotat.

- A rolling scaffold with an integral stair tower will allow personnel to access the top of the stacked panel after they are in the final position. The rolling scaffold will be moved around the cryostat floor as the TPC installation progresses.

Figure 7–7: Raised-panel floor to protect the cryostat's primary membrane

7.3.3   Clean Area

A clean-area enclosure in the range of class 10,000 (ISO 7 equivalent) will be constructed near the entrance to the cryostat to keep the area around the open hatch isolated. The assembly practices used by the MicroBooNe experiment may serve as an example of what is required for a surface detector. The enclosure will have an area for personnel to gown with the appropriate clean-room clothing and safety shoes. A large, closable door, next to which the TPC-storage containers can be parked, will allow unloading of the TPC components directly from the container into the clean area. The TPC components will be cleaned to a level suitable for installation into the crysotat as part of the TPC production process and will be delivered to the Far Site in clean containers.
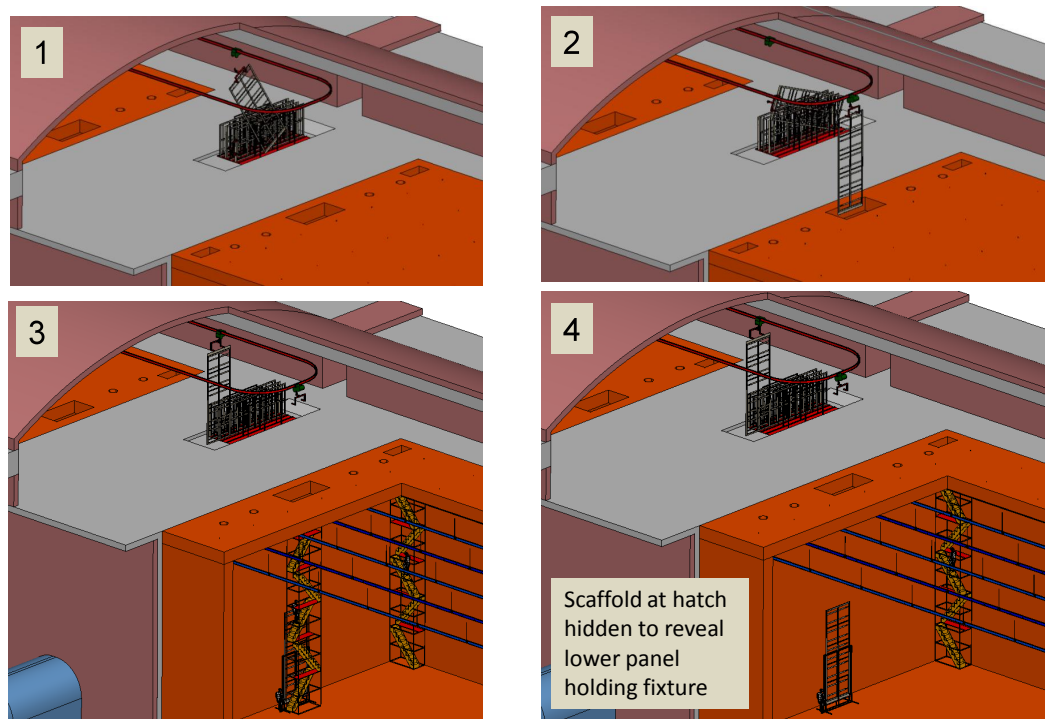
Figure 7–8: The bottom APA and CPA panels of the TPC are lowered through the cryostat hatch and held temporarily by a holding fixture

The Double Chooz detector developed a cleanliness plan to ensure that dust contamination did not contribute more than a specified amount to the detector signal. Measurements were made of the activity of rock in that experiment's underground laboratory which was assumed to be the source of airborne dust. Maximum allowable dust concentrations and the clean-room class and cleanliness practices were determined such as to meet the requirements for contamination. The Installation and Commissioning group will need to evaluate the dust sources in the LAr-FD detector pit and determine if a similar approach to setting the clean room requirements is appropriate.

7.3.4   Detector Electrical Ground

The LAr-FD will have approximately 300,000 channels of electronics with an intrinsic noise level of less than 1,000 electrons. These channels will be connected to wires that are seven meters long. Thus, grounding, shielding and power distribution are critical to the success of the experiment. In the reference design the entire detector pit will be treated as the detector ground for the following reasons:

- The cryostat has a large number of penetrations for supporting the APAs that extend to the support structure above the cryostat. There are also 15 signal feedthrough ports which connect to racks located on the top of the cryostat. Achieving and maintaining adequate AC isolation on such a large structure during construction will be difficult. In addition, the pit has very few connections to the outside world so it is much easier to isolate it as a whole than the individual pieces.

- Secondly, it is necessary to provide a conductive body with a large enough self-capacitance that its voltage changes only negligibly when electric charge flows onto it. In this way the detector pit can serve as a sink of unwanted current without generating noise in the detector.

7.3.4.1   Reference Design

Earth ground will be provided by the Ufer grounding system in the concrete walls and other concrete support structures. This ground will be attached to the rock bolts in the detector pit walls and augmented by the large amount of steel in the roof-support trusses and the upper metal floor. To be an effective ground, all of the steel support structure will be welded together. The welds need not be structural; their use is only to assure reliable long-term electrical connections.

In order for this system to work, the detector pit must be kept noise-free, i.e., all connections, except AC power, between the detector and the outside world must be electrically isolated either by dielectric breaks or optical isolators. Electric motors will be restricted to three-phase

induction motors except for special, well-controlled cases. Electric heaters will be controlled by switches rather than SCRs. Digital equipment such as network switches will be run at frequencies of 30 MHz or higher whenever possible so that the noise remains outside the bandwidth of the TPC preamplifier. Some equipment, such as switching power supplies, will still need special attention to ensure that they do not generate noise in the detector.

As the only conducting link to the outside world, the AC power must be filtered to eliminate any electrical noise. Since the currents are large, it is most economical to implement a filter using the inductance of the power cable itself along with some capacitors to form a capacitor-inductor filter.

The AC power design will have a 2.5-MVA transformer that feeds the compressors and pumps of the cryogenic equipment and a 750-kVA transformer shown in Figure 7–9 (top) that feeds the purification equipment and detector. The detector transformer will have double faraday shielding with the primary shield returned on the ground wire to the substation. The second shield will be connected to the local Ufer ground and to the pit by the required grounding wire. The 480-V power will be transmitted from the substation to a separate switch gear for each detector in the Detector Hall. The switch gear will directly distribute power to all of the 480-V loads. The switch gear will also feed 50- or 100-KVA single faraday-shielded transformers that power relay racks located on the cryostats. The number and size of the transformers may change depending on the final loads and additional optimization of the isolation of the detector power.

A saturable inductor between the two transformer shields will be used to isolate the primary and secondary shields and separate their grounds. The secondary shield and transformer frame are connected to Earth ground at the transformer. The ground wire running back to the substation is only locally grounded through the saturable inductor but it is fully grounded at the substation. A fault between the secondary and primary shields would trip the substation breaker due to current flowing in the return ground wire. If this wire were disconnected, the current would flow through the saturable inductor to Earth ground and also trip the substation breaker. Figure 7–9 (bottom) shows an inductor used at D-Zero and the voltage developed across the inductor as a function of the fault current. The inductance is completely saturated by 100 A and the developed voltage is still safe.

7.3.4.2   Ground Features

It is important that all the components inside each detector module be connected to a common ground. The best candidate for this common ground, and the one chosen for the reference design, is the top of the cryostat. The APAs will have ground braid connections to the roof at two points on each panel. The lower APAs will be connected to the upper ones by their mechanical mounting connections. The front-end boards, phototube ground and the reference ground for the bias voltages will all be connected to the APA frame.

Block diagram of the AC power for the detectors

Saturable inductor used for ground isolation

Voltage developed across the inductor as a function of the fault current
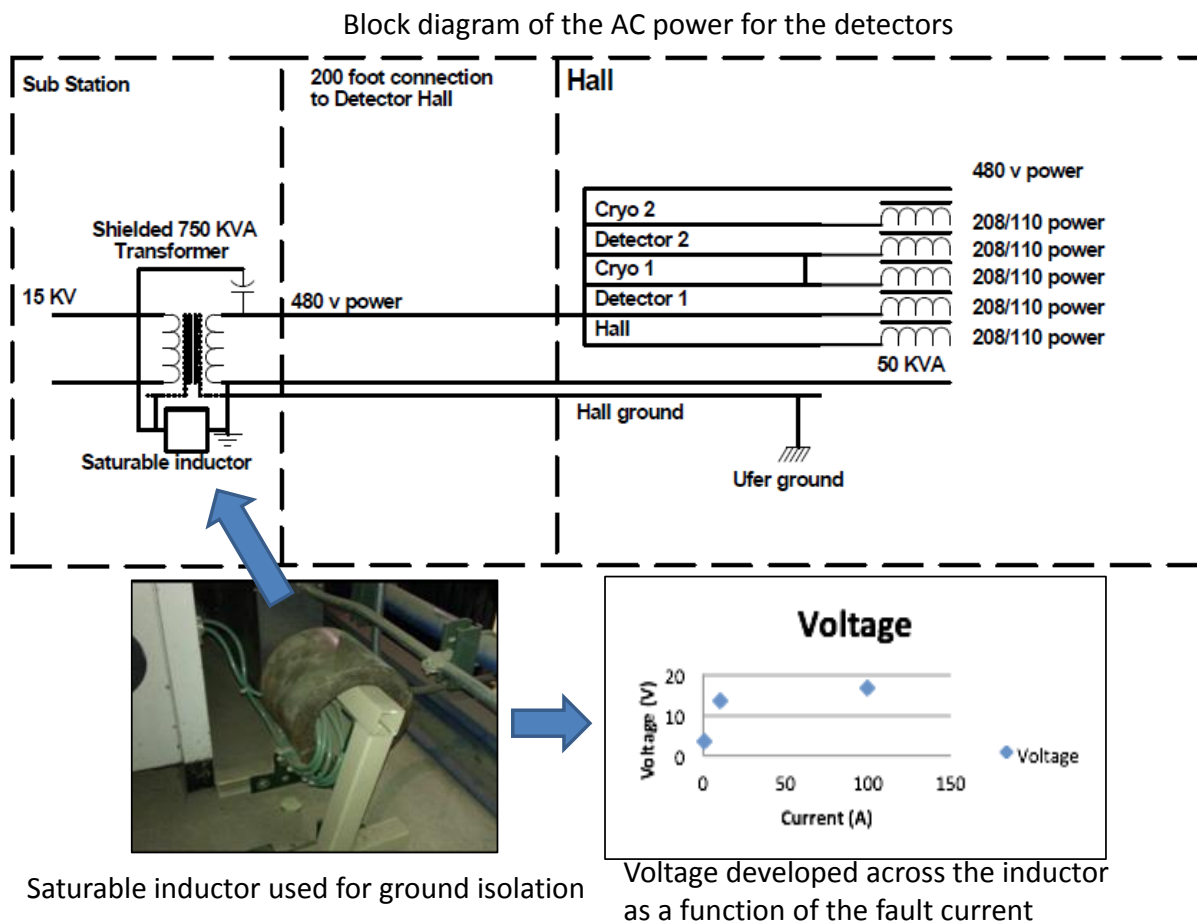
Figure 7–9: Block diagram of the AC power for the detector modules with a saturable inductor to separate the grounds of the transformer shields

The top of each cryostat is made of 1.2-mm or 2.0-mm-thick stainless steel, a poor conductor, and therefore does not serve as an adequate ground plane. The best solution would be to add a copper sheet directly on top of the cryostat, however this is difficult to do. Instead the copper sheet will be installed over the insulation that is on top of the cryostat membrane, about one meter from the cryostat, and connected to it via a grid of connections spaced 2.5 m apart. This spacing will give good electrical performance up to 12 MHz – well above the input bandwidth of the amplifier. The connections will be made with copper strips that fit in gaps in the insulation. Power supplies and power-supply filters (including the cathode supply) will all be grounded to this plane.

A port is located above every other APA junction and each port will serve the four APAs located directly underneath it. Cables for the bottom two APAs will be routed through the hollow cable frames to provide both mechanical support and electrical shielding. The digital cables will be located in the left frame member, and the power and bias lines will be routed through the right frame member. The horizontal portion of the cable run will be outside of the wire planes, so the use of doubly shielded cable such as "Amphenol skew clear" may be adequate. If not, then custom metal shields will be mounted on the front-end circuit boards.

The racks will be mounted either directly over the ports or adjacent to them with an extension to the rack that covers the port. All cables can be brought out of the cryostat into a grounded and shielded enclosure. The plan is to use 36-in-deep racks and construct a shielded area on the back side of the rack to hold the excess cable. Fifteen racks will be required for each cryostat, and rack space will be shared between the TPC and photon-detection system readout and power supplies. A modest number of racks will be required for the DAQ in the control room. All relay racks will be equipped with rack protection and monitoring. The racks will be supplied by the detector installation effort.

The digital electronics does not present a grounding issue in the strict sense, but it does affect noise. The plan is to operate the digital system with at least a 32-MHz clock that is well above the upper bandwidth of the input amplifier (the 3-db point is less than 1 MHz).

The 35-ton prototype will provide an opportunity to test some aspects of the system. Measurements of electrical noise in this prototype cryostat will be performed before and after installation of the TPC.

7.4 Detector Installation Activities

The following list of detector components and systems will be installed in the Detector Hall and cryostats:

- Relay Racks with rack protection (15 on each cryostat plus a few in the control room)

- Cable trays and power distribution to racks from power panels provided by CF

- Cable inside and outside of the cryostat including cable feedthrough flanges

- DAQ crates and power supplies in the relay racks

- The 60 APAs per cryostat with integrated photon detectors

- The 80 CPAs per cryostat

- Cryogenic instrumentation not installed by the cryostat construction vendor (e.g. purity monitors)

- Temporary ventilation, lighting and access equipment

- Note: Support rails and hangers are installed during cryostat construction
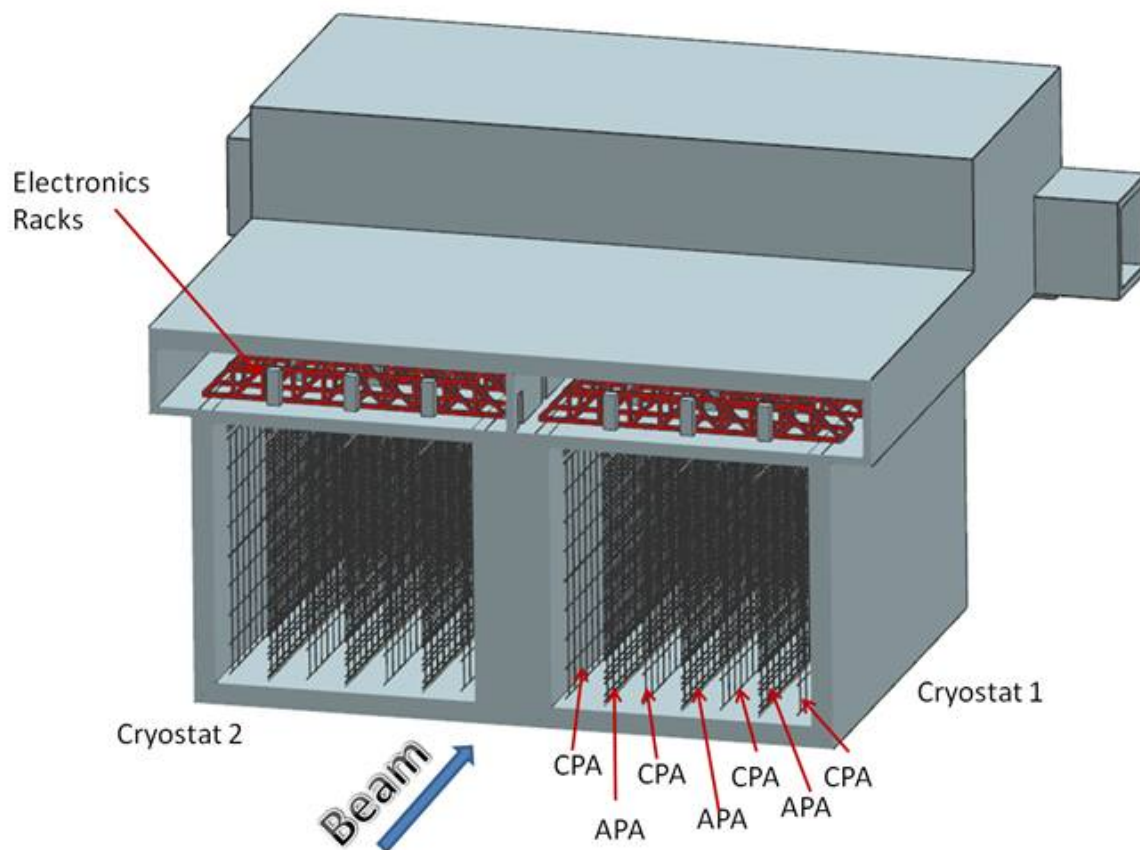
Figure 7–10: TPC panels installed in cryostats

7.5   TPC Installation

Each APA and CPA panel will be carefully tested after transport into the clean area and before installation into one of the cryostats. Immediately after a panel is installed it will be rechecked. Throughout the installation period it will be checked periodically. Testing is described more fully in Section 7.8. The serial stacking of the APA and CPA panels along the rails means that removing and replacing one of the early panels in the row after several others are installed would be very costly in effort and time. Therefore, to minimize the risk of damage, as much work around already-installed panels as possible will be completed before proceeding with further panels.

The installation sequence is planned to proceed as follows:

1. Install the monorail or crane in the staging area outside the cryostat, near the equipment hatch.

2. Install the relay racks on the top of the cryostat and load with the DAQ and power-supply crates.

3. Dress cables from the DAQ on the top of the cryostat to remote racks.

4. Construct the clean-room enclosure outside the cryostat hatch.

5. Install the raised-panel floor inside the cryostat.

6. Insert and assemble the stair tower and mobile scaffold.

7. Install the transfer rail with switches and the staging platform inside the cryostat

8. Install protection on (or remove) existing cryogenics instrumentation in the cryostat.

9. Install the cryostat feedthroughs and dress cables inside the cryostat along the support beams.

10. Begin regular transport of TPC panels in shipping boxes into the Detector Hall.

11. Install TPC panels:

    (a) Install a connected APA-CPA panel pair.

    (b) Connect power and signal cables.

    (c) Test each APA wire for expected electronics noise. Spot-check electronics noise while cryogenics equipment is operating.

    (d) Connect field cage in sections as the APA and CPA installation progresses.

    (e) Perform electrical test on CPAs and field cage.

    (f) Remove temporary floor sections as the TPC installation progresses.

    (g) Install sections of argon-distribution piping as the TPC installation progresses.

12. Complete the field cage.

13. Remove the transfer rail, holding fixture, movable scaffold and stair towers.

14. Temporarily seal the cryostat and test all channels for expected electronics noise.

15. Seal the access hatch.

16. Perform final test of all channels for expected electronics noise.

In general, APA and CPA panels will be installed in order starting with the panel furthest from the hatch side of the cryostat and progressing back towards the hatch. The field cage will be installed in stages as the installation of APA and CPA panels progresses. After the stacked panel is attached to the support rods the electrical connections will be made to cables that were already dressed to the support beams and electrical testing will begin. Periodic electrical testing will continue to assure that nothing gets damaged during the additional work around the installed panel.

The TPC installation will be performed in three stages, each in a separate location; the locations, or zones, are shown in Figure 7–11 (this illustration was made for a 34-kton, in-line underground detector, but the work zones are also applicable for the 10-kton surface siting). First, in the clean room vestibule, a crew will move the APA and CPA panels from storage racks, rotate to the vertical position and move them into the cryostat. Secondly, in the panel-staging area immediately below the equipment hatch of the cryostat, a second crew will transfer the lower panels from the crane to the staging platform, connect the upper and lower panels together, route cables to the top of stacked panels and finally transfer the stacked panels on to the monorail trolley that moves within the cryostat. A third crew will reposition the movable scaffolding and use the scaffold to make the mechanical and electrical connections at the top for each APA and CPA as they are moved into position. The monorails inside and outside the cryostat will each have two motorized trolleys so that work can be conducted by all three crews in parallel. The steady-state rate for installation, given this work plan and a single-shift schedule, is estimated to be two stacked panels per day.

The requirements for alignment and survey of the TPC are under development. Since there will be plenty of cosmic rays in the surface detector, significant corrections can be made for any misalignment of the TPC. The current plan includes using a laser guide or optical transit and the adjustment features of the support rods for the TPC to align the top edges of the APAs in the TPC to be straight, level and parallel within a few mm. The alignment of the TPC in other dimensions will depend on the internal connecting features of the TPC. The timing of the survey will depend on understanding when during the installation process the hanging TPC elements are in a dimensionally stable state. The required accuracy of the survey is not expected to be finer than a few mm.
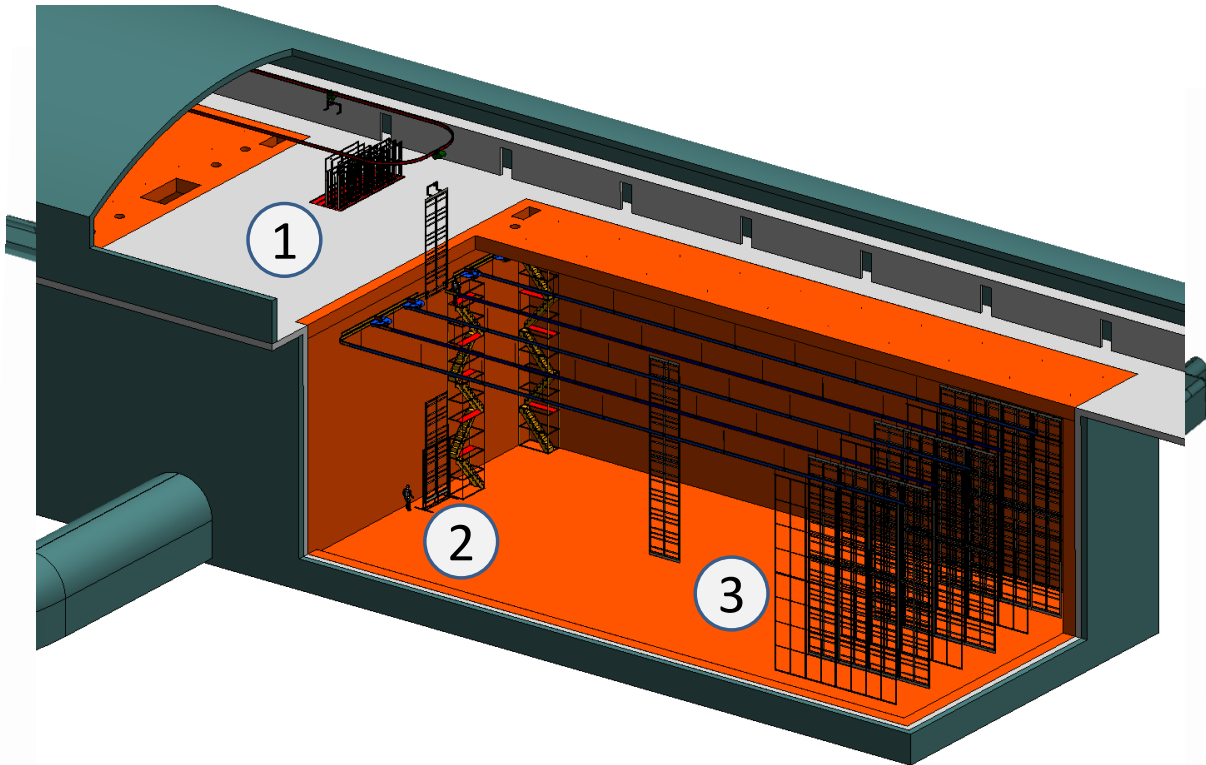
Figure 7–11: The three main work zones for TPC Installation. TPC components are lowered into the cryostat in zone 1. TPC components are connected together in zone 2, transferred to the support rails and then rolled into final position (zone 3). (The figure does not show reference design configuration, but the concept applies.)

The detector installation system is also responsible for developing and implementing the procedure for monitoring the integrity of the membrane-cryostat primary liner during installation. The space between the primary liner and the secondary liner will be held under vacuum during installation. The vacuum level will be automatically monitored and will alarm if any leaks develop in the primary membrane during TPC installation.

7.6   Installation Equipment Prototype

A full height mock TPC section will be constructed as part of an installation prototyope in a suitable location at Fermilab, e.g. the Wideband lab or the CDF or DZero assembly hall. See Figure 7–12. The installation equipment prototype is intended to test and verify the key elements of the equipment and the process for TPC installation and to serve as a training tool for personnel who will perform the TPC installation. The initial testing of the equipment at Fermilab will be used to verify or refine the installation concepts. Complete testing of the final equipment and operations will occur at Fermilab before the installation equipment is moved to the Far Site.

This prototype will include a representation of the roof hatch opening, APA and CPA rail supports and feedthroughs. Multiple mock-ups of APA and CPA stacked panels will be installed. The APAs will include all mechanical mounting points and electrical connections such as optical-fiber readout cables and power cables. Prototype versions of the special equipment required for TPC installation will be used, including the lower-panel staging platform, a transfer rail with trolley, and rolling-cart scaffolding. Scaffolding elements will be rented and the scaffolding will be erected by a contract or as part of a training program.

Initial tests, where appropriate, will be peformed at a low elevation. For example, the installation trolley and single-switch rail segment will be tested at a low elevation with a dummy weight. After successful demonstration of the features in this position, the components will be moved to a high elevation for testing with full-size mock-up panels.

7.7   Training

Installation and Commissioning will be responsible for the personnel, equipment and procedures for providing Detector Hall access controls after cryostat construction is complete. Members of the installation crew will be trained on specific installation tasks and must pass a qualification test. The training will use mock-up APAs constructed for the installation equipment prototype. The training program will be developed in collaboration with Fermilab and SURF ES&H personnel.

Installation and Commissioning will provide all of the general tools and equipment needed

Figure 7–12: An Installation equipment prototype, mockup TPC section in blue, will be built and tested in a Fermilab assembly building like Wideband lab shown here

to support the personnel in their installation work. It will include hand tools, power tools, material-handling equipment, ladders, lifts, electrical meters and personal protective equipment (PPE). The detector sytem groups will provide any special equipment to check out or debug the power and read-out chain of the detectors. The detector groups will also provide system experts at the far site to check out the detector systems before and after installation.

7.8   Detector Startup and Commissioning

The detector installation and commissioning activities will be staged such that both TPCs can be tested cold while one cryostat still remains available as a potential storage vessel in case a repair is needed. Once both TPCs are known to work properly at LAr temperature, the second fill will take place.

7.8.1   Commissioning Sequence

The commissioning sequence, illustrated in Figure 7–13, will start with the installation of the TPC into cryostat 1 (installed on the north side). During this time, the leak testing and cleaning of cryostat 2 will be completed and, where possible, the setup for TPC installation will begin. After the TPC is completely installed in cryostat 1, its purge and cool-down can begin. These processes are described in Section 2.7.1.

Following the purge and cool-down, the LAr fill of cryostat 1 will take approximately two months, assuming continuous LAr deliveries. LAr purification will begin when the liquid level is high enough to start the recirculation pumps. The commissioning of the cryogenics system can also begin at this point, but its full commissioning will require a fully loaded cryostat. In-vessel purity monitors will operate during this time.

When the cryostat is full with LAr, the TPC will undergo testing for approximately one month to establish that the TPC will be able to achieve the tracking requirements and to confirm that no further access will be needed to the cryostat and TPC. Additional testing will occur after the other cryostat is filled and is thus no longer available as a storage vessel.

Installation of the TPC in cryostat 2 will begin during the LAr fill of cryostat 1. After TPC installation and electronics testing, the purging and cooling for cryostat 2 can proceed. The LAr from cryostat 1 will be transferred to cryostat 2, and once it is full, its TPC will undergo a month of initial testing. During this time, cryostat 1 will be maintained cold via continuous circulation of gaseous Ar. After it is established that no further access will be required, cryostat 1 will be refilled with LAr and begin a five-month commissioning period. Testing during the commissioning period will demonstrate that the detector performance parameters for CD-4 have been achieved.

Cryostat 1   **Cryostat 2**

Install TPC

Step 1 – 4 months

Test Cryostat
and Start Setup

Cool down and fill with LAr   Start TPC installation

Step 2 – 3 months

Complete TPC installation

Test TPC in LAr

Step 3 – 1 months

Transfer LAr ~ 2 months
Test TPC   ~ 1month

Keep Cryostat cold

Step 4 – 3 months

Refill with LAr

Operate

Step 5 – 2 months
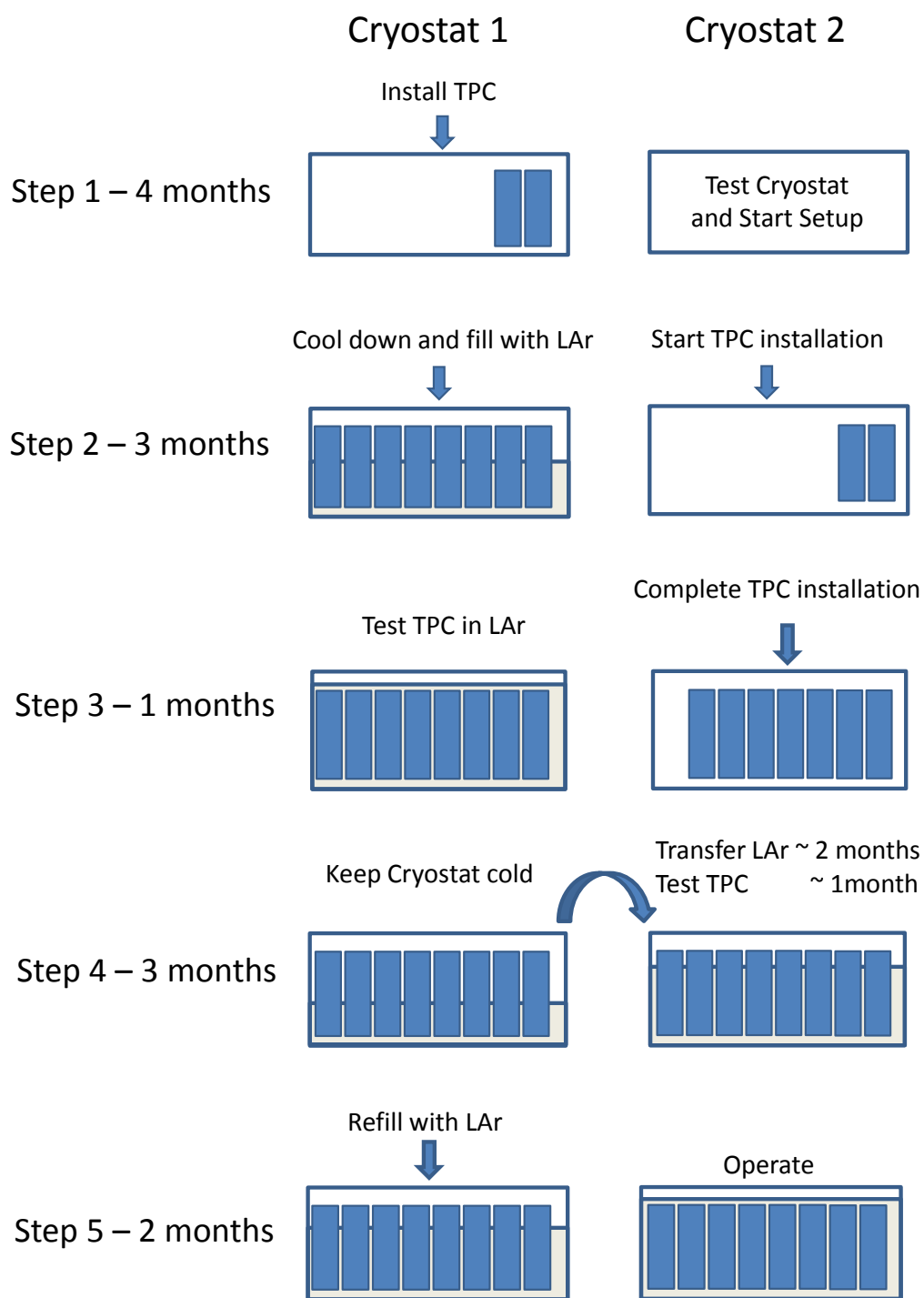
Figure 7–13: Startup and Commissioning Sequence

This sequence provides for a continuous flow of work and optimizes the use of the crews that will install the detectors and maintain the cryogenics systems. The operations crew is required from the start of the purge and cool down of the first cryostat through the commissioning phase. The cost/risk management benefit of other sequences will be evaluated as more experience is gained with the detector systems.

Several opportunities for system checkout arise throughout the detector installation, startup and commissioning phases as illustrated in Figure 7–14. Since the full DAQ system will be operational at the start of TPC installation, a full suite of tests can be made within the HV operating limits.

7.8.2   TPC, DAQ and Electronics Testing

After delivery to the Far Site and before installation, the following tests will be performed on the TPCs:

- The wires of the APA will be visually inspected for breakage or sagging.

- The leakage current will be measured on the APA wire bias terminals.

- A DAQ station will be connected to the APA cables to run electronics calibration to identify bad channel/wire connections.

- The CPA and field cages will be visually inspected. The resistance will be measured between the frame and the bias electrodes.

- The integrity of the resistors and the resistance between the field-cage strips will be measured.

These tests will be repeated and the mechanical connections will be checked after the APA and CPA are installed in a cryostat and the field cage is connected. The resistance between the field cage and the APA will be measured, and any individual broken or sagging APA wires will be removed. Wire integrity will be confirmed by measuring the Equivalent Noise Charge (ENC) of each electronics channel and comparing it with the expected noise for a properly connected wire. The wire-integrity test also ensures that coherent noise sources, e.g., a mechanical connection between the detector ground and the Ufer ground, are discovered promptly. As the TPC installation progresses, periodic electrical testing will continue on previously installed panels to ensure the wire and electronics integrity and the collective noise performance. Error budgeting, regular noise monitoring and mitigation will ensure that the TPC reaches and maintains the required noise performance before the cryostat is cooled down.

Testing at production/assembly site (days – weeks)	A

Transport to FD site

Testing upon delivery to FD site (days - weeks)	B
Recheck before installation (1 day)	C

Install APA in final position

Initial testing after APA is in final position (overnight)	D
Periodic testing while balance of TPC is installed (month)	E

Entire TPC installed

Testing before cryostat cover is sealed (days)	F
Testing after purge and cooldown (days)	G
Testing during argon fill (1-2 months)	H
Testing after argon fill is complete and during purification (1 month)	I

Commitment to begin fill of other cryostat

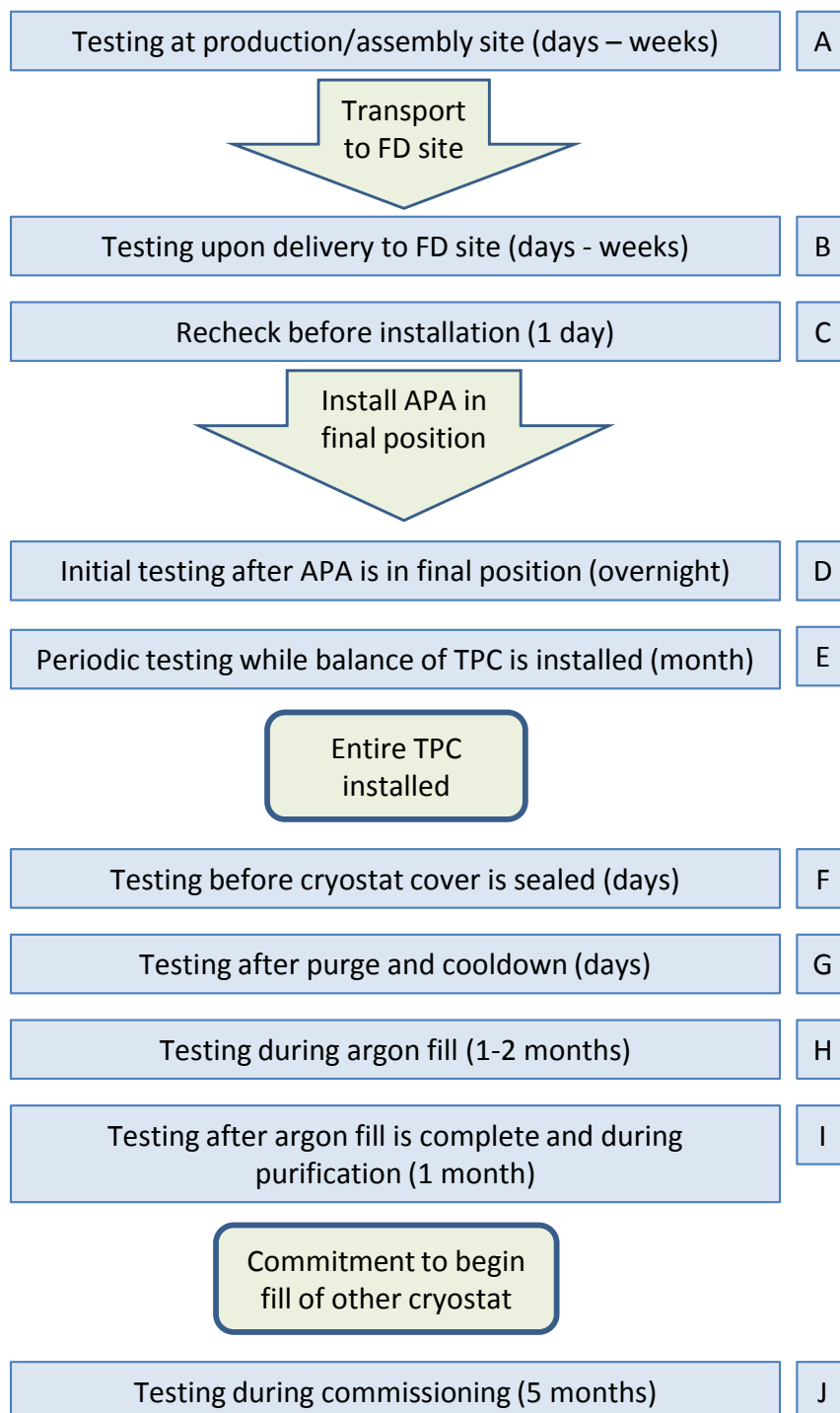|	
Testing during commissioning (5 months)	J

Figure 7–14: Several opportunities exist for checkout of the detector systems as the installation and startup progresses. The approximate durations are listed with each opportunity.

After cool-down and during LAr filling the electronics and wire integrity will be tested to ensure that no damage occurred during the temperature drop. Once the fill is complete, the TPC can be tested at full high voltage for the first time. The electronics testing at this point will be relatively quick, however, a demonstration that the TPC is fully operational, i.e., observation of tracks in each drift cell, requires achieving sufficient electron lifetimes in the LAr, which may take some time. Information from operation of the 35-ton prototype (Section 8.3.8) is expected to inform and confirm the simulations and to help estimate the time required to achieve sufficient LAr purity for testing operations.

7.9   ES&H

Careful consideration for ES&H will be demonstrated in the planning and execution of the installation and commissioning. Safety professionals will be involved in all phases. Hazards of note for the TPC installation include work at elevated heights and work in the confined space of the cryostat. During the detector installation no atmospheric hazards are expected inside the cryostat, thus for normal TPC installation work the cryostat should not require any special access permits. Procedures for access and egress will be prepared that include sign-in and sign-out for cryostat entry and for two-person work. Communication equipment will be available that works within the cryostat and between the interior and exterior of the cryostat. Emergency response procedures will be developed that include provisions for evacuation and rescue from the cryostat. Temporary ventilation and light systems will include air monitoring and high-sensitivity smoke detection. Crane operation and operator certification methods will be established. In general the detector installation operations are such that most of the installation tasks will involve preparing a written hazard analysis.

8 Detector Development Program

8.1 Introduction

This chapter describes the development program designed to ensure a successful and cost-effective construction and operation of the massive, dual-cryostat LArTPC detector for LBNE and to investigate possibilities for enhancing the performance of the detector. The feasibility of the LArTPC as a detector has been demonstrated most impressively by the current state of the ICARUS experiment currently taking data at Gran Sasso.

It is understood that for succesfull operation an LArTPC has stringent requirements on

- argon purity which must be of order 200 ppt O_2 equivalent or better

- long-term reliability of components located within the liquid argon; in particular, the TPC and field cage must be robust against wire-breakage and must support a cooldown of over 200 K

- the front-end electronics which must achieve a noise level ENC of $1000e$ or better

The design of the LBNE LArTPC has evolved significantly from earlier concepts based on standard, above-ground, upright cylindrical LNG storage tanks which envisioned single TPC sense and high-voltage planes spanning the full width of the tank – essentially a direct scaling of previous detectors. Problems with the actual construction of such massive planes and with the logistics of being able to construct the TPC only after the cryostat was complete are avoided in the present design. In our design, TPC 'panels' are fully assembled and tested – including the electronics – independently of the cryostat construction. This modular approach is a key feature of the design. It has the benefit not only of improving the logistics of detector construction, but also the individual components can be of manageable size. It should also be noted that the cryostat itself is formed of modular panels designed for quick and convenient assembly.

8.2   Components of the Development Program

Programs of ongoing and planned development to allow the construction of massive LArTPCs in the U.S. have been developed and were described in the *Integrated Plan for LArTPC Neutrino Detectors in the US* [11]. To advance the technology to the detectors proposed for LBNE, the U.S. program has three aspects:

- a demonstration that the U.S program can reproduce the essential elements of the existing technology of the ICARUS program

- a program of development on individual elements to improve the technology and/or make it more cost-effective

- a program of development on how to apply the technology to a detector module

A summary of the items in the program is given in the following tables. Table 8–1 lists the activities that are part of the LBNE Project ("on-project") described in this chapter, a short description of the information needed and the LBNE milestone corresponding to when the information is required. Table 8–2 lists off-project activities, the aspect of these activities that is applicable to LAr-FD and the LBNE milestone at which the information is required. These aspects will be described in more detail in the following sections. As will be explained below, these are not R&D activities, but rather elements of the preliminary engineering design process.

8.3   Scope and Status of Individual Components

8.3.1   Materials Test System

An area for LAr detector development, shown in Figure 8–1, has been established in the Proton Assembly Building at Fermilab. The Materials Test System (MTS) has been developed to determine the effect on electron-drift lifetime of materials and components that are candidates for inclusion in LAr-FD. The system essentially consists of a source of clean argon (< 30 ppt O_2 equivalent), a cryostat, a sample chamber that can be purged or evacuated, a mechanism for transferring a sample from the sample chamber into the cryostat, a mechanism for setting the sample height in the cryostat so that it can be placed either in the liquid or in the gas ullage above the liquid, a temperature probe to measure the temperature of the sample, and an electron-lifetime monitor. The system is fully automated and the lifetime data are stored in a single database along with the state of the cryogenic system.

Table 8–1: LBNE on-project development activities

Activity	LAr-FD Information	Need by
In-liquid Electronics	Low noise readout, long lifetime	CD-2
TPC Construction	Mechanical design	CD-2
35-ton Prototype, Phase I	Cryostat construction, purity demonstration	CD-2
35-ton Prototype, Phase II	Test major components of LAr-FD	CD-2

Table 8–2: LBNE off-project development activities

Activity	LAr-FD Applicability	Status	Need by
Yale TPC	None	Completed	NA
Materials Test System	Define requirements	Completed	NA
	Materials testing	Operating	As Req'd
Electronics Test Stand	Electronics testing	Operating	As Req'd
LAPD	Purity w/o evac.	Operating	LBNE CD-2
	Convective flow	Operating	LBNE CD-2
Scintillation Photon Detector Development	Photon Det. Definition	Completed	LAr1 Construction
	Industrialization	Not started	LBNE CD-3
ArgoNeuT	Analysis tools	On-going	LBNE CD-2
MicroBooNE	Electronics tests	Construction	LBNE CD-3
	DAQ algorithms	In development	LBNE CD-3
	Analysis tools	In development	LBNE CD-2
	Lessons learned	Not started	LBNE CD-3

Figure 8–1: Liquid argon area at the Proton Assembly Building at Fermilab

A noteworthy feature is the novel bubble-pump filter inside the cryostat. In case of argon contamination, this can filter the cryostat volume in a few hours, allowing us to continue studies without having to refill. A schematic of the MTS is shown in Figure 8–2.
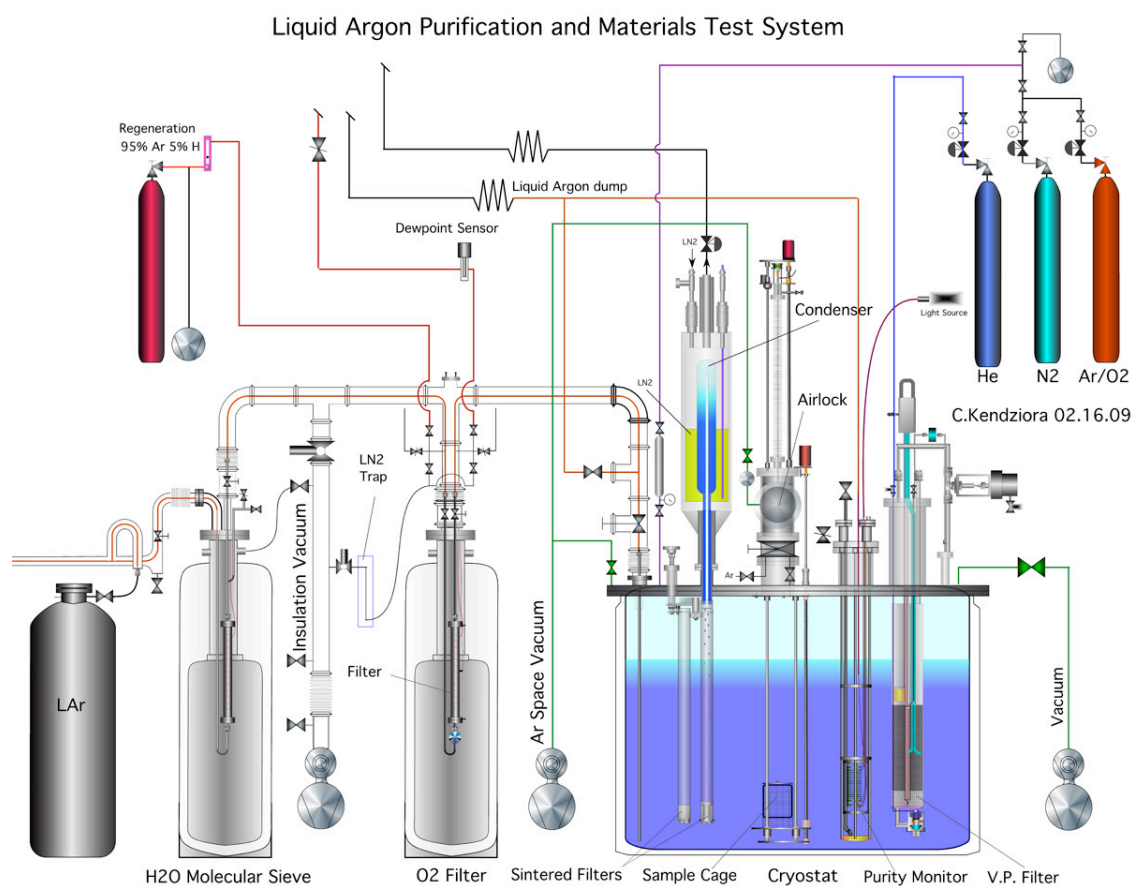
Figure 8–2: Schematic of the Materials Test System (MTS) cryostat at Fermilab

The major conclusions of the studies to-date are summarized here. No material has been found that affects the electron-drift lifetime when the material is immersed in liquid argon – this includes, for example, the common G-10 substitute, FR-4. On the other hand, materials in the ullage can contaminate the liquid; this contamination is dominated by the water outgassed by the materials and as a result is strongly temperature-dependent. Any convection currents that transport water-laden argon into the LAr and any cold surfaces on which water-laden argon can condense will fall into the LAr and reduce the electron lifetime. Conversely, a steady flow of gaseous argon of a few ft/hr away from the LAr prevents any material in the gas volume from contaminating the LAr.

These results are taken into account in the design of both MicroBooNE and LAr-FD. For LBNE they have been cast as detector requirements. The MTS will continue to be used by MicroBooNE and LBNE to test detector materials such as cables that will reside in the ullage.

8.3.2   Electronics Test Stand

The Electronics Test Stand is also installed in the Proton Assembly Building at Fermilab. It consists of a cryostat, served by the same argon source as the Materials Test System, and a TPC with a 50-cm vertical drift terminating in three planes of 50 wires each, arranged at 120 degrees. Figure 8–3 shows the TPC being inserted into the cryostat.Two sets of small scintillation counters outside the cryostat are used to trigger the system on cosmic rays. The data from this system provide a crucial check of simulations of the electron drift and the signals induced on the wires.

The front-end electronics and the crucial shaping filters for the ArgoNeuT experiment were developed on this system from the sort of data shown in Figure 8–4. These data also led to the development of the FFT technique for reconstructing track hits. A hybrid pre-amplifier has been successfully tested in LAr and has demonstrated excellent noise performance.

The ASIC front-end amplifiers for LBNE will also be tested, providing assurance that bench measurements are reproducible in a functional TPC.

8.3.3   Liquid Argon Purity Demonstrator

The Liquid Argon Purity Demonstrator (LAPD) is a significant-scale system, 30 tons, consisting of a complete cryogenic recirculation system and a vessel capable of achieving large-drift LArTPC purity specifications without initial evacuation. While large cryogenic systems have been built by U.S. groups, this is the first with a purification system intended specifically for an LArTPC. As such it is providing valuable experience and data for the construction of future systems. Figure 8–5 shows the filtration system and the LAPD tank in place at Fermilab's PC-4 facility.

The tank is instrumented with several systems. An array of sniffers measures the oxygen concentration at six heights during the gas-purge; a system of temperature monitors can be lowered and raised inside the tank to measure temperature gradients; an ICARUS-style purity monitor is deployed on the input line to the tank; and four ICARUS-style purity monitors measure electron-drift lifetime within the tank.

Analytic instrumentation includes a water meter and an oxygen meter, both with ppb sensitivity, and a nitrogen meter with 10-ppb sensitivity, installed for the purpose of taking measurements throughout the system. The scheme for displacing the air (at atmospheric pressure) in the cryostat interior volume by introducing and purifying LAr consists of several steps: a gas purge with argon, gas recirculation with purification, an LAr fill while venting (to drive out any contaminants remaining in the gas) and recirculation of the LAr through the purification system.

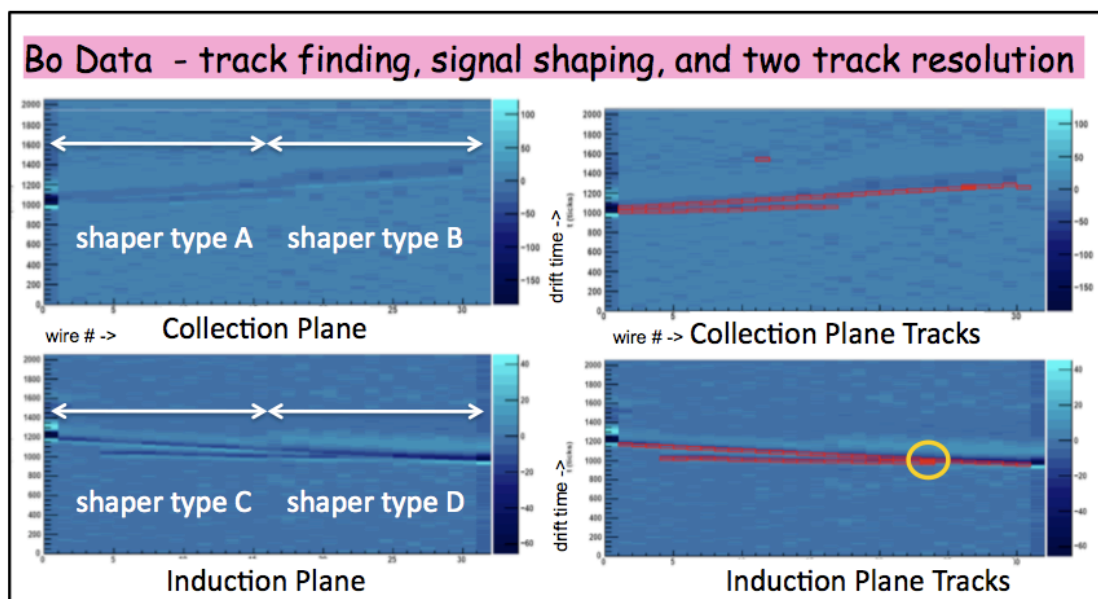**Figure 8–3:** Electronics test TPC insertion into cryostat

Figure 8–4: A cosmic ray with a delta electron as seen in the Electronics Test Stand TPC. Note the different width of the shaded portions along the tracks in the left panels. These are due to the two shaping circuits being tested. The readout scheme for MicroBooNE and LBNE uses digital signal processing and has minimal filtering before the ADC.

The primary motivation of LAPD is to demonstrate an electron-drift lifetime of several milliseconds, which has now been accomplished. LAPD began purging with argon gas in September 2011. The tank was filled with LAr to the 40% level on November 1, 2011. A drift electron lifetime of 3 ms was achieved in late November after some re-work was done on the filter material containment system. The filters became saturated (with water) in mid December, were regenerated and were returned to service in late January 2012. The drift-electron lifetime reached 3 ms after four days of operation and continued to improve through February.

Now that high purity has been achieved, the effect of varying the conditions (gas and/or liquid recirculation, different recirculation rates, no recirculation) can be investigated. The size of the tank allows use of the measurements from the temperature-monitor system to check the accuracy of ANSYS simulations of the temperature profile within the tank. This will check the simulations and should confirm the small temperature gradients and resulting low velocities of the convection flows predicted for large LArTPCs.

A problem was found with the building electrical system in early March 2012 that necessitated ending the planned suite of LAPD tests prematurely. The current plan is to perform additional re-work on the filter material containment system over the next few months, followed by a second phase of testing. At this time, LAPD management and operations will be transferred to LBNE to support the 35-ton membrane-cryostat prototype described in Section 8.3.7.
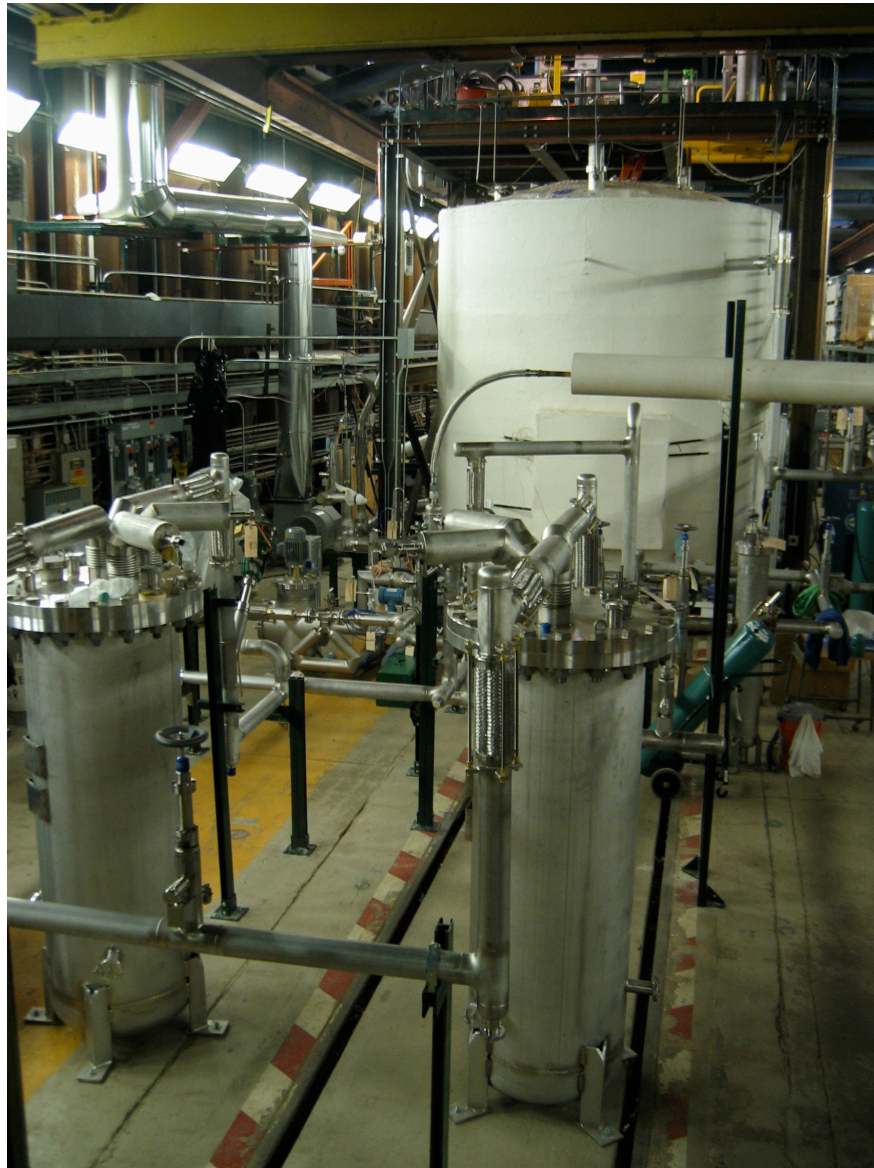
Figure 8–5: Liquid Argon Purity Demonstration filtration and tank at the PC-4 facility

8.3.4   Photon Detection

The development program for Photon Detection is based on a promising, new, cost-effective scheme for light collection in LArTPCs as described in a NIM article by Bugel et al [28]. The design is based upon lightguides fabricated from extruded or cast acrylic and coated with a wavelength-shifter doped skin. Multiple acrylic bars are bent to guide light adiabatically to a single cryogenic PMT. Prototypes of the basic detector elements have been shown to perform well. These lightguides have a thinner profile than the usual TPB-coated PMT-based system, occupying less space in an LAr vessel and resulting in more fiducial volume. Another advantage of this system is that the bars are inexpensive to produce. The most convenient place for the paddles is between the wire planes that wrap around the APAs.

Lightguide R&D has advanced rapidly since the initial publication resulting in $\sim 3 \times$ higher light yields. The development is now sufficiently advanced to provide a technical basis for the LAr-FD reference design. On-going design efforts at MIT, Indiana University, and Fermilab are directed toward industrial-scale production and the evaluation of lower-cost fluors that are effective in converting VUV photons. These efforts also include investigating PMTs with increased quantum efficiency as well as other efficient light-collection technologies, such as Geiger-mode avalanche photodiodes (commonly known as Silicon Photomultipliers, or SiPMs).

Discussion of efforts that contribute to development of the LBNE photon-detection system design follows.

8.3.4.1   Light-Guide Testing

The test apparatus shown in Figure 8–6 was built at and funded by Indiana University. It consists of a jacketed LHe dewar that has been fitted with a frame to support light guides. The hold time for LAr in this dewar is significantly increased with LN2 in the outer jacket. Since the purity of the LAr is vital in these test measurements (as described by the MIT group [28]) and high-purity LAr is quite expensive, the increased hold time is an important advantage to this setup. The 1-μCi Am^{241} α source generates the scintillation photons in LAr and can be moved up and down a shaft to illuminate the light guide along its length. The electronics are fast enough (1.4 GB/s) to read out the waveform of the prompt 1.6 ns signal and the fast waveform digitizer has enough memory to see the late signal as well.

8.3.4.2   Alternative Waveshifters

A program at Indiana University has been comparing the waveshifting properties of TPB, bis-MSB, and p-Terphenyl under analogous conditions. For the initial tests, polystyrene
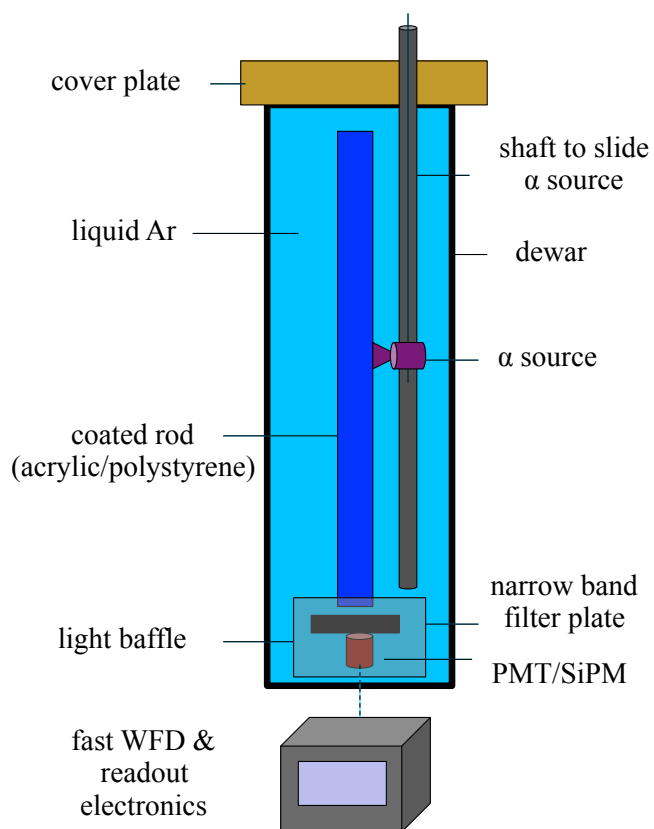
Figure 8–6: Apparatus for testing light guides in LAr. *left*: schematic of light guide testing apparatus; *right*: light guide testing apparatus.

bars have been extruded with a co-extrusion layer that contains 3% waveshifter and 97% polystyrene. These bars will be tested in two ways. First, it is necessary to test their absolute light output with the McPherson vacuum VUV monochromator at Fermilab. These measurements will be at room temperature. A NIST-calibrated photodiode has already been purchased and the monochromator will be calibrated in the near future. This investigation will directly compare the absolute optical-light output from these bars when illuminated by UV light from 100 nm to 200 nm to determine the efficiency for UV-to-optical light conversion for the different waveshifters.

These bars will be tested in LAr at IU in a test apparatus similar to that shown in Figure 8–6. These tests will measure the relative light output for the different waveshifters with the same concentration in the same type of co-extruded light guide. The monochromator measurements and the measurements in 35-ton prototype and/or LAPD should give enough information to make an optimum choice for the waveshifter.

The doping concentration will be optimized after the waveshifter has been selected. For these tests, different concentrations of waveshifter will be loaded into the co-extrusion then the light output will be measured with the VUV monochromator and in the LAr test apparatus. Since the costs of the waveshifters are known, these are studies that trade light for cost to produce light guides with adequate light for the funding available.

8.3.4.3   Cast-Acrylic Light Guides

As seen in Figure 6–17, cast acrylic has a significantly longer attenuation length than extruded polystyrene. In fact, the relatively short attenuation length for extruded polystyrene may prove a barrier to this technology for a 2.3-m light guide. A second advantage of cast acrylic is that it offers the potential to cast a single, monolithic adiabatic paddle, instead of four light guides that must be assembled into a paddle. In this case, a thin, flat paddle would be drawn into the square shape of the PMT. However, several issues associated with cast-acrylic light guides require investigation.

The first issue is whether light paddles can be cast into the required shape that adiabatically tapers a flat paddle into the square PMT profile. A second issue is whether this method would be cost-effective. If silicon photomultipliers (SiPMs) prove to be a realistic alternative to PMTs in their light-gathering power, however, a complicated mold may not even be necessary since the SiPMs could be manufactured to populate the edge of a flat panel and no bending would be necessary. It must be demonstrated that cast-acrylic paddles or light guides be made with equal uniformity to those from commercial off-the-shelf cast-acrylic stock.

A final issue is the uniform coating of light paddles with waveshifter. Hand-coating the 4,800 light guides by dissolving the waveshifter in polystyrene + toluene and air-brushing the

mixture onto the cast acrylic paddless (as is currently done at MIT for MicroBooNE) would be very labor-intensive and would likely introduce significant variations in the coatings. Two paths for coating the bars will be pursued. (1) Casting the light guides with the waveshifter in the mold. It is unknown whether this can be achieved. (2) The development of a machine to coat the bars. There is experience from MINOS and NOνA in developing machines to deposit the uniform coatings of glue for assembly of these experiments, which seems to be a very similar problem. It is clearly important to learn how these coatings would perform in LAr.

8.3.4.4   SiPMs

At Fermilab, the development plan includes the continuing work on the absolute calibration of SiPMs. In addition, the plan includes tests directed at detecting VUV light in LAr using SiPMs coated with TPB [32]. This work has already begun.

The Indiana University group has been awarded a research grant to purchase a small number of Hamamatsu SiPMs. These will be substituted for the R8520-MOD PMTs on the extruded light guides and comparison tests of them in LAr will be made.

8.3.5   TPC Design

The design for LBNE has adopted the basic ICARUS multi-plane, single-phase TPC concept and has incorporated new features suitable for a very large detector. The main emphasis of the development program is to develop a TPC design that is highly modular, low-cost, robust and easily installed inside a finished cryostat.

A significant effort has been focused on minimizing the dead space between detector modules to improve the fiducial versus total LAr-volume ratio. The APA reference design accomplishes this goal but requires making $\sim$2 million high-quality wire terminations. The wire-termination scheme used by ICARUS has proven to be very reliable but it is too labor-intensive to fabricate for a million-channel detector system. Instead, the wire-solder + wire-epoxy termination scheme that has been used for decades on drift chambers and proportional wire chambers to mount Cu-Be wires has been adopted. The termination scheme was used to terminate 2.5 million anode wires in the CMS end-cap muon system. Cu-Be wires have excellent mechanical properties and the advantage of low resistance compared to stainless steel. A study is currently underway within the LAr-FD L2 Project to identify the optimum wire-bonding parameters. The focus is currently on finding a commercial epoxy that optimizes the qualities of bond strength, cure time and low-temperature operation.

8.3.6 Electronics Development

The work to-date on cold electronics has established that no show-stoppers exist. The remaining activities outlined here concern performance optimization of the CMOS ASICs, the evaluation of several widely available CMOS technologies, and the development of readout architectures appropriate and timely for various scenarios of very large detectors.

8.3.6.1 CMOS Transistors: Lifetime Verification and Technology Evaluation

The results of the design of the CMOS electronics for operation at LAr temperature (87 K), performed so far by the MicroBooNE and LBNE collaborations, as well as by a large collaboration led by Georgia Inst. of Technology, are summarized in Section 4.3.

Briefly, the fundamentals are: charge-carrier mobility in silicon increases at 87 K, thermal fluctuations decrease with kT/e, resulting in a higher gain (transconductance/current ratio $= g_m/i$), higher speed and lower noise. For a given drain-current density the same degree of impact ionization (measured by the transistor substrate current) occurs at a somewhat lower drain-source voltage at 87 K than at 300 K. The charge trapped in the gate oxide and its interface with the channel causes degradation in the transconductance (gain) of the transistor and a threshold shift. The former is of major consequence as it limits the effective lifetime of the device (defined in industry and the literature as 10% degradation in transconductance). Thus an MOS transistor has equal lifetime due to impact ionization at 87 K and at 300 K at different drain-source voltages. This is illustrated in Figure 8–7.

This feature offers a tool for accelerated-lifetime testing by stressing the transistor with both increased current and increased voltage, and monitoring the substrate current and the change in g_m due to impact ionization. In these conditions, the lifetime can be reduced arbitrarily by many orders of magnitude, and the limiting operating conditions for a lifetime in excess of ∼20 years can be determined. With this foundation, more conservative design rules (lower current densities and voltages) can be derived and applied in the ASIC design, as has been done for the ASIC described in Section 4.1. The goal of this part of the program is to verify by accelerated testing the expected lifetimes for the several widely available CMOS technologies under consideration (TSMC, IBM, AMS). It should be noted that this is a standard test method used by the semiconductor industry. These methods are used to qualify electronics for deep space NASA missions as well as commerical PCs.

8.3.6.2 Readout Architectures, Multiplexing and Redundancy

Some degree of multiplexing after digitization of signals is essential for a TPC with 154,000 readout wires in order to reduce the cable plant and the attendant outgassing. Just how high
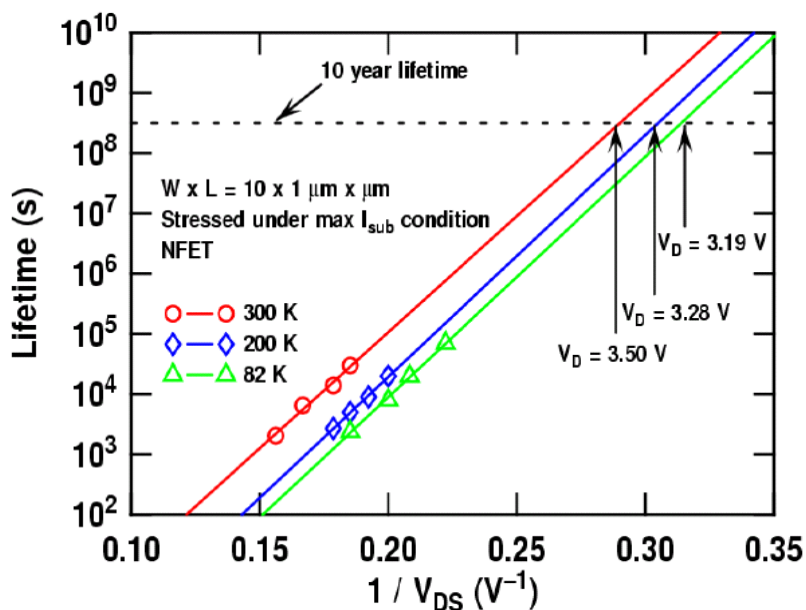
Figure 8–7: Lifetime at different temperatures vs V_{DS}

a multiplexing factor should be chosen is a matter of study, considering the risk of losing one output data link. A part of the program will include system designs with redundant links and redundant final multiplexing stages to minimize the risk of losing the data from a significant fraction of the TPC (note that even with a multiplexing factor of 1/1024 and no redundancy, one failed link would result in a loss of 0.2%).

8.3.7   35-ton Prototype, Phase I: Cryostat Development

The next step in the cryostat-prototype program is intended to address project-related issues: (1) to gain detailed construction experience, (2) to develop the procurement and contracting model for LAr-FD and (3) to incorporate the design and approval mechanism in the Fermilab ES&H manual. (Membrane cryostats are designed in accordance with European and Japanese standards.) Construction of a smaller but similar membrane cryostat (to the LAr-FD cryostat design) will accomplish these goals and in addition demonstrate high-purity operation in this type of cryostat and the suitability of the planned LAr-FD construction techniques and materials.

The LBNE project has contracted with the Japanese company IHI to build a 35-ton prototype membrane cryostat. As of late summer 2012, the construction, under the supervision of IHI personnel, is nearing completion at Fermilab's PC-4 facility where LAPD is located. See
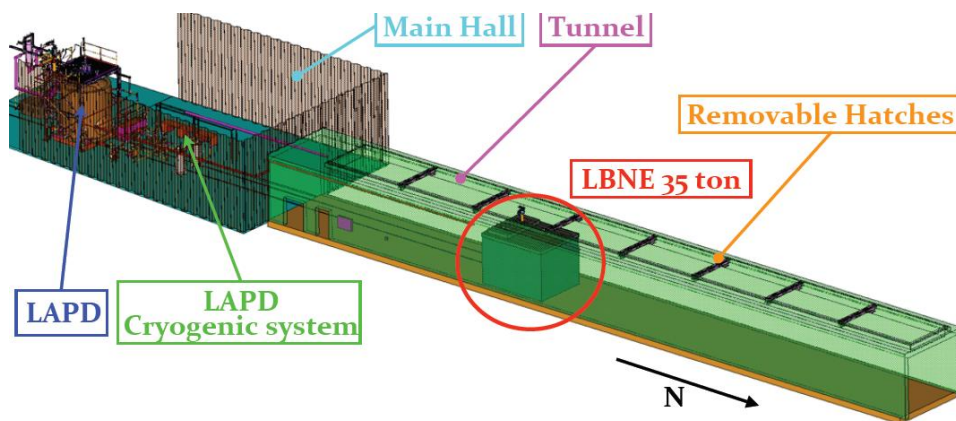
Figures 8–8 and 8–9.

Figure 8–8: Layout of 35-ton prototype at Fermilab's PC-4 facility

The prototype membrane cryostat's total size, including insulation and concrete support, is approximately 4.1 m × 4.1 m ×5.4 m, and will hold approximately 38.6 tons of LAr. The insulation thickness will be 0.4 m rather than the 0.8 m chosen for the LAr-FD reference design. Welding of corrugated panels, removal of leak-checking dye penetrant or ammonia-activated leak-detecting paints, and post-construction-cleaning methods will be tested for suitability of service. Residual contamination measurements at different elevations during the initial GAr purge process will be compared to computational predictions and will validate the purge-process modeling of a large rectangular vessel. The prototype membrane cryostat will be filled with LAr. Purity levels of the liquid with time and electron-drift times will be measured using purity monitors installed in the liquid bath. Heat-load measurements will be made and compared to calculations.

8.3.8   35-ton Prototype Phase II: Detector Development

Once the 35-ton prototype's Phase 1 goals are achieved, it will be exploited for a detector development program since it is the largest cryostat that LBNE will have access to until the Far Detector is constructed. In addition to testing detector components, this program will provide an opportunity for LBNE collaborators to participate in both the planning and operation of a large LArTPC system.

The first element of the detector development program involves insertion of pre-production,
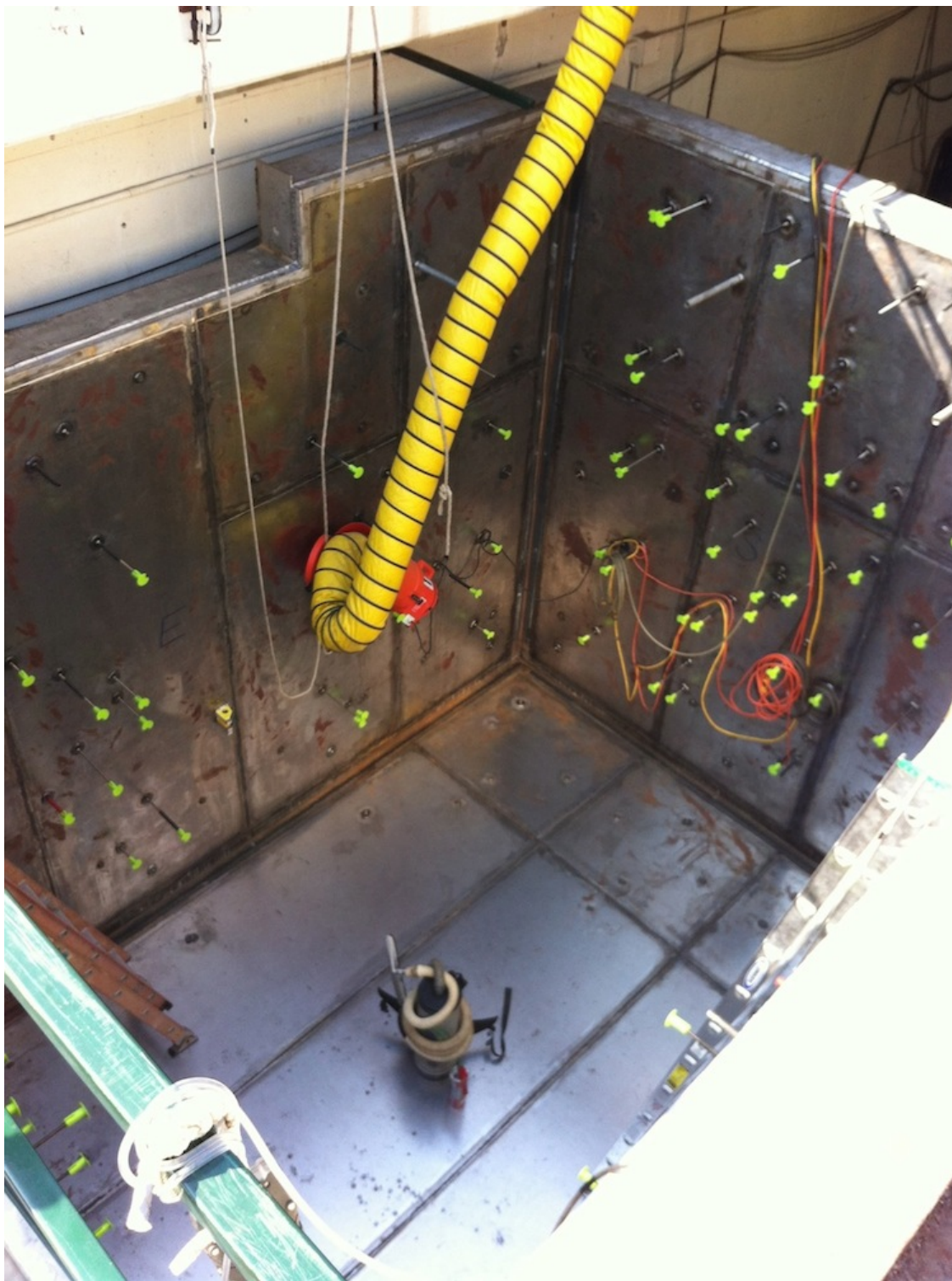
Figure 8–9: 35-ton prototype, with vapor barrier installed and inspected, Aug. 1, 2012 *Credit: D. Montanari*

reduced-scale subsystem components into the cryostat to explore each subsystem's response to cosmic ray tracks as well as its sensitivity to mechanical and electrical issues in the LAr environment. The impact of the subsystem and infrastructure materials on the LAr purity will also be studied.

Later, once the necessary production components have been procured, a full system test of a scaled-down version of the Far Detector will take place to ensure that these components will perform as designed. This system test will include a TPC, a photon-detection system, cold electronics, and a DAQ system. The size of the 35-ton cryostat precludes installing a full-size APA/CPA, however the components used in the testing program will be as similar as possible to the actual full-scale detector.

Since the 35-ton cryostat is located at the surface with no shielding overburden, the cosmic ray flux will be more extreme than what the actual Far Detector will experience. The TPC drift volumes will be configured to provide diagnostic data on space-charge effects expected to arise from the high flux. These data together with the response of the TPC and photon-detection systems to the high flux will provide important information for development of robust LBNE reconstruction software.

Figure 8–10 shows a side view of the 35-ton cryostat. The volume directly below Plate B remains committed to the cryogenic hardware (pumps and instrumentation). Except for the passage of wires and cables, the prototype detector components are limited to the volume shown within the dashed green area. This available volume is roughly 2.7 m × 2.4 m × 2.2 m (length × width × height), or about 20 tons of LAr.

In order to install detector components with dimensions on the order of the available volume, it will be necessary to remove the Phase 1 Plate B and either rework it or replace it with another Plate B that has a larger access flange. Figure 8–11 illustrates a new Plate B flange with a larger aperture. Existing anchors built into the ceiling membrane of the 20-ton volume can be used to mount detectors (again, see Figure 8–10).

The actual configuration of the full system-test detectors is still under consideration. Details as to the number of TPC drift volumes (one or two) will be determined based upon the needs of of the Far Detector. For example, asymmetric drift volumes may provide higher sensitivity to study space-charge effects since a higher electric field can be produced in the smaller volume. Figure 8–12 shows a possible orientation of a symmetric two-drift-volume TPC, using one APA and two CPAs. Approximately 2000 channels of electronics would be needed to instrument the ∼2-m width of the APA.

Whenever the 35-ton cryostat is down for installation purposes, the LAr will be transferred to LAPD, for storage and to contribute to LAPD test programs. It is also possible that LBNE could negotiate to have access to LAPD for additional prototyping use.
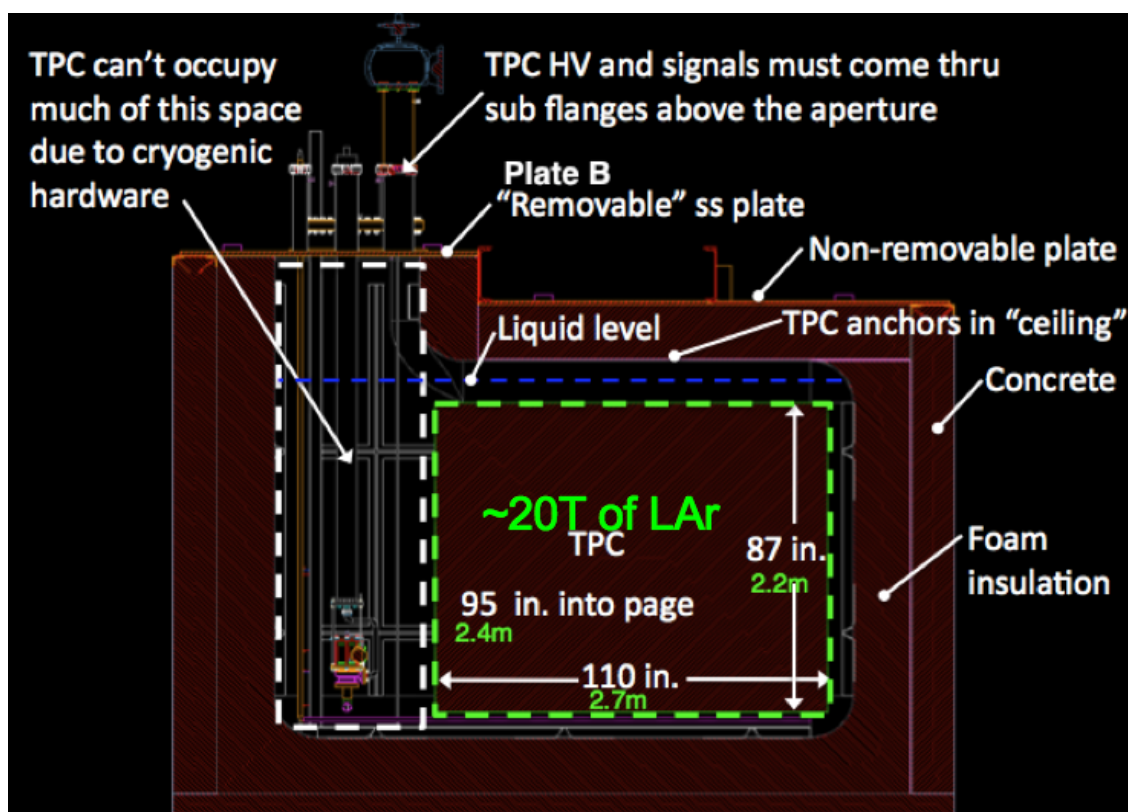
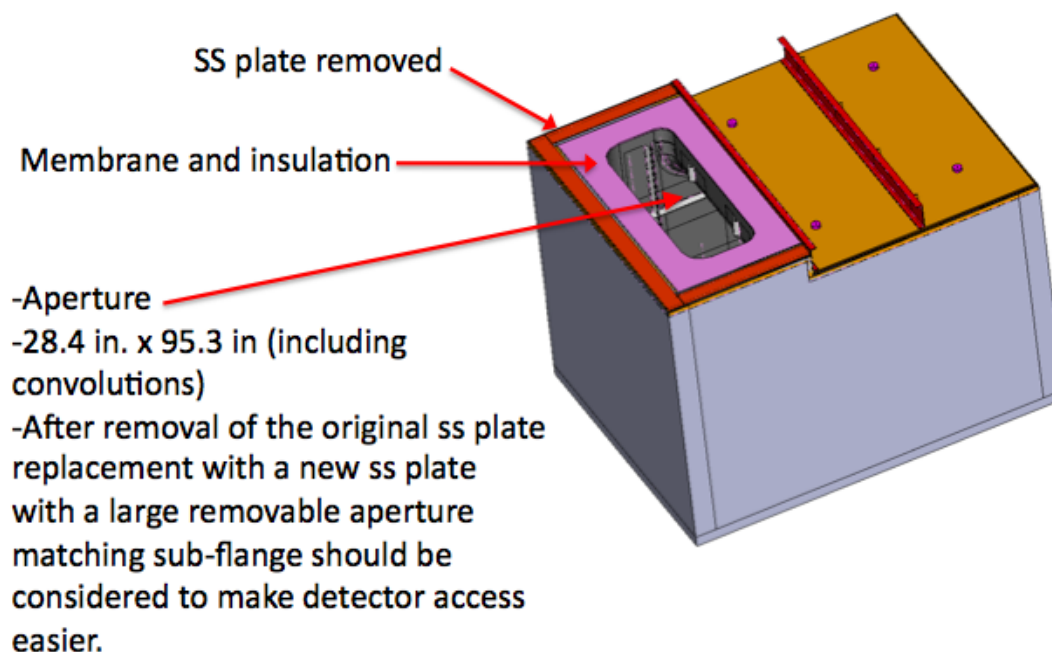**Figure 8–10:** 35-ton prototype cryostat showing volume available for detector prototyping

Figure 8–11: 35-ton cryostat showing aperture for detector installation
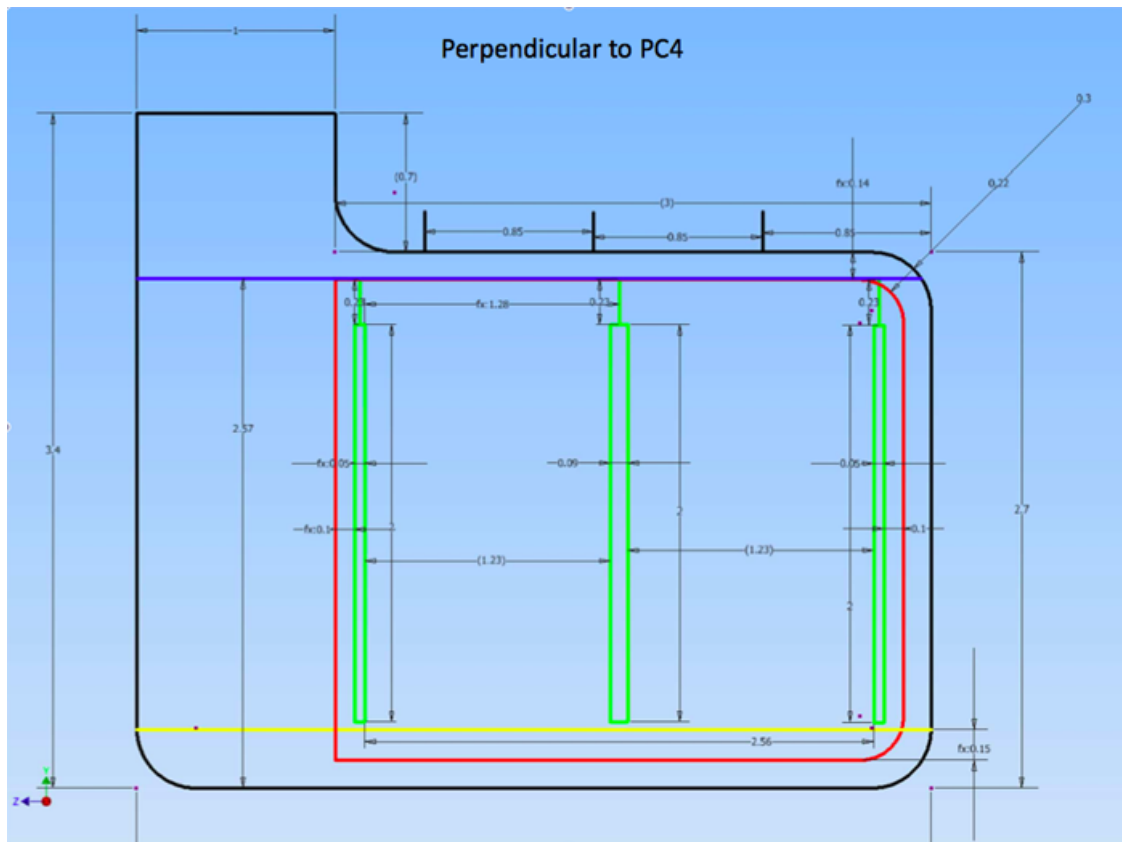
Figure 8–12: 35-ton cryostat showing possible TPC configuration with two drift regions

8.3.9   Physics Experiments with Associated Detector-Development Goals

Two projects, ArgoNeuT and MicroBooNE, which are physics experiments in their own right, are also contributing to the development of the LBNE experiment. Their most important role is in providing data and motivation for the development of event reconstruction and indentification software.

8.3.9.1   ArgoNeuT - T962

The Argon Neutrino Test (ArgoNeuT) is a 175-liter LArTPC which completed a run in the NuMI neutrino beam. The 0.5 m × 0.5 m × 1 m LArTPC was positioned directly upstream of the MINOS near detector, which served as a muon catcher for neutrino interactions occurring in ArgoNeuT.

ArgoNeuT began collecting data using the NuMI anti-muon neutrino beam in October 2009 and ran until March 1, 2010. ArgoNeuT's ∼10k events motivate the development of analysis tools, and are the basis for the first measurements of neutrino cross sections on argon. An event with two π^0 decays is shown in Figure 8–13. ArgoNeuT was also the first LArTPC to be exposed to a low-energy neutrino beam and only the second worldwide to observe beam-neutrino interactions. The ArgoNeuT collaboration is currently preparing (1) a NIM paper that documents the detector performance using NuMI beam muons and (2) the first physics paper on muon-neutrino charged-current differential cross sections on argon. See Figures 8–15 and 8–16.

A deconvolution scheme using an FFT has been applied to the ArgoNeuT data. This procedure eliminates a problem with the ArgoNeuT electronics (which were D-Zero spares and could not be modified for ArgoNeuT). Another more significant benefit of deconvolution is that bi-polar induction-plane signals can be transformed into uni-polar collection-plane signals. An example of this is shown in Figure 8–14. A selection of figures from the draft NIM paper are reproduced below.

The applicability of ArgoNeuT is that it provides a set of data in the same range of energy as the LBNE neutrino beam, enabling the development of analysis algorithms that can be utilized for LAr-FD physics analysis with little or no modification.

8.3.9.2   MicroBooNE E-974

The MicroBooNE experiment is an 86-ton active mass LArTPC, (170-ton argon mass) in the construction phase. It has both a physics program and LArTPC development goals.

MicroBooNE received stage 1 approval from the Fermilab director in 2008, partial funding
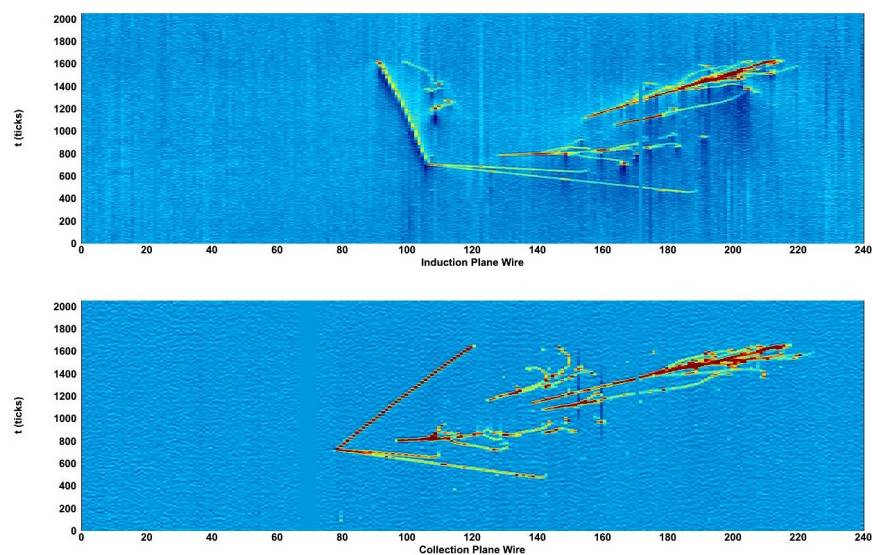
Figure 8–13: A neutrino event with four photon conversions in the ArgoNeuT detector. The top (bottom) panel shows data from the induction (collection) plane after deconvolution.
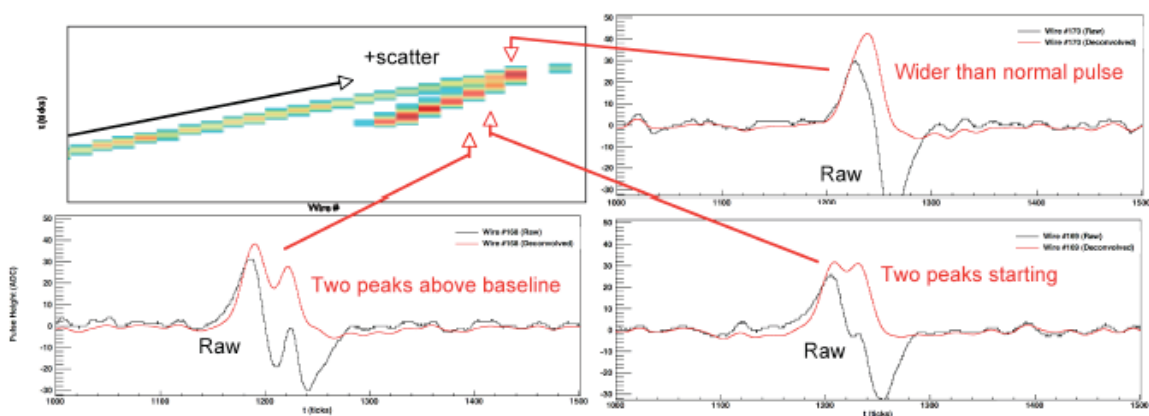
Figure 3: (Upper left) A set of tracks as seen on the (deconvoluted) induction plane. The wire views on three adjacent wires are also shown in order to demonstrate the effects of deconvolution on the raw wire pulses. The raw data can be seen in black and the deconvoluted data can be seen in red.

Figure 8–14: Figure from the ArgoNeuT draft NIM paper.
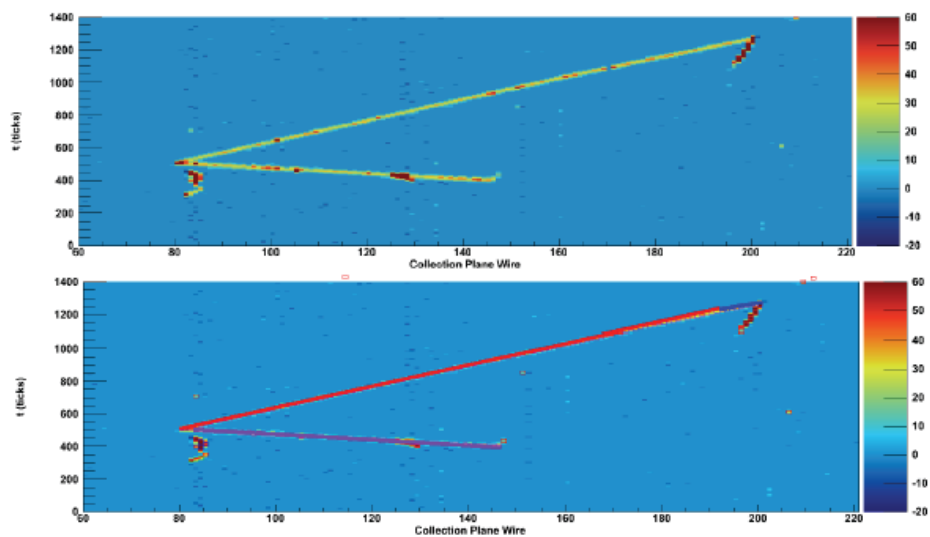
Figure 6: (Top) A neutrino candidate in ArgoNeuT as seen on the collection plane. (Bottom) The Hough lines found with the line-finding algorithm overlaid on the particle tracks.

Figure 7: The neutrino event shown in Figure 6 reconstructed in three dimensions.

Figure 8–15: Figure from the ArgoNeuT draft NIM paper showing the status of 3D reconstruction

Figure 13: dQ_0/dx distribution (in ADC/cm) obtained for the through-going muon data sample having corrected for the electron lifetime and quenching effect on the ionization charge and properly taken into account the contribution due to δ-rays, as reported in the previous Section. A Landau-Gaussian fit is also reported.
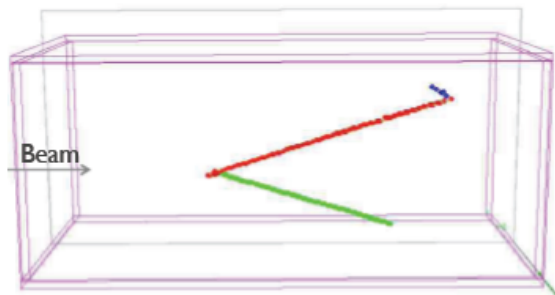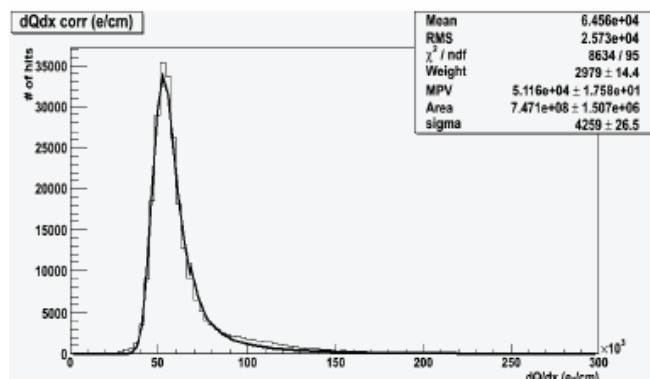
Figure 8–16: Figure from the ArgoNeuT draft NIM paper showing the status of calorimetric reconstruction.

through an NSF MRI in 2008 and an NSF proposal in 2009. MicroBooNE received DOE CD-0 Mission Need in 2009 and CD-1 in 2010, and CD-2/3a review in September 2011. It plans to start running in early 2014.

As well as pursuing its own physics program, MicroBooNE will collect a large sample (∼100k) of low-energy neutrino events that will serve as a library for the understanding of neutrino interactions in LAr. Because MicroBooNE is at the surface, it will also have a large sample of cosmic rays with which it can study potential backgrounds to rare physics. The process of designing MicroBooNE has naturally stimulated several developments helpful to the LBNE program. Studies of wire material, comparing Be-Cu with gold-plated stainless steel in terms of their electrical and mechanical properties at room and LAr temperatures, and techniques for wire-tension measurement are immediately relevant for LBNE. Expertise has been developed generating simulations of electrostatic-drift fields as well as simulations of temperature and flow distributions in LAr cryostats which is being applied to the LAr-FD TPC and cryostat. MicroBooNE will use the front end of the proposed in-liquid LBNE electronics as the wire-signal amplifiers. The DAQ developed for MicroBooNE will exploit compression and data-reduction techniques to record data with 100% livetime.

In summary, MicroBooNE's LArTPC development goals that are pertinent to LAr-FD are

- large-scale testing of LBNE front-end electronics

- testing of continuous data-acquisition algorithms

- refinement of the analysis tools developed in ArgoNeuT

- provide costing and construction lessons-learned

8.4 Summary

Impressive progress has been made in the development of LArTPC technology over the last few years. All elements of the development program have completed the R&D phase. Credible conceptual designs exist for all systems in LAr-FD. The technical activities described in this chapter are properly characterized as preliminary engineering design.

It is worth noting that the experiment-agnostic development of offline software, particularly that aimed at fully-automated event reconstruction has not been discussed in a dedicated way within this chapter. However, algorithms have been developed within the LAr community and are being successfully applied to ArgoNeuT data as well as to simulated MicroBooNE data. The algorithms have individually shown that the high efficiency and excellent background rejection capabilities of an LArTPC are achievable. As a physics experiment, MicroBooNE experiment will provide an excellent opportunity for synthesizing these algorithms into a cohesive package as well as further developing them.

9   Alternatives Not Selected

Alternative detector configurations and design parameters that were considered but ultimately rejected for other designs are discussed in this chapter.

9.1   Detector Configuration

9.1.1   Double Phase Readout

The European GLACIER study group is pursuing a novel double-phase readout detector technology that has potential advantages. In this scheme, ionization electrons are drifted upwards under the influence of an electric field towards the liquid-vapor interface. The electrons are extracted from the liquid into the vapor by an electric field of 2.5 kV/cm. The electrons then drift to two stages of Large Electron Multipliers (LEM). Electrical signals are induced on segmented electrodes on the LEM.

This method requires far fewer readout channels than our reference design, however significant R&D is required to demonstrate the viability of this technique for a large detector. This design requires very long electron-drift lengths (~ 20m) in order to be cost-effective.

9.1.2   Cryostat Shape

Storage tanks can be classified by shape (upright cylinder, horizontal cylinder, rectangular parallelepiped) and means of support (self supporting, externally supported).

A horizontal cylindrical tank would require significant structural support to withstand the gravitational load. On the other hand, upright self-supporting cylindrical tanks are commonly used for surface storage of cryogenic liquids. The proposed above-ground LArTPC experiment FLARE utilized a tank of this configuration. An upright cylindrical tank is also proposed for the 100-kton GLACIER underground detector. In contrast, the 600-ton ICARUS detector is a rectangular parallelepiped.

A study was performed [33] to compare the cost for three deep-underground configurations of equivalent active mass: upright cylindrical cryostat (soup can), rectangular parallelepiped externally-supported cryostat (membrane) and the rectangular parallelepiped self-supporting cryostat (modular). The study considered the cost of rock excavation, the cost of the total inventory of LAr required for a detector with a fixed active mass and a rough estimate of the cryostat cost.

The active/total mass fraction for the three configurations ranges between 70% and 74% and is therefore not a significant factor in the cost difference. The major cost factor is the volume of rock that must be excavated for these configurations. There is a significant amount of unused cavern space if an upright cylindrical tank is located within a rectangular parallelepiped cavern. The amount of unused space can be reduced by excavating a cylindrical cavern but the excavation cost would increase significantly ($\sim 30\%$).

The study results show a cost range of 10% - 20% for the different configurations. This is within the uncertainty of the estimates ($\sim 50\%$) so none of the options can be rejected purely on economic grounds given our current state of knowledge. Given sufficient resources, all configurations could be more fully developed to make a more informed decision, however any potential value would be offset by the cost of pursuing multiple design paths.

The study results also indicate that a membrane cryostat is the most cost-effective solution for a detector sited deep underground. It clearly maximizes the use of the excavated rock volume. A membrane cryostat is also inherently more cost-effective than a self-supporting cryostat since the hydrostatic pressure of the liquid is constrained by the cavern walls and not the cryostat walls, thereby reducing the amount of structural steel required.

9.1.3   Modular Cryostat

The modular LANNDD detector concept was considered. The main benefit of the LANNDD concept is that the cryostat is evacuable. However, reinforcing members within the cryostat would be required to withstand the vacuum load. Physics cuts around these members would reduce the fiducial mass of the detector significantly relative to the membrane-cryostat reference design. Results from the Liquid Argon Purity Demonstrator have shown that cryostat evacuation is not required to achieve excellent LAr purity.

9.2   Depth Options

9.2.1   800L

In addition to the reference design described in this CDR for a detector at the surface, a candidate design for the 800L was also developed [9] that was intended to achieve all the science goals of LBNE. At this depth, there is an unacceptable level of background to $p \to \nu K^+$ due to the creation of K0L by cosmic ray muons in the surrounding rock, which subsequently charge exchange within the LAr detector to create an isolated K^+. To mitigate this effect, a large-area veto system was included in the 800L design, in order to tag muons which could generate such background and thereby eliminate candidate proton decay events in coincidence with a detected muon. Given the goal of essentially zero background for the proton decay search ([34] quotes a background rate on the order of 1 event in 30 years), the veto system would be required to be extremely efficient, and therefore essentially completely hermetic. However, due to the practical engineering considerations of how to implement a veto system extending 7 m into the rock at both top and bottom of the main detector, it proved difficult to achieve the required hermetic coverage. In addition, at the position of the proposed cavern at the 800L, the cosmic ray flux – angle and energy – depend on the details of the surface topography, which would require extensive simulations to be able to be assured of the efficacy of the veto system for reducing the background to the required level.

Cosmic ray muons passing through the LAr detector itself can produce spallation products with lifetimes too long to allow signals resulting from their subsequent decay to be vetoed by observing the muon that created them. These would create backgrounds that could compromise low-energy physics searches, of which the observation of neutrinos from a distant core-collapse supernova is the prime example. The spectrum of spallation products of argon is not well known, nor is the spectrum of low-energy searches that the LBNE LAr-FD may be called upon to do, so it is difficult to quantify the effect of such background. Since the spallation backgrounds cannot be vetoed, the only way to reduce them is to move the detector to greater depth or abandon this physics.

9.2.2   4850L

The LBNE Collaboration Executive Committee, in its meeting in December 2011, issued a statement that "There was a very strong preference for siting the experiment at the 4850L depth" based on the considerations described in the preceding sections as well as the fact that siting LBNE at the 4850L would help enable other deep underground science in the U.S. At the present time, there are insufficient funds to site the detector below-ground.

9.3   Cryogenics Plant

9.3.1   LAr Supply using a Temporary Air-Separation Plant

The provision of a temporary, dedicated air-separation plant could be justified based on the elimination of LAr losses due to boil-off during transportation, elimination of vehicle movements and the potential increase in the supply reliability. These advantages must be offset against the net capital cost of the temporary plant, the operating cost of the plant and the relative inefficiency of the small temporary plant as compared to a large commercial plant. LAr suppliers have advised that this would not be cost-effective.

9.3.2   LAr Storage

It would be desirable to provide temporary storage of LAr to decouple the delivery schedule from the detector construction schedule. Ideally, temporary storage could reduce the schedule by several months since argon deliveries can occur in parallel with detector construction. This is only possible if construction of the temporary storage facility occurs concurrently with other activities.

Temporary storage would also mitigate the risk of a detector failure necessitating access to the cryostat. If a sudden detector-wide failure occurred and temporary storage were not available, the argon would be vented to the atmosphere and the investment in LAr would be lost. The cryostat filling sequence described in Chapter 7 effectively eliminates the likelihood of failure during detector commissioning. A sudden detector-wide failure occurring during operations is highly unlikely. It is more likely, but still unlikely, that a gradual degradation of detector performance would occur over an extended period of time, allowing time for a decision to be made to construct a storage tank.

9.4   Cryostat Insulation

The original LANNDD modular cryostat included the use of a vacuum-insulated space between the inner and outer tanks, resulting in a significant decrease in the required refrigeration load. This benefit would need to be weighed against the added capital cost of a vessel that can withstand the vacuum load. Arup eliminated the vacuum-insulated option during the screening process, citing the benefit of not having an outer tank designed for a full vacuum load.

The use of a vacuum-jacketed cryostat was rejected. The most serious concern is an accident scenario that would result in a significant leak in the inner vessel. The outer tank and the

argon venting system would need to be designed to cope with the large volume of released gas.

9.5 TPC

9.5.1 TPC Configuration

9.5.1.1 Reference Design 1a

The first proposed Reference Design, 1a [35], relied on a minimal extrapolation of the MicroBooNE TPC module design. The detector would be installed in a cavern with drive-in access and would consist of a rectangular stack of TPC modules that had been constructed above-ground.

A modest extrapolation of the MicroBooNE module design parameters does not introduce large cost uncertainty if done properly. The extrapolations are in dimensions that do not challenge the limits of the technology. Rather, this detector configuration suffers from a poor fiducial/total mass fraction. Only 56% of the LAr in the detector would be useful for physics and the cost is ~3 times the cost of the reference design.

9.5.1.2 Reference Design 2a

Reference Design 2a [36] is similar to the selected reference design. The major difference is the use of room-temperature, accessible electronics. The concept is shown in Figure 9–1.

Short low-impedance cables route wire signals from the Anode Plane Assemblies (APAs) to a cold feedthrough which is kept at ~ 120 K. The readout electronics are located within the feedthrough. The benefit of this design is that the electronics boards can be replaced without removing LAr from the detector.

There are a number of disadvantages to this concept, however. The cable lengths must be kept to ~ 1 m and the wire angle reduced from $45^{\deg}$ to $30^{\deg}$ in order to achieve a marginally acceptable signal-to-noise ratio. As a result, the track resolution in the vertical direction would be ~ 1 cm. A large number of feedthroughs are required in order to keep the cable lengths short. One feedthrough containing 576 electronics channels is required for every 53 cm along the top of each APA. Each feedthrough would be 34 cm × 22 cm in cross section and would be ~ 2 m long.
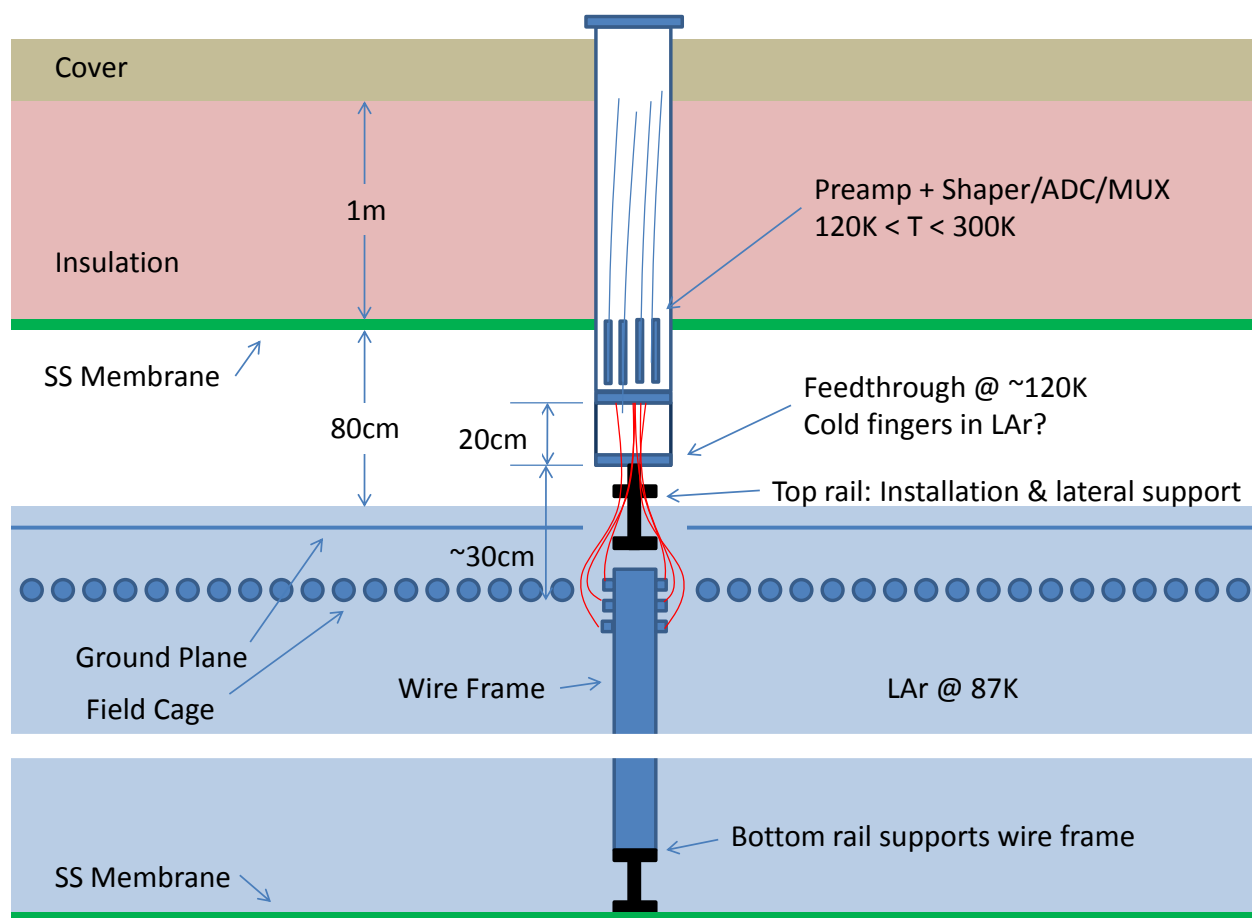
Figure 9–1: Reference Design 2a, showing cable routing from an Anode Plane Assembly to a cold feedthrough. The warm readout electronics are located within the feedthrough.

9.5.2 Wire Spacing

The distinguishing feature of the LArTPC is the ability to distinguish one MIP electrons from 2 MIP electron-positron pairs close to the interaction vertex. A wire spacing smaller than the design (5 mm) would have smaller signal-to-noise ratio (S/N) commensurate with the wire spacing. Reducing the wire spacing below 5 mm will only offer minimal benefit since the background from NCπ^0 events is already quite small.

9.5.3 Number of Wire Planes

The reference design includes three instrumented wire planes and one un-instrumented grid plane. Reducing the number of instrumented planes to two would reduce the detector cost by a few \$M with a negligible loss of ν_e identification efficiency. This would also reduce

the readout redundancy, however, and potentially affect the long-term reliability of detector operations. We do not consider this a credible value-engineering option.

The un-instrumented grid plane could be eliminated, saving $\sim$ \$1M. The grid plane is used to create equal signal levels in both induction planes. The signal level in the first induction plane would be reduced by $\sim$2 times if the grid plane were eliminated. The grid plane also provides electrostatic discharge protection for the instrumented wires. We may reconsider this option in the future.

9.5.4   Drift Length

Selection of the design drift length is highly coupled with the expected LAr purity, the wire spacing and the required ν_e identification efficiency and background rejection. The ICARUS detector is currently operating with a drift electron lifetime of 5 to 7 ms. We expect the LAr purity in LAr-FD to be equal or superior to ICARUS. Increasing the drift distance beyond the reference design would result in significant cost savings but tracks would suffer significant distortion due to space charge from the high cosmic ray flux.

9.6   DAQ Cable Routing

The concept of routing raw signals from all wires out of the cryostat, as ICARUS does, was considered. The large data rate would require a huge number of cables and feedthroughs with little benefit since the vast majority of the sampled wire signals have no information. The large cable plant would be a major contributor to LAr impurities.

9.7   Installation & Commissioning

The initial Installation and Commissioning concept was to support the TPC on the floor of the cryostat. Cross-bracing in both directions would be required to ensure mechanical stability and would compromise the TPC design. Hard points in the cryogenic insulation would be needed which would likely require design modifications to the standard vendor-supplied membrane-cryostat insulation system.

Several alternatives for accessing the top of the detector during installation were considered. A scissors lift was considered and rejected due to concerns that the lift could sway and damage detector components. Consideration was given to a moveable platform that would traverse the top of the detector on rails, or alternatively, using a temporary catwalk. These systems would provide access to the top of the detector but not at intermediate heights.

Several installation sequences were considered; row-wise versus column-wise installation of APAs and CPAs. The current installation sequence was deemed superior in that it minimizes work activities in previously installed sections of the detector. This reduces the risk of damage during installation.

9.8   Photon Detection

Most LArTPCs use TPB-coated PMTs to detect scintillation light. Light emitted more than a few meters from a PMT is diffused by Rayleigh scattering ($\lambda \approx 90$ ccm), so PMTs would need to be placed between drift cells. This configuration is not compatible with the APA concept. Conceptually, each interior cathode plane can be replaced with two cathode planes separated by sufficient space for an array of PMTs. This would increase the width of the detector and the cavern by ~ 1m and result in a lower fiducial mass.

A variety of options are still being considered for the wavelength-shifting scheme and the light guides.

References

[1] P. Benetti *et al. Nucl.Instr. and Meth. A*, vol. 574, p. 83, 2007.

[2] V. Gehman *et al.*, "Fluorescence Efficiency and Visible Re-emission Spectrum of Tetraphenyl Butadiene Fils at Extreme Ultraviolet Wavelengths," *Nucl.Instr. and Meth. A*, vol. 654, p. 1, 2011.

[3] Particle Physics Project Prioritization Panel, "US Particle Physics: Scientific Opportunities; A Strategic Plan for the Next Ten Years," 2008. `http://science.energy.gov/~/media/hep/pdf/files/pdfs/p5_report_06022008.pdf`.

[4] T. Akiri and others, "The 2010 Interim Report of the Long Baseline Neutrino Experiment Collaboration Physics Working Groups." arXiv:1110.6249.

[5] LBNE Project Office, "LBNE Project Management Plan," tech. rep., FNAL, 2011. LBNE Doc 2453.

[6] S. Amerio *et al.*, "Design, construction and tests of the ICARUS T600 detector," *Nucl. Instrum. Meth. A*, no. 527, 329, 2004.

[7] `http://t962.fnal.gov/`.

[8] `http://www-microboone.fnal.gov/`.

[9] Arup USA, Inc., "Concept Report LAr40 at 800L," tech. rep., 2011. LBNE Doc 4314.

[10] B. Baller, "TPC Wire Angle Optimization." LBNE Doc 2836, 2010.

[11] B. Baller, B. Fleming, "Integrated Plan for LArTPC Neutrino Detectors in the US," tech. rep., FNAL, 2010. LBNE:DocDB-2113.

[12] "SDSTA-Fermilab-LBNL MOU regarding the LBNE Project."

[13] LBNE LAr-FD L2 Project, "LAr-FD Requirements spreadsheets." LBNE Doc 3747.

[14] LBNE LAr-FD L2 Project, "LAr-FD Requirements traceback reports." LBNE Doc 5185.

[15] LBNE LAr-FD L2 Project, "LAr-FD Parameter Tables." LBNE Doc 3383.

[16] M. Adamowski, "Cryostat Insulation Purge Design Basis and Sizing," tech. rep., FNAL, 2011. LBNE Doc 4303.

[17] Freedonia Group, "Executive Summary - Specialty Gases to 2013," tech. rep., 2010. LBNE Doc 2371.

[18] M. Adamowski, "Purification Design Basis and Filter Sizing," tech. rep., FNAL, 2011. LBNE:DocDB-3609.

[19] Fermilab, "Fermilab ES&H Manual ." `http://esh.fnal.gov/xms/FESHM`.

[20] H. Jostlein, "FNAL APA prototype and wire holding tests." LBNE Doc 3037, 2010.

[21] E. Voirin, "Liquid Argon Circulation, Temperature Profile, and Impurity Distribution in the 10kT LBNE Cryostat," tech. rep., FNAL, 2012. LBNE:DocDB-6140.

[22] G. De Geronimo *et al.*, "Front-end ASIC for a Si Compton telescope," *IEEE Trans. Nucl. Sci.,*, vol. 55, no. 4, 2008.

[23] IEEE The International Conference on Dependable Systems and Networks (DSN-04), *The impact of technology scaling on lifetime reliability*, June 2004.

[24] M. A. Alam and S. Mahapatra, "A comprehensive model of PMOS NBTI degradation," *Microelectronics Reliability*, vol. 45, no. 1, pp. 71–81, 2005.

[25] IEEE International Semiconductor Device Research Symposium, *CMOS device reliability for emerging cryogenic space electronics applications*, 2005.

[26] NOvA Collaboration, "The NOvA Experiment Technical Design Report." `http://lss.fnal.gov/archive/design/fermilab-design-2007-01.pdf`, 2007.

[27] MicroBooNE Collaboration, "The MicroBooNE Conceptual Design Report." `http://microboone-docdb.fnal.gov/cgi-bin/ShowDocument?docid=1821`, 2010.

[28] L. Bugel *et al. Nucl.Instr. and Meth. A*, vol. 640, p. 69, 2011.

[29] T. Doke *et al. Nucl.Instr. and Meth. A*, vol. 291, p. 617, 1990.

[30] B. Baller, LAr40 Photon Detection Ruminations, August 2011.

[31] T. Pollman, M. Boulay, and M. Kuzniak, "Scintillation of thin teraphenyl butadiene fils under alpha particle excitation," 2010.

[32] P. K. Lightfoot *et al. JINST*, vol. 4, p. P04002, 2009.

[33] B. Baller, "LAr20 Cryostat Configuration Cost Comparison," tech. rep., FNAL, 2009. LBNE Doc 355.

[34] A. Bueno, A. J. Melgarejo, S. Navas, Z. D. ai, Y. Ge, M. Laffranchi, A. M. Meregaglia, and A. Rubbia, "Nucleon decay searches with large liquid Argon TPC detectors at shallow depths: atmospheric neutrinos and cosmogenic backgrounds," *Journal of High Energy Physics*, vol. 2007, no. 04, p. 041, 2007.

[35] "LAr20 Reference Design 1a: Modified MicroBooNE TPC Modules in a Membrane Cryostat at Shallow Depth," tech. rep., FNAL, 2010. LBNE:DocDB-2117.

[36] "LAr20 Reference Design 2a: Membrane Cryostat with Wrapped TPC Modules and Accessible Electronics in a Deep Cavern," tech. rep., FNAL, 2010. LBNE:DocDB-644.